Electrochemical Oxidation of Aliphatic Carboxylates: Kinetics, Thermodynamics, and Evidence for a Shift from a Concerted to a Stepwise Mechanism in the Presence of Water

Marwa Khalil Abdel Latif

Dissertation submitted to the faculty of the Virginia Polytechnic Institute and State University in partial fulfillment of the requirements for the degree of

Doctor of Philosophy
In
Chemistry

James M. Tanko
Karen J. Brewer
Robert B. Moore
Amanda Morris
Gordon T. Yee

August 31, 2016
Blacksburg, VA, 24060

KEYWORDS: convolution voltammetry, dissociative electron transfer, aliphatic carboxylates, aryl carboxylates, concerted mechanism, stepwise mechanism, oxidation potential, anhydrous conditions, wet conditions, hydrogen bonding, shift from concerted to stepwise, diffusion coefficients, radical stabilization

Electrochemical Oxidation of Aliphatic Carboxylates: Kinetics, Thermodynamics, and Evidence for a Shift from a Concerted to a Stepwise Mechanism in the Presence of Water

Marwa K. Abdel Latif

Abstract

The mechanism and the oxidation potential of the dissociative single electron transfer for tetra-n-butylammonium acetate has been investigated via conventional (cyclic voltammetry) and convolution voltammetry. The oxidation potential for tetra-n-butylammonium acetate was determined to be 0.60 ± 0.10 (vs. Ag/ (0.1 M) $AgNO_3$) in anhydrous acetonitrile. The results also indicated the mechanism of oxidation was concerted dissociative electron transfer (cDET), rather than stepwise as was previously reported.

To further investigate the mechanism, a series of aliphatic and aromatic tetra-n-butylammonium carboxylates were synthesized and investigated via convolution and conventional methods under anhydrous conditions (propionate, pivalate, phenyl acetate, and benzoate). The reported results showed high reproducibility and consistency with a concerted dissociative electron transfer for aliphatic carboxylates with a systematic shift in the oxidation potentials (0.60 ± 0.09 V for acetate, 0.47 ± 0.05 V for propionate, and 0.40 ± 0.05 V for pivalate) within the series which is expected trend based on radical stabilization energies of the alkyl groups on the aliphatic carboxylates.

Hydrogen bonding was investigated as a possible source for the discrepancy between our results and the reported mechanism of the dissociative electron transfer. Because of the extreme hygroscopic nature of carboxylate salts, it was hypothesized that the presence of small amounts of water might alter the reaction mechanism. Deionized water and deuterium oxide additions to

anhydrous acetonitrile were performed to test this hypothesis. The mechanism was noted to shift towards a stepwise mechanism as water was added. In addition, the derived oxidation potentials became more positive with increasing concentrations of water. Several explanations are presented with regards to water effects on the shift in the electron transfer mechanism.

Indirect electrolysis (homogeneous redox catalysis) was also employed as an alternative and independent approach to quantify the oxidation potentials of carboxylates. A series of substituted ferrocenes were investigated as mediators for the oxidation of tetra-n-butylammonium acetate. Preliminary data showed redox catalysis was feasible for these systems. Further analyses of the electrochemical results suggested a follow-up chemical step (addition to mediator) that competes with the redox catalysis mechanism. As predicted from theoretical working curves, a plateau region in the i_p/i_{pd} plots (where no meaningful kinetic information could be obtained) was observed. Products mixture analyses verified the consumption of the mediator upon electrolysis, but no further information with regards to the nature of the mechanism was deduced.

In a related study the effects of hydrogen bonding and ions on the reactivity of neutral free radicals were examined by laser flash photolysis. The rate of the β-scission of the cumyloxyl radical is influenced by cations ($Li^+ > Mg^{2+} \approx Na^+ > {}^nBu_4N^+$) due to stabilizing ion-dipole interactions in the transition state of the developing carbonyl group. Experimental findings are in a good agreement with theoretical work suggesting metal ion complexation can cause radical clocks to run fast with a more significant effect if there is an increase in dipole moment going from the reactant to the transition state.

Electrochemical Oxidation of Aliphatic Carboxylates: Kinetics, Thermodynamics, and Evidence for a Shift from a Concerted to a Stepwise Mechanism in the Presence of Water

Marwa K. Abdel Latif

General Audience Abstract

Our work focuses on employing electrochemical techniques to investigate single electron transfer processes, which lead to unstable organic species that contain an odd number of electrons called radicals and radical ions. Many essential biological and environmental pathways are found to occur via radicals, i.e. photosynthesis, atmospheric degradation, enzyme catalyzed reactions in biology, autooxidation, DNA mutations, and more. Electrochemical techniques permit us to investigate the scientific fundamentals of radical processes by generating radicals and radical ions in a controlled manner with a higher efficiency.

We have combined electrochemical techniques with established physical organic theories of electron transfer to allow us to determine of the rate and mechanism of electron transfer for a selective group of chemical compounds, specifically anions derived from carboxylic acids (carboxylates). A fundamental understanding of single electron transfer processes for carboxylates allows for a prediction of chemical behavior and the future design of novel chemical compounds for alternative chemical functionality. Our findings are the first to report experimental evidence for a so-called concerted dissociative electron transfer mechanism for carboxylates, where the transfer of an electron is accompanied by the simultaneous breakage of a carbon-carbon bond yielding a radical and carbon dioxide. The mechanism has been shown to proceed in a stepwise fashion only in the presence of water. Our work highlights the environmental effects on radical stability such as water and metals ions.

Acknowledgments

First and foremost, I would like to thank my academic father Dr. Jim Tanko for his enormous support throughout my journey. Your brilliance, kindness, and wisdom have guided me through the years. You have always embraced my curiosity and allowed me to be driven by it. Your valuable guidance helped me to mature not only professionally, but personally. You continue to show me how proud you are of my achievements, and never stop to challenge me to ask new questions. Our shared laughter, frustrations, and scientific "EUREKA" moments will always remind me that true passion is in itself very rewarding.

I would like to extend my deepest appreciation to the late Dr. Karen Brewer who was taken way too soon. My fond memories of you will never fade away. Your words are never forgotten, and your support will continue to guide my way. You were a role model for all women scientists. You supported the uniqueness of my personality and scientific curiosity, and urged me to let it guide my way.

My sincere gratitude to Dr. Gordon Yee who always reminded me to have ownership of my work and earn my respect as a scientist. Your questions continue to challenge me and make me a better chemist. You have made me grow not only as a scientist but also as a teacher.

My deepest gratitude to Dr. Robert Moore who took me in as a student during one of the toughest moments of my academic journey. Your assurance and constructive criticism has helped me tremendously and thank you for teaching me a valuable lesson "to always keep it simple!"

My deepest gratitude to Dr. Amanda Morris who was the first to teach me about electrochemistry, my true passion. Throughout my journey, you have supported my efforts and welcomed my questions and concerns.

Dr. Jared Spencer, there are no words to describe my appreciation for all the help and mentoring you have provided me. You were like a big brother to me and were always willing to help in understanding electrochemical theory. I would not have survived the journey without you.

I would also like to thank my colleagues, staff, and students across campus and throughout the years that have guided me through my professional career. Our shared confusions, arguments, stimulating discussions, community activities, and continuous encouragement to each other are a treasure that I will hold on to always.

Thank you to my husband and partner, Theodore Canterbury. Your love, devotion, kindness, as well as your genuine curiosity for knowledge of science and technology has been nothing but complete inspiration that lit the way.

My journey as a refugee woman scientist has been anything but boring. I would not be the person I am without the love and support of my parents, siblings, and grandparents. My mother, Mona ElSherif, who I only aspire to be like, is an endless blessing. You have endured our being apart for

over a decade so I can grow to become the woman I am today. To my father, Khalil Abdel Latif, who has stood by my side, allowed me to dream, and encouraged me to never stop the fight to better myself, and taught me to give back to the world. Thank you.

To everyone I have ever met, I say thank you for being a part of my life, as you all have helped shape my journey.

Table of Contents

List of Abbreviations

A	Surface area of electrode
AcO$^-$	Acetate anion
B3LYP	Becke, 3-parameter, Lee-Yang-Parr
BE	Bulk electrolysis
C	Molar concentration
*C**	Bulk molar concentration
C_{2v}	Point group symmetry
CBS	Complete basis set
CI	Confidence interval
C_M*	Mediator bulk concentration
CV	Cyclic voltammetry
DE	Direct electrolysis
DET	Dissociative electron transfer
DFT	Density functional theory
D_o	Diffusion coefficient
E	Electrode potential
EC	Electron transfer followed by a chemical step (electrode mechanism)
EOS	Electro-oxidative synthesis
ERC	Electroreductive cyclization
ES	Electrochemical synthesis
ET	Electron transfer
E^o	Standard oxidation potential for a redox couple
E_p	Peak potential
$E_{p/2}$	Half-peak potential
E_{pc}/E_{pa}	Cathodic peak potential/ anodic peak potential
F	Faraday constant
G	Free energy
GC	Gas chromatography
GC	glassy carbon
GC-MS	Gas chromatography - Mass spectroscopy

$G^{\ddagger}$	Free energy of activation
HAT	Hydrogen abstraction transfer
HF	Hartree-Fock theory
HOMO	Highest occupied molecular orbital
HRC	Homogenous redox catalysis
H_f^o	Standard heat of formation
I	Applied current
Iconv	Convolutive current
I_l	Limiting convolutive current
I_p	Peak current
K_{eq}	Equilibrium rate constant
LFP	Laser flash photolysis
LSV	Linear sweep voltammetry
M	Mediator
MP2	Moller-Plesset 2
MS	Mass spectroscopy
N*HE*	Normal hydrogen electrode
NMR	Nuclear magnetic resonance
O/*R*	Oxidized/reduced species
PFG NMR	Pulsed field gradient nuclear magnetic resonance
QCISD	Quadratic configuration interaction for single and double substitutions
R	Molar gas rate constant
RSD	Rate determining step
RSE	Resonance stabilization energy
S	Substrate
SCE	Saturated calomel electrode
SET	Single electron transfer
SHE	Standard hydrogen electrode
S^o	Standard entropy
T	Temperature (Kelvin)
TBA	Tetra-n-butylammonium
TBABr	Tetra-n-butylammonium bromide

TBAP	Tetra-n-butylammonium perchlorate
TMA	Tetramethylammonium
$TS^{\ddagger}$	Transition state
UV-vis	Ultraviolet visible spectroscopy
W	Electrostatic constant
XPS	X-ray photoelectron spectroscopy
Z	Spherical charge
ZPE	Zero point energy
cDET	Concerted dissociative electron transfer
f	Ionic strength
i_p	Catalytic current
i_{pc}/i_{pa}	Cathodic peak current/ anodic peak current
i_{pd}	Current peak in absence of substrate
k_{ET}	Electron transfer rate constant assigned in mathematical models for electron transfer processes (such as Marcus theory) and for the homogenous electron transfer process in solutions (such as HRC)
k_{add}	Follow-up addition rate constant
k_c	Chemical step rate constant
k_f	Forward reaction rate constant
k_{heter}	Heterogeneous electron transfer rate constant assigned for electron transfer processes at the electrode surface
k_{obs}	Observed rate constant
k_s	Standard electron transfer rate constant
m_R	Molar concentration
n	Number of electrons per a mole of reactant
q	Charge
r	Spherical radii
sDET	Stepwise dissociative electron transfer
t	time
x	Distance from electrode
v	Scan rate
α	Transfer coefficient (unit of symmetry)
α_{avg}	Averaged transfer coefficient

γ	Excess factor
η	Overpotential
λ, λ_o, λ_i	Total reorganization energy, outer, and inner reorganization

Chapter 1. Mechanism of the dissociative electron transfer for Kolbe's electrolysis

1. Introduction.

1.1. Overview of Electro-synthesis and Kolbe electrolysis.

Electrochemical synthesis (ES) is an increasingly important area of interest for synthetic chemists, especially in light of the growing need for industrial approaches that are both more efficient and environmentally friendly. Industrial ES requires simple reusable and commercially-available instrumentation to perform direct reduction or oxidation reactions in an electrochemical cell. ES offers several advantages over traditional, reagent-based organic synthesis methods. Most importantly, traditional methods commonly employ aggressive or expensive chemical reagents (e.g., potent oxidizing agents) and must often be carried out at high temperature and pressure; in contrast, electrochemical methods are greener, milder, less costly, and typically provide higher yields.[1-7]

The high demand for electrochemical synthesis (when feasible) is not only due to its simplicity and cost effectiveness, but is also tied to the ease of initiating reactions reductively or oxidatively. A prominent contribution involving electro-reductive synthesis is the enhanced ability to produce key industrial chemicals such as inositols and cyanoaceticacid.[8] Other key advances include (a) the limitation of toxic metal-containing reagents in the synthesis of chemical intermediates such as glycols for C-glycoside and oligosaccharide formation;[9] (b) the enhancement of product-selectivity of 5-and 6-membered rings, such as in the synthesis of α-amino aldehydes; (c) the production of α,β- unsaturated aldehydes via electroreductive cyclization reactions (ERC);[10,11] and (d) the generation of highly reactive radical intermediates such as nitrite radicals for the synthesis of diacylated compounds.[12]

The classic electro-oxidative synthesis (EOS) reaction to be studied, the Kolbe electrolysis remains one of the most well-known synthetic approaches.[13] Kolbe electrolysis originally involved the oxidation of organic acids, which results in the dimerization of R groups (C-C bond formation) due to generation of alkyl radical intermediates upon decarboxylation (**Scheme 1.1**). Furthermore, carbon radicals can be further oxidized to form carbocations via what is generally referred to as the non-Kolbe process. The oxidation of carboxylates at the surface of the electrode is initiated by a one-electron transfer step, which is then followed by the rapid and irreversible decarboxylation of the acyloxyl radicals (**Eq 1.1-1.2**).[1,14] Decarboxylation rate constants have been found to be on the order of 10^9-10^{10} s^{-1} for aryl and aliphatic carboxyl radicals (with the exception of benzoyloxyl).[15]

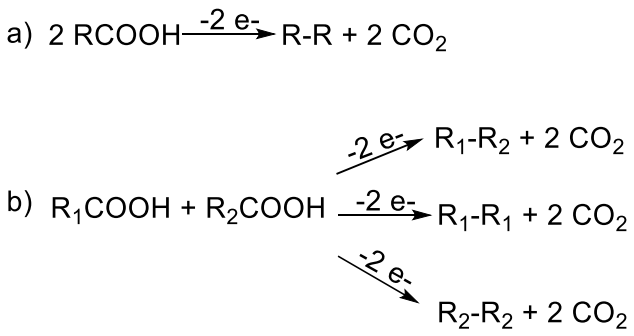

Scheme 1.1 The electro-oxidative reaction of carboxylic acids resulting in the dimerization of the alkyl groups upon decarboxylation, b) Representative variety of yields based on the nature of the R group.

Based on electrochemical studies, scientists have established that dissociative electron transfer is the rate determining step (rds) of the Kolbe reaction.[14,16-27] However, the precise mechanism by which dissociative electron transfer occurs is still disputed.[21] In the Kolbe electrolysis, electron transfer can occur via a *concerted* or a *stepwise* pathway. In concerted dissociative electron transfer (cDET), the electron transfer and fragmentation occur simultaneously.[7] In a stepwise dissociative electron transfer mechanism (sDET), the electron is

transferred in the first step, resulting in an acyloxyl radical intermediate (**Eq 1.2**), which is followed by fragmentation of the covalent bond to release carbon dioxide and alkyl radical as products.

$$RCOO^- \rightarrow RCOO^{\cdot} + e^- \quad \textbf{(1.1)}$$

$$RCOO^{\cdot} \rightarrow R^{\cdot} + CO_2 \quad \textbf{(1.2)}$$

$$R^{\cdot} \rightarrow R^+ + e^- \quad \textbf{(1.3)}$$

Despite a lack of precise mechanistic understanding of the Kolbe oxidative process, it has long been incorporated into a variety of synthetic applications due to its desirable generation of highly reactive alkyl radicals and cations following the fragmentation of the compound(**Eq 1.3**).[13] This chapter will present an overview of the historical contributions of the Kolbe mechanism, which has shaped electrochemical investigations over the decades—including the research detailed herein. In addition, we will present our new electrochemical approach to further enrich our fundamental knowledge of dissociative electron transfer utilizing Kolbe electrolysis.

1.2. Carboxylates as synthetic intermediates and electrode-modifying agents.

Carboxylic acids and their conjugate bases remain the focus of Kolbe electrolysis.[13] Their versatile nature as synthetic intermediates has heightened the interest of the research community in generating other functional groups.[1,2,15,25,28-31] Initially, reagent-based methods were utilized to initiate the formation of alkyl radical intermediates. For example, the Hunsdiecker reaction, also known as the Boroin reaction, employs silver (I) salts to perform a halogenations reaction, which is believed to generate carboxyl radical intermediates (**Scheme 1.2a**).[31-33] However, with the rise of electro-synthetic methods, similar results can be obtained by electrolysis at the surface of an electrode. Radical intermediates are formed by anodic oxidation of carboxylic acids to generate alkyl bromides in the presence of bromine (**Scheme 1.2b**). Therefore, electrolysis represents an

efficient reagent-free alternative for generating carbon-centered radicals, which can subsequently be employed to generate a wide variety of products, such as ketones, aldehydes, and alkenes.[1,2,34]

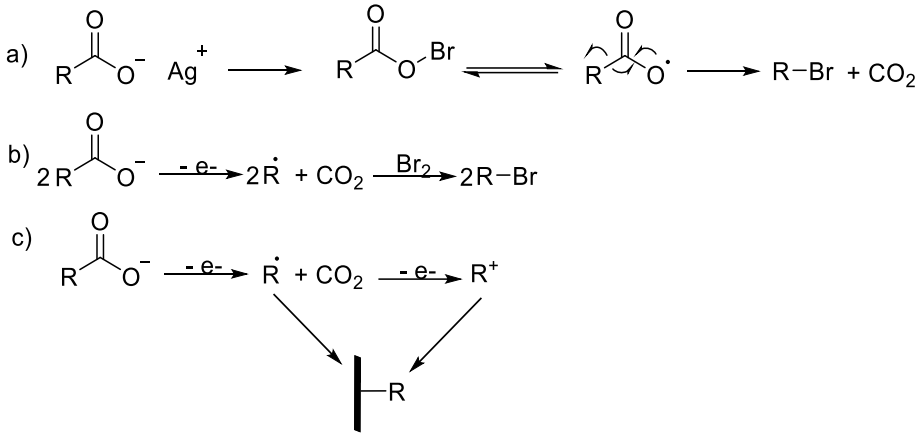

Scheme 1.2 a) Reagent-based decarboxylation with silver salts follows a radical intermediates pathway to generate alkyl bromide; b) electrodecarboxylation to generate alkyl bromide, c) electrolysis of carboxylates

While ES has become a popular synthetic approach to produce small molecules, the use of ES for modifying electrode surfaces represents one of the most promising and important advancements involving Kolbe electrolysis (**Scheme 1.3**). Regardless of whether or not the radical or the carbocation are produced via electro-decarboxylation, the resulting highly reactive intermediates can then be grafted onto metals and nonmetallic electrical components, and in particular, on glassy carbon electrodes. Indeed, electro-decarboxylation has been used advantageously in a wide variety of fields, most prominently in nanotechnology and materials science.[25,30,35-40] Over the last two decades, electro-grafting using carboxylates as starting material has been highly preferred—not only due to its efficiency and simplicity, but also due to its ability to introduce a variety of functional groups to the terminal of the carboxylates after they are grafted onto the surface of the electrode (**Scheme 1.3**).[25,28,30,35,40-44]

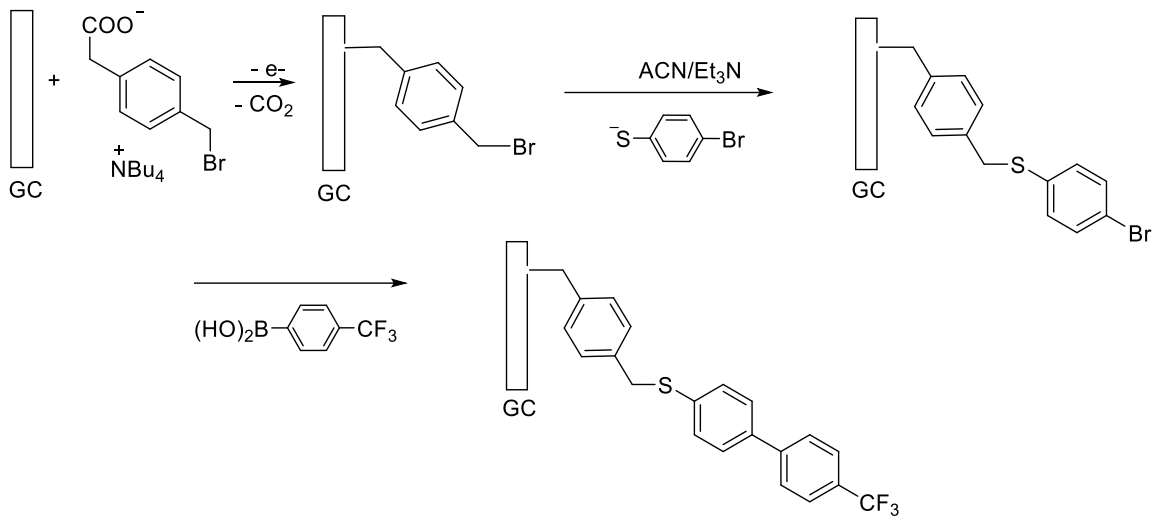

Scheme 1.3 Post functionalization of aryl groups on a glassy carbon (GC) electrode for development of sensors.[45]

1.3. Physio-chemical properties of the electron transfer mechanism of carboxylates.

Given the wide variety of synthetic products and industrial applications associated with Kolbe electrolysis, there has been some debate over the exact mechanisms and possible intermediates involved in this reaction. For example, a number of theories have been proposed as to the mechanistic pathway of Kolbe electrolysis, ranging from the formation of free or adsorbed alkyl radical species ($R^{\cdot}$) to acyloxyl radical ($RCOO^{\cdot}$) species; moreover, a carbocation (R^{+}) has been suggested as major mechanistic intermediate based on analyses of product mixtures.[16] Consequently, the goal of elucidating the physical and chemical fundamentals of the electron transfer process in Kolbe electrolysis has been a focal point in electrochemical research for many years—principally to enhance its practical applicability in industrial design and synthesis of products.

Both theoretical and experimental approaches have been undertaken to investigate the properties of these systems.[16] A number of competing mechanistic theories have been proposed for the initiation step and reactive intermediates for Kolbe electrolysis. Early workers argued for

the formation of an acyl peroxide intermediate (**Eq 1.4**), or the formation of an acyloxyl intermediate via an initiation by hydrogen peroxide (**Eq 1.5-1.8**) until the direct electrolysis of carboxylate at the electrode surface emerged as a more likely pathway. Mechanistic theories involving the formation of free radicals at the electrode surface were proposed via the formation of carbonium ion intermediates (**1.9-1.12**) or free radical intermediates (**Eq 1.13-1.15**), as summarized in **Table 1.1**.

Table 1.1
Alternative mechanistic hypotheses for the electrochemical oxidation of carboxylates.[16]

Acyl peroxide	$CH_3COO^- + CH_3COO^- \rightarrow CH_3COO^{\cdot} + CH_3COO^{\cdot} + 2e^-$ $\rightarrow CH_3COO - OOCH_3 \rightarrow 2CO_2 + C_2H_6$	**(1.4)**
Hydrogen peroxide	$2OH^- \rightarrow 2OH^{\cdot} + 2e^-$	**(1.5)**
	$2OH^{\cdot} \rightarrow H_2O_2$	**(1.6)**
	$2CH_3COO^- + H_2O_2 \rightarrow 2CH_3COO^{\cdot} + 2HO^-$	**(1.7)**
	$2CH_3COO^{\cdot} \rightarrow C_2H_6 + 2CO_2$	**(1.8)**
Carbonium ion	$CH_3COO^- \rightarrow CH_3COO^{\cdot} + e^-$	**(1.9)**
	$CH_3COO^{\cdot} \rightarrow CH_3^{\cdot} + CO_2$	**(1.10)**
	$CH_3^{\cdot} \rightarrow CH_3^+ + e^-$	**(1.11)**
	$2CH_3^+ + 2CH_3COO^- \rightarrow H_3CCOOCH_3 + C_2H_6 + CO_2$	**(1.12)**
Free radical	$2CH_3COO^- \rightarrow 2CH_3COO^{\cdot} + 2e^-$	**(1.13)**
	$2CH_3COO^{\cdot} \rightarrow 2CH_3^{\cdot} + 2CO_2$	**(1.14)**
	$2CH_3^{\cdot} \rightarrow C_2H_6$	**(1.15)**

Among these theories, the free radical theory was widely supported based on a growing body of experimental evidence from kinetic and byproduct studies.[16,46-52] Among the researchers investigating this field, Eberson,[14] Savéant,[24,25] Andrieux,[24,25] and González[26,27,53] all made significant contributions by utilizing electrochemical tools to ascertain the mechanism for these systems.[14,25,26,54] Our focus is on further enhancing our understanding of the chemical and physical properties of the dissociative electron transfer mechanism by employing a distinct approach, which allows one to determine both kinetic and thermodynamic properties of these systems.

1.4. Literature precedent for electron transfer mechanism of carboxylates: A theoretical approach to mechanism and oxidation potentials.

When early direct electrochemical measurements were still inconclusive as to the mechanism of the Kolbe electrolysis, Eberson's 1963 theoretical assessment emerged as an alternative approach for investigating associated mechanisms and subsequently quantifying the oxidation potentials (E^o) for carboxylates based on thermodynamic calculations. Eberson and coworkers adopted the free radical theory, and discussed two distinct and independent half-electrode processes in the electrolysis of carboxylates (**Figure 1.1**).[14,23,55]

The first process was a stepwise mechanism (sDET), which involved acetates forming an acyloxyl radical intermediate ($RCOO^{\cdot}$) via an electron transfer step, followed by the release of carbon dioxide and the formation of an alkyl radical ($R^{\cdot}$). The second process was a concerted mechanism (cDET), which involved electron transfer and the release of carbon dioxide and alkyl radical simultaneously. The distinct free energy findings for the electrode cDET and sDET processes, presented as $\Delta G_{(RCOO^-/R^{\cdot})}$ and $\Delta G_{(RCOO^-/RCOO^{\cdot})}$, respectively, were estimated by employing standard enthalpies and entropies ($\Delta G_{(RCOO^-/R^{\cdot})}$). The sample calculation for the formation of an acyloxyl radical ($RCOO^-/RCOO^{\cdot}$) at the electrode via a concerted mechanism is shown below (**Eq 1.16-1.19**).[14]

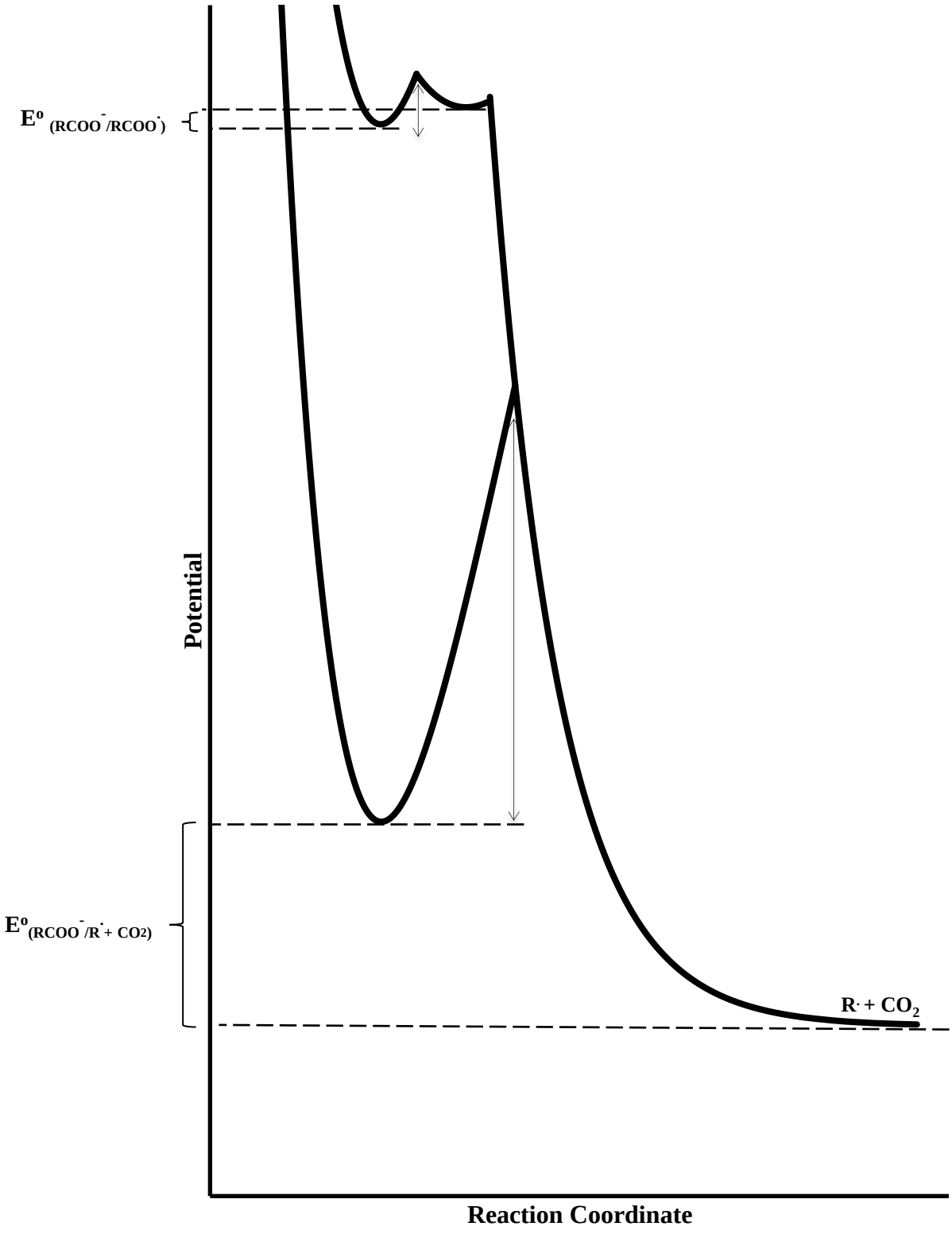

Figure 1.1. Morse potential curve illustrations of an activation barrier for concerted versus the stepwise dissociative electron transfer. Plot is modified from Savéant and coworkers.[56]

$$RCOO^{-}_{(aq)} + 2H^{+}_{(aq)} \rightarrow RCOO^{\cdot}_{(aq)} + {}^{1}/_{2}\, H_{2}{}_{(g)} \quad \textbf{(1.16)}$$

$$\Delta H^{\circ} = \Delta H_f^{\circ}[RCOO^{\cdot}]_{(aq)} + \tfrac{1}{2}\Delta H_f^{\circ}[H_2]_{(g)} - \Delta H_f^{\circ}[RCOO^{-}]_{(aq)} - \Delta H_f^{\circ}[H^{+}]_{(aq)} \quad \textbf{(1.17)}$$

$$\Delta S^{\circ} = S^{\circ}[RCOO^{\cdot}]_{(aq)} + \tfrac{1}{2}S^{\circ}[H_2]_{(g)} - S^{\circ}[RCOO^{-}]_{(aq)} - S^{\circ}[H^{+}]_{(aq)} \quad \textbf{(1.18)}$$

$$\Delta G^{\circ} = \Delta H^{\circ} - T\Delta S^{\circ} \quad \textbf{(1.19)}$$

It is critical to mention that these values are *estimates*. For instance, $\Delta H_f^{\circ}[RCOO^{-}]_{(aq)}$ is estimated from $\Delta H_f^{\circ}[RCOOH]_{(aq)}$ in acetic acid/H_2O; $\Delta H_f^{\circ}[RCOO^{\cdot}]_{(aq)}$ is estimated from acetyl peroxide; and $\Delta H_f^{\circ}[H^{+}]_{(aq)}$ is estimated from a gaseous proton.[57-62] Unlike $\Delta H_f^{\circ}[H_2]_{(g)}$, the other ΔH_f° values are estimated from various processes, which inevitably introduce a certain degree of error for each term.

Eberson employed estimated free energy to determine the standard oxidation potential of several derivatives of carboxylate. For instance, the oxidation potential of acetate ($\Delta G^{o} = -nF(E - E^{o})$, in particular, was found to be 2.41 V in water, and 1.30 V in acetonitrile, versus standard hydrogen electrode (SHE) for a stepwise mechanism. Conversely, the oxidation potential of acetates for a concerted mechanism was found to be 1.55 V in water versus SHE.[14] Based on these estimated oxidation potentials of acetates, Eberson proposed that decarboxylation would likely occur via a concerted mechanism. However, with the emergence of additional results, Eberson's suggestion was found to be inconsistent with newer empirical data which suggested a stepwise mechanism.[14,15,63-67] In addition, Eberson's theoretical approach was criticized as it failed to account for the reactivity of these radicals in solution.[13,24,26] It should also be noted that Conway and coworkers argued that the difference in reactivity based on the nature of the radicals—namely,

as free radical intermediates or adsorbed species at the surface of the electrode—was not taken into account in determining thermodynamic calculations.[17,21,23]

1.5. Mechanism of electron transfer via electrochemical approach: Historical experimental limitations.

Although advantageous in many respects, the use of Kolbe electrolysis for electrode grafting presents some serious challenges for fundamental electrochemical studies of the dissociative electron transfer mechanism. The highly reactive radicals that are generated lead to quick grafting of the electrode surface, which can then impede electrode activity. Moreover, electrode surfaces must be thoroughly cleaned following each scan to recover electrode functionality. The loss of electrode activity is an issue that must be addressed, as detailed in a number of studies. However, electrode fouling remains only one "minor" factor contributing to the complexity of Kolbe electrolysis, which is made more challenging based on several experimental factors such as the nature of the anode, the solvent, and most importantly, the structure and counter-ion for the carboxylates.[16]

Earlier work involving Kolbe electrolysis investigated a variety of product mixtures—both in solution and on the surface of the electrode as a function of the anode material.[13,64] Kinetic studies of electron transfer were challenging due to experimental limitations. Among several attempts, the use of precious metal anodes fabricated from platinum, gold, and ruthenium proved to be inappropriate since the surface oxide adsorbed the intermediates, rather than detecting Kolbe products (**Scheme 1.4**).[13,68] Ensuing modifications of the anode included incorporating thin films and even embedding the anode in gels. In addition, a variety of alkaline salts of carboxylic acids in aqueous solvents were investigated.[54,68-70] Nonetheless, these various experimental conditions resulted in the electrolysis of the solvent prior to the carboxylates, which limits the use of common electrochemical techniques for kinetics studies.[54,68-70] An additional experimental modification

includes employing glassy carbon in aprotic solvents as a new electrode material, which displayed an appropriate electrochemical signal in aprotic solvents.

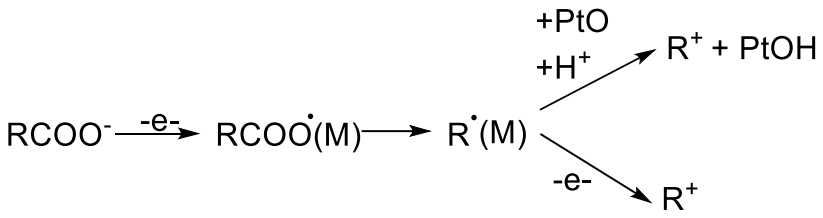

Scheme 1.4 Surface oxide adsorbed intermediates on metal (M) electrode (Top) in competition a chemical pathway for Kolbe electrolysis (Bottom) in the presence of water molecules.

1.5.1. Overcoming experimental limitations and the necessity of mathematical models for the Kolbe electrolysis.

Experimental conditions, especially the choice of anode material and solvent, have greatly limited our understanding of the Kolbe electrolysis. New mathematical models were also needed to effectively address the electrode kinetics for challenging systems such as the Kolbe electrolysis. This concern is particularly germane for cyclic voltammograms, the analysis of which became more feasible with Savéant's detailed mathematical mechanistic models for peak variations as a function of electrochemical mechanisms.[71-74] It was Savéant and coworkers who first reported the mechanism of dissociative electron transfer upon the oxidation of tetra-n-butylammonium salts of carboxylates on a glassy carbon anode in acetonitrile. The researchers examined the peaks corresponding to the oxidation of carboxylates, which enabled them to report the first kinetic analyses of dissociative electron transfer for arylcarboxylates. However, Savéant, et al. pointed out the limiting factor of irreversible and inconsistent peak current with consecutive cyclic voltammetry scans.[25] Subsequently, in 2012, González and coworkers adapted Savéant's approach to further investigate the oxidation of aliphatic carboxylates on a glassy carbon in acetonitrile in

order or address the persistent limitation of the pronounced fouling of the electrode, as well as the "minimal" loss of electrode activity due to absorbed material on the electrode surface.[36,75]

To date, all established experimental results involving the specific mechanisms of the Kolbe electrolysis for aliphatic and aryl carboxylates have been analyzed using conventional methods, as reported by Savéant and González.[24] The oxidation potentials and rate constants for the dissociative electron transfer of carboxylates are unobtainable via conventional analyses, and no attempts have been made to date to determine this information through other approaches. In order to elucidate the origin of these discrepancies using conventional electrochemical approaches to dissociative electron transfer, as well as discuss our proposed alternative approaches, it is critical to understand the mechanistic tool (alpha) and the theory pertaining to outer-sphere electron transfer processes occurring at the electrode surface. As all conventional electrochemical techniques are compatible with Marcus theory, the latter will be addressed with regards to its application to electrochemical processes.

1.5.2. Mechanisms of electrochemical process as indicated by the transition state symmetry coefficient (alpha).

1.5.2.1. What is alpha (α)? Transition state symmetry as it relates to the energy and the activation barrier for a chemical process.

Alpha is an electrochemical property which is quantifiable and usually utilized to diagnose the mechanism for an electrochemical process. It provides insight into the position of the transition state and relates the change in the free energy of activation and free energy of reaction ($a = \partial G^{\ddagger}/\partial G^{o}$). Alpha, which is also frequently referred to as the coefficient of symmetry in electrochemistry, ranges between 0 – 1 and is a fundamental chemical concept. Modeling of the transition state structure based on the thermodynamics and kinetics of a reaction

has been long established. It was first introduced by Leffler[76] and Hammond's postulate[77] and the same principles pertain to electrochemical processes.

For example, in any given chemical reaction, the structural model of a transition state correlates to the structures of the reactants and products. **Figure 1.2** shows free energy diagrams for a chemical process from reactants (R) to products (P). In accordance with Hammond's postulate and Leffler's model, during the course of a chemical reaction, the energy and structure of the transition state are governed by the free energy of reaction. If one assigns the structure of reactants as 0, and of products as 1, the location (symmetry) of the transition state can be mapped out based on these coefficients. If the reaction is an exothermic one, it is highly favored thermodynamically with a transition state structure resembling the reactant ($0 < TS^{\ddagger} < 0.5$). On the other end, if the reaction is highly endothermic, the energy of the transition state will closely resemble the product, and thus, the structure of the transition state will be a product-like ($0.5 \ll TS^{\ddagger} < 1$). With no driving force, the transition state will have an intermediate structure between the reactant and product.

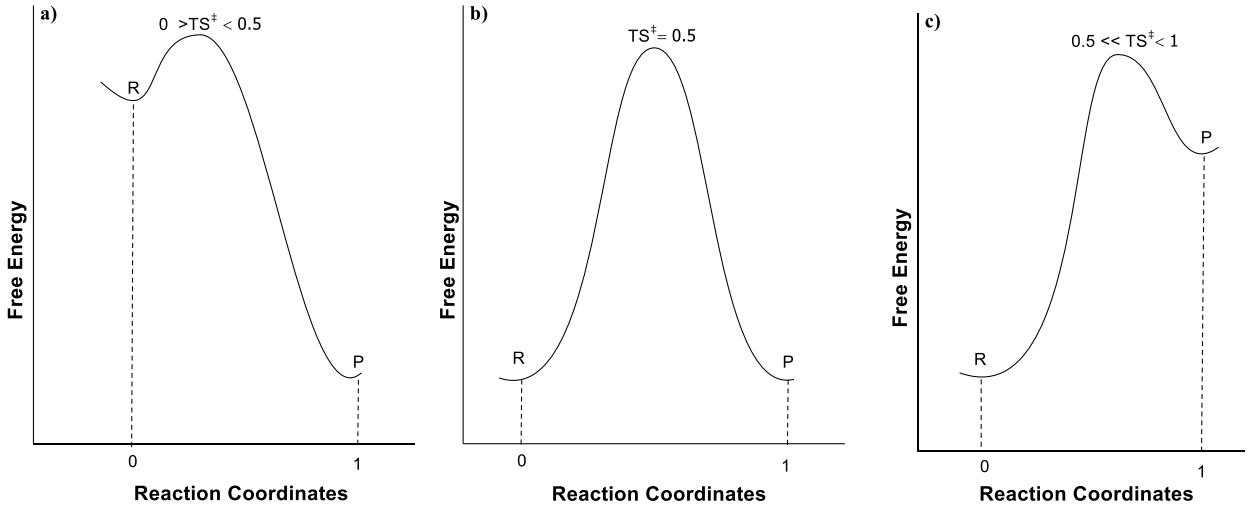

Figure 1.2. The structural changes in the transition as a function of the driving force of the reaction.

These free energy diagrams based upon the Hammond postulate, can be further presented as crossing Morse potential curves. As shown in **Figure 1.3**, the Morse potential curves show potential wells R and P representing the free energies of the reactants and the products respectively, with the point of intersection corresponding to the transition state ($TS^{\ddagger}$).

Modifications to the driving force, and hence the activation barrier, in a traditional chemical process are commonly achieved by structural alterations of the reactants. To force a reaction to become more or less favorable, either electron donating groups or electron withdrawing groups are usually employed for one of the reactants by taking the advantage of inductive and resonance effects.

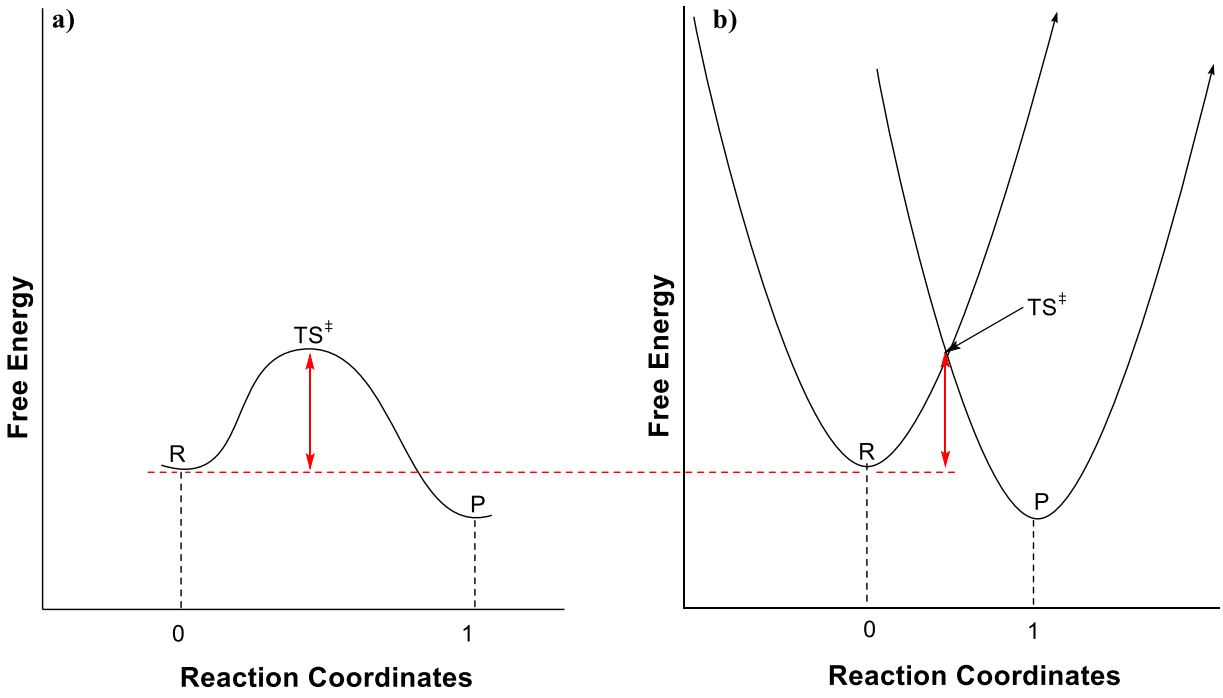

Figure 1.3. Morse's potential curves as an alternative illustration of the free energy diagrams reflecting the transition state as the interception of the two potential wells.

One example is the acidity constant of aliphatic carboxylic acids (pKa) as a function of substituents effects due to inductive effects. The acidity of a carboxylic acid with the structure of

(X-CH_2-CO_2H) is highly dependent on the nature of the substituent group (X). The acidity is increased as X becomes more electron withdrawing; such as $pKa\ for\ X = (NO_2) > F > (Cl) > (Br) > (I) > (H) > (CH_3) > (CO_2^-)$. Taking advantage of structural modifications with electron withdrawing groups on the acid allows for a thermodynamic shift with a more reactant-like transition state. However, these structural changes also alter the energetics and the nature of the products for each group (**Figure 1.4**). **Figures 1.4b-c** show the shift in the transition states as a function due to a shift in the energetics of the reactants with X = NO_2 and CO_2^-. These energy diagrams also indicate that energetics of the products are not the same as the structures of the reactants are different for each of the substituents. In other words, traditional chemical processes invoke a change in the intrinsic barrier accompanied by an alternation of the energetics of both the reactants and the products to favor a desirable product.

In contrast to common chemical processes, electrochemical processes hold several advantages. First, it allows for the investigation of only one compound of interest (reactant). The surface of an electrode serves as the other reactant whose potential can be used to shift the energetics of the reactants potential well without the need for any structural changes to the compound of interest. Second, as the structure of the reactants is held unvaried, no changes are made to the potential well of the products. Third, one electrode serves as an alternative to all substituents. The applied potential at the surface of the electrode is sufficient to alter the energetics of the reactants potential well (**Figure 1.5**). In other words, by employing an electrode, the energetics of the reaction can be varied due to the applied potential, while keeping the structures of reactants and products unvaried. Therefore, electrochemically, one can vary the free energy of reaction, and by extension, the activation barrier by adjusting the applied potential

of the electrode. Establishing a profile for the activation barrier as a function of driving force provides insight into the electrochemical mechanism.

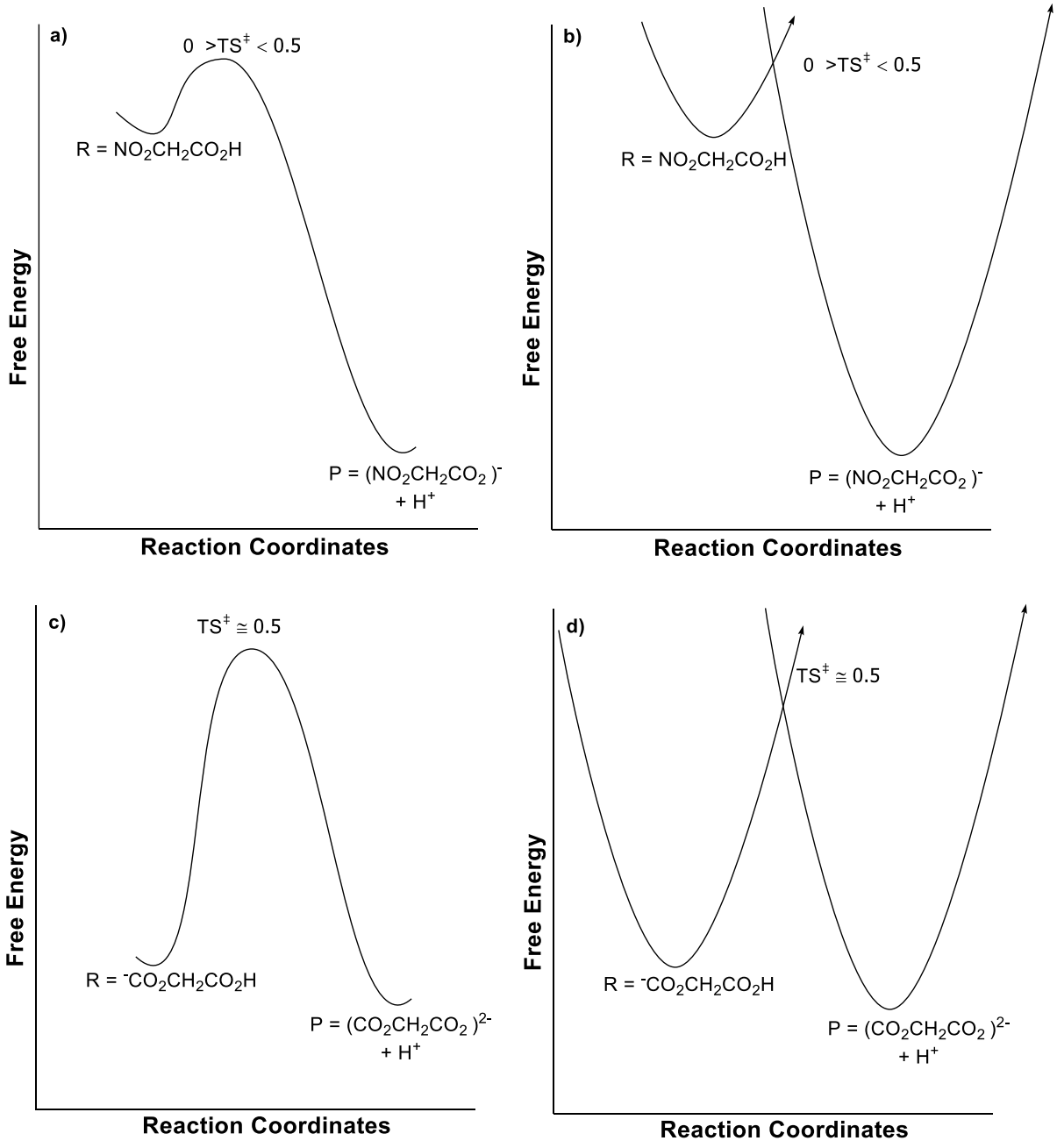

Figure 1.4. A shift in the transition state structure for a deprotonation of aliphatic carboxylic acid as a function of structural changes of the substituents on the acid.; a) A reactant-like transition state associated with lower intrinsic barrier for X = NO_2, b) A product-like transition state associated with higher intrinsic barrier for X = CO_2^-).

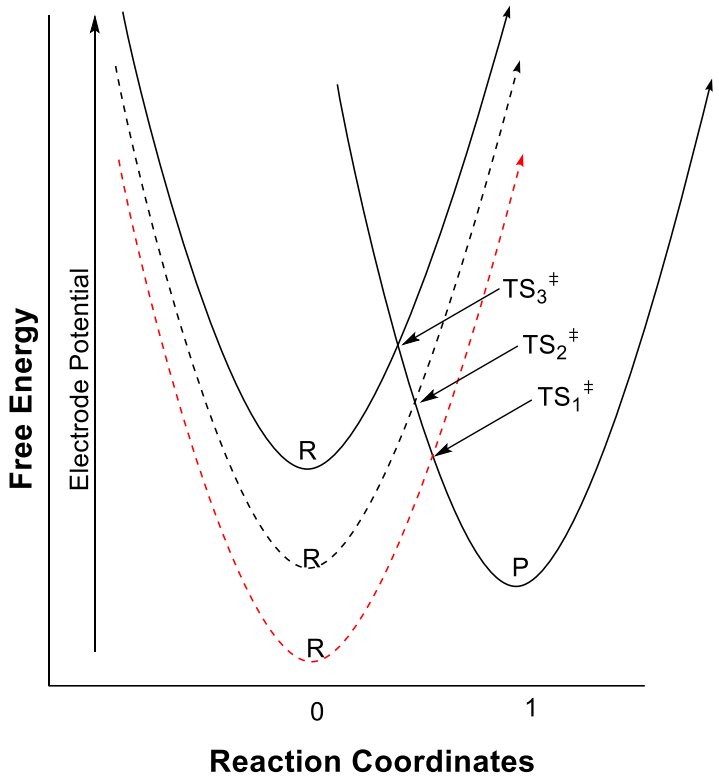

Figure 1.5. Increase electrode potential changes the energetics of the reactant without requiring any structural changes to the reactants or the products.

1.5.2.2. Alpha: qualitative approach to mechanism of an electron transfer.

Redox chemical processes are initiated by a single electron transfer for either a reduction or an oxidation process. In accordance with Marcus theory, the reactant has to overcome a minimum barrier for electron transfer to occur. If the chemical process involves only an electron transfer (**case A**), the barrier will be lower (attributed mainly to solvent reorganization) than the process coupled to breakage of a bond—which requires internal reorganization such as bond stretching (**case B**) (**Figure 1.6a-b**). Taking into consideration that these two cases are two distinct electrode mechanisms, they have a different activation-driving force relationship, and thus exhibit distinct alpha values. Electrochemically, quantifying alpha for a given chemical

process serves as a tool to distinguish between these mechanisms by providing an insight to the symmetry of the transition state.

As shown in **Figure 1.6**, at a zero driving force, both processes will not have the same reorganization energies but still hold a transition state symmetry of α = 0.5. To favor the forward process, an increase free energy will lead to a more exothermic reaction and decrease the free energy of activation. In **case A**, a slight increase in the free energy lowers the intrinsic barrier and allows the forward process to occur. The transition state symmetry will still remain close to α = 0.5. To drive a similar process for **case B** however, a much larger increase in the free energy is required to lower the intrinsic barrier sufficiently for an electron transfer to occur (**Figure 1.6c-d**). Thus, the transition state symmetry for an chemical process involving a bond breakage/formation is closer in energetics to the reactant and with alpha of $0.3 < a < 0.4$.

As electrochemical processes mimic chemical processes, the same concepts are applied with regards to the transition state positioning as a function of driving force and intrinsic barrier. The ability to shift the electrode potential allows for a change in the free energy of the electron transfer reaction. With the incremental increase in the potential at the electrode surface, a lower intrinsic barrier with another transition state symmetry is established. For a mechanism involving only electron transfer, the required overpotential is minimal and the transition state symmetry will correspond to 0.5. On the contrary, a large overpotential is required for an electron transfer requiring an additional bond breakage/formation with alpha of $0.3 < a < 0.4$. Thus far, alpha has been presented qualitatively, a quantitative approach to alpha will be discussed in terms of Marcus theory in **Section 1.6**.

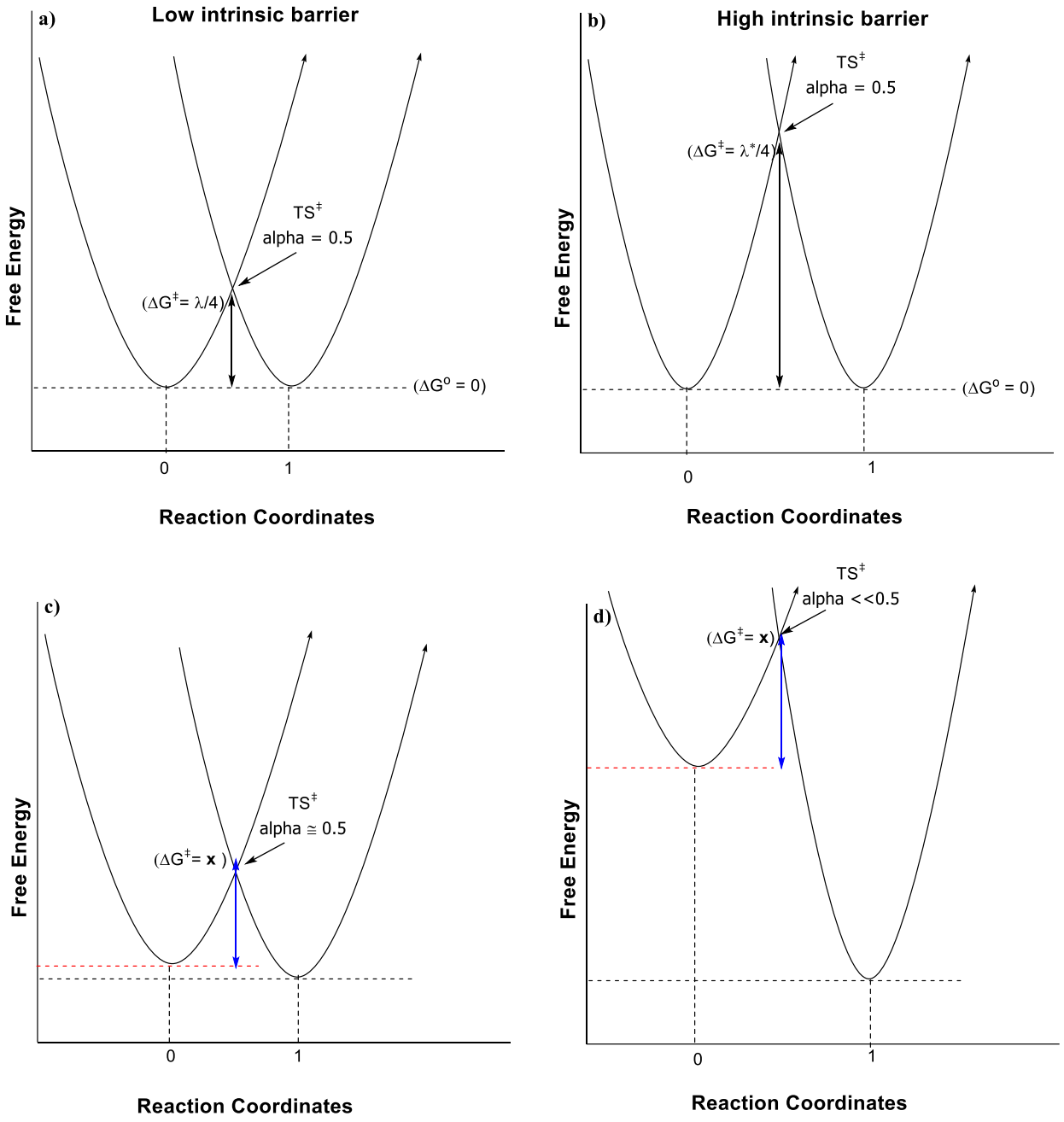

Figure 1.6. Alpha as a qualitative description of the transition state symmetry for two distinct electron transfer processes; a) Lower activation barrier associated with solvent reorganization energy at zero driving force with alpha = 0.5; b) High activation barrier associated with solvent reorganization energy in addition to bond breaking/forming at zero driving force with alpha = 0.5; c) A slight increase in the free energy is required to drive the electron transfer for low activation barrier process; d) A large increase in the free energy is required to drive the electron transfer for a high activation barrier process.

1.5.3. Overview of Marcus theory of heterogeneous electron transfer and applications to electrode kinetics through alpha

Electron transfer (ET) is one of the most fundamental chemical processes for chemical and biological systems. Protein interactions, sensors, artificial photosynthetic systems, molecular electronics from transistors to rectifiers and switches are all dependent upon electron transfer.[78-91] As such, the nature and rate of electron transfer has historically been of great interest.[92,93] Among the most prominent fundamental theories of electron transfer is Marcus theory, developed by Nobel Laureate Rudolph Marcus in 1956. Marcus theory is built on the Franck-Condon principle, which had earlier addressed a mechanism for electron transfer. Specifically, the Franck-Condon principle stated that nuclear motion is much slower than the movement of the electrons. In other words, the atomic positions are frozen during a gain or loss of an electron in a given solvated environment.[94,95] Hence, the molecular and structural changes within the solvent media are of utmost importance for electron transfer. These structural changes were also incorporated into Erying's "transition state theory," which states that the rate of a reaction is governed by the energy barrier of the transition state between reactants and products.[93,96,97]

Marcus theory evolved from these earlier studies, but with the added condition of an outer-sphere electron transfer mechanism whereby electron transfer could occur with minimal bonding interactions. Also—and most importantly—Marcus was a pioneer in formulating a quadratic mathematical model to relate the rate of a reaction (kinetics) to the driving force (thermodynamics), and in so doing contributed to the establishment of emerging fields of science such as solar energy and enzymatic activity.[98-102] This study investigates the one-electron transfer process involved in the electro-oxidation of carboxylates—either directly at the surface of the electrode, or indirectly by employing a series of readily oxidized mediators (**Scheme 1.5**).[103] In

either case, Marcus theory of outer-sphere electron transfer is still applicable, thus justifying a thorough overview of the theory and its applications.

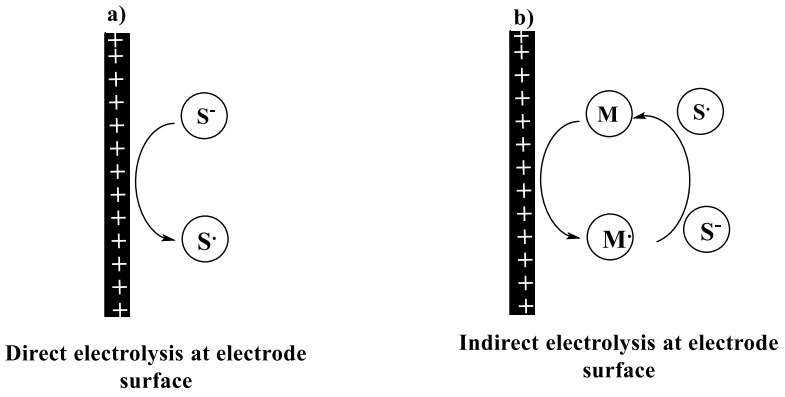

Scheme 1.5 Electro-oxidation of an anionic substrate (S^-) as a representative of carboxylate anions at the surface of the electrode through a) the direct method; and b) the indirect method, featuring a mediator that is easier to oxidize than the substrate at the surface of the electrode.

1.5.4. Outer-sphere electron transfer.

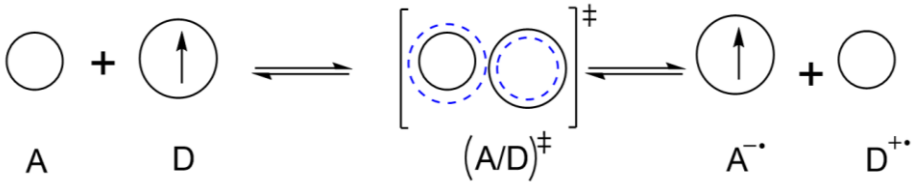

Scheme 1.6 Spherical models of outer-sphere ET between an acceptor (A) and a donor (D). (A & D) represent reactants (R) and ($A^{\bullet -}$ & $D^{\bullet +}$) represent products (P)

The Marcus electron transfer model treats both reactants as two colliding spherical entities (**Scheme 1.6**).[4,5,23] The physical model employs an oxidant A (electron acceptor) and a reductant D (electron donor) with spherical radii r_1 and r_2, respectively. The two spheres diffuse together at a distance $r_{12}= r_1+r_2$, after which they undergo thermal motion. Once they have obtained equal orbital energies ($[A/D]^{\ddagger}$) at room temperature, an electron can be transferred; the electron density

then shifts from the electron-rich reductant sphere (D) towards the oxidant sphere (A) (**Scheme 1.6**). Following electron transfer, the complex dissociates to two new species ($A^{\cdot -}$,$D^{\cdot +}$). [4,5]

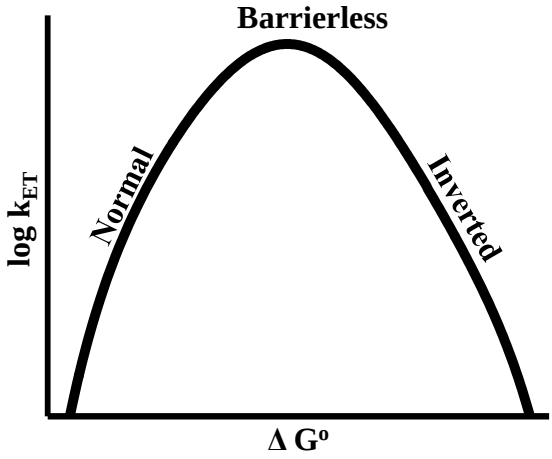

Figure 1.7. Marcus theory indicates the presence of three distinct regions relating the heterogeneous rate constant for an outer-sphere electron transfer to the driving force: (a) a normal region with a continuous increase in the rate constant as a function of increased driving force, (b) a barrierless region with no change in the rate constant, and (c) an inverted region with a decrease in the rate constant as a function of higher driving force.

Marcus theory provides a mathematical approach which involves a non-linear relationship between the free energy of the reaction (ΔG^o), which represents the favorability of the reaction, and the free energy of activation ($\Delta G^{\ddagger}$), which represents the energy barrier associated with it, as shown in **Eq 1.20**. As the driving force of the reaction increases, the activation barrier decreases and the reaction rate increases. However, due to the parabolic nature of the Marcus equation, at a specific point during the reaction a higher driving force leads to a slower reaction, which is referred to as the inverted region (**Figure 1.7 and 1.8D**). The decrease in the rate constant is caused by the re-introduction of the activation barrier, as shown in **Figure 1.8a - 1.8d**).

$$\Delta G^{\ddagger} = \frac{\lambda}{4}(1 + \frac{\Delta G^{o'}}{\lambda})^2 = \Delta G_o^{\ddagger}(1 + \frac{\Delta G^{o'}}{\lambda})^2 \qquad \textbf{(1.20)}$$

Equation **1.20** also introduces the reorganization energy (λ). This constant is defined at a

$(+\Delta \boldsymbol{G^o}, \Delta \boldsymbol{G^{\ddagger}} > \lambda/4)$ $(\Delta \boldsymbol{G^o} = \boldsymbol{0}, \Delta \boldsymbol{G^{\ddagger}} = \boldsymbol{\lambda/4})$

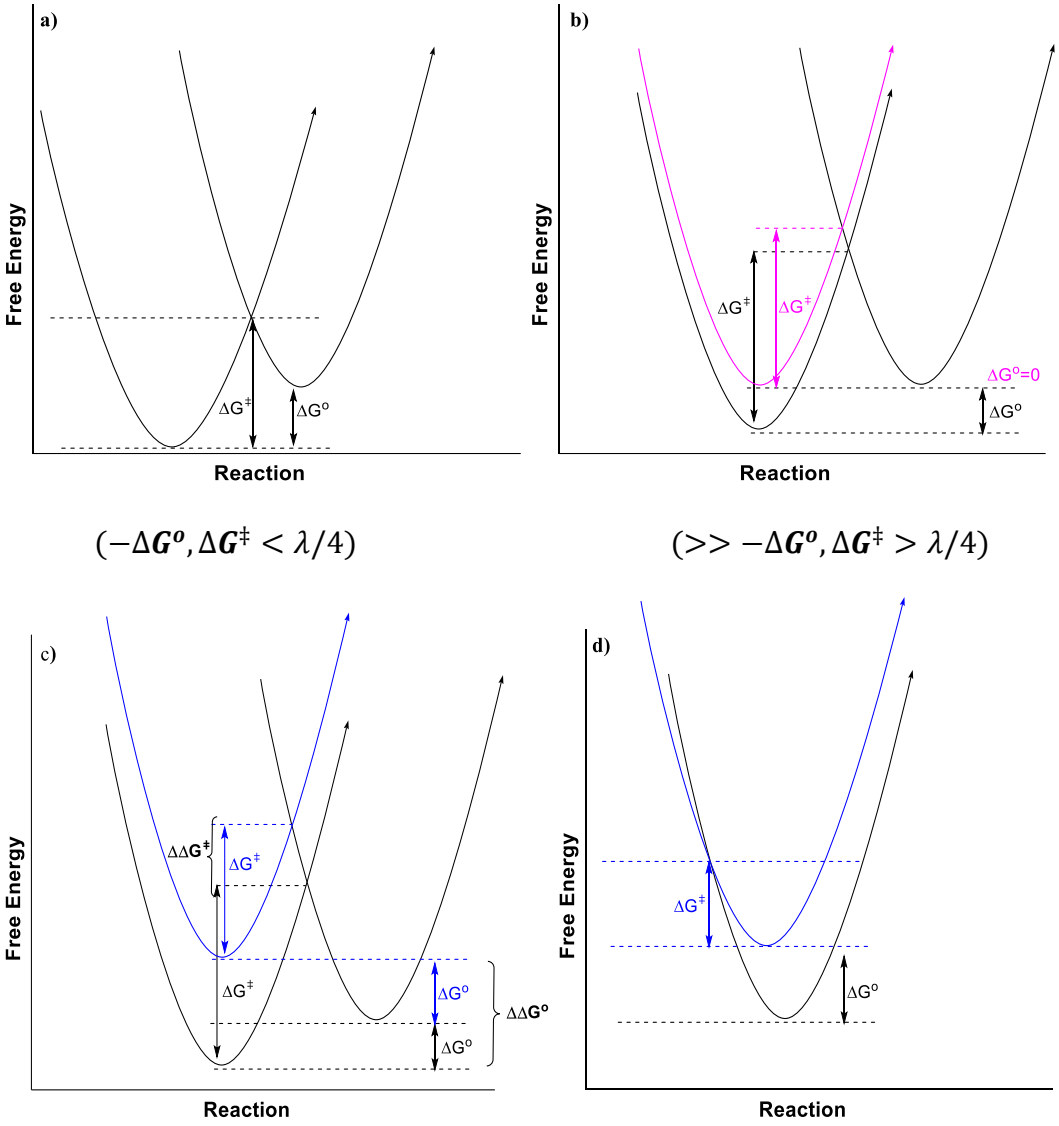

$(-\Delta \boldsymbol{G^o}, \Delta \boldsymbol{G^{\ddagger}} < \lambda/4)$ $(>> -\Delta \boldsymbol{G^o}, \Delta \boldsymbol{G^{\ddagger}} > \lambda/4)$

Figure 1.8. a) Parabolic curves for a free energy diagram illustrating the activation energy barrier associated with an outer-sphere electron transfer along reaction coordinates at a given thermodynamic energy, b) Electrochemical approach alters the activation barrier as the applied potential is varied, c) A net change in the activation energy is directly related to a net change in the applied potential for the electron transfer process, and d) Inverted region with re-introduced reorganization energy

zero driving force point ($\Delta G^o = 0$), at which point the free energy of activation ($\Delta G_o^{\ddagger}$) is equivalent to ($\lambda/4$). This barrier is a result of reorganizational changes ($\lambda = \lambda_o + \lambda_i$) from solvent

interactions with the charged species in solution (external reorganization energy; λ_o) and bond stretching and geometrical changes within the molecule (internal reorganization energy; λ_i). This reorganization energy is in agreement the Born-Oppenheimer approximation.[104,105]

It is critical to note that in the case of charged species, the electrostatic free energy must be accounted for. As shown in **equations 1.21** and **1.22**, the free energy term (ΔG^o) must be corrected for electrostatic forces of the reactive system, where Z_A and Z_D are the charges of each sphere, e is the charge of an electron, $r_{12}$is the radii distance between two nuclei, f is ionic strength, $\Delta G^{o'}$is the standard free energy corrected for electrostatic forces between acceptor and donor, and D is the dielectric constant of the solvent.

$$\Delta G^{\ddagger} = \frac{Z_A Z_D e^2 f}{D r_{AD}} + \frac{\lambda}{4}(1 + \frac{\Delta G^{o'}}{\lambda})^2 \qquad \textbf{(1.21)}$$

$$\Delta G^{o'} = \Delta G^{o} + (Z_A - Z_D - 1)\frac{e^2 f}{D r_{AD}} \qquad \textbf{(1.22)}$$

The Marcus equation can be re-expressed into a simplified form (**Eq 1.23),** which accounts for the electrostatic component of the system (W in kcal mol^{-1}). In cases of neutral species or solvents with low dielectric constants such as acetonitrile, the electrostatic component can be ignored and **Eq 1.20** is sufficient.

$$\Delta G^{\ddagger} = W + \Delta G_0^{\ddagger}(1 + \frac{\Delta G^{o'}}{\lambda})^2 \qquad \textbf{(1.23)}$$

Marcus theory has been utilized to predict a normal region for both exergonic and endergonic reactions. However, it was not until Miller and coworkers that an inverted region, which predicted that activation energy is reintroduced at particularly large driving force, was validated experimentally (**Figure 1.8d**).[55] One challenge with verifying the inverted region in Marcus theory was overcoming the diffusion limits between A and D. Specifically, intermolecular electron transfer is dependent on two distinct processes: the diffusion of A and D, and electron

transfer. Commonly, the reaction rate is limited by the electron transfer process in the normal region. The inverted region, however, is the location for highly exergonic reactions where electron transfer is still highly favored, but wherein occurs a more diffusion-controlled process.[106] By designing *A*−*D* linked molecules, Miller and coworkers established intramolecular electron transfer at lower observed rates due to the higher energy costs associated with electron transfer across several bonds.[106-109]

1.5.5. Application of Marcus theory to electrochemical methods.

This investigation was designed to determine the mechanistic and thermodynamic parameters for oxidative processes involving carboxylates throughout direct (heterogeneous) and indirect (homogeneous redox catalysis) electrolysis. As noted earlier, Marcus theory is fundamental for the quantitative analysis of the kinetics and thermodynamics of these systems. This section, therefore, first explores the mathematical concepts for electron transfer and the applicability of these mathematical approaches to electrochemical processes.

1.5.5.1. A qualitative electrochemical approach to kinetics and related mechanisms through Marcus theory.

For over half a century, electrochemical techniques have been used to explore the mechanisms and rate of reactions in a wide variety of scientific fields. These methods have evolved with advances in fundamental and quantitative electron transfer theories. Of particular interest is Marcus theory, which provides a quantitative approach for measuring the rate constants of electron transfer and oxidation potentials. Indeed, electrochemical methods routinely employed for mechanistic studies of electron transfer, cyclic voltammetry, and linear sweep voltammetry present significant advantages over traditional approaches.[110-113] For instance, a traditional approach for investigating the rate of electron transfer to reactant A (oxidation) involves a series of derivatives

of reactant B, substituted with either electron withdrawing or donating groups. This substitution is critical in order to change the driving force of the reaction, thereby enabling one to manipulate the forward rate of the reaction. In contrast, an electrochemical approach allows one to substitute the full series of the chemical reactant B with only an electrode surface, which can gradually be controlled by an applied potential to serve as either a rich or poor source of electrons. The variation in the applied potential (E) at the surface of the electrode and the oxidation potential of the substrate of interest (E^o) directly relate to the driving force of the reaction (G) through the equation: $\Delta G^o = -nF(E - E^o)$.

Consider the energy diagrams in **Figure 1.9** and assume that the reactant undergoes reduction. During the course of the reduction process at the electrode surface, a fraction of the substrate remains in its oxidized form (reactant) and reduced form (product) such as $f_o = O/(O + R)$, and$f_R = R/(O + R)$,which varies from $(0 \rightarrow 1)$. Ideally, as the applied potential at the surface of the electrode becomes more negative, a fraction of the oxidized species approaches 0, while a fraction of the reduced species approaches 1. Prior to the reduction of the reactant, the oxidized form of substrate (1) is present, but no reduced form (0). The reduction is initiated by a negative potential applied to an electrode to drive the electron transfer from the surface of the electrode to the electroactive species, which then drives the oxidized species to the reduced form of the substrate. If the potential at the surface of the electrode is insufficient, the forward electron transfer is hindered in favor of backward electron transfer (**Figure 1.9a**); this transition state resembles more of the oxidized species ($TS^{‡}$ symmetry = 0.0 –1.0).[114,115] Moreover, no current density is noted for the forward electron transfer in a cyclic voltammogram; instead; the reverse oxidation process would be observed. If the applied potential is sufficient to drive the reduction, an electron

transfer will occur. However, there are two distinct scenarios for electron transfer that must be noted. One scenario involves only an

electron transfer process, while the other involves a chemical process (in addition to the electron transfer) such as bond formation of breaking. Marcus theory purports that for any electron transfer to occur, a minimal energy input is needed to overcome the reorganization energy barrier. If

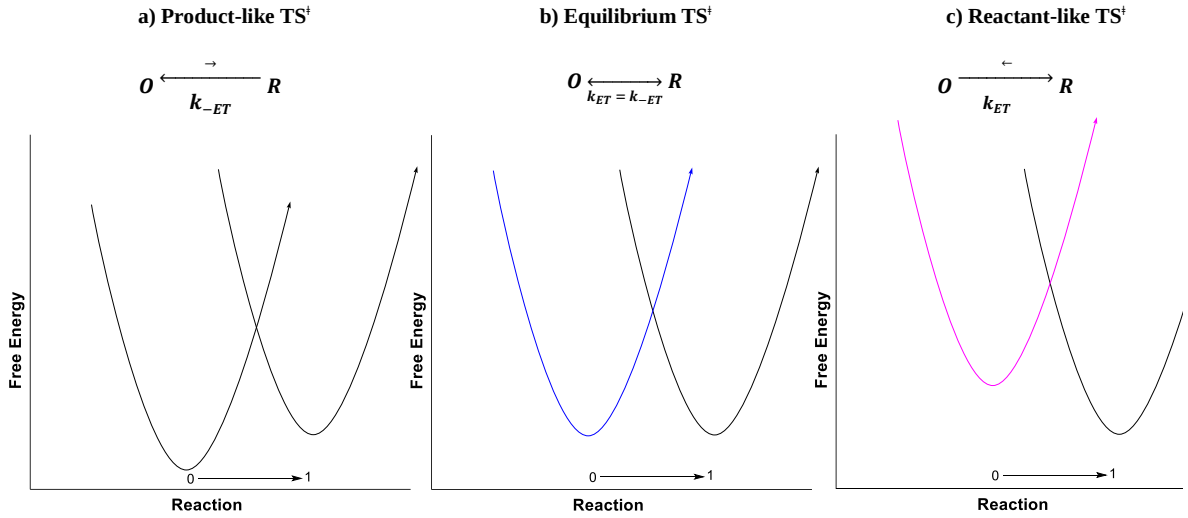

Figure 1.9. Applied potential to the electrode drives the electron transfer process for three distinct electrochemical scenarios, corresponding to specific transition states (TS‡), defined as the intercept of the curves. (a) corresponds to a potential at which forward electron transfer is unfavorable with a TS‡ similar to the reduced species; (b) corresponds to a potential when a is at equilibrium with the forward and backwards electron transfer equally favorable, which is associated with an intermediate TS‡. This is noted for well-behaved systems; (c) corresponds to an applied overpotential to favor the forward electron transfer.

additional electron transfer processes come into play, such as bond breaking and formation, electron transfer will require a higher applied potential, referred to as overpotential (η), since increased driving force is needed for electron transfer to occur (**Figure 1.9c**).

Electrochemically, a simple reversible and well-behaved system will undergo an electron transfer without additional bond breaking or formation processes; moreover such a system will require only slight overpotential for electron transfer to occur since the activation barrier is

minimal. In addition, the rates of the forward and backward electron transfer are equivalent, with a transition state structure that is between the reduced and oxidized forms of the species ($TS^{\ddagger}$ symmetry = 0.5, **Figure 1.9b**). The dissociative electron transfer for a carboxylate, however, is followed by a rapid chemical step, which does not favor backward electron transfer. Most importantly, forward electron transfer can proceed via either a stepwise or a concerted mechanism, both of which are initiated by an electron transfer. However, each mechanism has a distinct oxidation potential. In addition, the concerted mechanism proceeds with both electron transfer and bond cleavage occurring simultaneously as one step.

As shown in **Figure 1.1**, the concerted mechanism exhibits a large activation barrier due to the additional bond cleavage associated with the electron transfer when $RCOO^{-}$ converts to $R^{\cdot}$ and CO_2. For a stepwise mechanism, electron transfer occurs in two separate steps with an initial electron transfer step from $RCOO^{-}$ to $RCOO^{\cdot}$, which has a low activation barrier in comparison to the concerted mechanism. Decarboxylation occurs as a subsequent step to electron transfer. Therefore, a significantly higher overpotential is necessary to drive electron transfer via the concerted step method due to the higher activation energy (**Figure 1.7c**).

The electrochemical approach for distinguishing each mechanism is to measure the transfer coefficient alpha (α), which typically ranges from $0.5 < \alpha < 1$, providing insight into the transition state. The transfer coefficient is an electrochemical parameter that indicates the kinetic activation barrier (kinetics) required for an elementary electron transfer to occur at a given potential at the electrode, which is calculated as a function of applied potential (*E*) as illustrated in **Eq 1.24** where E, k_{ET}, and $G^{\ddagger}$ are the applied potential, rate constant of electron transfer, and activation energy respectively.[5] For a stepwise mechanism, low reorganization energy is required as evidenced by

the fact that α approaches 0.5. Conversely, a stepwise concerted mechanism requires a higher activation barrier in the range of $0.3 < \alpha < 0.4$.[41,116,117]

It is critical to mention that α is limited to electrode kinetics that describe an elementary electron transfer as the rate-determining step. Misinterpretations and invalid mechanistic conclusions have resulted from the misapplication of these kinetic equations and faulty definitions of α. Typically, electrode kinetics employ more complex processes than single elementary electron transfer, such as two-electron transfer, adsorption processes and dissociative rate-determining steps, which researchers indicate require special treatment for α.[118-120] Taking advantage of Erying's equation, the transfer coefficient can also be expressed directly in terms of heterogeneous rate constant, as shown in **Eq 1.24**.

$$\alpha = \frac{1}{F}\frac{\partial G_f^{\ddagger}}{\partial E} = -\frac{RT}{F}\left(\frac{\partial ln k_{het}}{\partial E}\right) \quad \textbf{(1.24)}$$

Moreover, in accordance with Marcus theory, the transfer coefficient can also be expressed in terms of reorganization energy and activation energy, as shown in **Eq 1.25**. These mathematical models of electrode kinetics can be employed to establish a relationship between the rate of heterogeneous electron transfer and driving force. One major downfall of conventional methods (e.g., cyclic voltammetry and linear sweep voltammetry) remains. The observed response represents both electron transfer as well as mass transport effects—the latter resulting from the diffusion of the substrate to the surface of the electron (refer to **Chapter 2**).[121] Moreover, it is critical to note that conventional methods provide an averaged α for the overall electron transfer mechanism. Therefore, Savéant and co-workers estimated α via alternative mathematical diagnostic criteria to estimate the rate constant of heterogeneous electron transfer.[54] Refer to **Chapter 2** for a detailed description of the limitations of electrochemical techniques for kinetic

analyses; this chapter also provides alternative diagnostic approaches to elucidate the mechanisms of electron transfer on electrode surfaces.[111]

$$\alpha = \frac{1}{2} + \frac{F(E - E^o)}{2\lambda} = \frac{1}{2} + \frac{F}{2\lambda}(E - E^o) \quad \textbf{(1.25)}$$

$$-\frac{RT}{F}\frac{\partial ln k_{het}}{\partial E} = \alpha = \frac{1}{2} + \frac{F(E - E^o)}{2\lambda} \quad \textbf{(1.26)}$$

In principle, if the rate constant for heterogeneous electron transfer could be measured (without the complication of diffusion), the α at every given potential could be obtained. Thereby, the oxidation potential of the compound through the application of Marcus theory can be determined. As illustrated in **Eq 1.26**, in the case when $E^o = E$, the second term of the equation becomes zero and α = 0.5. Convolution voltammetry eliminates the mass transport (diffusion effects) from the current signal generated via cyclic voltammogram; consequently, heterogonous rate constants (k_{het}) can be obtained as a function of applied potential at the electrode surface. Once values of k_{het} are calculated from convolutive currents, a non-linear plot (parabolic) for $\ln k_{het}$ as a function of applied electrode potential can be obtained. Using Marcus theory and the Erying equation, the first derivative of the non-linear best-fit equation is constructed to calculate a dimensionless parameter—namely α = 0.5 (**Eq 1.26**). The Erying equation is also utilized to determine other parameters such as the activation energy barrier ($\Delta G^{\ddagger}$) and reorganization energy (λ), as shown in **Eq 1.26**.

A second alternative approach, referred to as "homogeneous redox catalysis" (HRC) can be employed to measure the oxidation potential and rates of electron transfer (k_{ET}) by applying Marcus theory. Homogeneous redox catalysis is considered to be an indirect method for studying electron transfers between a substrate of interest (in this case carboxylates) in that it employs and monitors the electrochemical response of the mediator at the electrode (**Scheme 1.4**). The

mediators are well- behaved electrochemical compounds used to facilitate the electron transfer process for the compound of interest—principally because they produce well-known electrochemical responses at the surface of the electrode. In the presence of a given substrate, the concentration of the mediator at the electrode surface is impacted by a follow-up electron transfer step between the mediator and the substrate. Therefore, indirect methods are useful for monitoring the electrochemical behavior of a mediator as a direct response to the rate of homogeneous electron transfer between mediator and substrate.

Utilizing an indirect electrochemical approach is favored when direct heterogeneous methods provide limited information about electron transfer—say, for example, in cases when a substrate is likely to degrade upon electrolysis. The mediator, therefore, facilitates the oxidation process of the carboxylates because it undergoes oxidation at the electrode surface as an initial step, after which it diffuses into the solution and is then reduced by the carboxylates. Hence, rather than directly analyzing the behavior of the carboxylates, assessing the performance of the mediator can provide additional information about the system, thereby eliminating the dependency on the irreversible behavior of carboxylates to determine oxidation potentials.[122]

Indirect Electrochemical Process	Direct Electrochemical Process
$Fe(Cp)_2 \rightarrow Fe(Cp)_2{}^+ + e^-$	$RCOO^- \underset{k_{ET}}{\overset{k_{-ET}}{\rightleftarrows}} RCOO^{\cdot} + e^-$
$Fe(Cp)_2{}^+ + RCOO^- \underset{k_{ET}}{\overset{k_{-ET}}{\rightleftarrows}} RCOO^{\cdot} + Fe(Cp)_2$	$RCOO^{\cdot} \xrightarrow{k_{CO_2}} R^{\cdot} + CO_2$
$RCOO^{\cdot} \xrightarrow{k_{CO_2}} R^{\cdot} + CO_2$	

Scheme 1.7 A comparison between direct and indirect electrochemical approaches for examining the thermodynamics of the Kolbe process of carboxylates systems.

It must be noted that homogeneous redox catalysis is only applicable if several conditions are fulfilled. As illustrated in **Scheme 1.7**, the initial electron transfer occurs at the surface of the

electrode with ferrocene serving as a mediator. As the heterogeneous electron transfer step, it must be independent from the homogenous electron transfer phase that occurs in solution between the oxidized mediator (ferrocenium) and the acetate anion. In other words, heterogeneous electron transfer must not interfere with the redox reaction occurring in solution. Homogenous electron transfer must also behave in accordance with Marcus theory in that diffusion must be the initial step, which should then be followed by (a) electron transfer and (b) counter diffusion (**Scheme 1.6**). Furthermore, the oxidation potentials of the mediator and the substrate of interest must be relatively close in energies in order for homogeneous electron transfer to be feasible in solution and hence, both the forward and backwards homogenous electron transfer will be favored. Finally, a rapid follow-up step must take place that drives the forward homogenous electron transfer in solution. Once all conditions are satisfied, a wide range of redox mediators with similar electrochemical properties can be utilized to evaluate the thermodynamic parameter (E^o) of a given substrate.

As demonstrated in **Scheme 1.8**, in order to construct an HRC plot using a homogenous approach, a large variety of redox mediators with similar electrochemical properties is necessary. Based on research suggesting that ferrocene and its derivatives are well-ordered electroactive mediators, they were employed for the current investigation.[122] The change in the peak currents of the mediator in the presence of a carboxylate is directly related to the rate constant of electron transfer. (The rate constant for homogenous electron transfer can be estimated, as detailed in **Chapter 4**.)

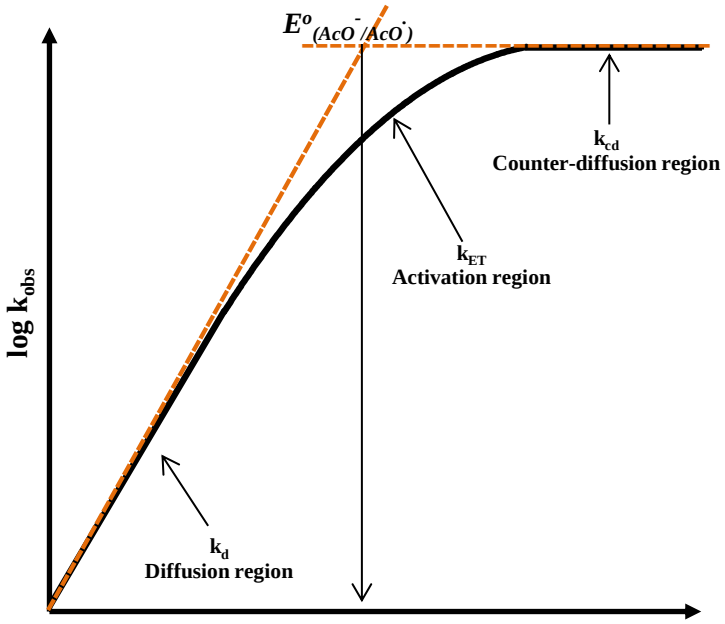

$$E^o_{(M/M^{\cdot+})} - E^o_{(AcO^-/AcO^\cdot)}$$

Scheme 1.8 The oxidation potential of a substrate is extrapolated from the plot of the rate constants of electron transfer as a function of oxidation potentials

1.6. Objectives and Aims.

The primary objective of this study was to determine the oxidation potentials of a series of carboxylates via two experimental approaches. First, we investigated the electrolysis process via **direct heterogeneous electron transfer,** by coupling convolution voltammetry and cyclic voltammetry. As noted earlier, direct heterogeneous electrolysis has represented the electrochemical technique of choice for investigating dissociative electron transfer.

As discussed, a series of aliphatic and aryl carboxylates were studied extensively using conventional analyses of cyclic voltammograms. There are, however, several important drawbacks using this conventional approach. First, cyclic voltammetry is quite limited in the case of irreversible processes—especially in systems with highly resistive solutions and sluggish heterogeneous kinetics, such as presented by aliphatic carboxylates. Second, the conventional approach is limited to measuring kinetic data based on only one or two data points collected from the entire cyclic voltammogram. In addition, the literature suggests that other approaches to kinetic and thermodynamic parameters are also not feasible.[25,26]

In this work, we employed convolution voltammetry to examine the rate constant of heterogeneous dissociative electron transfer, as was discussed by Savéant and co-workers.[111,121] We have utilized the convolution approach to determine the mechanism and kinetics of dissociative electron transfer, as well as couple it to Marcus theory to measure the thermodynamics (E^o) of the investigated carboxylate.

An additional objective of this study was to employ Marcus theory to examine thermodynamic data via an alternative approach known as homogeneous redox catalysis (HRC), with ferrocene and its derivatives serving as redox mediators. Based on prior investigations involving ferrocene and acetate, the oxidation potential of acetate served as the primary focus of this approach. Most recently, González and coworkers described HRC between ferrocene and

acetate for electrode modification purposes, but the kinetics and thermodynamics of the system were not investigated.[53] HRC proved to be a useful tool for our systems, since the direct oxidation of carboxylates is known be challenging. However, our results indicate that in addition to the catalytic process, another side reaction between the by-products of the acetate oxidation and ferrocene (and its derivatives) occurs, making the determination of thermodynamic data impossible. These findings will be presented with respect to possible applications and mechanistic schemes for this system.

1.7. Preliminary results and hypothesis.

Following previous work with aliphatic carboxylates,[25,27,53,123] our preliminary results for both conventional and convolution approaches involving tetra-n-butylammonium acetate pointed to a concerted mechanism, rather than the previously reported stepwise mechanism. Further investigations on the oxidation of acetate in wet acetonitrile indicated a stepwise mechanism, as established in literature. Replicate experiments under similar experimental conditions resulted in consistent and reproducible concerted dissociative electron transfer mechanisms (**Chapter 2**). In our approach, we employed rigorously anhydrous conditions. Thus, we suggest that the discrepancy between our findings and those previously reported are due in part to water impurities, combined with the hygroscopic nature of tetra-n-butylammonium carboxylates. The question remains, then, if, in fact, anhydrous conditions actually do have a profound impact on the electron transfer mechanism—and to what extent anhydrous conditions can be defined.

In terms of structure of the remainder of this dissertation, we present findings for both conventional and convolution results in the case of tetra-n-butylammonium acetate as our reference model under anhydrous and wet conditions in **Chapter 2**. Next, we extend our study to

investigate a series of aliphatic carboxylates to further determine the effects of radical stabilization energies on $E^{o}_{(RCO_2^{-}/R^{\cdot})}$ as well as the ET mechanism that drives that process (**Chapter 3**). The third chapter also includes findings with regards to hydrogen bonding effects as a possible interpretation for the discrepancy in reported ET mechanisms. **Chapter 4** presents our findings on the use of homogenous redox catalysis for investigating the kinetics and thermodynamics of acetate as our reference model, which, in fact, revealed significant discrepancies from expected redox behaviors. Specifically, the homogeneous system deviated from catalytic behavior, and instead, a degradation of the redox catalysis mediator (ferrocene and its derivatives) was observed. **Chapter 4** details these findings with comprehensive evidence for the degradation of the redox mediators, as well as highlights other possible alternative mechanisms for this system. Finally, **Chapter 5** describes the use of laser flash photolysis as an alternative method to further investigate the effects of water and ions on the rate of β-scission on the demethylation of cumyloxy radicals (**Scheme 1.9**). This investigation was inspired by our electroanalytical observations of the mechanistic shift of electron transfer from a stepwise to a concerted pathway due to hydrogen bonding effects; we then extended this research to include the effects of ions on the radical stability of β-scission reaction. The temperature dependence of the activation energy profile for each range of electrolyte and water/D_2O concentrations was also investigated, with findings presented in **Chapter 5**.

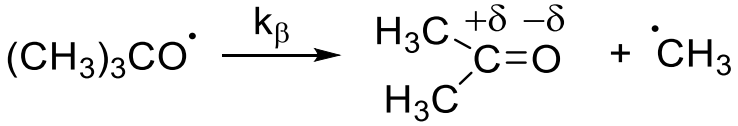

Scheme 1.9 Demethylation of cumyloxyl radical v*ia* a β- scission

References

(1) Workentin, M. S.; Maran, F.; Chiba, K.; Savéant, J. M.; Electrochemical Society. Organic and Biological Electrochemistry Division.; Electrochemical Society. Meeting *Organic electrochemistry : proceedings of the Fifth International Manuel M. Baizer Symposium in honor of Professor Jean Michel Savéant*; Electrochemical Society: Pennington, NJ, 2002.

(2) Lund, H. H., O. *Organic Electrochemistry: An Introduction and a Guide*; 3rd ed.; Marcel Dekker: New York, 1991.

(3) Tajima, T.; Fuchigami, T. *Chem-Eur J* **2005**, *11*, 6192.

(4) Eberson, L. *Electron Transfer Reactions in Organic Chemistry* Berlin, 1987; Vol. 25.

(5) Bard, J. A. F., L.R. *Electrochemical Methods: Fundamentals and Applications*, 2001.

(6) Downard, A. J.; bin Mohamed, A. *Electroanalysis* **1999**, *11*, 418.

(7) Sperry, J. B.; Wright, D. L. *Chem. Soc. Rev.* **2006**, *35*, 605.

(8) Hudlicky, T.; Claeboe, C. D.; Brammer, L. E.; Koroniak, L.; Butora, G.; Ghiviriga, I. *J. Org. Chem.* **1999**, *64*, 4909.

(9) Parrish, J. D.; Little, R. D. *Tetrahedron Lett.* **2001**, *42*, 7371.

(10) Maeda, H.; Maki, T.; Ashie, H.; Ohmori, H. *J. Chem. Soc., Chem. Commun.* **1995**, 871.

(11) Little, R. D.; Fox, D. P.; Van Hijfte, L.; Dannecker, R.; Sowell, G.; Wolin, R. L.; Moens, L.; Baizer, M. M. *J. Org. Chem.* **1988**, *53*, 2287.

(12) Shono, T.; Soejima, T.; Takigawa, K.; Yamaguchi, Y.; Maekawa, H.; Kashimura, S. *Tetrahedron Lett.* **1994**, *35*, 4161.

(13) Schäfer, H.-J. In *Electrochemistry IV*; Steckhan, E., Ed.; Springer Berlin Heidelberg: 1990; Vol. 152, p 91.

(14) Eberson, L. *Acta Chem. Scand.* **1963**, *17*, 2004.

(15) Hilborn, J. W.; Pincock, J. A. *J. Am. Chem. Soc.* **1991**, *113*, 2683.

(16) Vijh, A. K.; Conway, B. E. *Chem. Rev. (Washington, DC, U. S.)* **1967**, *67*, 623.

(17) Conway, B. E.; Vijh, A. K. *Electrochim. Acta* **1967**, *12*, 102.

(18) Dickinson, T.; Wynne-Jones, W. F. K. *Trans. Faraday Soc.* **1962**, *58*, 382.

(19) Dickinson, T.; Wynne-Jones, W. F. K. *Trans. Faraday Soc.* **1962**, *58*, 388.

(20) Dickinson, T.; Wynne-Jones, W. F. K. *Trans. Faraday Soc.* **1962**, *58*, 400.

(21) Eberson, L. *Electrochim. Acta* **1967**, *12*, 1473.

(22) Conway, B. E.; Dzieciuch, M. *Can. J. Chem.* **1963**, *41*, 21.

(23) Eberson, L. *Acta Chem. Scand., Ser. B* **1984**, *38*, 439.

(24) Andrieux, C. P.; Gonzalez, F.; Saveant, J. M. *J. Electroanal. Chem.* **2001**, *498*, 171.

(25) Andrieux, C. P.; Gonzalez, F.; Saveant, J. M. *J. Am. Chem. Soc.* **1997**, *119*, 4292.

(26) Galicia, M.; Gonzalez-Fuentes, M. A.; Valencia, D. P.; Gonzalez, F. J. *J. Electroanal. Chem.* **2012**, *672*, 28.

(27) Galicia, M.; Gonzalez, F. J. *J. Electrochem. Soc.* **2002**, *149*, D46.

(28) Vase, K. H.; Holm, A. H.; Norrman, K.; Pedersen, S. U.; Daasbjerg, K. *Langmuir* **2007**, *23*, 3786.

(29) Kayser, R. H.; Pollack, R. M. *J. Am. Chem. Soc.* **1977**, *99*, 3379.

(30) Allongue, P.; Delamar, M.; Desbat, B.; Fagebaume, O.; Hitmi, R.; Pinson, J.; Savéant, J.-M. *J. Am. Chem. Soc.* **1997**, *119*, 201.

(31) Reichenbacher, P. H.; Liu, M. Y. C.; Skell, P. S. *J. Am. Chem. Soc.* **1968**, *90*, 1816.
(32) Li, J. J. C., E.J. *Name Reaction for Functional Group Transformations*; John Wiley & Sons: New Jersey, 2007.
(33) Xue, L.; Su, W.; Lin, Z. *Dalton Trans.* **2011**, *40*, 11926.
(34) Yoshizawa, S.; Takehara, Z.; Ogumi, Z.; Matsubara, M.; Tsuji, T. *J. Appl. Electrochem.*, *6*, 403.
(35) Jouikov, V.; Simonet, J. *Langmuir* **2012**, *28*, 931.
(36) Hernández-Muñoz, L. S.; Fragoso-Soriano, R. J.; Vázquez-López, C.; Klimova, E.; Ortiz-Frade, L. A.; Astudillo, P. D.; González, F. J. *J. Electroanal. Chem.* **2010**, *650*, 62.
(37) Hernández-Muñoz, L. S.; González, F. J. *Electrochem. Commun.* **2011**, *13*, 701.
(38) Bhugun, I.; Saveant, J. M. *J Electroanal Chem* **1995**, *395*, 127.
(39) Belanger, D.; Pinson, J. *Chem Soc Rev* **2011**, *40*, 3995.
(40) Delamar, M.; Desarmot, G.; Fagebaume, O.; Hitmi, R.; Pinson, J.; Saveant, J. M. *Carbon* **1997**, *35*, 801.
(41) Workentin, M. S.; Donkers, R. L. *J. Am. Chem. Soc.* **1998**, *120*, 2664.
(42) Pinson, J.; Podvorica, F. *Chem Soc Rev* **2005**, *34*, 429.
(43) Maeda, H.; Maki, T.; Ohmori, H. *Chem. Pharm. Bull.* **1994**, *42*, 1041.
(44) Maeda, H.; Yamauchi, Y.; Hosoe, M.; Li, T.-X.; Yamaguchi, E.; Kasamatsu, M.; Ohmori, H. *Chem. Pharm. Bull.* **1994**, *42*, 1870.
(45) Coulon, E.; Pinson, J.; Bourzat, J.-D.; Commerçon, A.; Pulicani, J.-P. *J. Org. Chem.* **2002**, *67*, 8513.
(46) Fichter, F. *Zeitschrift Fur Physikalische Chemie--Stochiometrie Und Verwandtschaftslehre* **1927**, *130*, 49.
(47) Fichter, F.; Zumbrunn, R. *Helv. Chim. Acta* **1927**, *10*, 869.
(48) Glasstone, S.; Hickling, A. *J. Chem. Soc.* **1936**, 820.
(49) Glasstone, S.; Hickling, A. *J. Chem. Soc.* **1934**, 1878.
(50) Shukla, S. N.; Walker, O. J. *Trans. Faraday Soc.* **1931**, *27*, 35.
(51) Shukla, S. N.; Walker, O. J. *Trans. Faraday Soc.* **1932**, *28*, 457.
(52) Eberson, L.; Nyberg, K. *J. Am. Chem. Soc.* **1966**, *88*, 1686.
(53) Hernández, D. M.; González, M. A.; Astudillo, P. D.; Hernández, L. S.; González, F. J. *Procedia Chem.* **2014**, *12*, 3.
(54) Andrieux, C. P.; Gonzalez, F.; Savéant, J. M. *J. Electroanal. Chem.* **2001**, *498*, 171.
(55) Eberson, L. *Reactivity and Structure:Concepts in Organic Chemistry*, 2012; Vol. 25.
(56) Andrieux, C. P.; Robert, M.; Saeva, F. D.; Saveant, J. M. *J. Am. Chem. Soc.* **1994**, *116*, 7864.
(57) Corey, E. J.; Casanova, J. *J. Am. Chem. Soc.* **1963**, *85*, 165.
(58) Evans, F. W.; Skinner, H. A. *Trans. Faraday Soc.* **1959**, *55*, 260.
(59) Canady, W. J.; Papee, H. M.; Laidler, K. J. *Trans. Faraday Soc.* **1958**, *54*, 502.
(60) Wadso, I. *Acta Chem. Scand.* **1962**, *16*, 487.
(61) Jaffe, L.; Prosen, E. J.; Szwarc, M. *J. Chem. Phys.* **1957**, *27*, 416.
(62) In *Z. Phys. Chem. (Muenchen, Ger.)* 1954; Vol. 1, p 340.
(63) Isse, A. A.; Gennaro, A.; Maran, F. *Acta Chem. Scand.* **1999**, *53*, 1013.
(64) Saveant, J. M. *Acc. Chem. Res.* **1993**, *26*, 455.

(65) Costentin, C.; Robert, M.; Savéant, J.-M. *Adv. Chem. Phys.* **2006**, *324*, 40.
(66) Kanoufi, F.; Bard, A. J. *J. Phys. Chem. B* **1999**, *103*, 10469.
(67) Eberson, L. N., K. *Acta Chem. Scand.* **1964**, *18*, 1568.
(68) Weinberg, N. L.; Tilak, B. V. *Technique of electroorganic synthesis*; Wiley, 1974.
(69) Isse, A. A. G., Armando; Maran, Flavio *Acta Chem. Scand.* **1999**, *53*, 1013.
(70) Oliveira Neto, A.; Giz, M. J.; Perez, J.; Ticianelli, E. A.; Gonzalez, E. R. *J. Electrochem. Soc.* **2002**, *149*, A272.
(71) Nadjo, L.; Savéant, J. M. *J. Electroanal. Chem. Interfacial Electrochem.* **1973**, *48*, 113.
(72) Imbeaux, J. C.; Savéant, J. M. *J. Electroanal. Chem. Interfacial Electrochem.* **1970**, *28*, 325.
(73) Imbeaux, J. C.; Savéant, J. M. *J. Electroanal. Chem. Interfacial Electrochem.* **1971**, *31*, 183.
(74) Savéant, J. M.; Vianello, E. *Electrochim. Acta* **1967**, *12*, 629.
(75) Astudillo, P. D.; Galano, A.; Gonzalez, F. J. *J Electroanal Chem* **2007**, *610*, 137.
(76) Leffler, J. E. *Science* **1953**, *117*, 340.
(77) Hammond, G. S. *J. Am. Chem. Soc.* **1955**, *77*, 334.
(78) Creager, S.; Yu, C. J.; Bamdad, C.; O'Connor, S.; MacLean, T.; Lam, E.; Chong, Y.; Olsen, G. T.; Luo, J.; Gozin, M.; Kayyem, J. F. *J. Am. Chem. Soc.* **1999**, *121*, 1059.
(79) Yu, C. J.; Wan, Y.; Yowanto, H.; Li, J.; Tao, C.; James, M. D.; Tan, C. L.; Blackburn, G. F.; Meade, T. J. *J. Am. Chem. Soc.* **2001**, *123*, 11155.
(80) Weiss, E. A.; Ahrens, M. J.; Sinks, L. E.; Gusev, A. V.; Ratner, M. A.; Wasielewski, M. R. *J. Am. Chem. Soc.* **2004**, *126*, 5577.
(81) Bertin, P. A.; Georganopoulou, D.; Liang, T.; Eckermann, A. L.; Wunder, M.; Ahrens, M. J.; Blackburn, G. F.; Meade, T. J. *Langmuir* **2008**, *24*, 9096.
(82) Trammell, S. A.; Moore, M.; Lowy, D.; Lebedev, N. *J. Am. Chem. Soc.* **2008**, *130*, 5579.
(83) Meade, T. J.; Gray, H. B.; Winkler, J. R. *J. Am. Chem. Soc.* **1989**, *111*, 4353.
(84) Bowler, B. E.; Meade, T. J.; Mayo, S. L.; Richards, J. H.; Gray, H. B. *J. Am. Chem. Soc.* **1989**, *111*, 8757.
(85) Risser, S. M.; Beratan, D. N.; Meade, T. J. *J. Am. Chem. Soc.* **1993**, *115*, 2508.
(86) D'Alessandro, D. M.; Keene, F. R. *Chem. Soc. Rev.* **2006**, *35*, 424.
(87) D'Alessandro, D. M.; Topley, A. C.; Davies, M. S.; Keene, F. R. *Chemistry* **2006**, *12*, 4873.
(88) Beratan, D. N.; Onuchic, J. N.; Winkler, J. R.; Gray, H. B. *Science* **1992**, *258*, 1740.
(89) Gray, H. B.; Winkler, J. R. *Annu. Rev. Biochem.* **1996**, *65*, 537.
(90) Gray, H. B.; Winkler, J. R. *Proc. Natl. Acad. Sci. U. S. A.* **2005**, *102*, 3534.
(91) Mayo, S. L.; Ellis, W. R., Jr.; Crutchley, R. J.; Gray, H. B. *Science* **1986**, *233*, 948.
(92) Franck, J.; Dymond, E. G. *Trans. Faraday Soc.* **1926**, *21*, 536.
(93) Laidler, K. J.; King, M. C. *J. Phys. Chem.* **1983**, *87*, 2657.
(94) Anonymous *Physical Review* **1926**, *27*, 637.
(95) Condon, E. U. *Phys. Rev.* **1928**, *32*, 858.
(96) Eyring, H. *J. Chem. Phys.* **1935**, *3*, 107.
(97) POLANYI, J. C. *Science* **1987**, *236*, 680.

(98) Blumberger, J. *Chem. Rev. (Washington, DC, U. S.)* **2015**, *115*, 11191.
(99) Godovsky, D. *Org. Electron.* **2011**, *12*, 190.
(100) Khopde, S. M.; Priyadarsini, K. I. *Biophys. Chem.* **2000**, *88*, 103.
(101) Marcus, R. A. *J. Chem. Phys.* **1956**, *24*, 966.
(102) Moser, C. C.; Dutton, P. L. In *Photosystem I: The Light-Driven Plastocyanin:Ferredoxin Oxidoreductase*; Golbeck, J. H., Ed.; Springer Netherlands: Dordrecht, 2006, p 583.
(103) Marcus, R. A. *Ann. Rev. Phys. Chem.* **1964**, *15*, 155.
(104) Tully, J. C. *Theor. Chem. Acc.* **2000**, *103*, 173.
(105) EU, C. *Phys Rev* **1926**, *28*, 1182.
(106) Closs, G. L.; Calcaterra, L. T.; Green, N. J.; Penfield, K. W.; Miller, J. R. *J. Phys. Chem.* **1986**, *90*, 3673.
(107) Beitz, J. V.; Miller, J. R. *J. Chem. Phys.* **1979**, *71*, 4579.
(108) Closs, G. L.; Miller, J. R. *Science* **1988**, *240*, 440.
(109) Siders, P.; Marcus, R. A. *J. Am. Chem. Soc.* **1981**, *103*, 748.
(110) Pletcher, D.; Greff, R.; Peat, R.; Peter, L. M.; Robinson, J. In *Instrumental Methods in Electrochemistry*; Robinson, D., Ed.; Woodhead Publishing: 2010, p 76.
(111) Pletcher, D.; Greff, R.; Peat, R.; Peter, L. M.; Robinson, J. In *Instrumental Methods in Electrochemistry*; Robinson, D., Ed.; Woodhead Publishing: 2010, p 178.
(112) Pletcher, D.; Greff, R.; Peat, R.; Peter, L. M.; Robinson, J. In *Instrumental Methods in Electrochemistry*; Robinson, D., Ed.; Woodhead Publishing: 2010, p 356.
(113) In *Instrumental Methods in Electrochemistry*; Robinson, D. P. G. P. M. P., Ed.; Woodhead Publishing: 2010, p 388.
(114) Guidelli, R.; Compton Richard, G.; Feliu Juan, M.; Gileadi, E.; Lipkowski, J.; Schmickler, W.; Trasatti, S. In *Pure Appl. Chem.* 2014; Vol. 86, p 245.
(115) Antonello, S.; Maran, F. *J. Am. Chem. Soc.* **1999**, *121*, 9668.
(116) Maran, F. W., M. *Electrochem. Soc. Interface* **2002**, *149*, 44.
(117) Donkers, R. L.; Maran, F.; Wayner, D. D. M.; Workentin, M. S. *J. Amer. Chem. Soc.* **1999**, *121*, 7239.
(118) Gileadi, E., Kirowa-Eisner, E., Penciner, J. *Interfacial Electrochemistry, An Experimental Approach*; Addison-Wesley: Reading, MA, 1975.
(119) Pure, I. U. o.; Applied Chemistry. Physical Chemistry Division. Commission on Symbols, T.; Units; Paul, M. A. *Manual of symbols and terminology for physicochemical quantities and units: 1973 edition adopted by the IUPAC Council at Munich Federal Republic of Germany on 31 August 1973*; Butterworths, 1975.
(120) Matejec, R. *Zeitschrift für Elektrochemie, Berichte der Bunsengesellschaft für physikalische Chemie* **1958**, *62*, 400.
(121) Imbeaux, J. C.; Savéant, J. M. *J. Electroanal. Chem. Interfacial Electrochem.* **1973**, *44*, 169.
(122) Francke, R.; Little, R. D. *Chem. Soc. Rev.* **2014**, *43*, 2492.
(123) Galicia, M.; González-Fuentes, M. A.; Valencia, D. P.; González, F. J. *J. Electroanal. Chem.* **2012**, *672*, 28.

Chapter 2. Conventional and convolution approaches to the kinetic and thermodynamic behavior of heterogeneous dissociative electron transfer for acetate salts as a model reference for Kolbe's electrolysis

Chapter 2 compromises original work toward the completion of Ph.D. degree of Marwa Abdel Latif. Acknowledgement and thanks are given to major contributors to this work. Dr. James Tanko, Chair of the committee, and Dr. Jared Spencer, a former doctoral researcher and senior member of the Tanko's group, have contributed significantly to the intellectual content. Bryce Kidd, a doctoral researcher in Dr. Madsen's group, provided the PFG NMR measurements and its intellectual content.

2. Introduction.

2.1. Electrochemical methods for determining the kinetics of the electron transfer mechanism.

The complexity and functionality of substituted groups on carboxylates tend to make it more challenging to assign one particular pathway via post-electrolysis analysis of the product-mixture by-products.[1-9] There is definite literature precedent for the involvement of both acetoxyl and methyl radicals as possible reactive intermediates based on product mixture,[1,2,10-13] and for this investigation, the results were insightful but inconclusive. Nonetheless, the electrochemical approach still provides an unequivocal advantage in that one can investigate the kinetics of the dissociative electron transfer mechanism, which is not feasible otherwise.

An extensive body of work has addressed the kinetics and mechanism of the electron transfer for acetate systems. While it is known that the oxidation generates a free radical intermediate, it is not clear whether this occurs via a stepwise or a concerted pathway. For over a decade, electrochemists have utilized a variety of approaches to investigate mechanistic and thermodynamic parameters about a number of chemical systems; favored approaches utilize mathematical operations to describe the current-potential (*i*-*E*) relationship for a variety of electron

transfer mechanisms. However, the electrode kinetics for an elementary electron transfer mechanism is deduced via alpha (α), known as either the transfer coefficient or the coefficient of symmetry.[14-16] Alpha (α) is a dimensionless constant used to describe the kinetics of electrode processes. First introduced by Butler to describe the electrostatic potential energy impacting electron transfer at the surface of an electrode, this transfer coefficient (α) was later incorporated into a kinetic expression to describe electrode kinetics (**Eq 2.1**). Refer to **Section 1.5.4** for detailed description of alpha.

Originally, experimental values for α using Kolbe's electrolysis were first calculated from the Tafel's slope ($\partial V/\partial lni$), which relates the electrode overpotential to the log of current densities. Conway and co-workers investigated the kinetics of an overall kinetic reaction scheme (**Scheme 2.1**) on the surface of metal electrodes to identify the rate-determining step (rds) for Kolbe's electrolysis.[17-19]

$$RCOO^-(M) \rightarrow RCOO^{\cdot} + e^-$$

$$RCOO^{\cdot}(M) \rightarrow R^{\cdot}(M) + CO_2$$

$$R^{\cdot}(M) + R^{\cdot}(M) \rightarrow R - R$$

$$R^{\cdot}(M) + RCOO^- \rightarrow R - R + CO_2 + e^-$$

Scheme 2.1 Representative reaction scheme for Kolbe's electrolysis at the surface of metal electrode (M) with each step treated as a possible rate-determining step.

The slope of the linear region of Tafel plots can be generated theoretically based on kinetic models developed according to the Frumkin-Temkin logarithmic isotherm; results can then be compared to experimental values.[20-23] Kolbe's electrolysis for carboxylic acids under various experimental conditions indicated $\alpha > 2RT/F$, which corresponds to dissociative electron transfer as the rds step with $0.25 < \alpha < 0.5$.[7-9,13,17-19,24] However, a further analysis of concerted and stepwise DET is not yet feasible.

$$\alpha = \left(-\frac{RT}{nF}\right)\left(\frac{\partial ln|i|}{\partial V}\right) \quad \textbf{(2.1)}$$

It was not until the late 20th century that Savéant, Parker and Evans established reliable mechanistic diagnostic criteria for electron transfer.[25-29] Specifically, they developed mathematical diagnostic criteria to distinguish small differences observed in voltammograms based on complex or competitive pathways for electron transfer at the surface of an electrode. Researchers have routinely employed these approaches in electrochemical assessments of mechanisms, including Kolbe's electrolysis.[30,31] In particular, the nature of the intermediates can be deduced and specific electron transfer mechanisms can be determined via cyclic voltammetry, based on the shape of the peak and the current-potential response. Two major diagnostic criteria for Kolbe's system are the values of $\partial E_p/\partial log v$ and peak width $(E_p - E_{p/2})$, which represent another approach for evaluating α as a mechanistic parameter—specifically for electron transfer as the rate-limiting step ($n = 1$). While the transfer coefficient (α) can be calculated via this conventional approach, researchers have reported that it is somewhat limited in that it relies on a single-point or two-point measurements, $\partial E_p/\partial log v$ $[(\partial E_p/\partial log v) = 1.15RT(F/\alpha)]$ and peak width $\Delta E_p = (E_p - E_{p/2})$ $[E_p - E_{p/2} = 1.85RT/(F/\alpha)]$, which are obtained via cyclic voltammetry.[32-35] Therefore, it is necessary to vary the scan rate by at least two orders of magnitude to obtain accurate information.

Moreover, instrument-related limitations can be problematic since convection becomes more significant at very low scan rates, while high non-faradiac current becomes more significant at high scan rates. Conventional analytical approaches for determining the dissociative ET mechanisms for aliphatic and aryl carboxylates were first reported by the González group and the Savéant group. For example, González and coworkers proposed a stepwise DET mechanism for a

series of aliphatic carboxylates based on measured α values of 0.55 and 0.58 from the estimated peak width ($E_p - E_{p/2}$) of 86 V/s and from ($\partial E_p/\partial log v$) of 50.1 mV, respectively, but at a limited scan range of 0.1 – 2 V/s.[35,36] Conventional analysis of a series of arylmethyl carboxylates was also undertaken by Savéant and coworkers, who similarly proposed a stepwise mechanism—the difference being that they reported scan rates ranging from 0.1 to 100 V/s.[33] It must be noted that the transfer coefficient for aliphatic carboxylates was deduced from a limited range of scan rates; it is also not feasible to obtain the experimental oxidation potential of carboxylates *via* a conventional approach since do not obey Nerstian behavior. Thus, estimated oxidation potentials for this investigation are reported by theoretical estimations only (refer to **section 1.4**).[10]

2.2. Purpose.

The primary objective of this study was to employ an alternative approach to conventional methods in order to clarify the mechanisms associated with dissociative electron transfer, and most importantly, to evaluate the oxidation potential for acetate anions (**Scheme 2.2**). Convolution voltammetry was applied to experimental data from the cyclic voltammograms to overcome the limitations posed by conventional methods. Specifically, the major advantage of using convolution voltammetry is eliminating the effect of mass transport and peak potential dependency on the resulting scan rate; hence, all collected cyclic voltammograms were utilized directly to calculate the rate constant of heterogeneous dissociative electron transfer as a function of applied potential. (Refer to sections **2.3**, **2.4** and **2.5** for a detailed discussion of scan rate dependence of mass transport using conventional methods.) Consequently, this approach enables one to determine both the thermodynamic parameter (E^o) and the kinetic parameter (α) with higher accuracy.

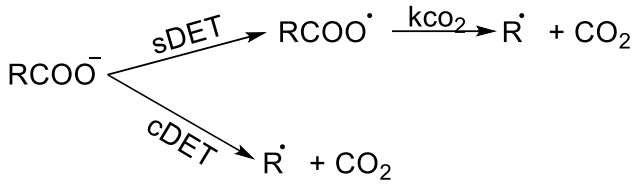

Scheme 2.2 Elementary dissociative electron transfer (DET) occurring via concerted (cDET) or a stepwise mechanism (sDET)

2.3. Convolution Voltammetry.

Convolution voltammetry originated in the early 1970s with the theoretical work of Oldham. Andriéux and Savéant later adapted his principles to provide a mathematical basis for the direct application of convolution voltammetry to cyclic voltammograms using high output data processors.[29,37-47] Specifically, they derived a convolution current function that is independent of the scan rate and applied potential, which can then be applied directly to generated experimental *i(t)- vs. E* cyclic voltammograms. In accordance with **Eq 2.2**, the "normal" current, i_u in a given cyclic voltammogram is transformed to yield the convoluted current, I_{conv}. Although the transient peak current (i_p) is sweep-rate dependent, I_{conv} is utilized to determine a sweep-rate independent current, which is referred to as the limiting current (I_l).[39,40,48] In addition, other significant characteristics involved in the ET process can be estimated: the number of electrons (*n*), the diffusion coefficient (D_o), and the Faraday's constant (*F*). As shown in **Eq 2.3**, A is the surface area of the electrode, and C is the bulk concentration of the analyte. The convolution function (I_{conv}) can be easily programmed using computing software. The *i(t)-t* data from cyclic voltammograms can then be background subtracted and convoluted via a visual basic code in Microsoft Excel written in-house and in accordance with **Eq 2.3** (**Appendix A**).[49] Background subtractions are essential for eliminating non-faradaic current contribution to the faradaic current.

$$I_{conv} = \pi^{-\frac{1}{2}} \int_0^{\tau} \left[\frac{i_u}{(t-u)^{\frac{1}{2}}}\right] du \qquad \textbf{(2.2)}$$

$$I_{conv} = \pi^{-\frac{1}{2}} \int_{j=i}^{j=k} \left[\frac{i_{\left(j\Delta t - \frac{1}{2}\Delta t\right)} . \Delta t^{1/2}}{\sqrt{(k-j+\frac{1}{2})}}\right] du \quad \textbf{(2.3)}$$

$$I_l = nFAD^{1/2}C_{bulk} \quad \textbf{(2.4)}$$

As indicated by Savéant and coworkers, eliminating the dependence of mass transport on scan rate is of primary significance. Specifically, the researchers utilized convoluted current in conjugation with the experimental voltammetric current to characterize the kinetic mechanisms at the surface of the electrode through a linear logarithmic relationship of the current function $\ln((I_l - I_{conv)})/i_t)$ to the applied potential (E).[41-45] It must be noted, however, that the relationship presented in **Eq 2.5** is specific to an irreversible system with a heterogeneous electron transfer, which is then followed by a rapid chemical step to accommodate our systems, where n is the number of electrons, F is Faraday's constant, R is ideal gas constant, k_s is standard rate constant of the electron transfer, T is temperature, and D^o is the diffusion coefficient. The convoluted voltammetric currents were incorporated in order to estimate an averaged α value for electron transfer from all collected data in the cyclic voltammogram, as well as a corresponding rate constant for the ET (k_{ET}) at any applied potential (E) in the voltammogram (**Eq 2.6**). Subsequently, and in accordance with Marcus theory, the oxidation potential can be estimated from a plot of α vs. E, and extrapolating to α = 0.5 (**Eq 2.7**).[29,31,37,49-53] Note that these equations are presented for reductions in the literature. The only difference is in the sign that applies to the oxidation process, which is only taken into consideration if applied potential (E) is included in the equation, such as shown in **Eq 2.7**. The difference in sign (from -1 to +1) originates from the expression of a reduction half potential at the surface of an electrode as $\Delta E = E^o_{red} - E$); whereas oxidation half potential is expressed as $\Delta E = E - E^o_{ox}$].

$$E = -\frac{RT}{\alpha nF} ln \frac{D^{o\,1/2}}{k_s} + \frac{RT}{\alpha nF} ln \frac{I_l - I_{conv}}{i_t} \quad \textbf{(2.5)}$$

$$lnk_{ET} = lnD^{1/2} - ln\frac{I_l - I_{conv}}{i_t} \quad \textbf{(2.6)}$$

$$\alpha = \frac{\partial G^{\ddagger}}{\partial G^o} = \frac{RT}{F}\frac{\partial lnk_{ET}}{\partial E} = \frac{1}{2} - F\frac{(E - E^o)}{2\lambda} \quad \textbf{(2.7)}$$

2.4. Results and discussion.

2.4.1. Conventional and convolution analysis of tetra-n-butylammonium acetate.

The electrolysis of acetate anion was reported recently in the published work of González and coworkers.[36,55] Due to instrumental limitations, the oxidation of 4 mM tetra-n-butylammonium acetate reported in this work was performed within the scan range of 0.1 - 2.0 V/s in neat acetonitrile. Experiments were performed in anhydrous conditions inside a glovebox due to the extreme hygroscopic nature of carboxylates. The resulting cyclic voltammograms showed the expected irreversible behavior with a shift in the peak potential as a function of scan rate under a diffusion-controlled process (**Figure 2.1a & 2.1b**).

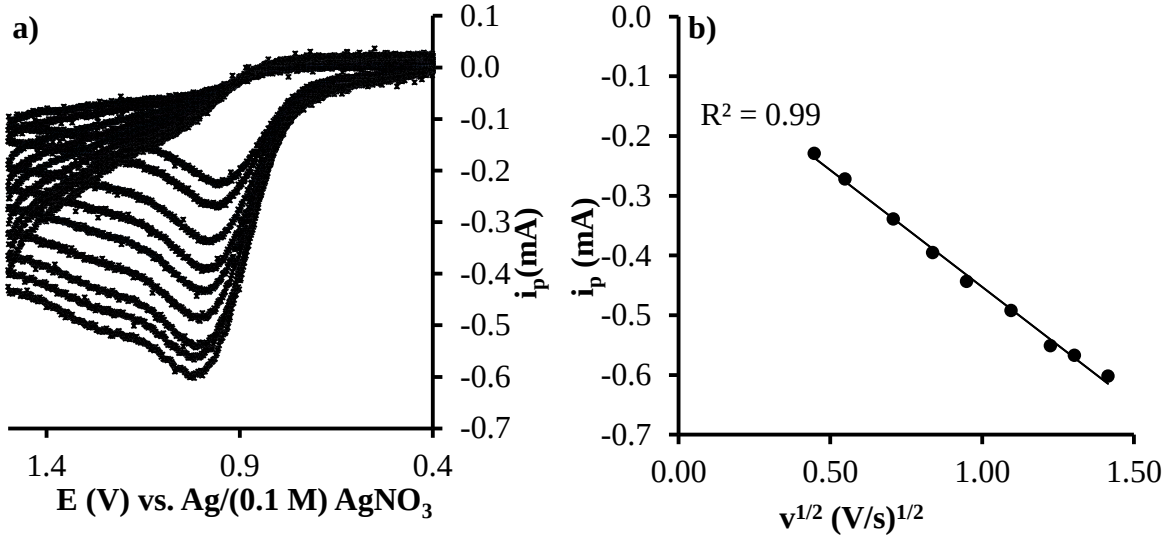

Figure 2.1. a) Cyclic voltammograms of 4 mM TBA-acetate in 0.45 M TBAP/neat CH_3CN vs. Ag/ (0.1 M) $AgNO_3$ (glovebox conditions); b) Linearity of the peak current as a function of scan rate to half power is indicative of diffusion controlled process.

Surprisingly, the α values calculated from $\partial E_p/\partial log v$ [$(\partial E_p/\partial log v) = 1.15RT(F/\alpha)$] and peak width $\Delta E_p = (E_p - E_{p/2})$ [$E_p - E_{p/2} = 1.85RT/(F/\alpha)$] had an average value of 0.33 ± 0.04, which is strongly suggestive of a concerted mechanism with ΔE_p = 150 ± 0.02 mV (**Figure 2.2a** & **2.2b** and **Table 2.1**). Note that conventional analysis for ($E_p vs. log v$) plots is limited to only one datapoint from the cyclic voltammogram at each scan rate. Thus, such an approach is predicted to have higher errors and less accuracy due to the limited scan rate range. Moreover, instrumental limitations and higher observed non-faradaic currents with increased scan rates are also problematic.

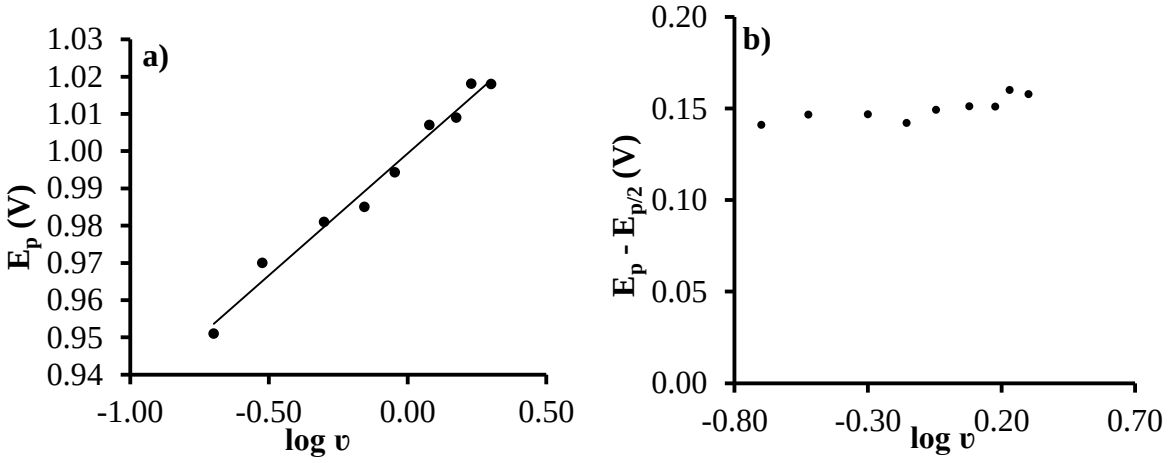

Figure 2.2. Conventional analysis of CV for 4 mM TBA-acetate under anhydrous conditions. a) Peak potential versus log scan rate with scan rates range of 0.1 - 2.0 in V/s. Alpha values calculated from the slopes of the plot were discarded as standard deviation was more pronounced, b) Peak width vs. log of scan rate indicative of a concerted mechanism as peak width averaged around 140 mV.

It is also critical to note the consistency between the value of α calculated from the peak width and $\partial E_p/\partial log v$, as stated by Savéant and coworkers.[33] In contrast to the conventional approach, utilizing calculated peak widths has the advantage of incorporating two datapoints (E_p

and $E_{p/2}$) in the cyclic voltammogram instead of one (E_p). These two datapoints are intrinsically related, since the peak potential corresponds to the potential at the highest peak current is passed; while the half peak potential corresponds to the potential when half the current peak is passed. Most importantly, the calculated α values based on peak width are independent of the scan rate; hence, higher accuracy is predicted ($\Delta E_p = (E_p - E_{p/2})$ $[E_p - E_{p/2} = 1.85RT/(F/\alpha)]$).

Based on the limited range of scan rates, the calculated α from the peak widths is reported for this body of work. Therefore, given that the averaged α calculated via conventional method is more reliable using peak width measurements, we utilized convolution voltammetry as described earlier to further investigate the mechanistic parameter α, as well as to estimate other parameters such as D_o and E^o for the system based on all experimental datapoints from our voltammograms (**Eq 2.2 - 2.5**).

In accordance with **Eq 2.7,** the ($i(t)$-E) CV profile was convoluted and (I_{conv}-E) profiles were obtained at each scan rate. Note that regardless of the scan rate, the convoluted current as a function of applied potential was independent of the scan rate (υ) or mass transport. Thus, it is critical to perform appropriate background subtractions to eliminate the possibility of significant errors that could propagate through the data analysis. As shown in **Figure 2.3**, the convoluted currents for a background-corrected voltammogram show a proper sigmoidal fitting in comparison to the raw data. As noted in **Eq 2.3**, the convolution is a summation function, which means that the contribution from the non-faradaic current is significant. In contrast, the convoluted currents without proper background subtractions show higher peak current (I_l) and a continuous increase in current in the linear plateau region. Therefore, high quality CV is needed with proper current-to-noise signal and background subtractions to achieve reliable data.

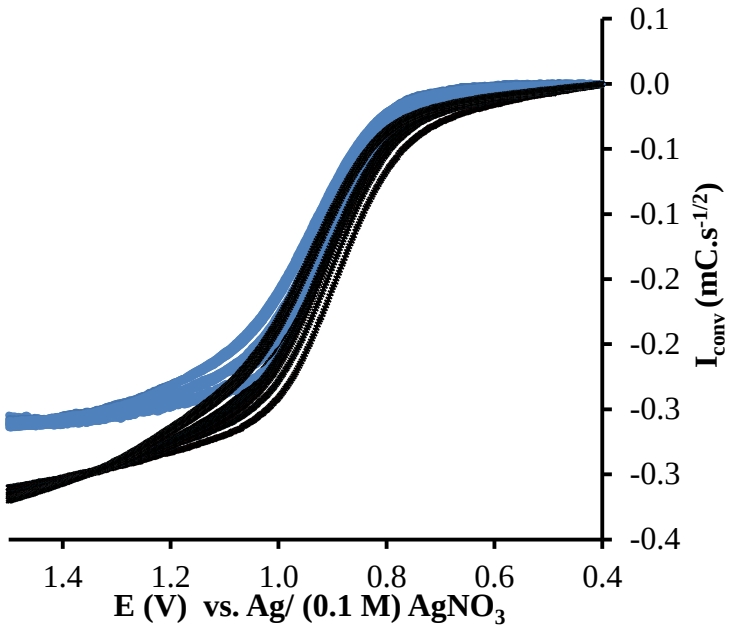

Figure 2.3. Convolution voltammograms applied to cyclic voltammograms of 4 mM tetra-n-butylammonium acetate in 0.45 M TBAP/neat CH_3CN vs. Ag/ (0.1 M) $AgNO_3$ (glovebox conditions) for with (top) and without (bottom) with background subtraction.

In accordance with Saveant's convolution model for irreversible systems, voltammetric and convoluted currents are employed to determine α from the slope of the (E *vs.* $\ln((I_l - I_{conv)})/i_t)$ plot. As shown in **Figure 2.4**, linearity is noted over the convoluted current region as a function of the applied potential. The calculated α obtained via convolution at every scan rate yields an averaged α = 0.31± 0.02 for the oxidation of tetra-n-butylammonium acetate under anhydrous conditions. This finding is strongly indicative of a concerted mechanism as evidenced by the fact that more overpotential is applied to overcome both bond breaking and electron transfer (*vide infra*). Hence, there is agreement between both electrochemical approaches regarding an observed concerted mechanism for the electron transfer process.

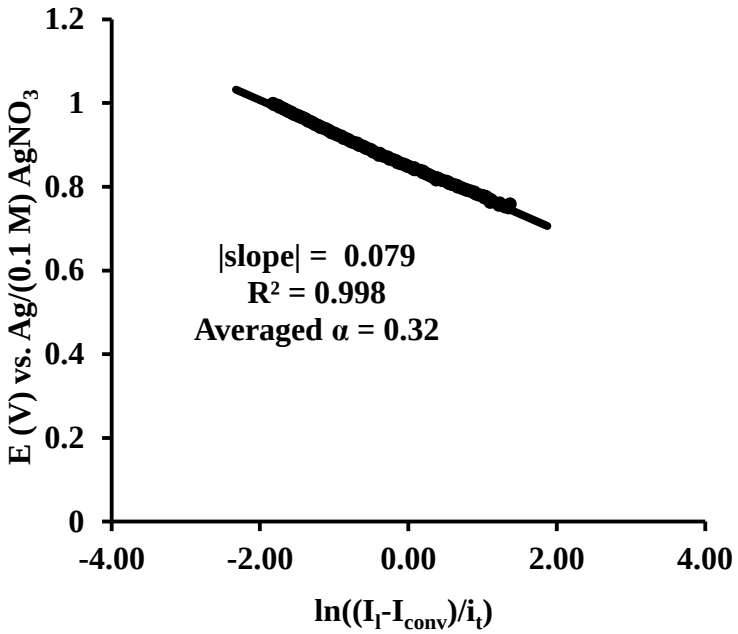

Figure 2.4. Representative linear plot of applied potential as a function of ln((I_l-I_{conv})/i_t) for 4 mM tetra-n-butylammonium acetate in neat acetonitrile with 0.45 M tetra-n-butylammonium perchlorate at 0.5 V/s vs. Ag/(0.1 M) $AgNO_3$.

2.4.2. Determination of the E^o for the heterogeneous DET for acetate.

Plots for the *ln* k_{ET} as a function of the applied potential (*E*) at the surface of an electrode (**Eq 2.6**) were constructed. Similar to the predicted normal region using Marcus theory, an increase in the rate constant was noted with increasing driving force ($\Delta G^o = -nF\Delta E^o$). The data was curve-fit according to the Marcus equation and the first derivative yielded a linear plot of α vs *E* plot using TableCurve 2D (**Figure 2.5a** and **2.5b**).[54] The extrapolation to α = 0.5 (corresponding to ΔG^o = 0) allows an estimate of E^o = 0.60 ± 0.10 V vs. Ag/ (0.1 M) $AgNO_3$ (1.20 ± 0.10 V vs. NHE) for tetra-n-butylammonium acetate under anhydrous conditions, as illustrated in **Figure 2.5b**.

Eberson and coworkers predicted a concerted mechanism for tetra-n-butylammonium acetate based on thermodynamic cycles with a theoretical E^o in CH_3CN under anhydrous conditions of 1.30 vs. SHE, which is consistent with our experimental results. Conway and

coworkers later challenged Eberson's calculations for not taking into account the difference in reactivity based on the nature of the radicals as free radical intermediates or adsorbed species at the surface of the electrode.[55-58] In summary, the relative consistency between our results via conventional and convolution approaches with respect to theoretical estimations further confirms the presence of a concerted mechanism. However, these findings diverged from published findings,[34] thereby necessitating further research to validate our results. Refer to **Appendix D** for other detailed conventional and convolution analyses for a series of concentrations of tetra-n-butylammonium acetate.

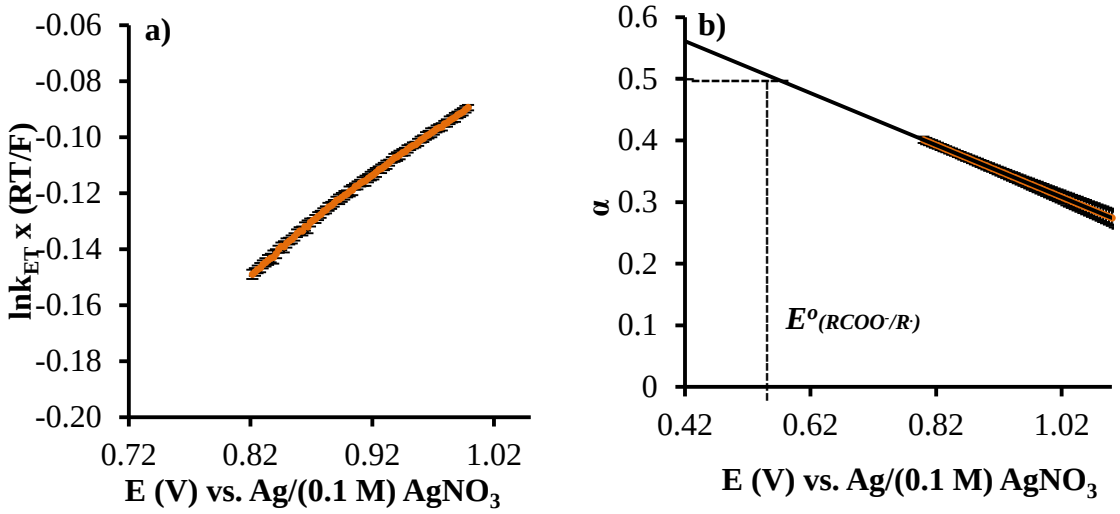

Figure 2.5. a) 4mM TBA-acetate in 0.45 M TBAP/neat CH_3CN. A representative averaged plot for the ln k_{ET} vs E for scan range of 0.1-2.0V/s with 95% CI error, b) 4mM TBA-acetate in 0.45 M TBAP/neat CH_3CN. A representative averaged plot for the apparent α vs E for scan range of 0.1-2.0V/s with 95% CI error bars.

2.4.3. Experimental conditions and mechanisms of ET.

In order to validate and ensure the reproducibility and accuracy of findings, we conducted a series of experiments by varying the concentration of the substrate and supporting electrolyte, while maintaining at least a ten-fold excess of supporting electrolyte. As the molarity of the tetra-n-butylammonium acetate was increased, there was no significant effect on the reported α values

as confirmed by convolution and conventional analyses. It is critical to note that a significant error associated with α from ($\partial E_p/\partial log v$) was observed—which was expected due to the limited range of scan rates, as well as the lower concentrations of substrate associated with the higher noise-to-signal ratio. Concentrations of 1 mM and 2 mM of substrate are sufficiently significant to be detected by cyclic voltammetry. However, due to the extended electrical connections between the instrumentation and the glovebox, the noise was higher than expected; thus, our investigations were performed at higher concentrations.

Findings from convolution analysis confirmed a larger standard deviation at lower concentrations among a range of scan rates; however, significantly higher accuracy for all concentration was noted once all voltammetric datapoints had been incorporated. It should also be noted that results from both analyses indicated a concerted mechanism, with consistent values for calculated α from the peak width and the convolution analysis that fall within experimental error as shown in **Table 2.1**. Refer to **Appendix B** for detailed mathematical approach for error analysis of α.

Table 2.1
Conventional and convolution analysis for kinetic and thermodynamic parameters, with scan rates ranging from 0.1 – 2.0 V/s.

Molarity $^{n}Bu_4N^{+}CH_3CO_2^{-}$ *(mM)*	α $(E_p - E_{p/2})$	α $(\partial E_p/\partial log v)$	α *(convolution)*	E^o *(V) vs. Ag/(0.1 M)* $AgNO_3$
2.7	0.32 ± 0.02	0.40 ± 0.20	0.30 ± 0.03	0.62 ± 0.11
3.0	0.33 ± 0.02	0.37 ± 0.07	0.30 ± 0.03	0.62 ± 0.13
3.2	0.32 ± 0.01	0.29 ± 0.07	0.30 ± 0.02	0.62 ± 0.04
4.0	0.33 ± 0.01	0.38 ± 0.08	0.33 ± 0.01	0.58 ± 0.07
8.0	0.29 ± 0.01	0.33 ± 0.11	0.31 ± 0.02	0.57 ± 0.07
[a]Average	0.32 ± 0.01	0.35 ± 0.09	0.30 ± 0.02	0.60 ± 0.10

[a]The calculated entries are reported with 95% confidence interval with an average reported for concentrations between 3.0 to 8.0 mM.

Varying the concentration of the supporting electrolyte produced some unexpected results and added to the complexity of this investigation. Specifically, as the molarity of the supporting electrolyte increased, a continuous decrease in the peak current was noted, as illustrated in **Figure 2.6**. The peak current decreased significantly by 33.8% as the concentration of the supporting electrolyte increased from 0.1 M to 0.45 M under anhydrous conditions. In contrast, no significant difference in the apparent peak potential and peak width was noted. One possible explanation for this finding is that when the molarity of the electrolyte increases, the viscosity of the solution is also increases (resulting in a lowered diffusion-coefficient for the analyte).

Because cyclic voltammetry is a diffusion-dependent process, the concentration of the tetra-n-butylammonium salts is critical. The diffusion process is not only impacted by the size of the ions in solution, but also by the following parameters: ion-ion interactions, ion-solvent interactions, and the concentration of the electrolyte.[59-61] In our investigation, the calculated diffusion coefficients of the acetate anion decreased with an increased molarity of tetra-n-butylammonium salts, which corresponded to lower peak current in obtained cyclic voltammograms.

In contrast, no significant difference was noted for the reported α and E^o values at any given electrolyte concentration (**Table 2.2**), and the oxidation potential of acetate was found to be 0.60 ± 0.09 V. Therefore, concentration profile studies confirmed a concerted electron transfer mechanism with a consistent calculated E^o, but with a decreased peak current as a function of electrolyte concentration. The decrease in peak current is likely associated with a lower transfer coefficient resulting from the increased solution viscosity at high electrolyte concentrations.

Table 2.2
Diffusion coefficients run in PFG NMR in deuterated acetonitrile versus diffusion coefficients calculated from convolution analysis.

Molarity of TBAP (M)	*[a]Averaged α*	*E^o (V)*	*(D_o x 10^{-5}) cm^2/s convolution*	*(D_o x 10^{-5}) cm^2/s PFG NMR*
0.10	0.32 ± 0.01	0.73 ± 0.10	2.46 ± 0.13	3.41 ± 0.01
0.20	0.30 ± 0.01	0.74 ± 0.08	2.10 ± 0.15	2.89 ± 0.01
0.30	0.30 ± 0.01	0.70 ± 0.09	1.93 ± 0.19	2.71 ± 0.01
0.45	0.32 ± 0.01	0.60 ± 0.10	1.82 ± 0.10	2.60 ± 0.01

[a]Alpha is an averaged value calculated from the peak width and the convolution for 4 mM tetra-n-butylammonium acetate in neat CD_3CN vs. Ag/ (0.1 M) $AgNO_3$ at 27 °C

2.4.4. Diffusion coefficient of acetate anion as a function of solution viscosity.

In order to further validate the effects of electrolyte concentration on the diffusion of the acetate anion, convolution voltammetry and pulsed field gradient (PFG) NMR were utilized simultaneously, since these methods are both capable of estimating diffusion coefficients as a function of the increased molarity of the supporting electrolyte in solution (*vide infra*). Assuming a one-electron transfer for the oxidation of an acetate anion in non-deuterated acetonitrile, the peak current from convolution voltammograms, referred to as I_l, was utilized to estimate D_o as stated in **Eq 2.4**. However, since the proton signal for a methyl group on an acetate anion cannot be detected in light acetonitrile, NMR samples were prepared in deuterated acetonitrile for PFG NMR analysis. Under such conditions, the NMR signal for an acetate anion's methyl group coincides with the NMR signal of the solvent. Preliminary measurements obtained for D_o via both methods indicate a similar trend of decreasing diffusion coefficient with an increase in the concentration of the supporting electrolyte.

This investigation also gave rise to additional questions about the mechanisms involved in the diffusion coefficient of acetate anion as a function of solution viscosity. For example, what are the effects of deuterated solvent on D_o values and how does its incorporation impact the overall

mechanism? Is it even useful to compare values obtained from convolution voltammetry and PFG-NMR? What levels of consistency can reliably be expected from these independent methodologies?

In order to address these questions, we designed a series of experiments to elucidate these relationships. First, electrochemical analysis of the oxidation of acetate anion via convolution analysis was performed in deuterated and non-deuterated neat acetonitrile to investigate the effects of a deuterated solvent on associated mechanisms and the resulting diffusion coefficients. As listed in **Table 2.3**, we observed a small, but statistically significant, difference between the reported D_o values with a slightly higher diffusion coefficient in light acetonitrile, which based on prior findings was expected. Convolution analysis also confirmed a concerted mechanism with α values within experimental errors, regardless of choice of solvents. In conclusion, we confirmed via our electrochemical testing that the mechanisms involved in the diffusion coefficient of acetate anion as a function of solution viscosity, related oxidation potentials, and diffusion coefficients were experimentally consistent.

In addition, to further confirm the observed slight decrease in diffusion coefficient in deuterated acetonitrile, convolution analysis was performed on ferrocene as a reference model. In contrast to anionically-charged acetate, ferrocene is a neutral, well-behaved model for electrochemical studies. Similar to an acetate system, the calculated diffusion coefficient results for ferrocene obtained from convolution voltammetry for both the deuterated and non-deuterated systems were identical and within experimental error. Therefore, our findings confirmed that neither deuterated nor non-deuterated acetonitrile play any role in the observed kinetic and thermodynamic parameters of acetate anion.

Table 2.3
Oxidation of 4 mM tetra-n-butylammonium acetate performed with 0.2 M TBAP. Oxidation of 4 mM ferrocene performed with 0.45 M TBAP. Scan rates range between 0.1 - 2.0 V/s.

Substrate	*Solvent*	$^{a}E^{o}$	α	$^{b}D_o$
Tetra-n-butylammonium acetate	CD_3CN	0.62 ± 0.03	0.33 ± 0.02	1.42 ± 0.05
	CH_3CN	0.64 ± 0.02	0.33 ± 0.02	1.82 ± 0.05
Ferrocene	CD_3CN	0.03 ± 0.01	--	2.60 ± 0.10
	CH_3CN	0.03 ± 0.01	--	2.71 ± 0.03

$^{a}E^{o}$ (V) vs. Ag/ (0.1 M) $AgNO_3$ and $^{b}D_o$ in (x 10^{-5} cm^2/s)

Given that PFGNMR represents a reliable tool for evaluating diffusion coefficients under precise experimental conditions for cyclic voltammetry, one can reasonably predict the number of electrons based on a comparison between calculated diffusion coefficients via convolution and PFG NMR. Moreover, based on the difference between reported values of diffusion coefficients based on n = 1 obtained via convolution analysis, a one electron transfer process is confirmed which is consistent with the findings of Gonzales and coworkers.[35]

To investigate the slight discrepancy between the diffusion coefficients measured by PFG NMR and convolution analysis, studies of ferrocene in deuterated acetonitrile were performed utilizing samples of ferrocene prepared from an electrochemical bulk solution. An averaged value of D_o from three PFG-NMR runs was found to be 2.19 (± 0.01) x 10^{-5} cm^2/s in deuterated acetonitrile for 4 mM ferrocene in 0.45 M TBAP; in comparison, findings from convolution analysis over a scan range of 0.1 -2.0 V/s resulted in an averaged D_o of 2.60 (± 0.12) x 10^{-5} cm^2/s. Both methods are considered to be consistent with a slight discrepancy between 0.28 cm^2/s and 0.54 cm^2/s. However, comparing a wide range of substrate concentrations is necessary for accuracy. Therefore, the calculated D_o was averaged at 2.38 (± 0.18) x 10^{-5} cm^2/s with 95% confidence interval for 2, 4, and 6 mM of ferrocene in deuterated acetonitrile with 0.45 M TBAP; in comparison, the analogous findings utilizing convolution analysis were D_o = 2.58 (± 0.26) $x\ 10^{-5}$ cm^2/s over a scan range of 0.1 -2.0 V/s. Hence, based on a well-behaved system such as

ferrocene, reported diffusion coefficient results were consistent and within experimental error. It is reasonable, therefore, to assume that both techniques are compatible.

To further compare the PFG NMR and convolution voltammetry methodologies, electrochemical bulk solutions in deuterated acetonitrile were prepared and analyzed using both approaches. The discrepancy between the calculated diffusion coefficient results via convolution and PFG NMR for acetate anions appeared to be less significant, and approximated analogous results for the ferrocene model, with a discrepancy of $\pm$ 0.60 x 10^5 cm^2/s for the range of 0.2 to 0.3 M TBAP. Findings show a higher discrepancy for diffusion coefficients at 0.45 M TBAP ($\pm$ 1.5 x 10^5 cm^2/s). Therefore, one can reliably infer that the range of 0.20 M and 0.30 M TBAP will provide higher accuracy, since the discrepancy for the reported D_o values between PFG NMR and convolution analysis more closely approximates the ferrocene model. It is important to note, however, that even though diffusion coefficient values indicated a higher discrepancy at 0.45 M TBAP, it does not necessary refute earlier reported data under similar conditions due to the fact no differences were reported for the alpha and oxidation potentials for the acetate system.

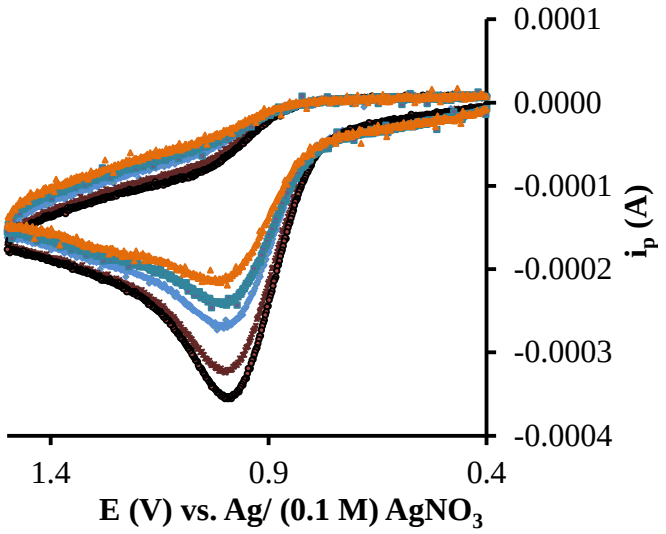

Figure 2.6. Cyclic voltammograms of 4 mM tetra-n-butylammonium acetate in CH_3CN vs. Ag/ (0.1 M) $AgNO_3$ (glovebox conditions) with TBAP (M): 0.1, 0.2, 0.3, 0.4, and 0.5 (Top to bottom).

The question remains, then, whether the dramatic increase in the concentration of electrolyte from 0.2 M to 0.45 M only impacts the diffusion coefficient of the acetate anion. Note that a slight but continuous decrease in reported peak currents via cyclic voltammetry was observed for the oxidation of the 4 mM acetate when the concentration of TBAP was increased from 0.2 M to 0.45M. This decrease was insignificant for 4 mM ferrocene since the TBAP concentration was increased to 0.45 M. Based on the fact that both ferrocene and acetate are expected to undergo one electron transfer, the significant decrease in the peak current, as well as the discrepancy between the calculated diffusion coefficient values for the acetate anion at higher concentrations, is compared to analogous ferrocene results (**Appendix E**). Nonetheless, the findings were further confirmed by convolution analysis. For the oxidation of 4 mM ferrocene in 0.2 M and 0.45 M TBAP, the averaged I_l was found to be (-3.4 ± 0.1) x 10^{-4} C/$s^{-1/2}$ for a scan rate range of 0.1 – 2.0 V/s. Conversely, the I_l for 4 mM of acetate decreased with increased viscosity, as shown in **Table 2.4**. The findings for the limiting currents indicate a reduced current signal due

to the concentration of electrolytes. Hence, because acetate anions are charged molecules, ionic interactions and the ionic strength of the solution are expected to play a role. It should also be noted that while pipetting, the solutions appeared to be more viscous with increasing concentrations of electrolytes.[62]

Table 2.4
Decrease in the reported limiting current from convolution analysis once the concentration of the supporting electrolyte is increased for the direct electrolysis of 4 mM tetra-n-butylammonium acetate

Molarity of TBAP (M)	*(I_l x10^4) Convolution $C/s^{-1/2}$*
0.10	2.58 ± 0.01
0.20	2.40 ± 0.01
0.30	2.25 ± 0.02
0.45	1.18 ± 0.09

2.5. Conclusions.

Tetra-n-butylammonium acetate was utilized as a reference model to establish a protocol for investigating the dissociative electron transfer of Kolbe's electrolysis via convolution voltammetry. Conclusive findings can be made with regards to the dissociative electron transfer mechanism for acetate anion.

- A concerted dissociative electron transfer is observed via conventional analytical approaches for the electrolysis of acetate with a reported average of $\alpha = 0.32 \pm 0.02$. The findings are in disagreement with the stepwise dissociative electron transfer mechanism as reported by Gonzáles and coworkers. The latter reported a one-electron electrode process with $\alpha \pm 0.55$.
- Convolution voltammetry for addressing the mechanism of Kolbe's electrolysis is first reported in this work. The convolution data was in agreement with our reported conventional analytical approaches. Contrary to established literature, both

methods confirmed dissociative electron transfer via a concerted mechanism with an agreement in the reported value of an average α = 0.32 ± 0.02. Due to the extremely hygroscopic nature of the carboxylate anions, even more rigorous experimental conditions were followed and thus, we hypothesize that trace amount of water play a role in the observed discrepancy in this study and the published work of Gonzáles and coworkers. These effects will be addressed to a great extent in **Chapter 3**.

- Convolution voltammetry was successfully utilized to evaluate an experimental value for the oxidation potential (E^o) of the tetra-n-butylammonium acetate which is found to be 0.60 ± 0.10 V vs. Ag/(0.1 M) $AgNO_3$ (0.121 ± 0.10 vs. NHE). The value is found to be consistent with the thermodynamically estimated value by Eberson and coworkers (1.30 ± 0.10 V vs. NHE).[55]
- The effects of varying the concentration of TBAP supporting electrolyte and tetra-n-butylammonium acetate were investigated to ensure consistency and reproducibility. Despite the fact that a decrease in both peak and limiting currents was noted for higher concentrations of TBAP, no significant difference was reported for the calculated alpha and oxidation potentials for acetate anions under anhydrous conditions.
- PFG NMR and convolution analysis were utilized to further investigate the effects of higher concentrations of the supporting electrolyte on the diffusion coefficient of the substrate. Ferrocene was utilized as a neutral, well-behaved and reversible model for this series of experiments. PFG NMR produced diffusion coefficient values with a discrepancy of 0.5 x 10^{-5} cm^2/s in comparison to the lower values

generated via convolution analysis. Findings obtained from this comparative study indicate that an ideal system for investigating the electrochemical oxidation of an acetate system would feature a TBAP concentration range between 0.2 M to 0.30 M in order to reduce discrepancies between the diffusion coefficients reported by convolution voltammetry and PFG NMR. However, it is important to stress that the observed decrease in peak current had no significant effects on the kinetics or thermodynamic parameters of acetate anion, thus further validating findings. In addition, a comparative analysis of the diffusion coefficients obtained from these two techniques further confirm established findings of a one electron electrode process for the dissociative electron transfer mechanism of acetate.

- Deuterated acetonitrile had no significant impact on the reported mechanisms or oxidation potential of acetate anions or diffusion coefficients. Contrary to prior reports, both conventional and convolution analysis indicated the presence of a concerted mechanism. Given this discrepancy, it is important to further investigate this mechanism for other derivatives of aliphatic carboxylates that will undergo similar dissociative electron transfer as acetate (**Chapter 3**).

2.6. General Techniques.[49]

2.6.1. Linear sweep voltammetry (LSV) and cyclic voltammetry (CV).

Linear sweep voltammetry (LSV) and cyclic voltammetry (CV) represent conventional electroanalytical approaches for studying the electrode reactions kinetics of organic and inorganic compounds. Both techniques involve varying the electrode potential in a linear fashion with respect to time, with the goal of inducing a reduction (or oxidation) of the compound of interest. (The following discussion considers an electrochemical reduction, but the same principles apply for oxidations, with n = -1). Specifically, the current (*i*) passed over the course of the reaction (*t*) is related to the concentration (*C*) of the analyte as defined in Faraday's Law. Current can also be represented in terms of charge (q), as shown in **Eq 2.8.**

$$i = \frac{\partial q}{\partial t} = nF\frac{\partial C}{\partial t} \qquad \textbf{(2.8)}$$

The flow of electrons throughout the reaction, to or from the surface of the electrode, results in a circuit current. Monitoring the latter (as a linear function of applied potential, see below) will generate a cyclic voltammogram, which features distinctive characteristics corresponding to the particular phases in the electrode reaction, as discussed below.

The applied potential at any given time (E_t) during the course of a reaction is defined in **Eq 2.8** and **2.9**, where E_i is the initial applied potential, υ is the scan rate, t is time and λ is time at switching potential point. Let us assume that a system featuring reduced (R) and oxidized species (O) is present (**Eq 2.11**); under such circumstances, an electron transfer (e^-) will occur at certain potentials. When the applied potential at the electrode surface approaches the reduction potential of the substrate (O), a significant increase in the current will occur. The current will then diminish when all the O species at the electrode surface are eliminated. In short, the depletion of the O

species at the electrode causes the current to drop; at that point the system becomes limited by the diffusion of the O species in the electrode region (**Figure 2.7**).

$$E_t = E_i - vt \quad \textbf{(2.9)}$$

$$E = E_i - 2v\lambda + vt \quad \textbf{(2.10)}$$

$$O + ne^- \rightarrow R \quad \textbf{(2.11)}$$

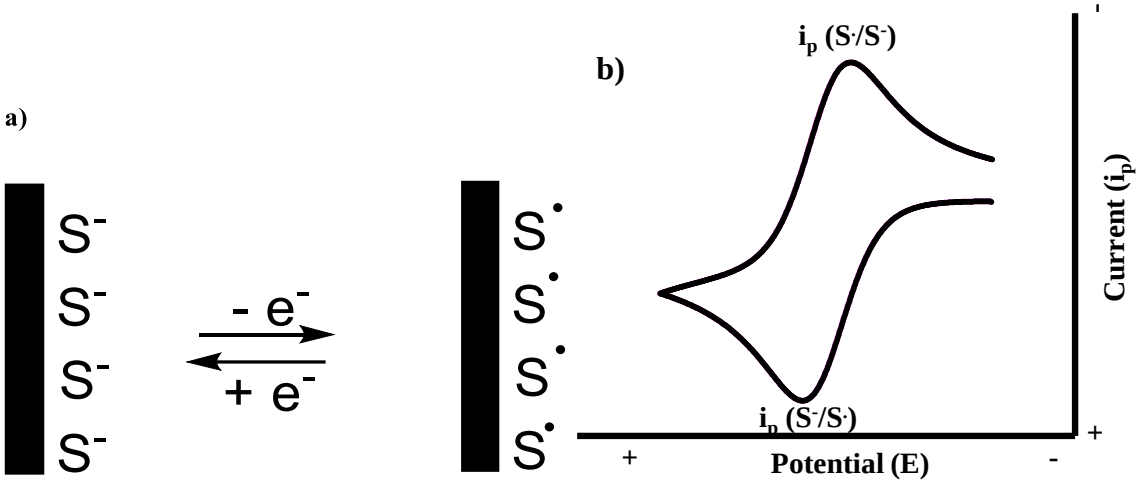

Figure 2.7. a) Represetative scheme of oxidation and reduction of a substrate (S) at the surface of the electrode, b) Corresponding cyclic voltammogram for a reversible system with with oxidative and reductive peak currents as a function of applied potential.

At a given time (t = λ), the direction of the applied potential is reversed, thereby inducing the oxidation of the R species, as well as a similar current wave in the opposite direction (**Eq 2.10**). If only one sweep is obtained, however, it is considered unidirectional and referred to as LSV (Linear Sweep Voltammetry). In the case of a bidirectional sweep—during which the O species is reduced and re-oxidized—it is known as CV (Cyclic Voltammetry). In the case of bidirectional sweeps, **Eq 2.9** is applied for the reduction sweep (forward wave), whereas **Eq 2.10** is specific for the oxidation sweep (reverse wave).

These two conventional electroanalytical approaches provide valuable insights into the thermodynamics and kinetic mechanisms of a given system—principally due to the fact that one can precisely tune the driving force by applied potential (thermodynamics) and measure the current (kinetics of the reaction) simultaneously. The applied potential can also be modified per unit time in a linear fashion to monitor changes in the kinetics at the surface of the electrode; the resulting data is known as the scan rate. For instance, one can oxidize a given electroactive compound at a scan rate of 0.1 V/s or 1.0 V/s, thereby examining any changes in the shape and characteristics of the obtained cyclic voltammograms as a result of altering the scan rate. These methodologies also provide data on reversibility, the number of transferred electrons, and the reduction potential of a species. For example, in considering a fully reversible system that exhibits Nernstian behavior (**Figure 2.7**), its reduction potential can be determined from the cyclic voltammograms, as shown in **Eq 2.12,** where E_{p_a} and E_{p_c} are anodic and cathodic potential peaks, respectively.

$$E^o = \frac{E_{p_c} + E_{p_a}}{2} \qquad \textbf{(2.12)}$$

A peak difference of 58 mV at 25 ^oC corresponds to a one-electron transfer process and characterizes a reversible wave. An electroactive compound that follows Nernstian behavior will reach thermodynamic equilibrium fairly rapidly due to the accelerated electron transfer kinetics between the reduced and oxidized forms at the electrode. The resulting cyclic voltammograms for an electroactive compound at the surface of the electrode (distance x = 0) with thermodynamic equilibrium will show full reversibility as evidenced by cyclic voltammograms at each scan rate. In addition to reduction potential, both the concentration and number of electrons in an electroactive compound can also be determined.

$$E = E^{o'} + \frac{RT}{nF} ln \frac{C_O(x=0)}{C_R(x=0)} \qquad \textbf{(2.13)}$$

Not all electroactive species, however, are well-behaved reversible couples. A significant number of essential electroactive species with significant potential for use in biochemical systems can result in either quasi-reversible or irreversible cyclic voltammograms with lesser cathodic peaks or no cathodic peak, respectively (**Figure 2.8**). Such quasi-reversible or irreversible behaviors indicate a system with no thermodynamic equilibrium. As the oxidized species is reduced, it becomes unavailable at the surface of the electrode for a follow-up reduction. This subsequent chemical reaction, which consumes the reduced species to form a product, is a one possible contributor to removing the generated oxidized species. Hence, upon switching the potential, the concentration of reduced species present on the surface of the electrode for oxidation is either reduced or eliminated—thus, little to no reversed peak will be observed in the CV.

The rate of which the follow-up chemical step proceeds represents a defining characteristic of each system. For quasi-reversible species, the chemical step is typically the rate-limiting step; as such, reversibility can be established if (and only if) the rate to re-oxidize the reduced species is faster than the rate of the follow-up chemical step. For example, the electrochemical oxidation of carboxylate salts will follow this trend; when the rate of follow-up chemical step is observed to be 10^9 M/s, the system will display complete irreversibility (no backward wave).[63] When the reversibility of a system cannot be reestablished experimentally, it becomes challenging to work with. Additionally, an irreversible system produces unwanted variations to the peak potential, which is a function of both the rate of the follow-up step (k) and the reduction potential of the species (E^o) (**Scheme 2.1** and **Figure 2.8**)

$$O + ne^- \rightarrow R \xrightarrow{k} Products$$

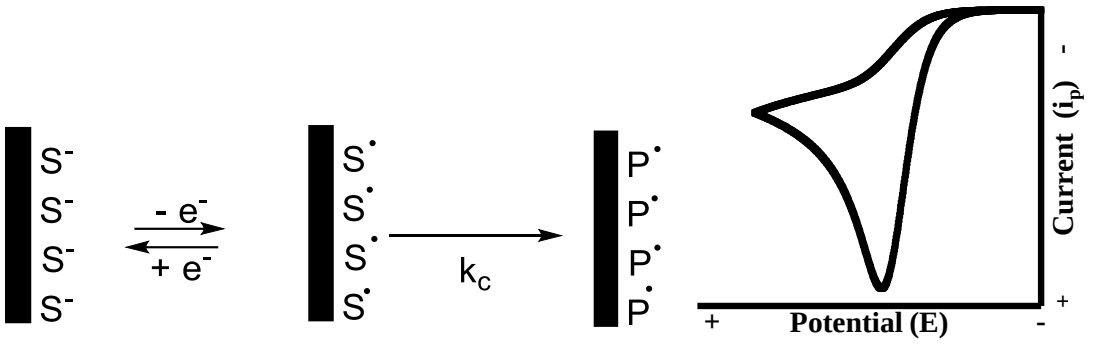

Figure 2.8: Follow-up chemical step depleting the oxidized form of the substrate ($S^{\cdot}$) at the surface of the electrode resulting in an irreversible CV profile

Despite the fact that thermodynamic information can be difficult to obtain for an irreversible system, other valuable kinetic information such as rate of electron transfer and associated mechanisms can be investigated (**Section 2.1.2**). Prior to investigating a particular system, however, one must determine whether electron transfer or the follow-up chemical step represents the rate-limiting step. In such cases, it is necessary to "diagnose" essential components of the cyclic voltammograms. As shown in **Table 2.5**, important diagnostic criteria are based on two datapoints (E_p *and* $E_{p/2}$) collected from each cyclic voltammogram in order to characterize the rate limiting step as either the electron transfer or the follow-up chemical step.[31,64]

Table 2.5
Diagnostic criteria established by Savéant and coworkers for electron transfer kinetics at the surface of the electrode

Rate limiting Step	$\boldsymbol{E_p - E_{p/2}}$ **(mV)**	$\boldsymbol{\partial E_p/\partial log v}$ **(mV)**
Electron Transfer	95	59
Chemical Step (first order)	48	30

Typically, scan rates that range over three orders of magnitude are required for elucidating the mechanisms of rate-limiting step. If dissociative electron transfer proves to be rate-limiting

step, further analysis is required to thoroughly evaluate its mechanisms and determine if it occurs via a concerted or stepwise pathway based on calculated transfer coefficient (see Savéant and coworkers)[35,36,65] (**Eq 2.14** and **2.15** where α_{avg} is the averaged transfer coefficient, $k_o$is the standard electron transfer rate, and $R, T, F, v, E^o, E_p, E_{p/2}$ are their normal definitions). Therefore, cyclic voltammetry represents an essential tool for investigating a system's kinetic and thermodynamic behavior. It must be noted, however, that CV is not without its drawbacks—particularly when used to investigate carboxylate systems.

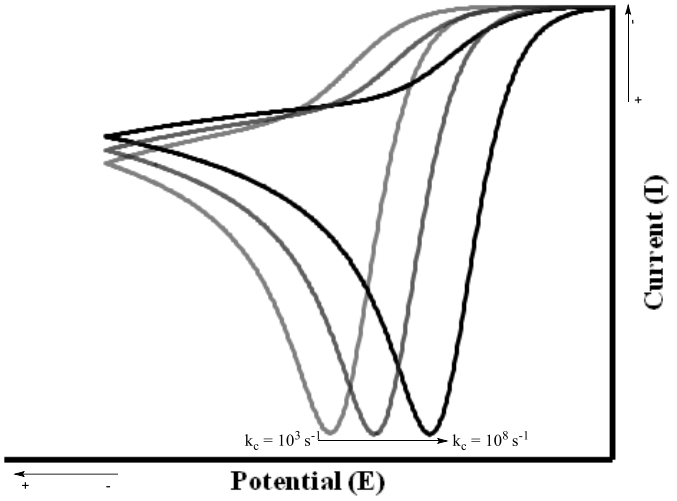

Figure 2.9. A shift in the peak potential as a function of the rate of the follow-up chemical step for irreversible systems. Cyclic voltammograms were generated by digital simulations using DigiSim software.

$$E_p = E^0 + 0.78\left(\frac{RT}{\alpha_{avg}F}\right) - \left(\frac{RT}{\alpha_{avg}F}\right)\ln\left(k_o\sqrt{\frac{RT}{\alpha_{avg}FvD_o}}\right) \quad \textbf{(2.14)}$$

$$E_p - E_{P/2} = 1.86\left(\frac{RT}{\alpha_{avg}F}\right) \quad \textbf{(2.15)}$$

2.6.2. Predicted mass transport and defaults in CV techniques.

The use of conventional electroanalytical techniques such as CV presents some inherent limitations when used to investigate systems that are not well behaved and/or irreversible. In particular, systems with highly resistive solutions and sluggish heterogeneous kinetics are difficult to investigate using these established techniques. Most importantly, while it is not possible to obtain data on the oxidation potential of a system under heterogeneous electron transfer control via LSV (or irreversible CV) (**Eq 2.14**), such information can be obtained using convolution voltammetry. The analytical potential of convolution voltammetry emerged from the reformulation of mathematical models for addressing mass transport via cyclic voltammetry. This section will address major the pitfalls associated with utilizing Fick's second law for determining the diffusion-controlled signal via cyclic voltammetry. To address the limitations in cyclic voltammetry, one must first elucidate the fundamental mathematical operations that govern the relationship between time-dependent mass transport and generated current signal, which applies to any electroactive species upon application of an electrode potential. This dissertation, however, will focus on experimental and instrumental limitations for cyclic voltammetry. For a more extensive list of other electroanalytical methods, the reader is referred to the work by authors such as Keith Oldham and Morten Grenness.[38-40]

2.6.3. Mass transport and linear diffusion (Cottrel Equation).

In electroanalytical techniques, a given current refers to a direct measurement of the number of electrons produced upon the reduction or oxidation of a particular concentration (C_o) of a molecule. The mechanisms involved in the mass transport of species to the surface of the electrode are important, especially since solutions are a dynamic media. In other words, the current is dependent on the concentration of species near the electrode surface. In the case of semi-infinite,

linear mass transport, three major mechanisms control the mass transport of electroactive species to the surface of the electrode: convection, migration and diffusion. Mass transport towards the electrode surface for a one-dimensional model is defined by the Nernst-Plank equation (**Eq 2.16**). This one-dimensional mathematical model reveals the flux of the species (J_x in mol/s cm^2) at a distance x as a function of these three mechanisms.[49]

The first, convection, results from perturbations in the solution (e.g., from stirring or vibrating), which then contributes to the overall rate of transport of the molecules towards the electrode. This relationship is defined in terms of the velocity of v(cm/s) of a species with a known concentration of C_o (mol/L) in a solution.[49] The second mechanism, migration, arises from the motion of an ion towards a charged electrode due to a potential gradient; this phenomenon can be defined in terms of the potential gradient ($\partial\phi/\partial x$), which is governed by the concentration (C_o) and known charge (z_o) of the species. The final mechanism, diffusion, results from the concentration gradient at a distance x ($\partial C/\partial x$) for a species with a known diffusion coefficient (D_o in cm^2/s).

$$J_o(x\,,t) = D_o\frac{\partial C_O(x,t)}{\partial x} + \frac{z_i F}{RT}D_o C_o\frac{\partial \phi(x)}{\partial x} + C_o v(x) \qquad \textbf{(2.16)}$$

$$J_o(x\,,t) = D_o\frac{\partial C_O(x,t)}{\partial x} \qquad \textbf{(2.17)}$$

$$\frac{\partial C_O(x,t)}{\partial t} = D_o\frac{\partial^2 C_O(x,t)}{\partial x^2} \qquad \textbf{(2.18)}$$

In the case of cyclic voltammetry, the diffusion of the electroactive species represents the most significant experimental contributor to current signal. Although all three mechanisms indicate the motion of electroactive species to the surface of an electrode in solution, both convection and migration can be eliminated experimentally, which results in a rather simplified mathematical model for mass transport (**Eq 2.17 – 2.18**). In the absence of any perturbations to the solution, one can eliminate increased mass transport due to convection. The addition of high

concentrations of fully dissociated supporting electrolyte ensures that no-charge migratory effects will occur due to a buildup of the electric gradient in the solution. The electric gradient is due to the capacitance charge buildup near the surface of the electrode as the potential is applied to the solution.

Even utilizing a simplified model, solution diffusion can be difficult to analyze—in part because it is highly dependent on several mechanisms that take place at the surface of an electrode over a given time period (*t*). For each applied potential as a function of time, the concentration gradient of the molecules at the surface of the electrode varies accordingly, which then inevitably impacts the resulting generated current. In other words, a concentration gradient of molecules for a given distance during an electrochemical process is a direct representation of the net number of moles of a given molecule per unit time per unit area. Hence, quantifying a given concentration of a molecule at a given distance from electrode (*x*) and time (*t*) is essential for evaluating any electrode reaction.[49]

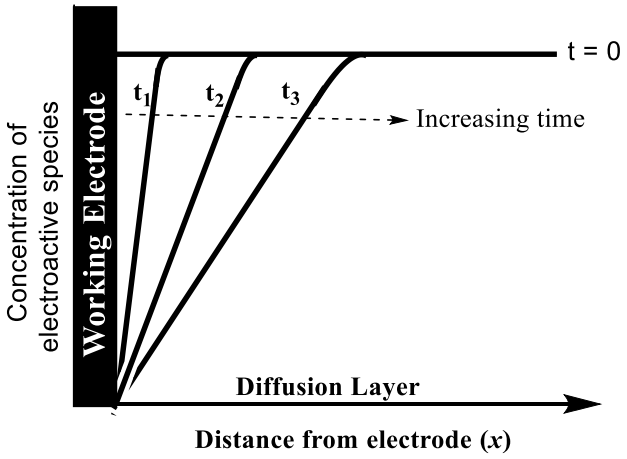

Figure 2.10. Representative scheme of the depletion of an electroactive species as a function of distance from the surface of the electrode ($\partial C/\partial x$) through the diffusion layer at a given scan rate (*v*/s).

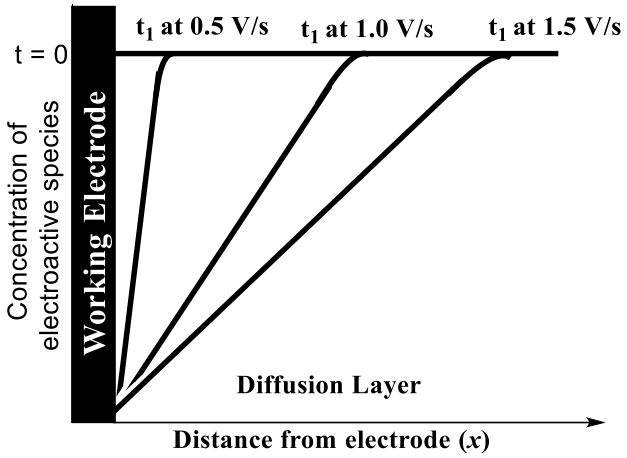

Figure 2.11. Representative scheme of the rate of depletion of an electroactive species based on the scan rate at the surface of the electrode. Faster scan rates result in higher rates of depletion

As mentioned previously, the use of cyclic voltammetry for investigating electrochemical processes is highly dependent on the diffusion process of a molecule to the surface of the electrode. Additionally, as shown in **Eq 2.18**, resulting diffusivity data is not only dependent on the diffusion properties of the molecule, but also on the geometry and nature of the electrode. Cyclic voltammetry, in particularly, features an electrode with a planar geometry; thus, linear diffusion must also be taken into account. The "linear diffusion assumption" is insufficient for solving Fick's second law—a set of initial and semi-infinite conditions is also necessary. Specifically, initial boundary conditions take into account the homogeneity of a solution prior to electrolysis (**Eq 2.19 - 2.20**); after electrolysis, a complete depletion of the species will occur near the electrode surface at a distance *x* with no disturbance to the bulk concentration occurs. In addition, potential sweep boundary conditions represent the changes in concentration gradient due to the applied potential over the course of the reaction (**Eq 2.21**).

$$C_O(x, 0) = C_O^* \quad \textbf{(2.19)}$$

$$\lim_{x\to\infty} C_O(x, t) = C_O^* \quad \textbf{(2.20)}$$

$$\frac{C_O}{C_R} = \theta S(t) = \exp[\frac{nF}{RT}(E_i - E^{0\prime})]\exp(\frac{nF}{RT}vt) \quad \textbf{(2.21)}$$

These boundary conditions simplify the solution to the concentration gradient. As a consequence, a direct current-time relationship at a given potential can be determined, which is known as the Cottrel equation, where D_o is the diffusion coefficient of a molecule in a given solution. Also important to note is that the solution is highly dependent on the starting potential (E_i) and scan rate (υ). For more detailed mathematical workup of the Cottrel equation, readers are referred to the citations herein. [66,67]

$$i_{(t)} = \frac{nFAD_o^{1/2}C_o^*}{\pi^{1/2}t^{1/2}} \qquad \textbf{(2.22)}$$

2.7. Experimental and instrumental limitations.

The principal advantage of various **e**lectroanalytical methods is their use in developing mathematical models to represent a time-dependent current response based on the concentration of species in a solution. The corresponding mathematical model for cyclic voltammetry assumes that the current corresponds *only* to the concentration of electroactive species undergoing electrolysis, which diffuses in a linear manner towards a planar electrode surface. The drawback of this model, however, is that the application of a potential at the surface of an electrode typically leads to the rearrangement of solvated ions in solution, which subsequently results in a buildup of a capacitance layer. When this occurs, a non-faradiac "capacitive current" is produced that is independent of the redox process for an electroactive species at the surface of an electrode (**Figure 2.12**). This accumulated capacitance varies with applied potential, which is a fundamental component of cyclic voltammetry. Thus, the capacitive current is an unavoidable process that contributes to the overall current generated via electrolysis.

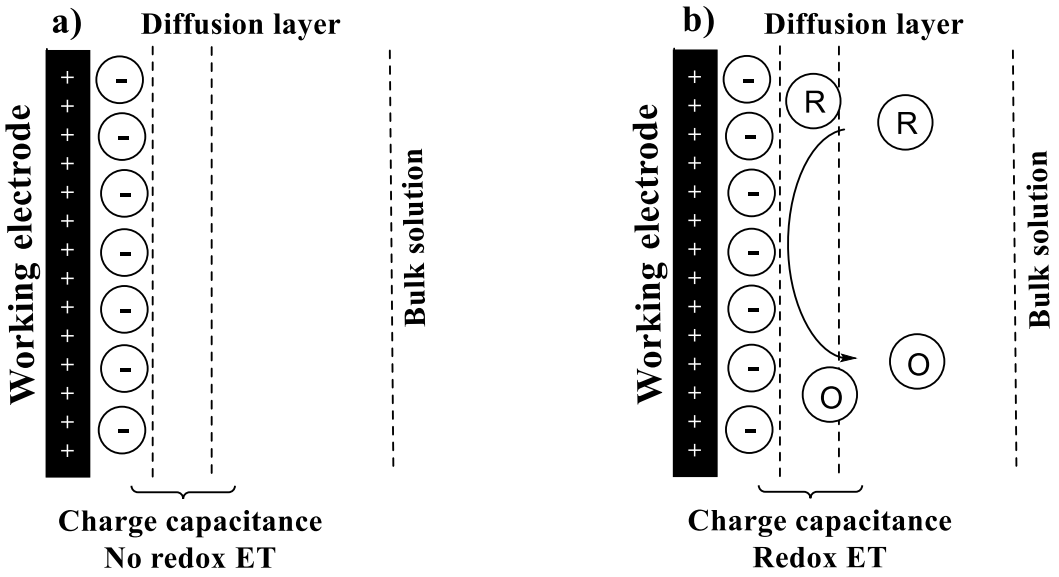

Figure 2.12 Applied potential at the surface of an electrode, resulting in a build-up of capacitive current a) in the absence, and b) in the presence, of a redox ET process for an electroactive species

It is critical to consider and compensate for the presence of a non-faradaic current—given that it contributes to the overall signal and can vary significantly with the range of scan rates applied to the surface of an electrode. For example, when one increases the scan rate, higher potential is applied over a shorter time interval, thereby generating a higher non-faradaic current. The latter is concurrent with the faradaic current generated by the electron transfer process. Research shows, however, a non-faradaic current can be minimized by compensating for background current in the absence of the species of interest in solution. [13,49]

One must also consider certain experimental assumptions associated with mass transport mathematical models, which may not be applicable under all experimental conditions. Recall that electroanalytical techniques are generally based on relating electrode concentration at a given time to the current response recorded by a potentiometer. This relationship is dependent on a mass transport occurring on a perfectly flat and planar electrode in a linear diffusion-based mode. Although the majority of the electrode surface area is indeed flat, curvatures and ill-defined edges

are typically present. Nonetheless, the current contribution from these areas is usually considered to be insignificant in comparison to the overall current generated from the surface of the electrode.[39,40]

2.8. Semi-integral and convolution voltammetry.

Convolution voltammetry is a well-established electrochemical tool that can be used in solving the Cottrell equation in a semi-integration approach in order to eliminate the time dependence ($t^{-1/2}$) of the current (i). Oldham and coworkers were the first to validate the use of the semi-integration operator $\partial^{-1/2}/\partial t^{-1/2}$ as mathematically linear and equivalent to the original semi-differentiation operator utilized for solving Fick's second law (**Eq 2.23**). This semi-integration method solves Fick's second law by incorporating similar initial and semi-finite boundary conditions as a semi-differentiation method.[38-40] However, since potential sweep boundary conditions are eliminated, it instead establishes a direct link between the concentration of electroactive species at the surface of an electrode and the faradaic current density (**Eq 2.24** and **2.25**). Consequently, the convolution model eliminates the dependence on both the scan rate and applied potential; nor does it require any additional assumptions concerning the kinetics or the specific mechanisms of electron transfer.[45,49]

$$J(0,t) = \frac{\partial C_O(x,t)}{\partial x} = D_o \frac{\partial^2 C_O(x,t)}{\partial x^2} = -\frac{1}{D^{1/2}} \frac{\partial^{1/2} C_O(x,t)}{\partial t^{1/2}} \quad \textbf{(2.23)}$$

$$J(0,t) = -\frac{C^* i(t)}{nF} = \frac{i(t)}{vF} \quad \textbf{(2.24)}$$

$$C_o(t) = C^* - \frac{1}{nFAD^{1/2}} \frac{\partial^{-1/2} i}{\partial t^{-1/2}}(t) \quad \textbf{(2.25)}$$

Based on Oldham's work, Savéant adopted a semi-integral approach for processing the (i-t) experimental output profile to generate a mass-transfer independent current (I_{conv}).[39,40,48] The convolution function (I_{conv}) can be determined easily through the use of computing software (**Eq**

2.26). More importantly, the experimental voltammetric current and the convoluted currents can be utilized to calculate the heterogeneous rate constant of the dissociative electron transfer for the *i(t)-E* data from cyclic voltammograms.

$$I_{conv} = \pi^{-\frac{1}{2}} \int_0^{\tau} \left[\frac{i_u}{(t-u)^{\frac{1}{2}}} \right] du \qquad \textbf{(2.26)}$$

$$I_{conv} = \pi^{-\frac{1}{2}} \int_{j=1}^{j=k} \left[\frac{i_{\left(j\Delta t - \frac{1}{2}\Delta t\right)} \cdot \Delta t^{\frac{1}{2}}}{\sqrt{(k-j+\frac{1}{2})}} \right] du \qquad \textbf{(2.27)}$$

2.9. Experimental Techniques.

2.9.1. Electrochemical instrumentation and electrochemical apparatus.

Cyclic voltammetry and controlled current coulometry were performed on an EG&G Princeton Applied Research (EG&G/PAR) Model 283 potentiosat/galvanostat.

2.9.1.1. Cyclic voltammetry (CV).

Cyclic voltammetry was carried out in a conventional three-electrode cell utilizing a 3.2 mm diameter glassy carbon (GC) electrode as a working electrode, with a measured active surface area of 0.18 cm^2. A platinum coil was used as an auxiliary electrode and the reference electrode was Ag/Ag^+ (0.1 M in CH_3CN, 0.337 V vs. SCE). The reference electrode potential was confirmed against ferrocene (E^o = 0.030 ± 0.005 V). Prior to use, the GC electrode was sanded and polished with alumina slurry (Buehler) in the decreasing order of 1.0 μM, 0.3 μM, and 0.05 μM on a micro-cloth. The electrode was then rinsed with an isopropyl/DI water solution and subsequently sonicated in isopropyl alcohol/water solution prior to use. Due to adsorption of carboxylates by-products to the surface of the electrode during consecutive scans, the GC was polished with a damp microcloth treated with with 0.05 μM alumina and rinsed several times with acetonitrile solution.

The active surface area of the electrode was determined via voltammetric measurements to be 0.18 cm^2 (**Appendix C**). All voltammetric measurements were performed inside the glovebox at 27 ^oC, as measured by a thermometer, unless stated otherwise. All experiments were performed under inert atmosphere (glovebox) with dried glassware stored in an oven at 110 ^0C; all CVs were performed with 95% IR compensation. Scan rates varied from 0.05 – 2.5 V/s. It is important to note that the solution was stirred prior to each scan. Thus, any decrease in the observed peak current does not reflect the decrease in the concentration of the reactant at the electrode surface, but rather a decline in electrode activity. The latter became more apparent for more highly concentrated solutions in which a drastic decrease in peak current was observed between consecutive runs.

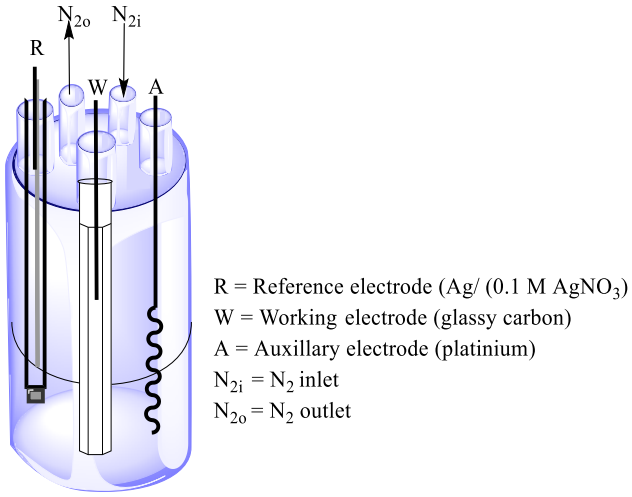

Figure 2.13. Specialty design five neck electrochemical cell for cyclic voltammetry

2.9.2. PFG NMR.

All ^1H PFG-NMR diffusometry experiments were performed using a 600 MHz Bruker Avance III NB NMR spectrometer, equipped with a TBI probe and 5 mm ^1H coil coupled to a single-axis (z-

axis) gradient system. In the PFG NMR experiment, measured signal amplitude *I* as a function of gradient strength, *g*, was fit to the Stejskal-Tanner equation,[68-70]

$$I = I_o e^{-D\gamma^2 g^2 \delta^2 (\Delta \frac{\delta}{3})} \quad \textbf{(2.28)}$$

where I_0 the signal amplitude at g = 0, γ the gyromagnetic ratio, δ the effective gradient pulse length, Δ the diffusion time between gradient pulses, and *D* the self-diffusion coefficient. The simple and robust pulsed-gradient stimulated echo (PGSTE) sequence was used with a $\pi/2$ pulse length of 13.7 μs. A repetition time of 5.3 s, effective gradient pulse length of δ = 5 ms (actual pulse length = 1.57 x effective gradient pulse length for the half sinusoid gradient pulse), and a diffusion time Δ = 500 ms were used for ^{1}H diffusion measurements. Maximum gradient strengths were adjusted in the range 25 – 62 G cm^{-1} to achieve 80% signal attenuation in 16 steps. Sufficient signal-to-noise ratio (SNR) for each data point was achieved with 4 – 8 scans and an acquisition time of 4.8 s.

2.10. Materials.

HPLC-grade solvents were utilized as received unless otherwise stated. All glassware was stored at 110 ^{o}C prior to assembling. A fractional distillation setup was designed with specially designed glassware to ensure that a sealed apparatus was utilized. The apparatus was purged with dried nitrogen for 30 minutes prior to being sealed. Acetonitrile was stirred over calcium hydride overnight prior to distillation. HPLC-grade acetonitrile was distilled slowly at 70 ^{o}C over calcium hydride under dried nitrogen passed over a column of 4A molecular sieves. Distilled acetonitrile was stored over dried molecular sieves and sealed prior to being disconnected and transferred to the glovebox. Distilled acetonitrile was then passed over activated alumina before use. All solvents and starting materials were obtained from Sigma-Aldrich unless otherwise stated.

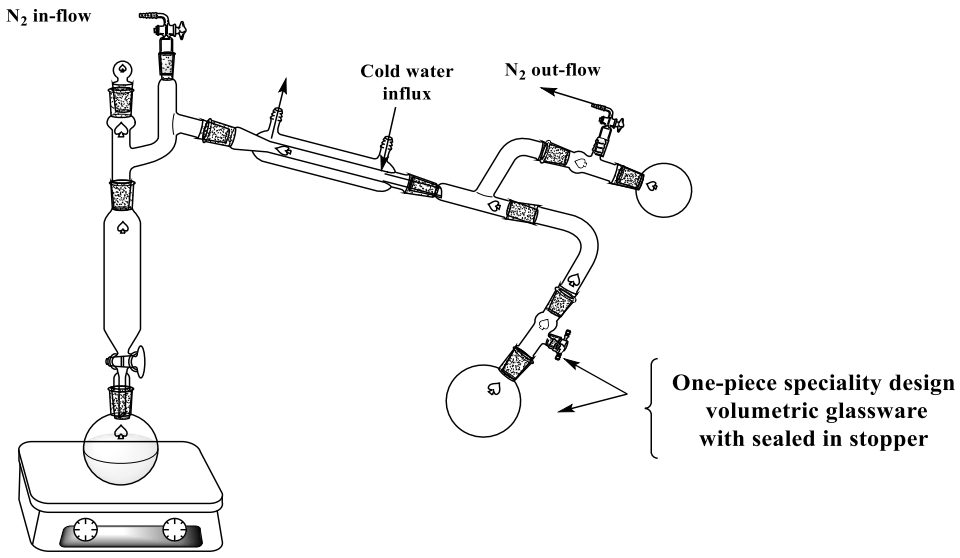

Figure 2.14 Fractional distillation of the HPLC grade acetonitrile over calcium

2.11. Experimental Syntheses

2.11.1. Tetra-n-butylammonium methoxide.

Tetra-n-butylammonium bromide was dissolved in a minimal amount of methanol. An equimolar ratio of silver oxide powder was added slowly to the solution while stirring with a magnetic bar for an hour. The glassware was covered with a wash glass to avoid evaporation of methanol over time. A greenish-grayish powder was formed that settled to the bottom of the beaker. Additional silver oxide (1/3 ratio) was added to the solution and allowed to stir for an additional two hours. The supernatant of the solution was tested for bromide with a diluted nitric acid solution. If yellowish-white precipitate was observed, additional silver oxide was added and allowed to stir. After a negative bromide test, the mixture was filtered over Celite column.

2.11.2. Tetra-n-butylammonium acetate.

Tetra-n-butylammonium hydroxide (Aldrich, 1 M in methanol) was added to an equal molar ratio of acetic acid (Aldrich, anhydrous) at 22 ^{o}C. The reaction mixture was rotovapped at 45 ^{o}C under vacuum and the resulting white salt was recrystallized with ethyl acetate. The crystals were filtered

and stored in a vacuum oven at 68 ^{o}C overnight, and dried over P_2O_5 in a vacuum desiccator for 24 hours. The sealed desiccator was placed into the glovebox prior to opening.1H NMR ($CDCl_3$, 400MHz) δ 0.95-1.05 (t, 12H), 1.95 (s, 3H), 1.35-1.45 (sex, 8H), 1.52-1.65 (quin, 8H), 3.20-3.30 (t, 8H). The findings are consistent with reported literature.[71]

2.11.3. Tetra-n-butylammonium perchlorate (TBAP).

Tetra-n-butylammonium perchlorate (Bu_4NClO_4) was prepared via an ion exchange reaction. Tetra-n-butylammonium bromide was fully dissolved in deionized water (DI) using a magnetic stirrer and a heat gun. 70% perchloric acid was added in an equimolar ratio to tetra-n-butylammonium bromide. The resulting Bu_4NClO_4 was washed with cold DI water (2 L) until clear aliquots were noted and tested for a neutral pH with litmus paper. The solid was dried overnight in a vacuum oven at 78 ^{o}C. For recrystallization, the solid was dissolved in a minimal amount of ethyl acetate with continuous controlled heating and continuous stirring with a magnetic bar to yield a transparent solution. Small aliquots of hexane were added to the hot solution to yield a slowly forming, but rapidly disappearing, white precipitant. The addition of hexane and the heating of the solution continued until a persistent white precipitant was formed. The solid was dissolved into solution with heating till a transparent solution was obtained. The solution was cooled to form white needle-like crystals. The recrystallization was performed 3-5 times from ethyl acetate/hexane then dried at 80 ^{o}C in a vacuum oven for 24 hours. A white crystalline solid with 85% yield with a melting point of 213 ^{o}C was dried over P_2O_5 in a vacuum desiccator and then transferred under vacuo into the glovebox. Typically, the melting point of TBAP ranges between 207-214 ^{o}C as evidenced by literature reports.[72]

References

(1) Eberson, L.; Nyberg, K. *J. Am. Chem. Soc.* **1966**, *88*, 1686.

(2) Leung, M.; Herz, J.; Salzberg, H. W. *J. Org. Chem.* **1965**, *30*, 310.

(3) Shukla, S. N.; Walker, O. J. *Trans. Faraday Soc.* **1931**, *27*, 722.

(4) Glasstone, S.; Hickling, A. *J. Chem. Soc.* **1934**, 1878.

(5) Glasstone, S.; Hickling, A. *J. Chem. Soc.* **1936**, 820.

(6) Pande, G. S.; Shukla, S. N. *Electrochim. Acta* **1961**, *4*, 215.

(7) Dickinson, T.; Wynne-Jones, W. F. K. *Trans. Faraday Soc.* **1962**, *58*, 400.

(8) Dickinson, T.; Wynne-Jones, W. F. K. *Trans. Faraday Soc.* **1962**, *58*, 382.

(9) Dickinson, T.; Wynne-Jones, W. F. K. *Trans. Faraday Soc.* **1962**, *58*, 388.

(10) Eberson, L. *Acta Chem. Scand.* **1963**, *17*, 2004.

(11) Koehl, W. J. *J. Am. Chem. Soc.* **1964**, *86*, 4686.

(12) Kochi, J. K. *J. Am. Chem. Soc.* **1963**, *85*, 1958.

(13) Vijh, A. K.; Conway, B. E. *Chem. Rev. (Washington, DC, U. S.)* **1967**, *67*, 623.

(14) Guidelli, R.; Compton Richard, G.; Feliu Juan, M.; Gileadi, E.; Lipkowski, J.; Schmickler, W.; Trasatti, S. In *Pure Appl. Chem.* 2014; Vol. 86, p 245.

(15) Butler, J. A. V. *Trans. Faraday Soc.* **1924**, *19*, 729.

(16) Butler, J. A. V. *Trans. Faraday Soc.* **1924**, *19*, 734.

(17) Conway, B. E.; Dzieciuch, M. *Can. J. Chem.* **1963**, *41*, 21.

(18) Conway, B. E.; Dzieciuch, M. *Can. J. Chem.* **1963**, *41*, 38.

(19) Conway, B. E.; Dzieciuch, M. *Can. J. Chem.* **1963**, *41*, 55.

(20) Bagotzky, V. S.; Vasilyev, Y. B. *Electrochim. Acta* **1964**, *9*, 869.

(21) Gelbshtein, A. I.; Airapetova, R. P.; Shcheglova, G. G.; Temkin, M. I. *Zh. Neorg. Khim.* **1964**, *9*, 1502.

(22) Temkin, M. I. *Doklady Akademii Nauk Sssr* **1965**, *165*, 615.

(23) Smirnov, I. A.; Morozov, N. M.; Temkin, M. I. *Doklady Akademii Nauk Sssr* **1963**, *153*, 386.

(24) Conway, B. E.; Gileadi, E. *Trans. Faraday Soc.* **1962**, *58*, 2493.

(25) Andrieux, C. P.; Nadjo, L.; Savéant, J. M. *J. Electroanal. Chem. Interfacial Electrochem.* **1970**, *26*, 147.

(26) Andrieux, C. P.; Savéant, J. M. *J. Electroanal. Chem. Interfacial Electrochem.* **1970**, *28*, 446.

(27) Andrieux, C. P.; Savéant, J. M. *J. Electroanal. Chem. Interfacial Electrochem.* **1970**, *26*, 223.

(28) Andrieux, C. P.; Nadjo, L.; Savéant, J. M. *J. Electroanal. Chem. Interfacial Electrochem.* **1973**, *42*, 223.

(29) Pletcher, D.; Greff, R.; Peat, R.; Peter, L. M.; Robinson, J. In *Instrumental Methods in Electrochemistry*; Robinson, D., Ed.; Woodhead Publishing: 2010, p 178.

(30) Nadjo, L.; Saveant, J. M. *J. Electroanal. Chem.* **1973**, *48*, 113.

(31) Nadjo, L.; Savéant, J. M. *J. Electroanal. Chem. Interfacial Electrochem.* **1973**, *48*, 113.

(32) Andrieux, C. P.; Gonzalez, F.; Saveant, J. M. *J. Am. Chem. Soc.* **1997**, *119*, 4292.

(33) Andrieux, C. P.; Gonzalez, F.; Saveant, J. M. *J. Electroanal. Chem.* **2001**, *498*, 171.

(34) Galicia, M.; González-Fuentes, M. A.; Valencia, D. P.; González, F. J. *J. Electroanal. Chem.* **2012**, *672*, 28.

(35) Galicia, M.; Gonzalez, F. J. *J. Electrochem. Soc.* **2002**, *149*, D46.
(36) Andrieux, C. P.; Gonzalez, F.; Savéant, J. M. *J. Electroanal. Chem.* **2001**, *498*, 171.
(37) In *Instrumental Methods in Electrochemistry*; Robinson, D. P. G. P. M. P., Ed.; Woodhead Publishing: 2010, p 388.
(38) Oldham, K. B.; Spanier, J. *J. Electroanal. Chem. Interfacial Electrochem.* **1970**, *26*, 331.
(39) Grenness, M.; Oldham, K. B. *Anal. Chem.* **1972**, *44*, 1121.
(40) Oldham, K. B. *Analytical chemistry (Washington)*, *44*, 196.
(41) Nadjo, L.; Savéant, J. M.; Tessier, D. *J. Electroanal. Chem. Interfacial Electrochem.* **1974**, *52*, 403.
(42) Saveant, J. M.; Tessier, D. *J. Electroanal. Chem.* **1975**, *61*, 251.
(43) Savéant, J. M.; Tessier, D. *J. Electroanal. Chem. Interfacial Electrochem.* **1975**, *65*, 57.
(44) Savéant, J. M.; Tessier, D. *J. Electroanal. Chem. Interfacial Electrochem.* **1975**, *61*, 251.
(45) Imbeaux, J. C.; Savéant, J. M. *J. Electroanal. Chem. Interfacial Electrochem.* **1973**, *44*, 169.
(46) Amatore, C.; Nadjo, L.; Savéant, J. M. *J. Electroanal. Chem. Interfacial Electrochem.* **1978**, *90*, 321.
(47) Bieniasz, L. a. K.; SpringerLink *Modelling Electroanalytical Experiments by the Integral Equation Method*; Springer Berlin Heidelberg: Berlin, Heidelberg, 2015; Vol. 2015.
(48) Kissinger, P. T.; Heineman, W. R. *Laboratory techniques in electroanalytical chemistry*; Dekker, 1984.
(49) Bard, A. F., L. *Electrochemical Methods Fundamentals and Applications*; 2 ed.; John Wiley & Sons Inc., 2000.
(50) Antonello, S.; Maran, F. *J. Am. Chem. Soc.* **1999**, *121*, 9668.
(51) Antonello, S.; Maran, F. *J. Am. Chem. Soc.* **1997**, *119*, 12595.
(52) Antonello, S.; Benassi, R.; Gavioli, G.; Taddei, F.; Maran, F. *J. Am. Chem. Soc.* **2002**, *124*, 7529.
(53) Donkers, R. L.; Workentin, M. S. *J. Phys. Chem. B* **1998**, *102*, 4061.
(54) Jandel Scientific Software: San Rafeal, CA; Vol. 3.0 ed.
(55) Eberson, L. *Acta Chemica Scandinavica Series B-Organic Chemistry and Biochemistry* **1984**, *38*, 439.
(56) Conway, B. E.; Vijh, A. K. *Electrochim. Acta* **1967**, *12*, 102.
(57) Eberson, L. *Acta Chem. Scand., Ser. B* **1984**, *38*, 439.
(58) Eberson, L. *Electrochim. Acta* **1967**, *12*, 1473.
(59) Giesecke, M.; Meriguet, G.; Hallberg, F.; Fang, Y.; Stilbs, P.; Furo, I. *Phys. Chem. Chem. Phys.* **2015**, *17*, 3402.
(60) Kim, H.; Revzin, A.; Gosting, L. J. *J. Phys. Chem.* **1973**, *77*, 2567.
(61) Claridge, T. D. W. *High-resolution NMR techniques in organic chemistry*; Elsevier: Amsterdam;London;, 2009; Vol. 27.;27;.
(62) Riley, T.; Tomlinson, C.; James, A. M. *Principles of electroanalytical methods*, 1987.
(63) Hilborn, J. W.; Pincock, J. A. *J. Am. Chem. Soc.* **1991**, *113*, 2683.
(64) 4th ed. / ed.; Bernasconi, C. F., Ed.; Wiley: New York :, 1986.

(65) Galicia, M.; Gonzalez-Fuentes, M. A.; Valencia, D. P.; Gonzalez, F. J. *J. Electroanal. Chem.* **2012**, *672*, 28.

(66) Hempstead, M. R.; Oldham, K. B. *J. Electroanal. Chem. Interfacial Electrochem.* **1984**, *162*, 1.

(67) Nicholson, R. S. *Anal. Chem.* **1965**, *37*, 1351.

(68) Stejskal, E.; Tanner, J. *J. Chem. Phys.* **1965**, *42*.

(69) Callaghan, P. T. *Translational Dynamics and Magnetic Resonance: Principles of Pulsed Gradient Spin Echo NMR*; Oxford University Press: New York, 2011.

(70) Price, W. S. *Concepts in Magnetic Resonance* **1997**, *9*, 299.

(71) Yang, C. T.; Fu, Y.; Huang, Y. B.; Yi, J.; Guo, Q. X.; Liu, L. *Angew Chem Int Ed Engl* **2009**, *48*, 7398.

(72) House, H. O.; Feng, E.; Peet, N. P. *J. Org. Chem.* **1971**, *36*, 2371.

Chapter 3. Oxidative dissociative electron transfer mechanisms for aliphatic carboxylates: The effect of water, hydrogen bonding and structure on the reaction mechanism

Chapter 3 includes original work toward the completion of Ph.D. degree of Marwa Abdel Latif. The author acknowledges the major contributors of Dr. James Tanko, Chair of the committee, and Dr. Jared Spencer, a former doctoral researcher. Bryce Kidd, a doctoral researcher in Dr. Mattson's group provided the PFG NMR measurements and its intellectual content, and Dr. Yafen Zhang, a former doctoral researcher in Dr. John Morris's group provided the XPS measurements.

3. Introduction.

3.1. Substituent effects on carboxylate oxidation.

Several researchers have investigated the effects of substituents on the oxidation of carboxylates in terms of the resulting electron transfer mechanism (**Scheme 3.1**). Savéant et al. examined the effects of arylmethyl substituents on the carboxylate ions ($ArCR_2CO_2^-$) on dissociative electron transfer mechanisms using the conventional electrochemistry. Their findings strongly suggested a stepwise mechanism with $\alpha > 0.5$.[1-3]

Gonzáles et al. recently examined aliphatic carboxylates (RCO_2^-, with R = alkyl) with respect to their substituent effects on the dissociative electron transfer mechanism. Findings pointed to a stepwise mechanism with electron transfer as the rate limiting step for alkyl substituents with R = C_3H_7, C_5H_{11}. Competing rates for the electron transfer and decarboxylation steps were reported for substituents with electron donating and withdrawing groups with R = H_3C, OCH_3, $ClCH_2$. The researchers also reported no significant impact on the stability of the acyloxy radical by incorporating these substituted R-groups.[4] The Gonzáles group showed that the observed shift in the peak potentials align with the computed ionization energy of the carboxylate,

which also suggests a stepwise mechanism. No significant change in the peak potential for these alkyl aliphatic carboxylates was noted unless an electron withdrawing or donating group was present.[4] As discussed earlier, peak potential is a function of not only the oxidation potential, but also the rate of the follow-up chemical step. Therefore, it is challenging to form definitive conclusions regarding radical stabilization effects on the mechanism of the electron transfer for these alkyl carboxylates based only on limited scan range of measurements of E_p.

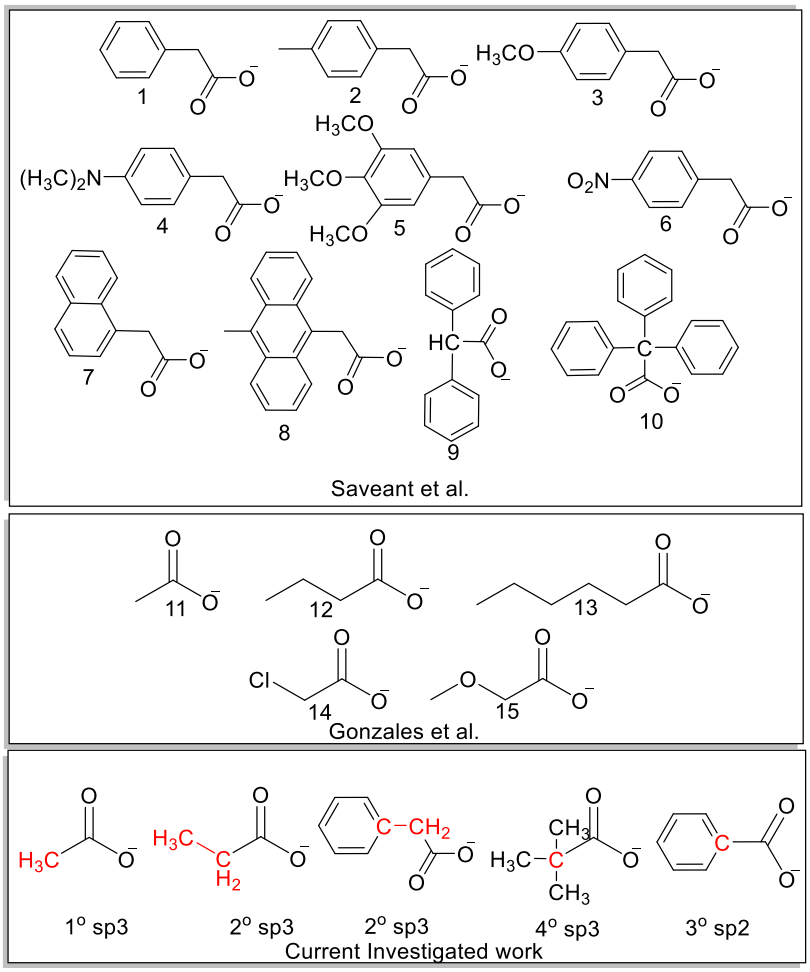

Scheme 3.1 Reported mechanistic studies for the listed carboxylates via conventional electrochemical methods

For this phase of the investigation, we utilized convolution voltammetry to examine the effect of substitution on the oxidation potential of several aliphatic carboxylates (rather than the peak potential, which as discussed, is ambiguous). Specifically, we utilized a relatively similar series of R-substituted aliphatic carboxylates, RCO_2^-, with R = C_2H_5, $t-C_4H_9$, $C_6H_5CH_2, C_6H_5$. Our hypothesis is that if the oxidation of these carboxylates proceeds by a stepwise mechanism, the R group will have little effect on the oxidation potential because this group does not interact directly with the carboxyl moiety: $RCO_2^- \rightarrow RCO_2^{\cdot} + e^-$. In contrast, if the oxidation were concerted ($RCO_2^- \rightarrow R^{\cdot} + CO_2 + e^-$), then the oxidation potential would vary as a function of the stability of the product alkyl radical ($R^{\cdot}$).

3.2. Anticipated effects of R-group on the dissociative electron transfer mechanism.

As discussed in **Chapter 2**, the concerted pathway was found for the dissociative electron transfer for the acetate anion, which implies simultaneous electron transfer and bond breaking to form alkyl radical ($R^{\cdot}$) and carbon dioxide. Substituting acetate's methyl group with an R group that would form a more stable radical is expected lower the oxidation potential if a concerted mechanism is operative. Hence, we anticipated two key results from our convolution experiments. First, the electron transfer mechanism for the investigated aliphatic carboxylates was expected to be consistent with our findings for acetate—i.e., concerted; second, a shift towards a lower oxidation potential ($E^o_{(RCOO^-/R^{\cdot}+CO_2)}$) was expected to follow the trend for radical stabilization energies.

As shown in **Figure 3.1,** the oxidation potential is dependent on the nature of the produced radical for a concerted mechanism; thus, a lower oxidation potential would result from the oxidation that produces a more stable alkyl radical. If the dissociative ET for carboxylate is a stepwise mechanism, there would be no significant shift in the net oxidation potentials between

acetate anion and the other aliphatic carboxylates due to the absence of additional stabilization of the acyloxyl radical by the alkyl groups($E^o_{net} = E^o_{(Rcoo^-/RCOO\cdot)} - E^o_{(RCOO^-/CH_3COO\cdot)}$). In contrast, the nature of the alkyl group is expected to contribute more significantly if a concerted mechanism is employed in the dissociative electron transfer process. The stability of the alkyl radical can be assessed according to the net difference in oxidation potentials between acetate and the other aliphatic carboxylates ($E^o_{net} = E^o_{(Rcoo^-/R\cdot + CO_2)} - E^o_{(RCOO^-/CH_3\cdot + CO_2)}$).

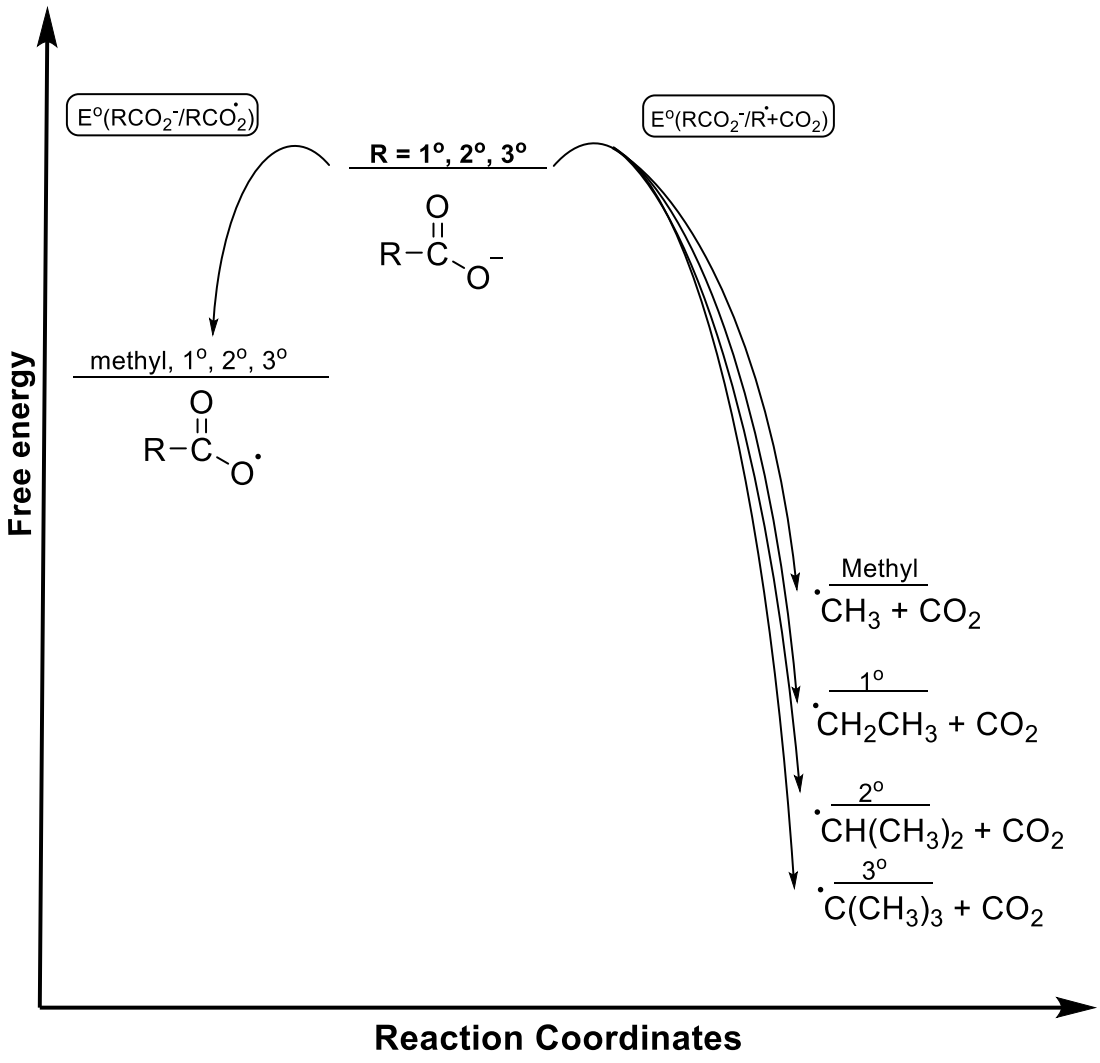

Figure 3.1.Reaction coordinate diagram for the predicted effects of R for the oxidation of RCO_2^- for a stepwise (left) and concerted (right)

If the acid dissociation constants (pK_avalues) of these aliphatic anions are assumed to be similar, then the oxidation potential will be directly related to the C-H bond dissociation energies for CH_4, CH_3CH_3, and $(CH_3)_3CH$ groups, with dissociation energies of 105, 101, and 96.5 kcal/mol, respectively (**Scheme 3.2**). The bond dissociation energies of R-H will reflect the relative stabilities of the corresponding alkyl radicals.

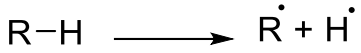

Scheme 3.2 Homolytic cleavage of R-H resulting in the formation of the alkyl radical and hydrogen atom.

Electrochemically, these stabilization energies can be measured as follows: every 23 kcal/mol is equivalent to 1 V shift in the oxidation potential. Hence, convolution voltammetry can be employed to estimate the oxidation potential of these aliphatic carboxylates, after which the experimental difference can be determined when acetate is employed as the reference carboxylate. In accordance with radical stabilization energies, the predicted differences in the oxidation potential with respect to acetate [($\Delta E^o_{net} = E^o_{CH_3COO^-} - E^o_{CH_3CH_2COO^-}$) and ($\Delta E^o_{net} = E^o_{CH_3COO^-} - E^o_{(CH_3)_3CCOO^-}$) are expected to be +0.14 V and +0.29 V for propionate and pivalate, respectively—if the mechanism is concerted (**Table 3.1**).

Table 3.1
Summary of the investigated carboxylates with the expected theoretical net differences in oxidation potential when acetate as the reference model.

R- groups	[a]k_{CO_2} (s^{-1})[5]	BDE (kcal/mol)[6]	Radical Stabilization energy[7] (kcal/mol)	[b]Net stabilization (kcal/mol)	[c]ΔE^o (V)
	10^7	113	-8.9	-8.9	-0.39
	$\approx 10^9$	105	0.0	0.0	0.00
	$\approx 10^9$	93	3.2	3.2	+0.14
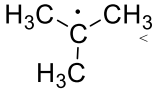	$>10^9$	96	6.8	6.8	+0.29
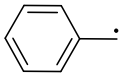	$>> 10^{10}$	90	---	15.0	+0.65

[a]The rate constant for decarboxylation is measured for $RCO_2 \rightarrow R^{\cdot} + CO_2$.[5] [b]The net radical stabilization energies were calculated from the difference in radical stabilization energies of carboxylates in reference to acetate anion except in the case of phenylacetate.,[6,7] [c]The net oxidation potential is representative of the difference between the oxidation potentials for the concerted mechanism ($\Delta E^o = E^o_{CH_3COO^-} - E^o_{RCOO^-}$).

3.3. Results and Discussions.

3.3.1. Conventional electrochemistry of aliphatic carboxylates.

The conventional analysis of the electrochemical oxidation of both propionate and pivalate suggests a concerted mechanism for dissociative electron transfer. **Figures 3.2a and 3.3a** show a linear decrease in the peak current (i_p) as a function of $v^{1/2}$, which corresponds to electron transfer under the diffusion controlled process. **Figures 3.2b - 3.3b** illustrate the peak width as a function of the log υ, indicating an average of 150 mV for both carboxylates with a value α of 0.33 and 0.34 for propionate and pivalate, respectively. Based on these findings, one can conclude that like acetate, both of these aliphatic carboxylates undergo a concerted dissociative electron transfer mechanism (see **Chapter 2**).

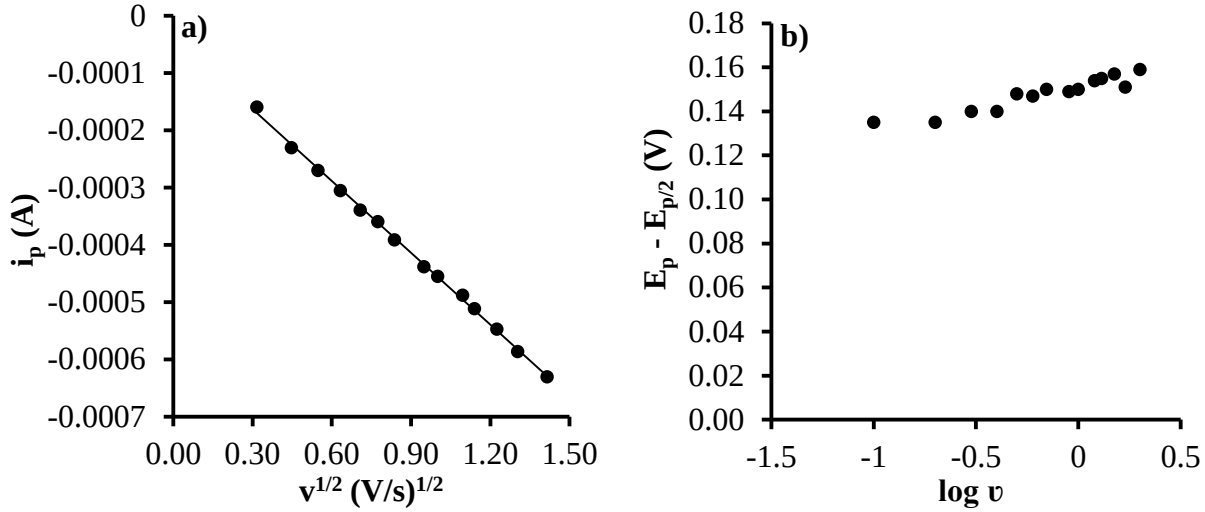

Figure 3.2. Representative plots for conventional analysis for the oxidation of propionate, (a) Linear peak current response to the square root of scan rate showing the electron transfer process under diffusion control, (b) a peak width of 0.14 V is noted as a function of *log v*, corresponding to electron transfer as the rate limiting step with a concerted mechanism and $\alpha = 0.34 \pm 0.01$.

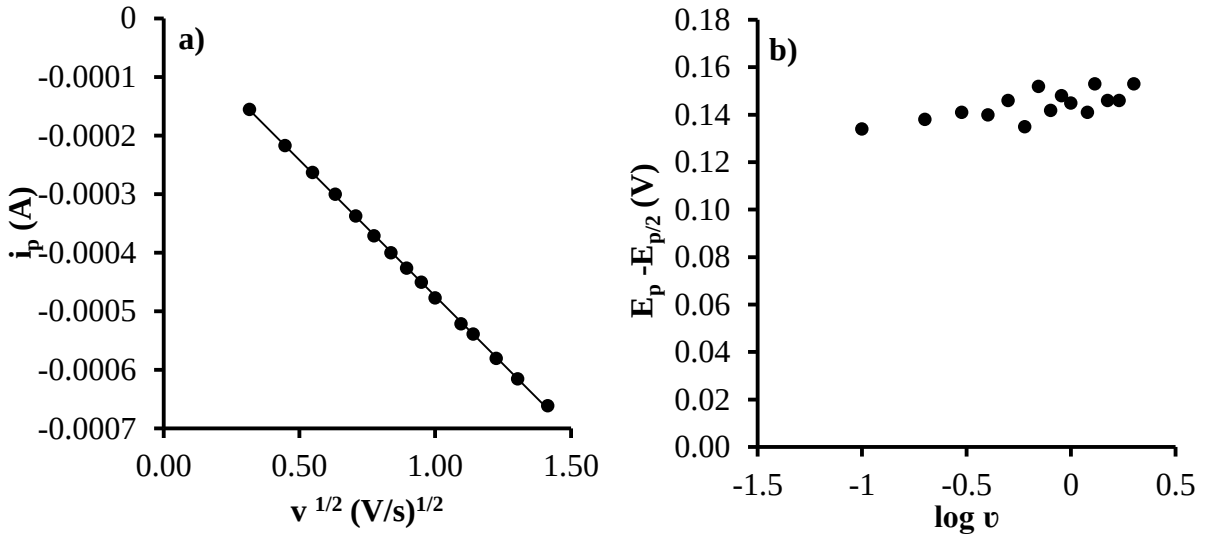

Figure 3.3.Representative plots for conventional analyses for the oxidation of pivalate, (a) Linear peak current response to the square root of scan rate showing the electron transfer process under diffusion control, (b) a peak width of 0.14 V is noted as a function of *log v*, corresponding to electron transfer as the rate limiting step with a concerted mechanism and alpha = 0.34 ± 0.01.

3.3.2. Convolution voltammetry as an alternative approach to determine oxidation potentials for aliphatic carboxylates.

Convolution voltammograms were obtained for propionate and pivalate using the same anhydrous conditions employed for the acetate anion (**Figure 3.4 – 3.7**). As predicted, our analysis confirmed a concerted mechanism for dissociative electron transfer for these carboxylates (**Table 3.2**). The derived oxidation potential for each compound was as follows: (a) 0.60 ± 0.09 V for acetate, (b) 0.47 ± 0.05 V for propionate, and (c) 0.40 ± 0.05 V for pivalate. In accordance with the thermodynamic calculations reported by Eberson et al., a concerted ET mechanism for propionate was predicted with an oxidation potential of 1.20 V in acetonitrile vs. NHE.[8,9] Yet again, the estimated oxidation potential did not differ significantly from our results of 1.07 ± 0.10 V vs. NHE.

Our experimental results confirmed a relative decrease in the oxidation potentials values of 0.13 ± 0.05 V and 0.20 ± 0.05 V for propionate and pivalate, respectively (error reported from the 95% confidence interval from 20 convolution voltammograms).The decrease in both of these estimated oxidation potential values $E^o_{(RCOO^-/R\cdot)}$was significant and parallels well with trends expected on the basis of radical stability.

Table 3.2
Summary of conventional and convolution analyses for 4 mM of carboxylates in 0.2 M TBAP under anhydrous conditions. Estimated oxidation potentials are obtained by the convolution method and Marcus theory.

[R-COO⁻]	*[a]$D^o x10^{-9}$ (m^2/s)*	*E_p - $E_{p/2}$ (V)*	*[b]Averaged α*	*E^o (V)*
CH_3-	4.58 ± 0.05	0.14 ± 0.01	0.30 ± 0.01	0.60 ± 0.09
CH_2CH_3-	4.53 ± 0.03	0.14 ± 0.01	0.35 ± 0.02	0.47 ± 0.05
$(CH_3)_3-$	3.21 ± 0.05	0.14 ± 0.01	0.34 ± 0.01	0.40 ± 0.04
$(C_6H_5)CH_2-$	3.80 ± 0.10	0.11 ± 0.01	0.44 ± 0.02	[c]0.46 ± 0.05

[a]Diffusion coefficients were averaged from convolution values. [b]Alpha values were averaged from the peak width and the convolution values. [c]$E^o_{(RCOO^-/RCOO\cdot)}$ rather than ($E^o_{(RCOO^-/R\cdot+CO_2)}$ for phenyl acetate vs. Ag/(0.1 M) $AgNO_3$

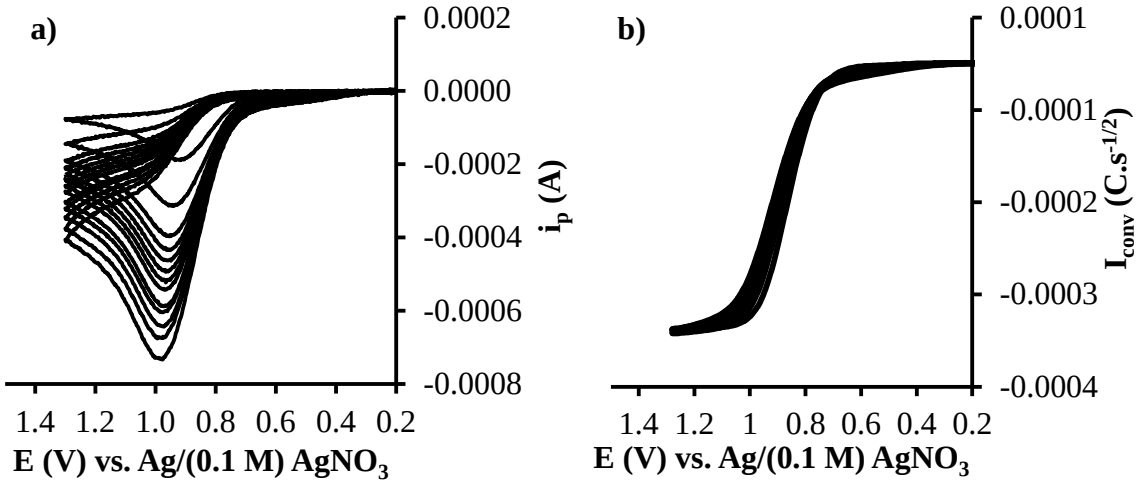

Figure 3.4. a) Cyclic voltammograms for the oxidation of 4 mM of tetra-n-butylammonium propionate in "neat acetonitrile" with 0.2 M TBAP vs. Ag/(0.1 M) $AgNO_3$ at scan rates of 0.1 -2.0 V/s , b) Corresponding convolution voltammograms under reported conditions.

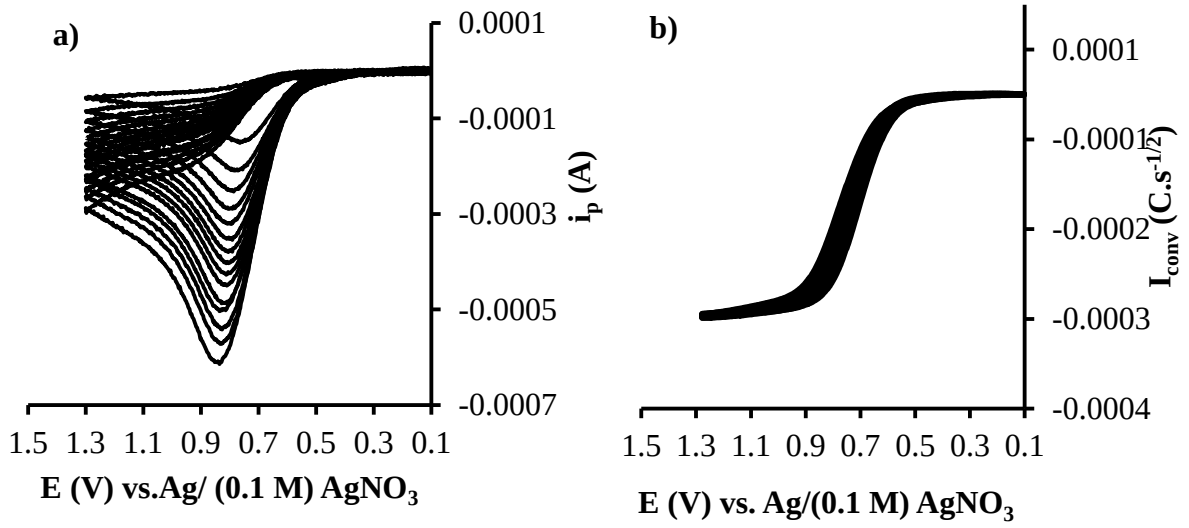

Figure 3.5. a) Cyclic voltammograms for the oxidation of4 mM of tetra-n-butylammonium pivalate in "neat acetonitrile" with 0.2 M TBAP vs. Ag/(0.1 M) $AgNO_3$ at scan rates of 0.1 - 2.0 V/s , b) Corresponding convolution voltammograms under reported conditions.

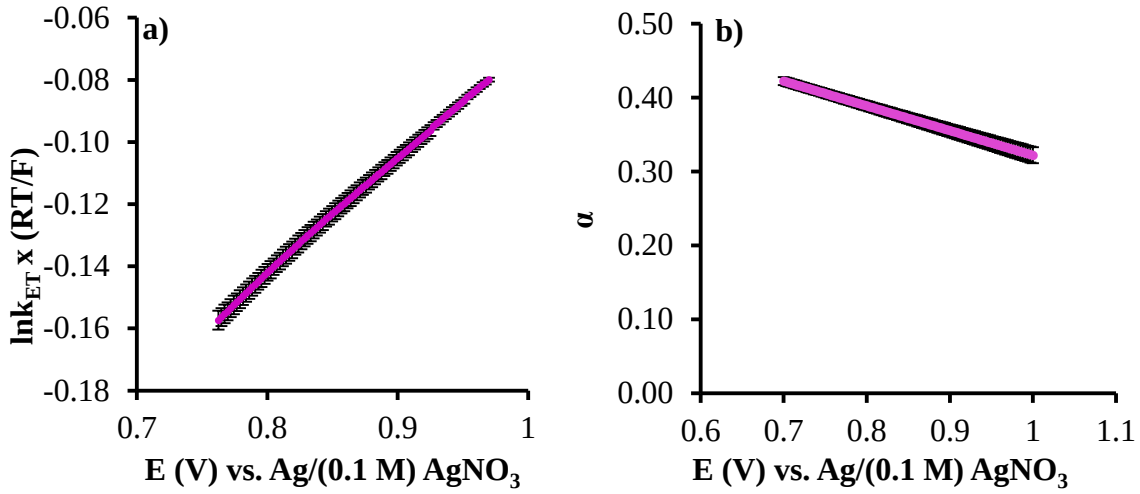

Figure 3.6. Representative convolution plots for for the oxidation of the 4 mM of tetra-n-butylammonium propionate at a GC electrode in neat acetonitrile with 0.2 M TBAP vs. Ag/(0.1 M) $AgNO_3$, a) fitting of Marcus equation in the averaged rate constant at each given potential, b) Corresponding alpha as a function of the applied potential as generated from the first derivative function.

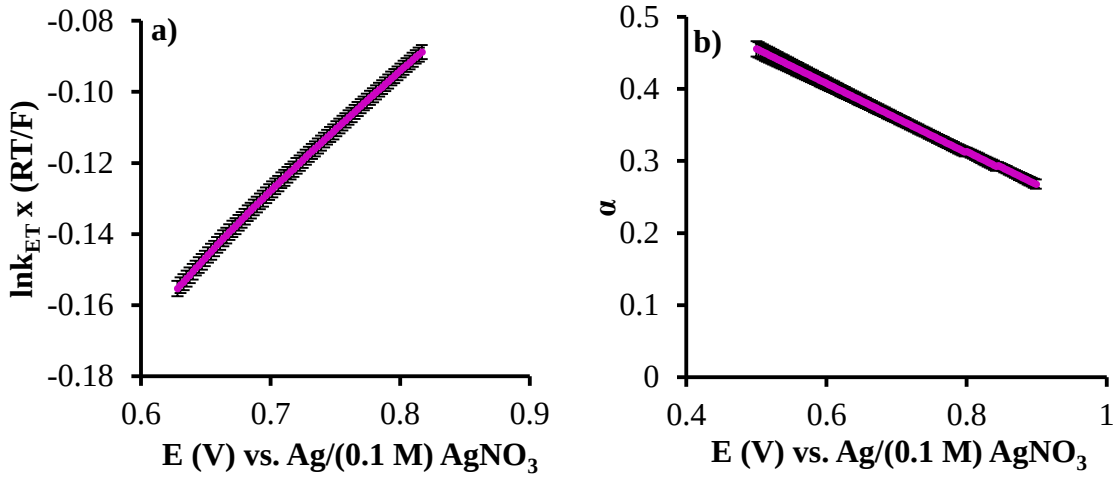

Figure 3.7. Representative convolution plots for the oxidation of 4 mM of tetra-n-butylammonium pivalate at a GC electrode in neat acetonitrile with 0.2 M TBAP vs. Ag/(0.1 M) $AgNO_3$, a) fitting of Marcus equation in the averaged rate constant at each given potential, b) Corresponding alpha as a function of the applied potential as generated from the first derivative function.

3.3.3. Discrepancies between the observed oxidation potentials based and estimated resonance stabilization energy (RSE).

Although the oxidation potentials for acetate, propionate, and pivalate parallel the stability of the resulting alkyl radical, the differences were not quite as large as anticipated. In order to address this potential discrepancy, and to assess whether the we were underestimating the effect of alkyl substitution on the carboxylate anion, we reviewed pK_avalues for carboxylic acids in aqueous solution: 4.56 for acetic acid, 4.67 for propanoic acid, and 4.83 for pivalic acid.[10] The pK_a's are significantly higher in acetonitrile solvent, because the resulting carboxylates are not stabilized by hydrogen bonding. For example, as measured by UV-Vis spectroscopy, the pK_avalues were reported to be 23.82 for acetic acid and 24.12 for butyric acid.[11] Assuming the difference in pK_a is a measure of the difference in the stability of the carboxylate anions, a maximum difference in 0.45 pK_a units corresponds to less than 0.03 V. Therefore, it is expected that the net difference in the oxidation potentials of the various carboxylates reflects the stability of the resulting radical ($R^{\cdot}$) to a much greater extent than differences in the free energy of solvation and relative energy of the starting carboxylate.[12]

3.4. Aryl carboxylates and dissociative electron transfer.

In addition to aliphatic carboxylates, two aryl carboxylates (benzoate and phenyl acetate) were also investigated with respect to dissociative electron transfer. Prior findings indicate that the decarboxylation rate for the benzoyloxyl radical ($k_{CO_2} \cong 10^6 s^{-1}$) is two orders of magnitude slower than aliphatic carboxyl radicals; in other words, relatively speaking, the benzoyloxyl radical is long-lived.[13-15] The low decarboxylation rate is attributed to the fact that phenyl radical is much less stable than 1°, 2°, or 3° alkyl radicals. On the other hand, phenyl acetate is expected to experience a faster decarboxylation and possibly undergo a concerted mechanism because the resulting benzyl radical is resonance-stabilized. As reported earlier, similar analyses were

performed using benzoate, with its poor behavior and adsorption to the surface of the electrode resulting in a significant loss in peak current signal upon anodic scanning (**Figure 3.8**).

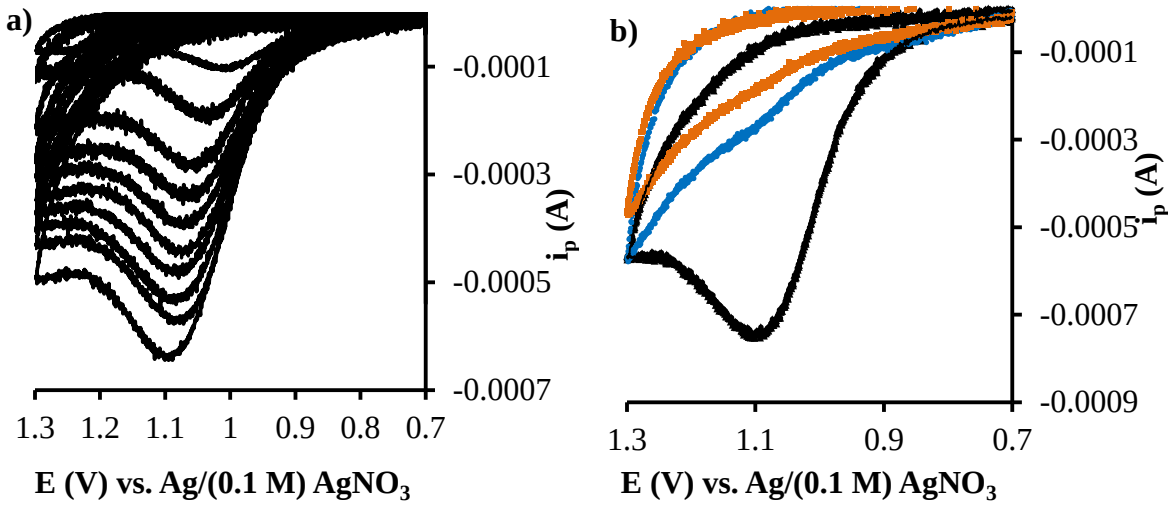

Figure 3.8. a) Representative cyclic voltammograms of 4 mM tetra-n-butylammonium benzoate in neat acetonitrile on a GC electrode with 0.2 M TBAP vs. Ag/ (0.1 M) $AgNO_3$, scan range 0.1-2.0 V/s, b) Representative cyclic voltammogram at 1.5 V/s under the same experimental conditions showing massive fouling of the GC surface electrode within one consecutive scan (blue), followed by complete passivation upon the second consecutive scan (orange).

Although our cyclic voltammograms exhibited a proper increase in the peak current as a function of the scan rate with similar irreversible behavior (**Figure 3.8b**), the significant signal loss revealed a lack of linearity of i_p as a function of $v^{1/2}$ (**Figure 3.9a**). The averaged $E_p - E_{p/2}$ was 0.094 ± 0.02 V with a corresponding averaged α of 0.52 ± 0.06, which points to a stepwise mechanism (**Figure 3.9b**). However, poor linearity, electrode fouling, and significant scattering made it difficult to draw definite conclusions about the mechanistic behavior of these systems. **Figure 3.9b** illustrates the major loss in current signal, and no current was observed after the second consecutive scan. This pattern has not been noted for any other carboxylate under

investigation. Hence, conventional analysis results were inconsistent and inconclusive; so, convolution analysis was not attempted for this system.

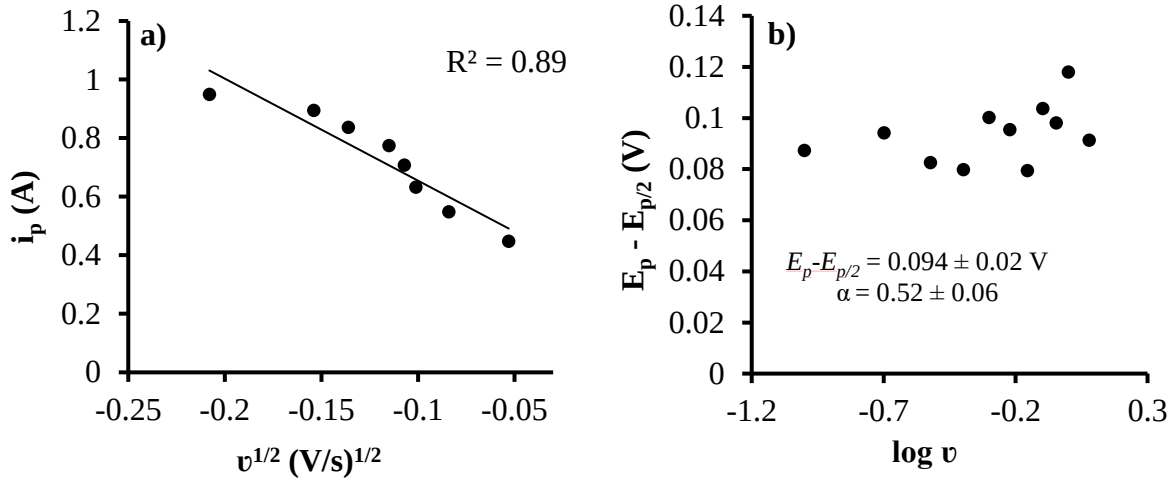

Figure 3.9. Representative conventional analyses plots for the oxidation of 4 mM of tetra-n-butylammonium benzoate at a GC electrode in neat acetonitrile with 0.2 M TBAP vs. Ag/(0.1 M) $AgNO_3$, with a scan range of 0.1 – 2.0 V/s, a) Poor linearity for the variation of the peak current as a function of the scan rate to the half power, b) Peak width scattered resulting in inconsistency and irreproducibility.

The apparent deactivation of the electrode surface was suggestive of significantly deposited material on the electrode surface. If the oxidation of the benzoate is occurring via a stepwise mechanism, a carbonyl-like compounds are expected to be deposited. As a result, fouling was examined by X-ray photoelectron spectroscopy measurements of the electrode surface, which detected the presence of a carbonyl-like signal at 286.5 and 288 eV. This data suggests that a relatively long-lived carboxyl radical intermediate is produced upon oxidation (**Figure 3.10**) by virtue of the fact that C-O and C=O functionalities were detected on the electrode surface.[16] Neither the XPS samples for background solution (tetra-n-butylammonium perchlorate in acetonitrile solution) nor the acetate exhibited any significant signal in these regions.

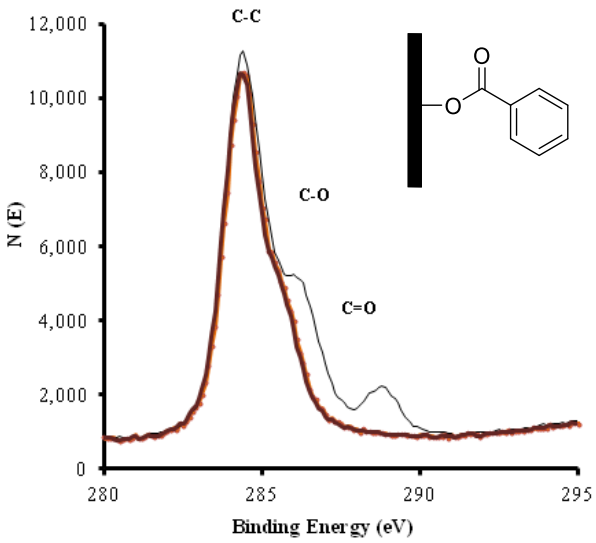

Figure 3.10. XPS for glassy carbon electrode surface upon the oxidation of 4 mM tetra-n-butylammonium benzoate in neat anhydrous acetonitrile with 0.45 M tetra-n-butylammonium perchlorate (black) in comparison to the glassy carbon surface upon the oxidation of 4 mM tetra-n-butylammonium acetate with tetra-n-butylammonium perchlorate (orange), and a background with tetra-n-butylammonium perchlorate (red).

In contrast, the results for phenyl acetate were more intriguing. Based on our results with acetate, we expected that phenyl acetate would undergo a concerted mechanism—because the resulting the benzyl radical ($(C_6H_5)CH_2^{\cdot}$) is resonance-stabilized. However, a stepwise mechanism was confirmed (supporting the earlier work of Savéant et al.), but featured just one electron based on our PFG-NMR measurements instead of two as noted by Savéant's group. Savéant's electrochemical studies were based on the *in situ* neutralization of the phenyl acetic acid with tetra-n-butylammonium hydroxide to produce the tetra-n-butylammonium anion. The overall number of transferred electrons for this oxidative process was based on the coulometric measurements of the observed current passed for the direct *in situ* neutralization of the phenyl acetic acid with hydroxide base. Neutralization unavoidably introduce other side reactions which interfere with the heterogeneous electron transfer such as water and hydroxide **(Figures 3.11** and **Table 3.2**). In other words, the discrepancy in the reported number of electrons can be explained

by the fact that Saveant's work includes an overall measured electron for the oxidative process but via *in situ* approach which is proposed to contribute to the observed number of electrons.

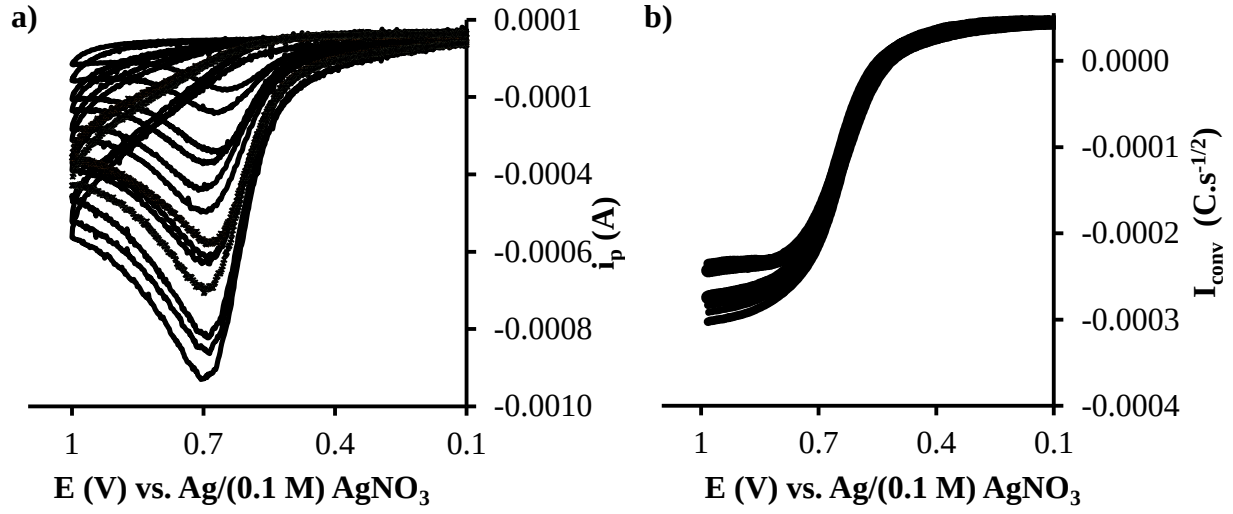

Figure 3.11. a) Representative cyclic voltammograms for the oxidation of 4 mM tetra-n-butylammonium phenyl acetate in 0.2 M TBAP/neat acetonitrile using a GC electrode vs. Ag/(0.1 M) $AgNO_3$, scan range 0.1-2.0 V/s, b) Corresponding convolution voltammograms under exact experimental conditions.

3.5. Solvent effects on the electrochemical oxidation of carboxylates.

3.5.1. Does the presence of water influence the reaction mechanism?

The discrepancy in the reported α values and the mechanism of the dissociative electron transfer for aliphatic carboxylates and the published work by González, et al. merits further discussion. We suspect that with much of this earlier work, the conditions for generating the carboxylate anion were such water may have been present in the system. For example, Savéant et al.'s investigation of methylaryl carboxylates was performed via an *in situ* neutralization reaction between an equimolar ratio of acid to tetra-n-butylammonium hydroxide in order to generate the tetra-n-butylammonium carboxylate. As the researchers reported, the formation of water is an unavoidable byproduct of this synthetic approach.[1] Gonzáles et al. utilized more rigorous anhydrous conditions involving the synthesis of tetra-n-butylammonium salt for their

electrochemical investigations. Although the tetra-n-butylammonium salts were synthesized *ex situ* and vacuum dried prior to use, no experimental details were provided with regards to the transfer of these extremely hygroscopic compounds,[4,17,18]

One goal of this investigation was to determine how and to what degree the presence of water impacts the electron transfer mechanisms. The hygroscopic nature of the aliphatic carboxylates we utilized in this investigation was challenging in terms of obtaining accurate mass measurements. Accordingly, a series of electrochemical studies were conducted under differing anhydrous conditions—from very rigorous environmental conditions within a glovebox to less anhydrous conditions outside a glovebox.

3.5.2. A possible shift from a concerted to a stepwise dissociative electron transfer mechanism with water additions.

To ascertain the influence of water on electron transfer, preliminary data were collected outside the glovebox under less anhydrous conditions with "as received" HPLC-CH_3CN (Sigma Aldrich) and tetra-n-butylammonium acetate and a supporting electrolyte. These initial experiments were performed under argon with continuous polishing with alumina oxide and washes with an isopropyl alcohol and water solution. The averaged α was found to be 0.38 ± 0.02 from both convolution and conventional methods, which were higher that analogous values obtained inside a glovebox. It is important to note that, regardless of whether we washed the polished electrode in acetonitrile/water solution or only acetonitrile, no differences in the α values were noted for the voltammograms obtained inside the glovebox. In addition to an α value that suggests more of a stepwise mechanism, a shift towards a more positive oxidative peak with E^o of 0.80 ± 0.05 V was found. In summary, the presence of trace water might have impacted the ET mechanisms and results reported herein—possibly through hydrogen bonding effects, which could account for the differences in our findings and previously published results.

3.5.3. Literature precedent for stabilization of radical intermediates/transition states by solvent.

The rates of several reactions of neutral free radicals have been shown to be sensitive to solvent effects.[19,20] Germane to this investigation are those that mimic aspects of the systems investigated herein, specifically the β-scission (decarboxylation) of a carboxyl radical. For example, as illustrated in **Scheme 3.3a**, the decarbonylation of acyl radicals were found to be slower in more polar solvents, as evidenced by the fact that k_{CO} decreased from 8.3 x 10^5 s^{-1} in hexane to 1.9 x 10^5 s^{-1} in acetonitrile.[21] A similar trend was found for the decarboxylation rate of the 4-methylbenzoyloxyl radical, with a reaction rate that is on the order of magnitude slower when acetonitrile is used instead of carbon tetrachloride (**Scheme 3.3b**).[22] In both these cases, the transition state is less polar than the reactant. Conversely, the reaction rate for the β-scission of tert-butoxyl radical to form methyl radical can be increased with more polar solvents, such as acetic acid, due to stabilizing the (more polar) transition state of the radical intermediate via dipole/dipole interactions (**Scheme 3.3c**).[2]

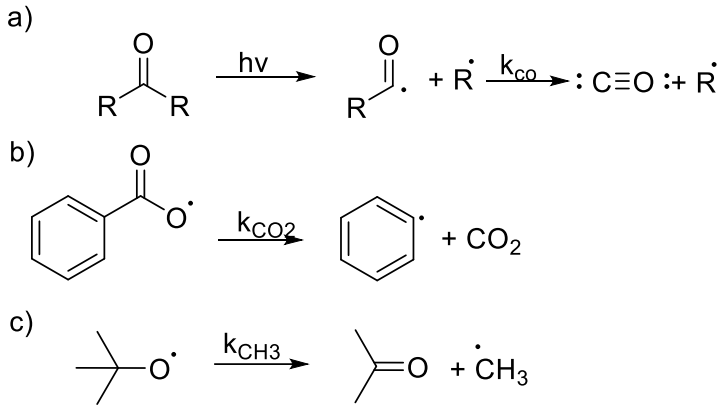

Scheme 3.3 Reaction rates of some neutral radicals are dependent on the polarity of the solvents.[15,19,21]

3.6. The effect of water on the DET mechanism of acetate.

The results reported herein suggest that the electrochemical oxidation of alkyl carboxylates (RCO_2^-, with R = CH_3, CH_2CH_3, and $C(CH_3)_3$) proceed via a concerted dissociative electron transfer process—in contrast to the previous work of Gonzáles, et al. A possible explanation for this discrepancy is that because of the nature of the experiments, hygroscopic nature of carboxylate salts, and the need to generate the carboxylate anion via acid/base chemistry, previous studies may have had small amounts of water present. Hence, one goal of this investigation was to determine if the mechanism of the oxidation of aliphatic carboxylates is affected by the presence of water.

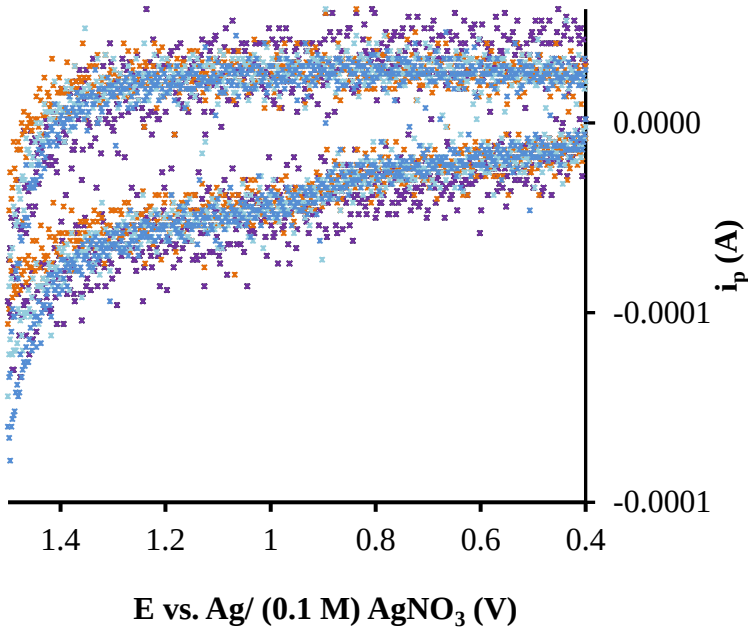

Figure 3.12. Anodic oxidation of background solution at 0.5 V/s in 0.45 M TBAP/neat acetonitrile (black), 0.05 M added DI H_2O (purple), 0.22 M added DI H_2O (orange), 0.5 M added DI H_2O (light green), 0.8 M added DI H_2O (blue).

To address this question, a series of experiments were performed whereby deionized water was introduced, with rigorously anhydrous CH_3CN, electrolyte, and tetra-n-butylammonium acetate serving as a control. Both conventional and convolution analyses were carried in the exact manner as discussed earlier. Additionally, appropriate background subtractions were performed to

ensure that only additions of water that yielded no increase in the background current were contributing to the observed response. Our results showed that water additions with concentrations higher than 0.8 M resulted in an increase in the non-faradaic current at more positive potentials (**Figure 3.12**).

To assess how "anhydrous" our reaction conditions were, a Karl Fischer titrator was utilized. The averaged water content for the bulk solution HPLC CH_3CN passed over alumina was found to be 3.65 ± 0.20 ppm. The bulk sample containing the salt was found to be 4.67 ± 0.57 ppm. Based on the Karl Fischer results, we estimate that for our "rigorously anhydrous" experiments, the mole ratio to be (460 ± 60):1 for carboxylate anion:H_2O. Hence, our experimental results confirmed that these systems were investigated under anhydrous conditions.

Table 3.3
Reported averaged values for the alpha and oxidation potential for tetra-n-butylammonium acetate for a range of water concentrations added to neat acetonitrile/0.45 M TBAP vs. Ag/(0.1 M) $AgNO_3$

Molarity D_2O or *H_2O* (mM)	**[a]α**	**E^o (V)**
Neat	0.31 ± 0.02	0.60 ± 0.10
55	0.40 ± 0.02	0.72 ± 0.03
	0.38 ± 0.04	*0.72 ± 0.08*
220	0.44 ± 0.02	0.87 ± 0.02
	0.42 ± 0.03	*0.80 ± 0.06*
493	0.45 ± 0.02	0.88 ± 0.04
	0.43 ± 0.05	*0.90 ± 0.05*

[a]A set of 4 replicates (2 mM, 3 mM, 4 mM, and 6 mM) of tetra-n-butylammonium acetate were performed for each concentration of H_2O (Italicized) and D_2O additions to a neat system.

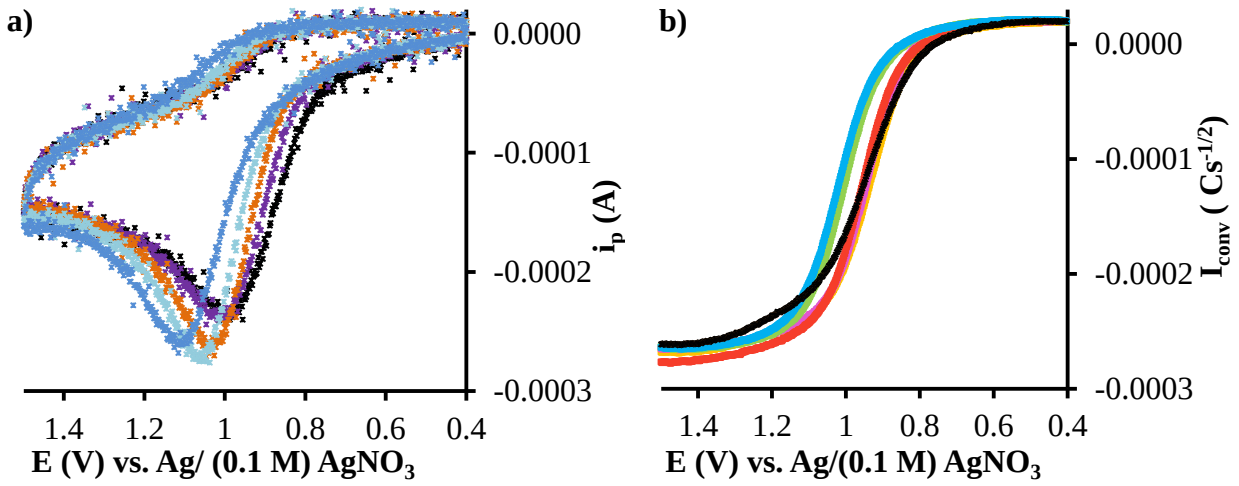

Figure 3.13. a) Cyclic voltammograms for the anodic oxidation of 4 mM TBA-acetate at 0.5 V/s in 0.45 M TBAP in neat acetonitrile (black), 0.05 M added DI H_2O (purple), 0.22 M added DI H_2O (orange), 0.5 M added DI H_2O (light green), and 0.8 M added DI H_2O (blue) (None are background-subtracted), b) Corresponding convoluted currents,

Figure 3.13 depicts representative cyclic voltammograms at 0.5 V/s for each of the water additions that illustrate three recurring features: a) a continuous shift in the peak potential to higher (more positive) values, b) a narrowing in the peak width, and c) a slight increase in the peak current. Subsequent convolution and conventional analyses showed a significant increase in the α value with increasing concentrations of water. Importantly, the shift towards higher α values is suggestive of a change in the dissociative electron transfer mechanism.

Furthermore, our convolution analyses results pointed to an initial increase in the oxidation potential upon the addition of water. However, no significant change was noted in the oxidation potential with incorporations of higher concentrations of water (i.e., 200 mM and 500 mM). Since carboxylates are anions, we anticipated that the solvation dynamics for these anions in the presence of water would differ significantly in comparison to results obtained in neat acetonitrile. This supposition is based on prior research indicating that acetate anions form up to five direct hydrogen bonds with water molecules in an inner solvation shell, which is further supported by a similarly structured outer solvation shell.[23]

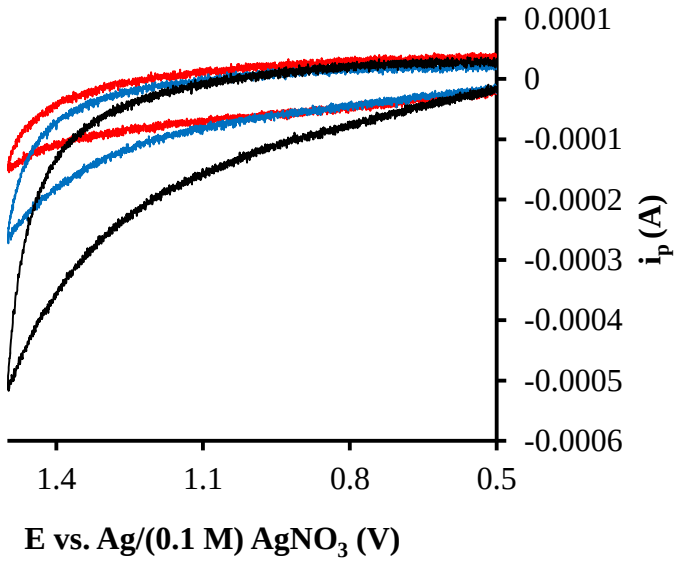

Figure 3.14. Cyclic voltammograms shows higher background current with increased water concentrations over 1.8% in neat acetonitrile with 0.45 M TBAP (0%, 2%, and 5% "added H_2O" from top to bottom).

Water-addition experiments were limited to 0.5 M H_2O concentrations because no increase in the additional background current was noted in comparison to neat conditions which could be indicative of an interference with the analysis (**Figure 3.14)**. Although water concentrations up to 1.0 M in solution did not result in any significant increase in background current as noted by cyclic voltammetry, higher water concentrations (e.g., 2 M and 3 M solutions) caused a significant current increase. We attributed this increase to electrolyte precipitation in the solution to form a milky appearance.

In general, an increase of about 13% in the peak currents *(i_p)* was noted in the cyclic voltammograms as the water concentration was increased to 0.5 M, which corresponded to less than 3% increase in convoluted currents. There was no evidence of an increase in the number of electrons being transferred upon oxidation of the acetate. Convolution analyses indicated 23% higher diffusion coefficients (1.2 ± 0.05) x 10^{-5} cm^2/s under anhydrous to (1.4 ± 0.07) x 10^{-5} cm^2/s

at 0.5 M water). Similarly, PFG NMR results showed an increase of 14.9% in the diffusion coefficient as the water concentration was increased to 0.5 M (4.70 ± 0.10) x 10^{-5} cm^2/s to (3.90 ± 0.10) x 10^{-5} cm^2/s). In other words, the modest increase in the peak current is attributed to a change in the diffusion coefficients.

3.7. Effect of D_2O vs. H_2O on the mechanism for the dissociative electron transfer of acetate.

To further confirm the role of water in shifting the mechanism of the dissociative electron transfer, we also examine the effect of added D_2O. As indicated in **Table 3.3** and **Figure 3.15,** results obtained with H_2O and D_2O were identical within experimental error suggesting no significant (measureable) isotope effect. The difference in the hydrogen bonding energy from O-H to O-D was found to be weakened by roughly 1- 2 kJ/mol (0.23 – 0.46 kcal/mol).[24] A 2 kJ/mol difference moving from a O-H to O-D should correspond to a range of 0.01 – 0.02 V shift towards a lower peak potential. This shift is difficult to note as it falls within experimental error of these electrochemical measurements. In summary, although we expect acetate anion to be stabilized by H-bonding in the presence of water, our measurements of oxidation potential are not sensitive enough to detect this isotope effect, even if it were occurring.

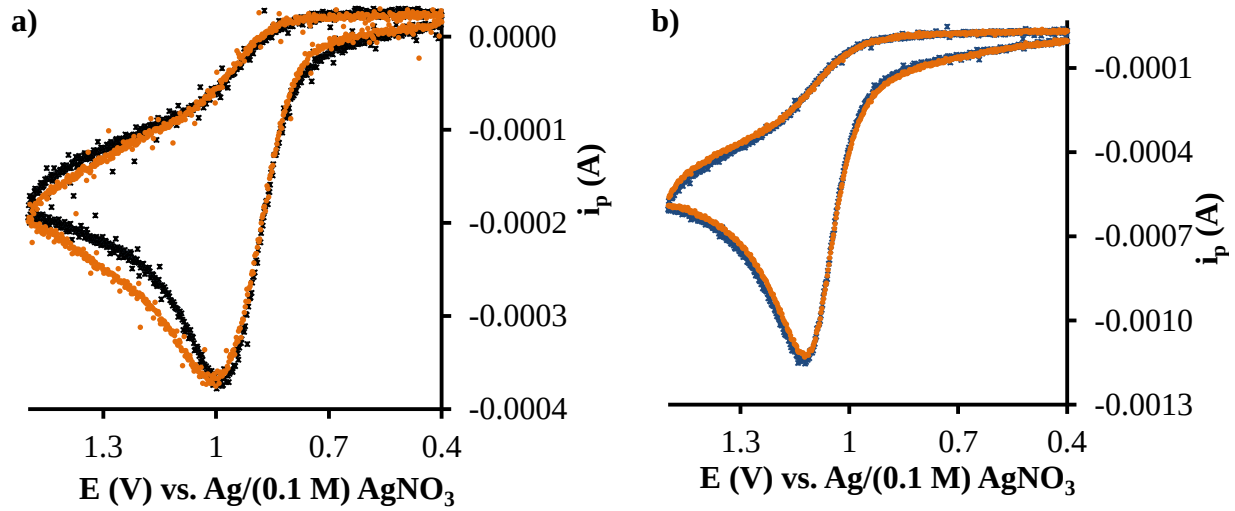

Figure 3.15. Cyclic voltammograms for the oxidation of 4 mM tetra-n-butylammonium acetate in 0.45 TBAP/acetonitrile vs. Ag/(0.1 M) $AgNO_3$ on a GC electrode with 0.0 55 M added DI H_2O (black) and D_2O (orange), a) at 0.5 V/s and b) at 0.9 V/s.

3.8. Effect of water on the mechanism of dissociative electron transfer for aliphatic carboxylates.

To further investigate the impact of incorporating water in solutions of acetate, propionate and pivalate carboxylate salts, electrochemical analyses were performed under the same synthetic conditions as those employed in our investigations with acetate. Water additions to an anhydrous system were performed and all resulting data obtained for our aliphatic carboxylates were constantly monitored for accuracy and precision. Proper functional electrochemical setup was monitored with a ferrocene as a reference control. Additionally, tetra-n-butylammonium acetate runs were performed concurrently to further undoubtedly assure reproducibility. As evidenced in **Table 3.4** and **Figure 3.16**, experimental results revealed similar trends and results to those reported for acetate when water is added. We noted a concerted mechanism with a consistent shift to higher oxidation potentials with increasing water concentrations, which corresponds to α values that confirm a stepwise dissociative electron transfer mechanism for these aliphatic carboxylates.

Table 3.4
Summary of conventional and convolution analyses for the 4 mM concentration of aliphatic carboxylates and phenyl acetate in 0.2 M TBAP under anhydrous and wet conditions.

[R-COO$^-$] (mM)	*[H_2O] (M)*	*$D^o x10^{-9}$ (m^2/s)*	*$E_p - E_{p/2}$ (V)*	*[b]Averaged α*	*[e]E^o (V)*
[a]CH_3-	Neat	4.58 ± 0.05	0.14 ± 0.01	0.30 ± 0.01	0.60 ± 0.09
	0.5	5.20 ± 0.10	*0.11 ± 0.02*	*0.43 ± 0.05*	*0.90 ± 0.05*
CH_3CH_2-	Neat	4.53 ± 0.03	0.14 ± 0.01	0.35 ± 0.02	0.47 ± 0.05
	0.5	5.46 ± 0.05	*012 ± 0.01*	*0.41 ± 0.02*	*0.73 ± 0.04*
$(CH_3)_3$-	Neat	3.21 ± 0.05	0.14 ± 0.01	0.34 ± 0.01	0.40 ± 0.04
	0.5	5.61 ± 0.08	*0.12 ± 0.01*	*0.41± 0.02*	*0.63 ± 0.04*
$(C_6H_5)CH_2$-	Neat	3.80 ± 0.10	0.11 ± 0.01	0.44 ± 0.02	[d]0.46 ± 0.05
	0.5	--	--	--	--

[a]Higher water concentrations were performed at 0.45 M TBAP for acetate as noted earlier concentration of TBAP only impacts diffusion coefficients. [b]alpha values were averaged from the peak width and the convolution values. [c,d]E^o ($RCOO^-/RCOO^\cdot$) rather than ($RCOO^-/R^\cdot$) for the other aliphatic carboxylates vs. Ag/(0.1 M) $AgNO_3$. Italicized indicate 0.5 M H_2O data.

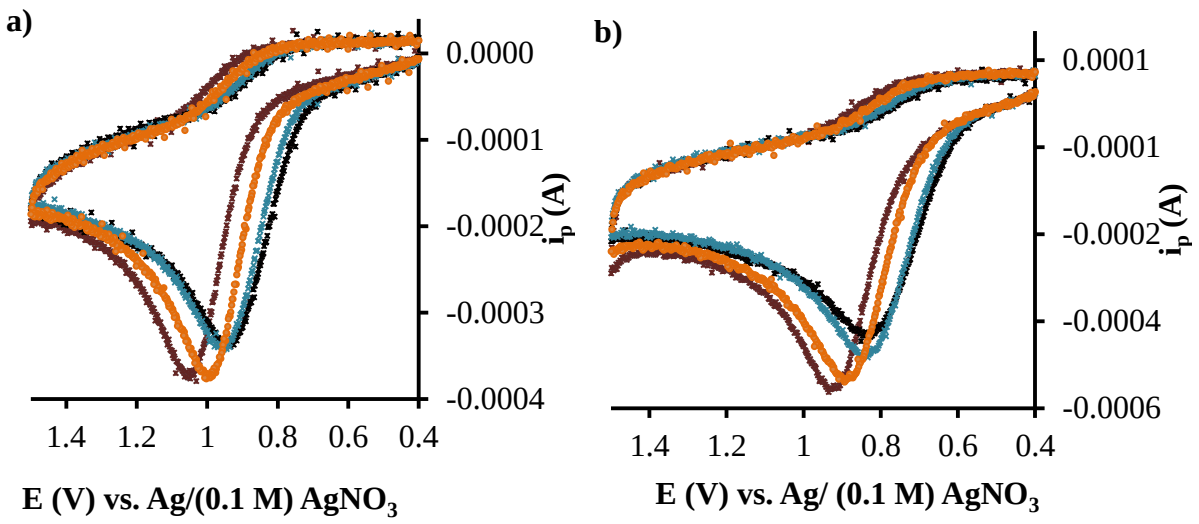

Figure 3.16. Representative cyclic voltammograms for the oxidation of 4 mM tetra-n-butylammonium carboxylate in 0.2 TBAP/acetonitrile at 0.5 V/s vs Ag/(0.1 M) $AgNO_3$ on a GC electrode at (-) neat acetonitrile, (-) 55 mM added water, (-) 0.22 mM added water, (-) 499 mM added water for: a) tetra-n-butylammonium propionate, and b) tetra-n-butylammonium pivalate.

3.9. Possible explanations for the effect of water on the apparent mechanism for the oxidation of acetate.

Under rigorously anhydrous conditions, the electrochemical oxidation of acetate is characterized by an early transition state (α = 0.3) and a large intrinsic barrier. This large intrinsic barrier indicates significant internal structural reorganization is needed to reach the transition state for electron transfer, and suggests the mechanism may be concerted DET. The fact that the derived oxidation potentials for RCO_2^- (with R = CH_3, CH_2CH_3, and $C(CH_3)_3$) parallel radical ($R^{\cdot}$) stability provides further evidence for a concerted mechanism. As water is added, the transition state is more symmetrical (α = 0.5), and the intrinsic barrier is lower.

We hypothesize several possible interpretations for the observed trends. One possibility is a shift in the mechanism. The mechanism of the dissociative electron transfer of aliphatic cabroxylates is concerted under anhydrous conditions, and it undergoes a gradual transition to stepwise as water is added. H-bonding may differentially stabilize the carboxyl radical, giving it sufficient lifetime that it can exist as an intermediate under the reaction conditions (**Scheme 3.4**).

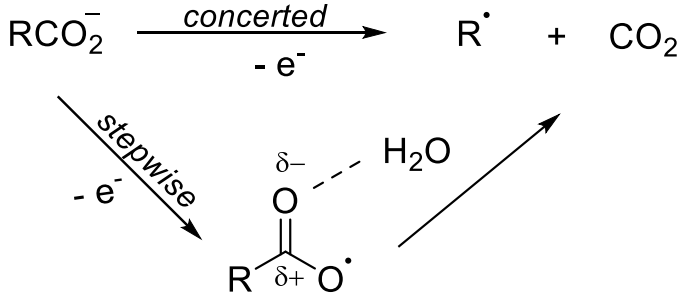

Scheme 3.4 Possible hydrogen bonding stabilization of the transition state results in (a) a longer-lived radical acyloxyl radical intermediate and (b) a mechanistic shift towards a stepwise mechanism.

In accordance with Marcus theory (and the Franck-Condon principle) solvent reorganization occurs prior to electron transfer. Presumably, the interaction of solvent (particularly H_2O) with acetate anion is much more significant (both energetically and with regard to structure) than with the acetoxyl radical. It may be reasonable to suppose that the acetoxyl radical formed

electrochemically will be "born" into the solvation shell that is more defined by the acetate anion, and the acetoxyl radical is stabilized by H-bonding.

A second hypothesis is a shift in the nature of the resulting carboxyl radical due to H-bonding. Depending on the nature of the orbital from which the electron is removed (π- vs. σ- in nature), there may be two different electronic states of $CH_3CO_2^{\cdot}$ being generated, with the π-state possibly becoming more favored when H_2O is present. (π- $CH_3CO_2^{\cdot}$ is presumed to have a higher barrier to decarboxylation than σ-) (**Scheme 3.5**)

The acetoxyl radical has two low electronic states, roughly referred to as π- (B_2) and σ- (A_1). Of the two, the former is lower in energy by ca. 2.4 kcal/mol in the gas phase.[25-27] These two states may have been observed experimentally.[3] It is assumed that the π-state will have a higher barrier to decarboxylation because the unpaired electron is in an orbital orthogonal to the cleaving bond.

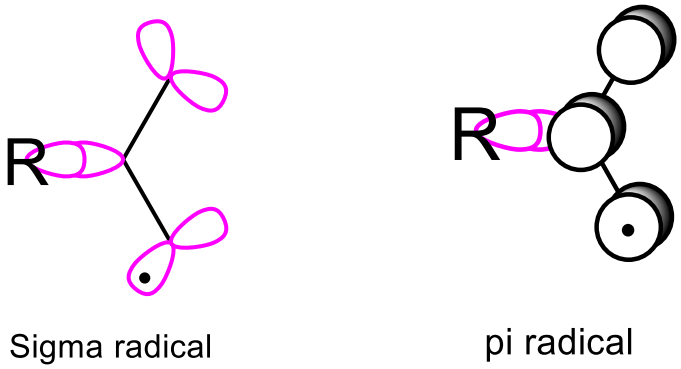

Scheme 3.5 Hydrogen bonding stabilization of the radical in a π orbital instead of the σ orbital.

For acetate, there are two, nearly degenerate HOMOs, one of which is more σ- like, the other more π-like. The relative energies of these are very close in energy, and may lead to different electronic states of the acetoxyl radical. Ab initio MO calculations have been reported by Bock et

al. on acetate anion, and acetate/water complexes, where up to six waters have been added in an inner solvation shell.[23] The main objective of this work seemed mainly to focus on structures, and the extent to which water stabilizes acetate anion. Simple MO calculations using Harttee-Fock (6-31G*) level of theory were performed by James Tanko suggests that the HOMO for acetate is π-like, while $HOMO_{-1}$ is σ-like. The energy difference was reported to be 0.09 eV. As water molecules are added, the energy difference decreases and in one case, the HOMO appeared to be more σ-like (**Table3.5**).

Table 3.5
Spartan simulations for acetyloxyl radical showing the lowest occupied molecular orbital in the absence of water molecules and in the presence of a water molecule using Hartree-Fock theory level with 6-31G*basis set with geometry optimization.

Structure Acetate Anion	**HOMO**	**$HOMO_{-1}$**
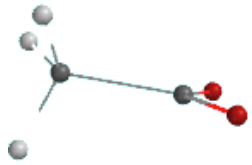	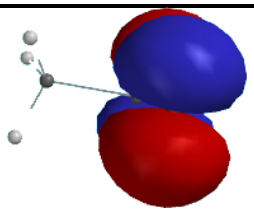	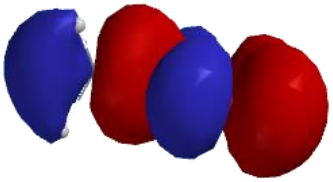
	-4.35 eV	-4.44eV
	-4.35 eV	-4.44 eV
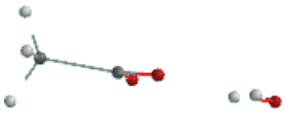	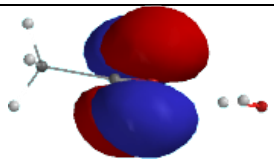	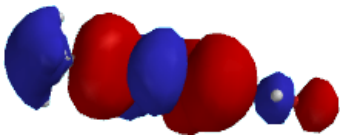
	- 5.37 eV	-5.39 eV
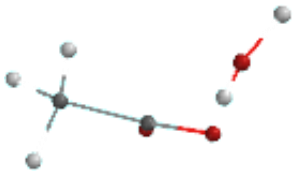	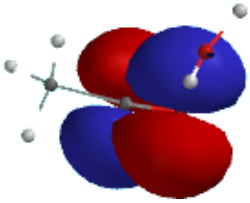	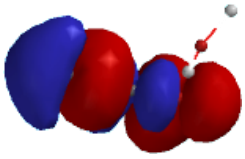

	- 5.18 eV	-5.22 eV
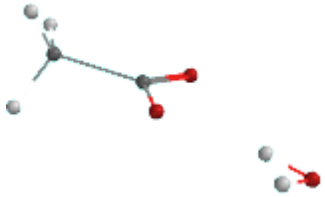	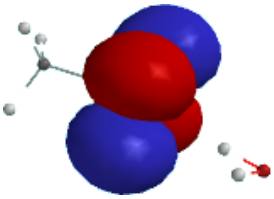	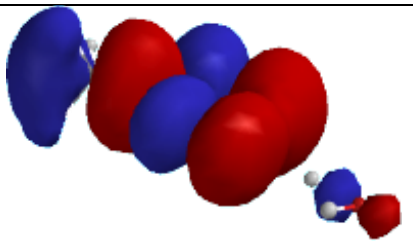
	- 5.18 eV	- 5.23 eV
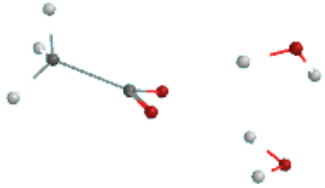	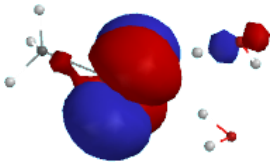	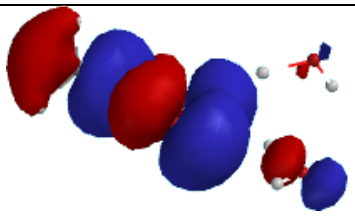
	- 6.03 eV	- 6.06 eV
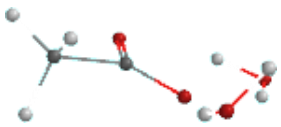	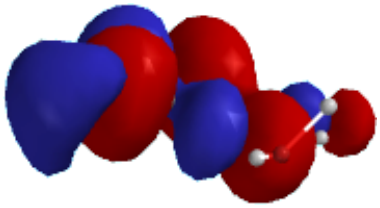	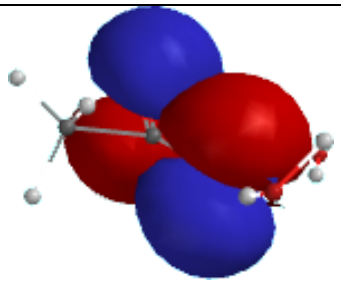
	- 6.06 eV	-6.09 eV
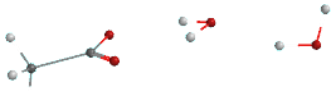	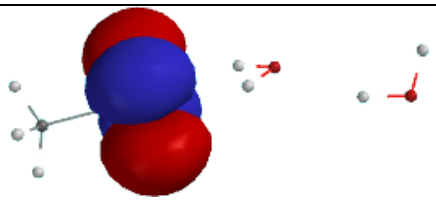	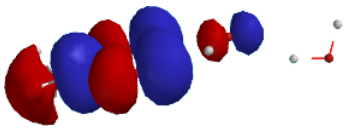
	- 5.75 eV	-5.78 eV
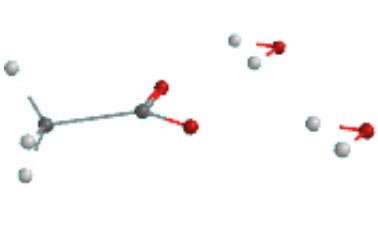	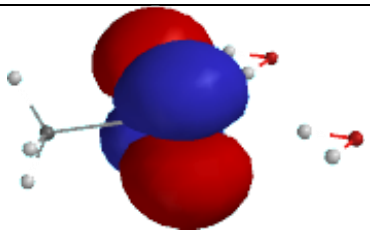	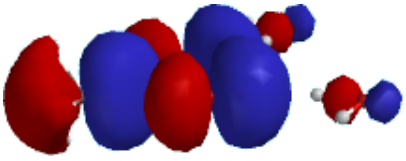

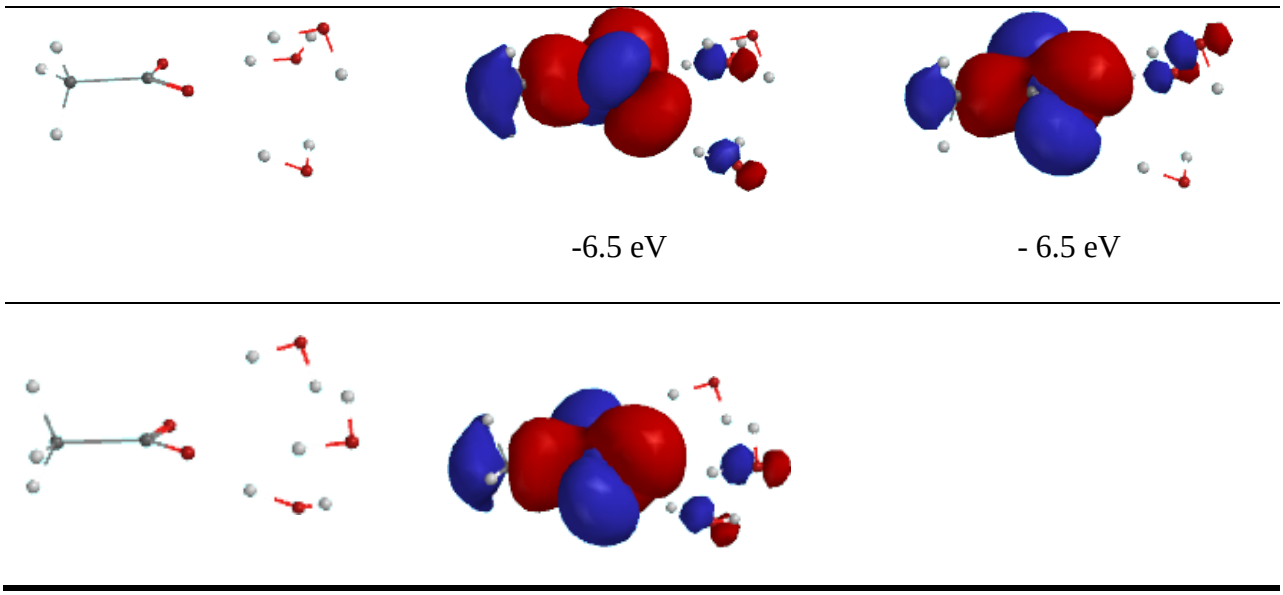

3.10. Conclusions.

The mechanisms associated with the dissociative electron transfer of a series of aliphatic carboxylates have been fully investigated. Our findings support the following conclusions:

- Under anhydrous conditions, for RCO_2^- (with R = CH_3, CH_2CH_3, and $C(CH_3)_3$), a low (ca. 0.3) alpha value was observed, suggestive of a concerted DET mechanism.
- Convolution voltammetry was successfully employed to determine oxidation potentials as derived from Marcus theory. For R = CH_3, CH_2CH_3, and $C(CH_3)_3$), the oxidation potentials were 0.60 ± 0.09, 0.47 ± 0.05, and 0.40 ± 0.04 V (vs. Ag/0.1M Ag^+) respectively, and the trend parallels the radical stability of $R^{\cdot}$.Moreover, the oxidation potentials were similar to the predicted values reported by Eberson and coworkers for a concerted mechanism.[9,28]
- Addition of water appears to significantly impact the DET mechanism, in that a significantly higher transfer coefficient value and oxidation potential were reported

for all these carboxylates in the presence of water, with an apparent shift from a concerted to a stepwise mechanism under wet conditions.

- The results obtained in the presence of H_2O vs. D_2O were identical within experimental error. To the extent there is an H/D isotope effect, the methods used in this study were not sensitive enough to detect it. This is reasonable because the predicted magnitude of the isotope effect on E^o is predicted to be very small.
- Our findings for the specific DET mechanisms for aliphatic carboxylates differed from published reports (earlier work by Gonzáles et al.); we attribute this discrepancy to possible contamination with trace water in the earlier work.
- Possible explanations for the effect of water on the DET mechanism were presented. Computational studies regarding solvation effects on the radical intermediate carboxyl radicals and carboxylate anions are needed to assess the viability of these hypotheses, and are currently being done in collaboration.
- In contrast to aliphatic carboxylates, our preliminary analyses of phenyl acetate indicate a stepwise mechanism, which agrees with published work—with the exception that it features a one-electron process instead of two. Further studies of aryl carboxylates and other substituted derivatives of phenyl-acetates are needed to elucidate the mechanistic behavior of these complexes.

3.11. Materials.

Acetonitrile. HPLC grade solvents were used as received unless otherwise stated. HPLC grade acetonitrile was distilled slowly at 70 ^{o}C over calcium hydride under dried nitrogen passed over a column of 4A molecular sieves. All glassware was stored at 110 ^{o}C prior to assembling. Distilled acetonitrile was stored over dried molecular sieves and sealed prior to being disconnected and transferred to the glovebox. Distilled acetonitrile was passed through activated alumina prior to use. All solvents and starting materials were obtained from Sigma-Aldrich unless otherwise stated.

3.12. Experimental techniques.

3.12.1. Electrochemical instrumentations and electrochemical apparatus.

Cyclic voltammetry and controlled current coulometry were performed on an EG&G Princeton Applied Research (EG&G/PAR) Model 283 potentiosat/galvanostat.

*3.12.1.1. **Cyclic voltammetry (CV).** Identical approach to **Section 2.3***

*3.12.2. **Pulsed field gradient NMR (PFG-NMR).** Identical to **Section 2.3***

3.12.3. X-ray photoelectron spectroscopy.

A glass rod of a GC electrode was cut without disturbing the Cu-rod connected to the glassy carbon plug. The GC was prepared in accordance to the described polishing procedure. Three consecutive scans were performed at 1.5 V/s and the GC electrode was molted on a 3 by 3 cm piece of glass using fast-glue. The sample was kept in a vial until dry. The XPS data presented in this article were obtained by employing monochromatic radiation from a Phi 5300 X-ray source (Mg K-alpha, 1253.6 eV) operating at 250 W (12 kV). Ejected photoelectrons were detected using a hemispherical energy analyzer (PSD input, Omni Focus II lens, 80-360 analyzer control) operated at a take-off angle of 45^{o} with respect to the surface. All high-resolution spectra were acquired in the region of interest using the following experimental parameters: pass energy of 17.90 eV; step

size of 0.1 eV and dwell time of 25 ms. The binding energy scales for all spectra were referenced to the C (1s) peak at 284.6 eV.

3.13. Experimental syntheses

3.13.1. Tetra-n-butylammonium zwitterion.

Tetra-n-butylammonium bromide was dissolve in a minimal volume of methanol. An equimolar ratio of silver oxide powder was added slowly to the solution while stirring with a magnetic bar for an hour. The glassware was covered with parafin to avoid evaporation of methanol over time. A greenish-grayish powder was formed that precipitated at the bottom of the beaker. Additional silver oxide (1/3 ratio) was added to the solution and allowed to stir for an additional two hours. The supernatant of the solution was tested for bromide with a diluted nitric acid in silver nitrate solution. If yellowish-white precipitate was observed, additional silver oxide was added and allowed to stir. After a negative bromide test, the mixture was filtered over a celite column.

3.13.2. Tetra-n-butylammonium perchlorate (TBAP). Identical to ***Section 2.3.3***

3.13.3. Tetra-n-butylammonium methoxide.

Tetra-n-butylammonium bromide was dissolve in a minimal volume of methanol. An equimolar ratio of silver oxide powder was added slowly to the solution while stirring with a magnetic bar for an hour. The glassware was covered with parafin to avoid evaporation of methanol over time. A greenish-grayish powder was formed that precipitated at the bottom of the beaker. Additional silver oxide (1/3 ratio) was added to the solution and allowed to stir for an additional two hours. The supernatant of the solution was tested for bromide with a diluted nitric acid in silver nitrate solution. If yellowish-white precipitate was observed, additional silver oxide was added and allowed to stir. After a negative bromide test, the mixture was filtered over a celite column.

3.13.4. Tetra-n-butylammonium carboxylates.

An equimolar solution of corresponding carboxylic acid in methanol was mixed with a tetra-n-butylammonium methoxide solution. The resulting solution was rotovapped under *vacuo* at 50 ^{o}C until a white solid formed. Methanol solvent was removed with several hexane washes in *vacuo* at 50 ^{o}C. The white solid was washed with hot cyclohexane to yield white flakes over dried ice. The cyclohexane was decanted and the white solid was dried over P_2O_5 for several days in a vacuum desiccator and transferred under *vacuo* into the glovebox.

3.13.1. Tetra-n-butylammonium propionate.

An equimolar solution of pivalic acid in methanol was used as the corresponding acid. ^{1}H NMR ($CDCl_3$, 400MHz) δ 1.00-1.10 (t, 3H), 2.10-2.20 (q, 2H), 3.47 (s, 12H). The findings are consistent with reported literature.[29]

3.13.2. Tetra-n-butylammonium pivalate.

An equimolar solution of pivalic acid in methanol was used as the corresponding acid. ^{1}H NMR ($CDCl_3$, 400MHz) δ 0.95-1.05 (t, 12H), 1.16 (s, 9H), 1.35-1.45 (sex, 8H), 1.52-1.65 (quin, 8H), 3.20-3.30 (t, 8H). The procedure was adopted from synthesis of tetra-n-butylammonium carboxylate.[29] Although no ^{1}H spectrum was available for this compound, the chemical shifts are identical in nature for a shift from the acid form into the tetra-n-butylammonium salt.

3.13.3. Tetra-n-butylammonium benzoate.

An equimolar solution of benzoic acid in methanol was used as the corresponding acid. ^{1}H NMR ($CDCl_3$, 400MHz) δ 0.95-1.05 (t, 12H), 1.35-1.45 (sex, 8H), 1.52-1.65 (quin, 8H), 3.20-3.30 (t, 8H), 7.15-8.15 (5H). The findings are consistent with reported literature.[30]

3.13.4. Tetra-n-butylammonium phenyl acetate.

An equimolar solution of phenyl acetic acid in methanol was used as the corresponding acid. ^{1}H NMR ($CDCl_3$, 400MHz) δ 0.95-1.05 (t, 12H), 1.35-1.45 (sex, 8H), 1.52-1.65 (quin, 8H), 3.20-3.30 (t, 8H), 3.55 (s, 2H), 7.05-7.5 (t (2 H), t (2H), d (1H)). The procedure was adopted from synthesis of tetra-n-butylammonium aryl succinimide and benzoate.[30] Although no ^{1}H spectrum was available for this compound, the chemical shifts are identical in nature for a shift from the acid form into the tetra-n-butylammonium salt.

References

(1) Andrieux, C. P.; Gonzalez, F.; Saveant, J. M. *J. Electroanal. Chem.* **2001**, *498*, 171.

(2) Walling, C.; Wagner, P. *J. Am. Chem. Soc.* **1963**, *85*, 2333.

(3) Lu, Z.; Continetti, R. E. *The Journal of Physical Chemistry A* **2004**, *108*, 9962.

(4) Galicia, M.; Gonzalez-Fuentes, M. A.; Valencia, D. P.; Gonzalez, F. J. *J. Electroanal. Chem.* **2012**, *672*, 28.

(5) Hilborn, J. W.; Pincock, J. A. *J. Am. Chem. Soc.* **1991**, *113*, 2683.

(6) Blanksby, S. J. E., G.B. *Acc. Chem. Res.* **2003**, *36*, 255.

(7) Hioe, J.; Zipse, H. *Org. Biomol. Chem.* **2010**, *8*, 3609.

(8) Eberson, L. *Acta Chem. Scand., Ser. B* **1984**, *38*, 439.

(9) Eberson, L. *Acta Chem. Scand.* **1963**, *17*, 2004.

(10) In *Applications of Ion Chromatography for Pharmaceutical and Biological Products*; John Wiley & Sons, Inc.: 2012, p 449.

(11) Kütt, A.; Leito, I.; Kaljurand, I.; Sooväli, L.; Vlasov, V. M.; Yagupolskii, L. M.; Koppel, I. A. *J. Org. Chem.* **2006**, *71*, 2829.

(12) *CRC Handbook of Chemistry and Physics*; 91 ed.; CRC Press: Coca Raton, FL, 2010; Vol. 53.

(13) Britt, P. F.; Buchanan, A. C.; Eskay, T. P.; Mungall, W. S. *Abstr. Pap. Am. Chem. Soc.* **1999**, *218*, U620.

(14) Britt, P. F.; Buchanan, A. C. *Abstr. Pap. Am. Chem. Soc.* **2012**, *244*.

(15) Chateauneuf, J.; Lusztyk, J.; Ingold, K. U. *J. Am. Chem. Soc.* **1988**, *110*, 2886.

(16) Crist, B. V. *Handbook of Monochromatic XPS Spectra: The Element of Native Oxides* Wiley, 2000.

(17) Galicia, M.; Gonzalez, F. J. *J. Electrochem. Soc.* **2002**, *149*, D46.

(18) Hernández, D. M.; González, M. A.; Astudillo, P. D.; Hernández, L. S.; González, F. J. *Procedia Chem.* **2014**, *12*, 3.

(19) Martinho, J. A. G., A.; Liebman, J. *Engergetics of Organic Free Radicals*; Blackie Academic & Professional: London, 1996; Vol. 4.

(20) Libman, J. A. M. S. A. G. J. F., Ed.; Blackie Academic & Profeesional; Vol. 4.

(21) Tsentalovich, Y. P.; Fischer, H. *J. Chem. Soc., Perkin Trans. 2* **1994**, 729.

(22) Chateauneuf, J.; Lusztyk, J.; Ingold, K. U. *J. Am. Chem. Soc.* **1988**, *110*, 2877.

(23) Markham, G. D.; Bock, C. L.; Bock, C. W. *Struct. Chem.* **1997**, *8*, 293.

(24) Rao, C. N. R. *J. Chem. Soc., Faraday Trans. 1* **1975**, *71*, 980.

(25) Yu, D.; Rauk, A.; Armstrong, D. A. *J. Chem. Soc., Perkin Trans. 2* **1994**, 2207.

(26) Rauk, A.; Yu, D.; Armstrong, D. A. *J. Am. Chem. Soc.* **1994**, *116*, 8222.

(27) Peyerimhoff, S. D.; Skell, P. S.; May, D. D.; Buenker, R. J. *J. Am. Chem. Soc.* **1982**, *104*, 4515.

(28) Eberson, L. *Electrochim. Acta* **1967**, *12*, 1473.

(29) Tonellato, U. *J. Chem. Soc., Perkin Trans. 2* **1978**, 307.

(30) Ośmiałowski, B.; Mroczyńska, K.; Kolehmainen, E.; Kowalska, M.; Valkonen, A.; Pietrzak, M.; Rissanen, K. *J. Org. Chem.* **2013**, *78*, 7582.

Chapter 4: Oxidation potential of acetate anion via homogenous redox catalysis (HRC)

Chapter 4 comprises original work toward the completion of the Ph.D. degree of Marwa Abdel Latif, the dissertation author. The author thanks and acknowledges the significant contributions of Dr. James Tanko, Committee Chair. Additionally, Dr. Jared Spencer, a former doctoral researcher, provided significant and essential content for advancing this research. Dr. Mehdi Ashraf-Khorassani, Senior Scientist, assisted with GC/GC-MS analyses. The author was also assisted by Mr. Brian Grossman, an undergraduate researcher, who was instrumental in contributing to the experimental procedures described herein and resulting data analyses.

4. Introduction.

4.1. The applicability of homogenous redox catalysis (HRC) to studies of the electron transfer rate of carboxylates.

Investigating the electrochemical response of a given substrate via direct electrochemical methods is one approach for studying the dissociative electron transfer rate and mechanism of dissociation carboxylates radicals. Alternatively, indirect electrochemistry can also be employed; this approach relies on monitoring the electrochemical response of a carrier molecule (mediator), which shuttles the electrons to/from the electrode surface to the substrate of interest in the solution. This approach is useful when direct methods provide only limited information about the dissociative electron transfer process.[1-6] Irrespective of the technique of choice, the oxidation of carboxylates always leads to decarboxylation and results in the fragmentation of these molecules. It must be noted, however, that the direct electrolysis of carboxylates shows irreversible behavior, with major fouling of the electrode surface.

An alternative approach for monitoring the behavior of the substrate is via the indirect method, which monitors the behavior of the mediator. The significance of this technique is that any change in the electrochemical response of the mediator corresponds directly to a compound's

homogenous electron transfer capability. In such cases, the mediator facilitates the oxidation process of the carboxylates by being oxidized to the reactive active form at the electrode surface where it diffuses into the solution and is reduced back to non-reactive form by the carboxylate. Hence, instead of directly analyzing the CV (coefficient of variation) profile of the carboxylates, the generated CVs of the mediator provide sufficient information about the system, thereby eliminating having to assess the irreversible behavior of carboxylates to determine oxidation potential.

Conditions must be met for the HRC process to occur. For example, employing an easily oxidizable mediator at the electrode surface is critical for this catalysis. The mediator must also feature reversible (Nernstian) behavior with a more negative oxidation potential than carboxylates ($(E^{o}_{M/M^{\cdot+}}) < (E^{o}_{S^{-}/S^{\cdot}})$). For our purposes, ferrocenes and their derivatives are well-known compounds for use in electrochemical studies, and thus are often utilized to serve as mediators. Ferrocenes have a distinctly reversible behavior with known, or easily measured, oxidation potentials. However, the reversibility will be lost with an increase in the anodic peak current if the HRC process occurs with an acetate anion (**Figure 4.1**).

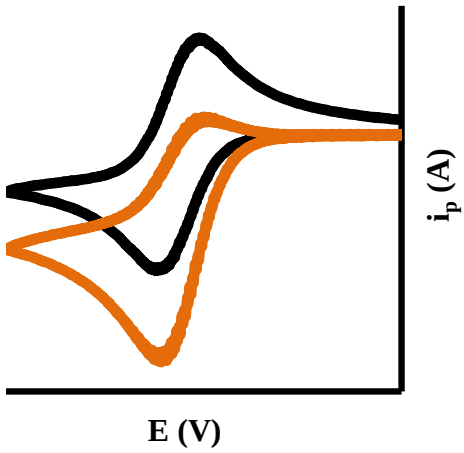

Figure 4.1. Representative cyclic voltammograms for a fully reversible mediator in the absence of the substrate of interest (black) and in the presence of the substrate of interest (orange) with an observed loss of reversibility and increased peak current.

Scheme 4.1 shows indirect electrolysis as being initiated via heterogeneous electron transfer from the mediator, as the mediator is easier to oxidize at the surface of the electrode in comparison to acetate anions. Specifically, as the oxidized form of the mediator diffuses into the solution and is reduced via homogenous electron transfer with acetate anions, the concentration of the oxidized species of the mediator becomes depleted at the surface of the electrode; as a result, the ratio of the oxidized and reduced species of the mediator is altered ($C_M/C_{M^{\cdot+}}$). Because the surface concentrations are determined via the Nernst equation, the system responds by generating more $M^{\cdot+}$, resulting in an increase in current.

The HRC process has other requirements in addition to the need to employ an easily oxidizable mediator. Importantly, the oxidation potential of both the mediator and substrate should be relatively close for homogeneous electron transfer to occur at a sufficient rate in solution. This requirement implies that backward homogenous electron transfer is as important as its forward counterpart. Thus, it is critical that forward homogenous electron transfer is (which is

thermodynamically unfavorable) is driven by a rapid and irreversible follow-up step such as a decarboxylation step.

In principle, either the homogeneous ET step, or chemical step can be the rate limiting step. Because of the high rate constants for decarboxylation of most acyloxyl radicals, it is suspected that electron transfer will be rate limited—a suspicion that can be tested experimentally.

If homogenous electron transfer is the rate-limiting step, the electrochemical response is dependent on the λ_{ET}(Eq. 4.2) which has a concentration term (C_M). If the chemical step is the rate-limiting step, response is a function of the composite rate constant $K_{ET}\mathrm{k_{cs}}$, where ($K_{ET} = \frac{k_{ET}}{k_{-ET}}$) which is concentration independent (the C_M terms in k_{ET} and k_{-ET} cancel). These criteria become essential for assigning and diagnosing the corresponding rate constant according to the nature of a system's kinetic behavior when undergoing HRC.

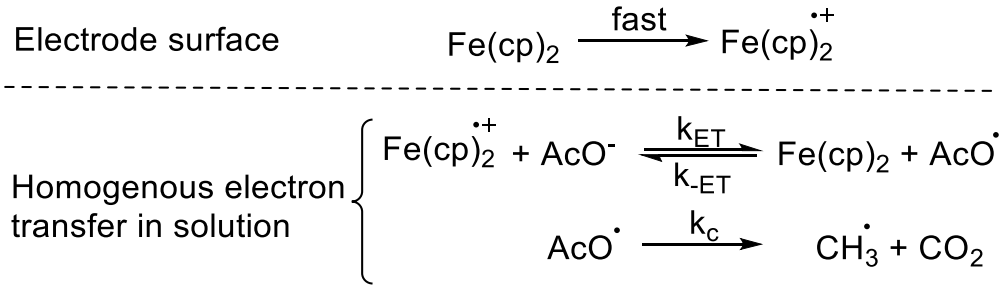

Scheme 4.1 Homogeneous redox catalysis applied to the electrochemical oxidation of acetate.

When used as a diagnostic tool for investigating the rate-limiting step in HRC, rate constants are typically expressed as dimensionless parameters. As shown in **Eq 4.1 – 4.3**, λ_{ET} and $\lambda_{CS}$are the dimensionless parameter for (a) the rate of homogenous electron transfer and (b) the chemical step rate constant, respectively, C_M^* is the mediator concentration in bulk solution, k_{ET} is the homogeneous electron transfer rate constant, and k_{cs} is the chemical step rate constant. (The other terms *v*, *R*, *T*, *n*, and *F* retain their normal meaning.[2]) Although a rate constant is typically

expressed in units that contain time and, depending on the order, concentration units, due to its contributing constituents (i.e., scan rate and concentration of mediator), a dimensionless rate constant is "unitless" since it is generated independently by eliminating these complicating factors. Hence, dimensionless forms can be considered as normalized forms, which can then be employed to compare the rate constants of processes featuring different molecularities.

$$\lambda_{ET} = \left(\frac{RT}{nF}\right)\left(k_{ET}\frac{C_M^*}{v}\right) \quad \textbf{(4.1)}$$

$$\lambda_{-ET} = \left(\frac{RT}{nF}\right)\left(k_{-ET}\frac{C_M^*}{v}\right) \quad \textbf{(4.2)}$$

$$\lambda_{CS} = \left(\frac{RT}{nF}\right)\left(k_{CS}\frac{1}{v}\right) \quad \textbf{(4.3)}$$

4.2. Preliminary data. Does the ferrocene/acetate system follow a homogenous redox catalysis process? Theoretical evidence for quasi- catalytic HRC process as performed and proposed by Dr. Jared Spencer.

Peak current variations in a mediator are a direct function of the dimentionless rate constant(s) when redox catalysis is occurring. Thus, the rate-limiting step for a redox catalysis with substituted ferrocenes in the presence of acetate can be investigated. In instances when the homogenous electron transfer is rate-limiting step, the concentration of the mediator is important. **Figure 4.2** illustrates ratio variations for the peak current of the mediator ($i_p/\gamma i_{pd}$) as a function of scan rate (υ). The parameters involved are (i_p)and (i_{pd}), which representthe peak current of the mediator in the presence of a substrate (catalytic current), and in the absence of the substrate (diffusion-only current), respectively, while γ is the excess factor between the mediator and carboxylates ($\gamma = [S]/[M]$).

The mediated oxidation of acetate was performed with ferrocene, vinyl ferrocene, and bromophenylferrocene—each featuring ten times the concentration of tetra-n-butylammonium acetate—in 0.1 M TBAP/acetonitrile under argon ($\gamma = 10$). Distinct variations in the measured ratio ($i_p/\gamma i_{pd}$) as a function of changing scan rate were noted for all three mediators, with a clear dependency on concentration as evidenced by a convergence in constructed plots once normalized for the molarity of the mediator. These findings indicate that homogeneous electron transfer is the rate limiting step.

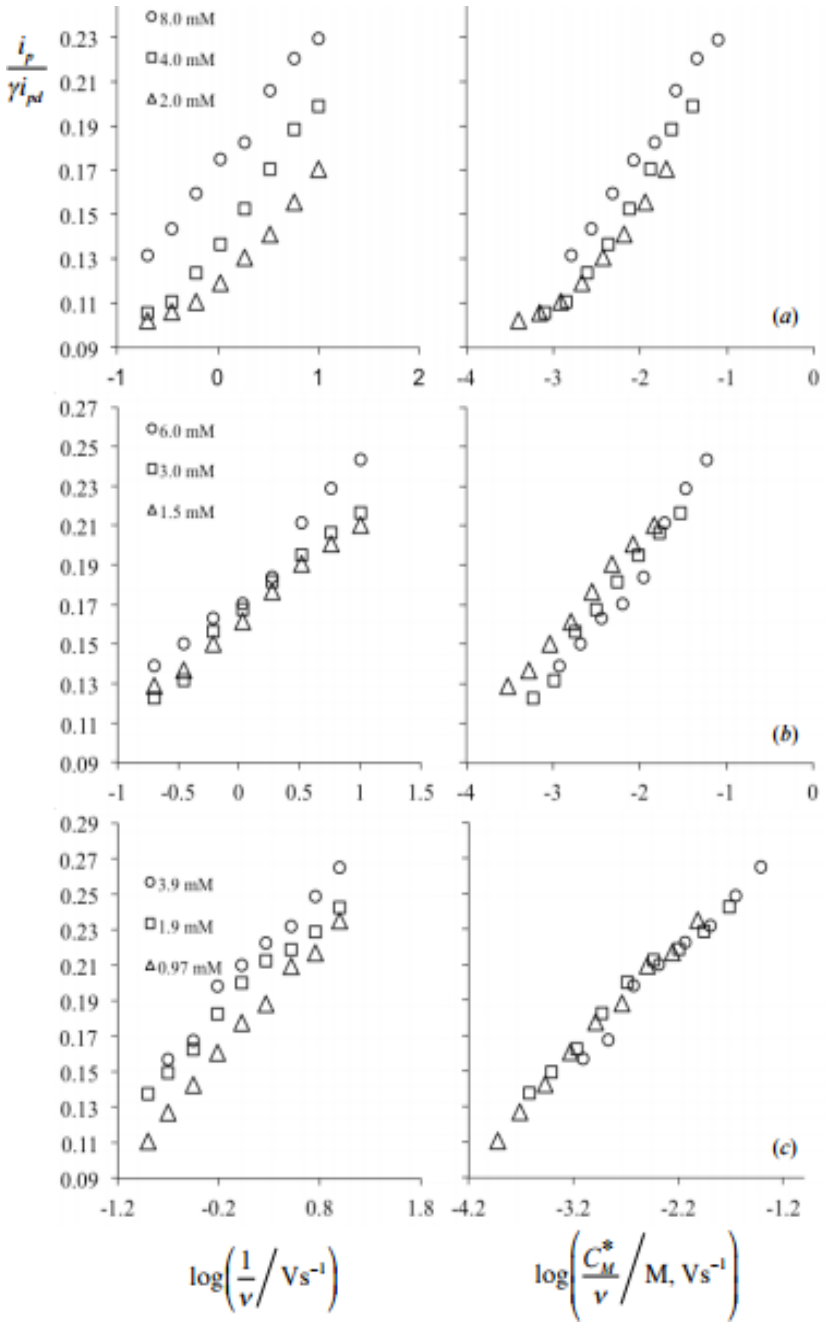

Figure 4.2. Mediated oxidation of tetra-*n*-butylammonium acetate in neat acetonitrile (0.1 M supporting electrolyte, γ = 10). Catalysis was assessed as the ratio of catalytic current (i_p) to diffusion current (i_{pd}) as a function of scan rate. Dependence of catalysis on mediator concentration indicates kinetic control via homogeneous electron transfer. Mediators from top to bottom: ferrocene, vinyl ferrocene, *p*-bromophenylferrocene.[7]

Although preliminary results are indicative of an HRC process, the experimental data fit to the theoretically generated dimensionless parameters indicate that the process is not completely

catalytic, possibly because the product radicals are consuming the mediator (**Figure 4.3 and Scheme 4.2**).[7] Refer to PhD dissertation by Jared Spencer for details.

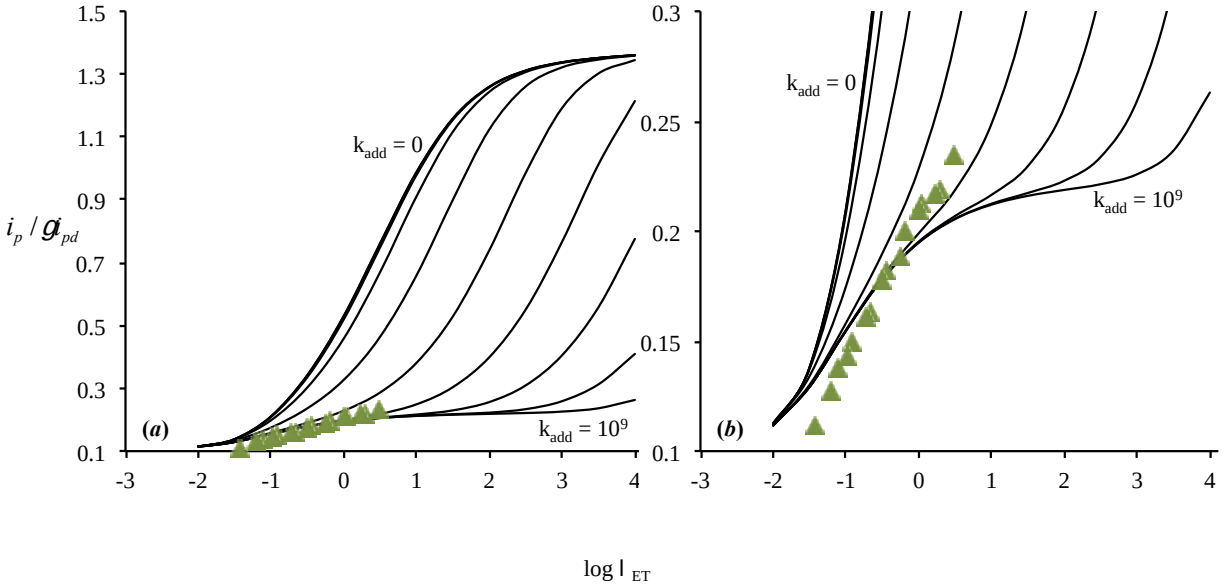

Figure 4.3. Representative schematics of simulated theoretical working curves (black lines) with superimposed experimental data for HRC runs of *p*-bromophenylferrocene with acetate (triangles) fit to the mechanism depicted in Scheme 4.2. (*a*) Full working curves where the top left curve corresponds to no addition of products to the activated mediator (k_{add} = 0 M^{-1} s^{-1}), and the bottom right curve corresponds to significant addition of products to the activated mediator (k_{add} = 10^9 M^{-1} s^{-1} (*b*) Same working curves with the y-axis scaled appropriately to better demonstrate data fitting.[7]

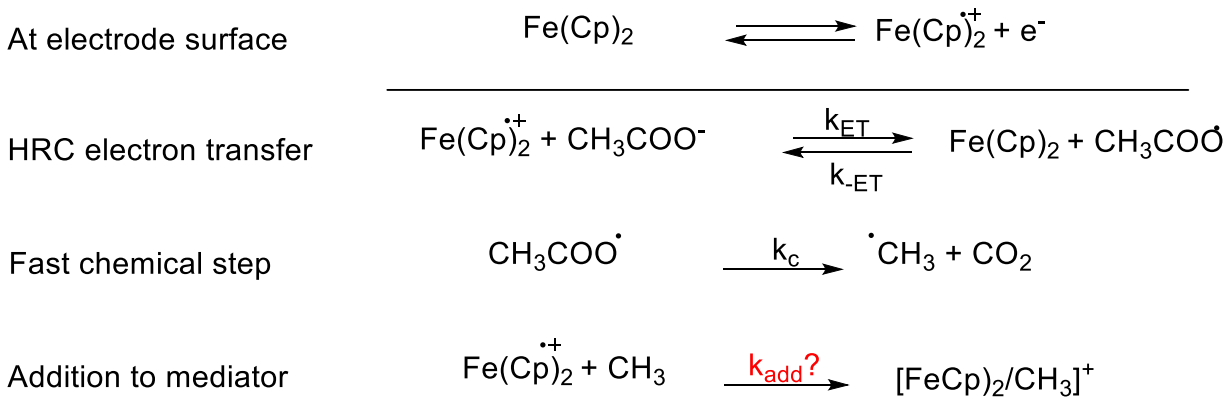

Scheme 4.2 Schematics of a competing mechanism with the catalytic homogenous electron transfer, which consumes the mediator as a result of the formation of an unstable radical. An addition reaction of the activated mediator to methyl radical, referred to as (k_{add}), is shown in Figure 4.2.

As summarized in **Figure 4.3,** one can draw three distinct conclusions from these findings, each of which should be addressed experimentally. First, the assumption of a purely catalytic mechanism associated with the HRC process in a ferrocene/acetate system is inaccurate; rather, one must assume the existence of an alternative pathway that competes with the catalytic step by which the consumption of the mediator occurs. The most likely pathway is the addition of methyl radical to the oxidized form of ferrocene. Second, the working curves suggest that when λ_{ET} increases, there will be a plateau region in the i_p/i_{pd} vs. λ_{ET} plot. In this region, it will be impossible to obtain any meaningful kinetic information. Third, the experimental fitting for *p*-bromophenylferrocene showed a higher rate of addition in comparison to analogous findings for ferrocene and vinyl ferrocene, which implies additional complexity due to substitutions on the phenyl ring. Fitted working curves for ferrocene and vinyl-ferrocene are provided as **Figure 4. 13** and **4.15** in **Appendix G**.

It is important to investigate these three conclusions experimentally. However, one is limited to either ferrocene derivatives with oxidation potentials closer to the substrate (acetate) or

inaccessible ranges of scan rates — such as very high or very low scan rates. As shown in Eq. 4.2, λ_{ET} increases with k_{ET} and inversely with sweeprate. Hence, ferrocene and its derivatives with electron withdrawing groups, which serve as more potent mediators (higher anticipated k_{ET}), were utilized in this follow up investigation. Some of these investigated derivatives of ferrocenes include *p*-cyanophenylferrocene, benzoylferrocene, and ferrocenecarboxaldheyde (**Scheme 4.3**). As a guiding hypothesis, we expected that with these mediators, k_{ET} would increase and we would enter the plateau region of the i_p/i_{pd} vs. λ_{ET} plot predicted by the theoretical working curves (**Figure 4.3**).

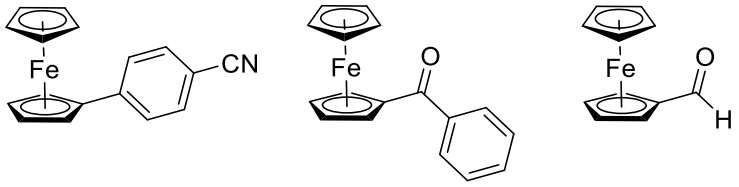

Scheme 4.3 Selected derivatives of ferrocene with oxidation potentials significantly more positive than ferrocene (E^o = 0.03 V) vs. Ag/(0.1 M) $AgNO_3$.

4.3. Results and Discussion.

4.3.1. Is HRC applicable to ferrocene/acetate systems? Experimental evidence for a non-catalytic HRC process.

Based on theoretical working curves and the mechanism proposed in **Scheme 4.2**, consumption of the mediator ought to be more significant with more potent mediators, and there will be a plateau region in the i_p/i_{pd}vs. log υ plots. This assumption can be verified by investigating HRC systems for other ferrocenes with higher oxidation potentials due to the presence of substituted electron withdrawing groups. Some electron-deficient derivatives of ferrocene include 4-cyanophenylferrocene, benzoylferrocene, and ferrocenecarboxaldehyde, which were each investigated with a series of excess factors (ɣ =0, 3, 4, 5, and 10) for a given mediator:acetate system. Ideally, a more potent mediator will display higher catalysis at a lower

mediator-to-substrate mole ratio compared to ferrocene. However, all other characteristics of the HRC process remain applicable: irreversibility, increased anodic peak currents in the presence of a substrate, and a decreasing ratio of (i_p/i_{pd})with increased scan rates.

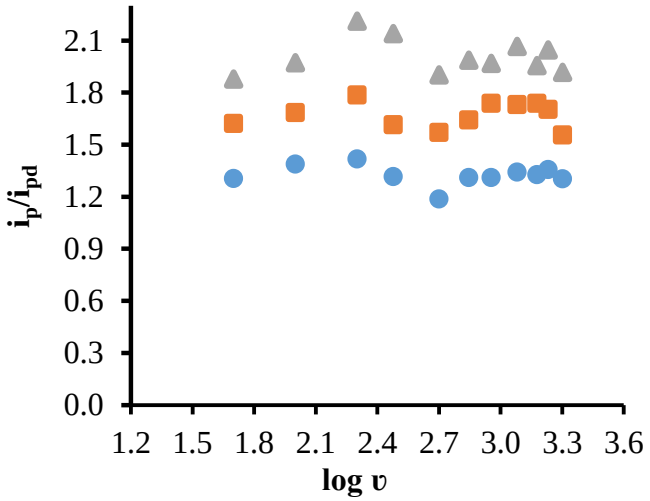

Figure 4.4. Redox catalysis of tetra-n-butylammonium acetate with 1-(-4-cyanophenyl) ferrocene with ɣ = 2, 4, and 6 (Bottom to top) at a scan range of 0.1 - 2.0 V/s in neat acetonitrile and 0.45 M TBAP at a glassy carbon vs. Ag/ (0.1 M) $AgNO_3$.

Among these mediators, only 4-cyanophenylferrocene showed a catalytic-like HRC process. Similarly to the ferrocene:acetate system, higher irreversible oxidative current peaks with no apparent shift in the peak potential were observed. Most importantly, a constant peak ratio was reported instead of the expected decreasing trend at faster scan rates (**Figure 4.4**). These findings indicate a significantly higher deviation from a purely catalytic HRC process in comparison to the analogous results when ferrocene served as a mediator. Hence, the plateau region predicted in theoretical working curves is confirmed via the use of 4-cyanophenylferrocene as a mediator.

Both benzoylferrocene and ferrocenecarboxaldheyde showed an even greater deviation from typical homogenous redox catalysis behavior in the presence of an acetate. Cyclic voltammograms displayed a loss of irreversibility, but the appearance of a pre-peak and shifts to

lower peak potentials were evident. **Figure 4.5a** shows a pre-peak with $\gamma = 1$ for benzoylferrocene:acetate. In contrast, the pre-peak in the catalytic current appeared to be absent at higher concentrations of substrate and at higher scan rates; instead, it was replaced with an overall peak potential shift in the CV profile. These observations were consistent for the catalytic peaks obtained for ferrocenecarboxaldehyde as well (**Figure 4.6**). The shift in the peak potential of the catalytic current is consistent with no further shift at higher scan rates with higher concentrations of acetate, as illustrated in **Figure 4.7b**. This type of catalytic behavior was investigated by Savéant and coworkers, who attributed the phenomenon to rapid catalysis occurring concurrently with the generation of the active form of the mediator. As a result, a pre-peak appeared due to the consumption of the substrate in the vicinity of the electrode surface, followed by a typical redox peak for the mediator as typically reported in the absence of a substrate.[2] These two features were noted in our investigation, with (a) the appearance of a pre-peak current at lower scan rates or lower acetate molarities, and (b) the replacement of the pre-peak with a potential shift in the catalytic current. The potential shift remains constant for the same system regardless of the scan rate, and increases with the increased molarity of the acetate (**Figure 4.8**).

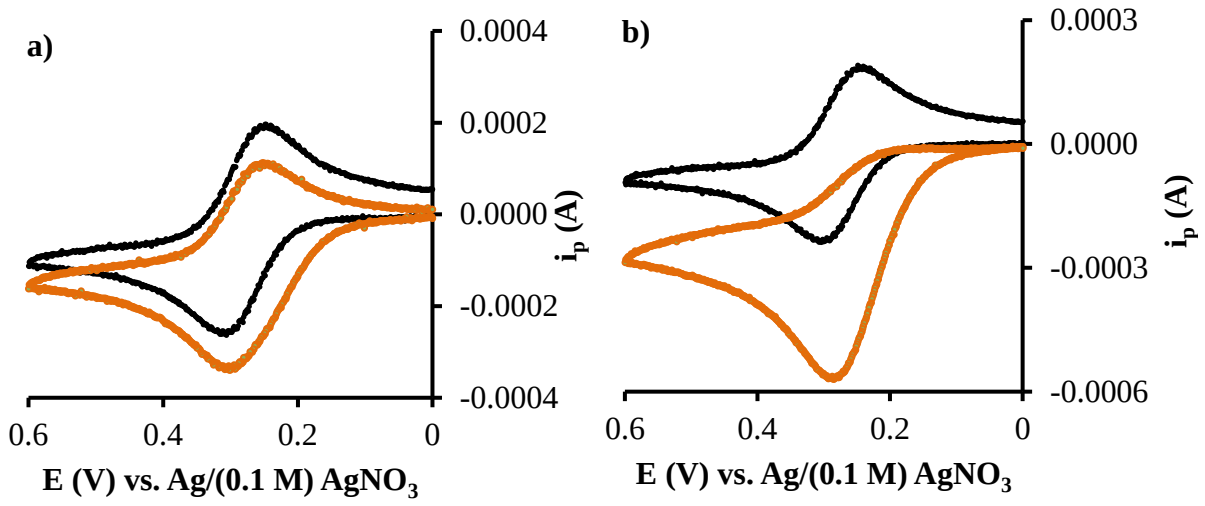

Figure 4.5. Representative cyclic voltammograms for benzoylferrocene in the absence (black) and presence of acetate (orange) with 0.45 TBAP in neat acetonitrile vs. Ag/ (0.1 M) $AgNO_3$. a) ɣ = 1 for a system of benzoylferrocene and acetate at 0.5 V/s; b) ɣ = 4 for a system of benzoylferrocene and acetate at 0.5 V/sat 0.5 V/s.

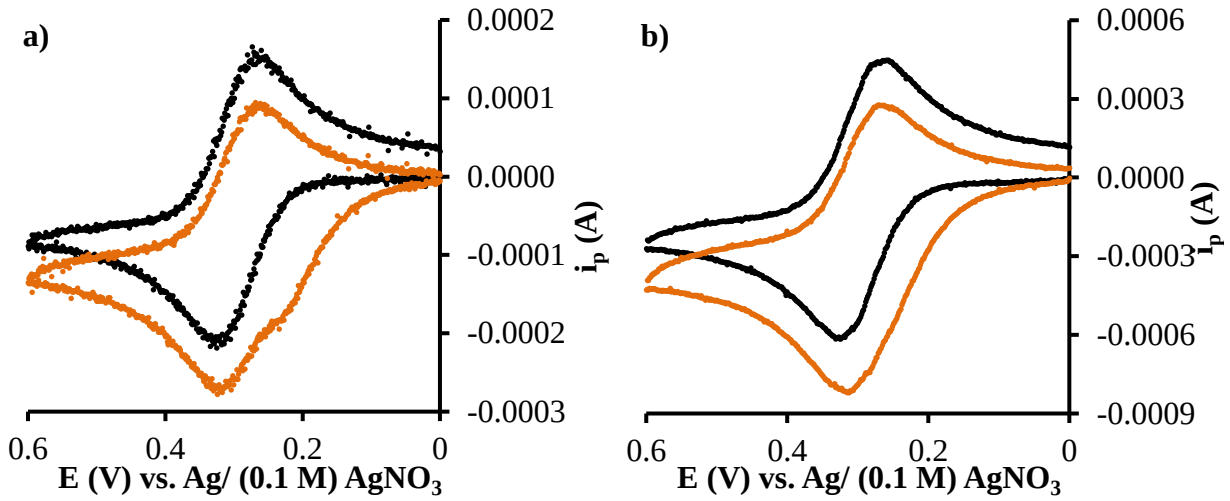

Figure 4.6. Representative cyclic voltammograms of ferrocenecarboxaldehyde with acetate in neat acetonitrile with 0.5 M TBAP vs. Ag/(0.1 M) $AgNO_3$.a)ɣ = 1 as a distinct pre-peak current is shown with a shift to lower peak potential at 0.1 V/s; b) ɣ = 1 with no evident peak current at 2.0V/s with a similar shift in the peak potential 2 V/s.

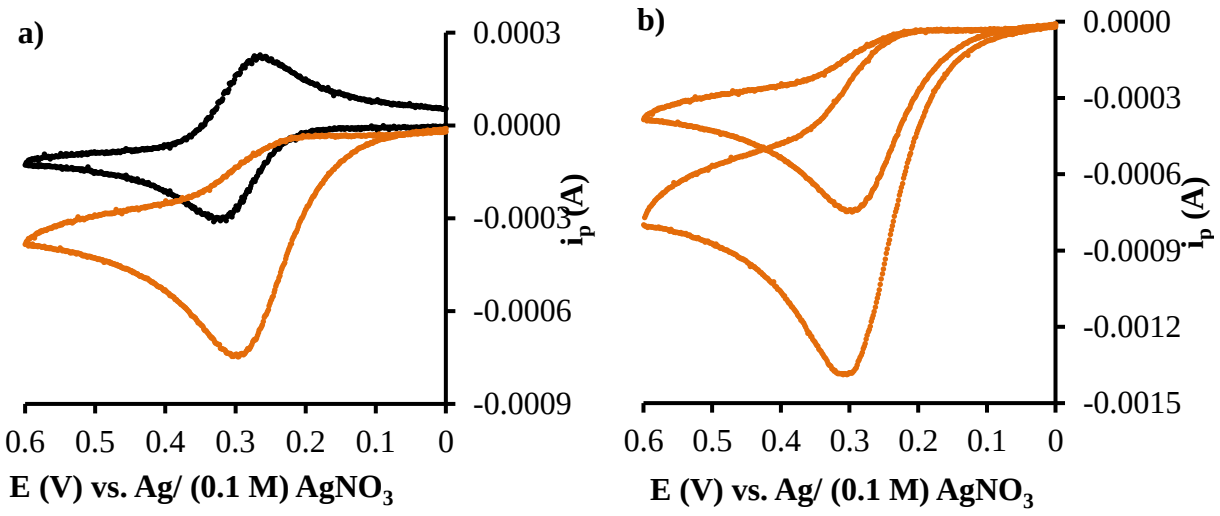

Figure 4.7. Representative cyclic voltammograms of ferrocenecarboxaldehyde with acetate in neat acetonitrile with 0.5 M TBAP vs. Ag/(0.1 M) $AgNO_3$.; a) ɣ = 4 under exact experimental conditions at 0.5 V/s. All higher excess factors are similar; b) Superimposed CVs for 0.5 V/s and 2.0V/s for ɣ = 4 of ferrocenecarboxaldehyde: acetate system indicating no additional peak shift with higher scan rates.

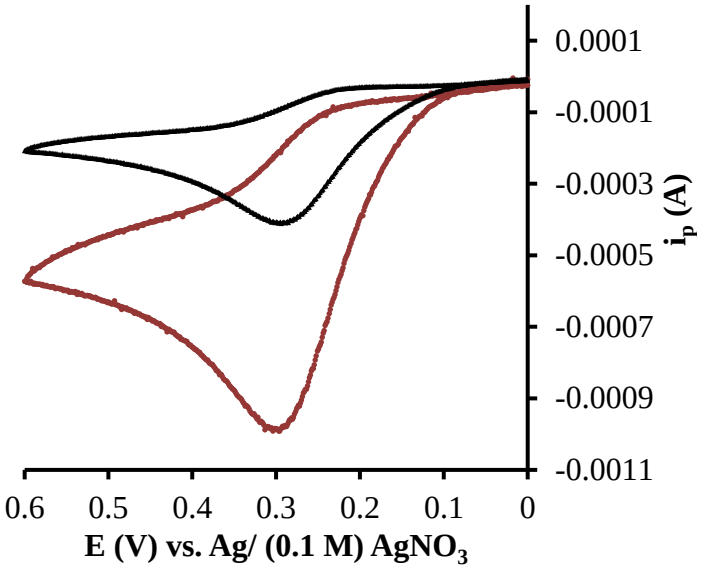

Figure 4.8. Representative CVs of ferrocenecarboxaldehyde with acetate in neat acetonitrile with 0.5 M TBAP vs. Ag/(0.1 M) $AgNO_3$.at 0.5 V/s with ɣ = 5 (black-top), and ɣ = 10 (maroon-bottom).

The fitting of experimental data in the simulated working curves indicated a higher deviation from a purely catalytic HRC process with more potent mediators—a relationship that was later supported experimentally. However, a number of questions remain as to the nature of the

competing pathway under HRC catalysis. Is the mediator being consumed? If so, how is it being consumed? Is the competing pathway a follow-up chemical reaction between the generated radical and the neutral ferrocene and/or the ferrocenium cation responsible for this phenomenon? Or is the competing pathway due to an addition of a radical to the cyclopentadiene or the metal center? Or perhaps the competing pathway is related to the addition of an acetate anion to the ferrocenium cation—or is it simply fouling? Given this level of ambiguity, it is important to confirm (or refute) the consumption of the mediator experimentally and rule out the contribution of fouling as a major competitor of homogenous redox catalysis.

4.4. Consumption of the mediator upon oxidation of ferrocenes in the presence of acetate anions: Experimental evidence for removing the mediator without subsequent fouling.

In order to elucidate the nature of possible competing mechanisms, one must first confirm if the mediator is, indeed, being consumed upon oxidation. **Figures 4.9 -4.12** illustrate electrochemical response results for ferrocene and 4-cyanophenylferrocene upon consecutive scans at the surface of a glassy carbon in the presence of acetate anions, with either no time interval between each consecutive scan, or with a pre-scan time interval of 5 seconds. Upon consecutive scans of the ferrocene in the presence of acetate anions with a 5 seconds pre-scan time interval, no significant decrease in the current was noted, which indicates that all ferrocenium ions were reduced back to ferrocene, or that the 5 second time delay was sufficient for concentrations at the electrode surface to have been replenished by diffusion (**Figure 4.9**). In contrast, results for the 4-cyanophenylferrocene indicated a continuous decrease and shift in the peak current under identical experimental conditions to a lower peak potential (**Figure 4.11**)—an observation that suggests that 4-cycnophenylferrocene is likely consumed, and that the 5 second interval is not enough time for the surface concentrations to be replenished. In addition to the decrease in the peak current, the

oxidative peak potential was noted to shift to the original peak potential noted for the 4-cyanophenylferrocene in the absence of the acetate anions. Consecutive scan results for the 4-cyanophenylferrocene with no pre-scan time interval showed a more prominent decrease in the peak current upon scans in comparison to one noted for the ferrocene (**Figure 4.10** and **Figure 4.12)**.

The constant peak current upon consecutive scans with pre-scan time interval was anticipated, due to replenishing of the diffusion layer with the mediator. The loss of current signal upon consecutive scans without a pre-scan time interval further confirmed the removal of the non-active form of the mediator at the vicinity of the electrode surface in the presence of excess acetate anions. In others words, if a purely catalytic HRC process was indeed the only mechanism occurring, the oxidized species of the mediator would be generated via homogeneous electron transfer, and the reduced species of the mediator would be present for a consecutive scan.

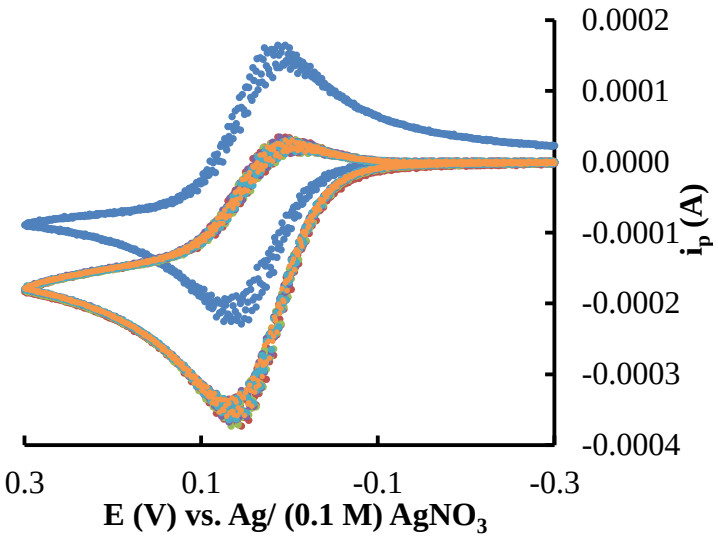

Figure 4.9: Representative multi-scan cyclic voltammograms of ferrocene in the presence of tetra-n-butylammonium acetate with a ɣ = 4 at scan rate of 0.1 V/s with 0.45 TBAP/ neat acetonitrile under anhydrous conditions vs. Ag/ (0.1 M) $AgNO_3$. Multi-scans were performed with *5 seconds pre-scan* time interval. (-) Ferrocene only (Top), (-) 1st scan with acetate, (-) 2nd scan with acetate, (-) 3rd scan with acetate, (-) 4th scan with acetate, and (-) 5th scan with acetate (Bottom- all CVs are superimposeable).

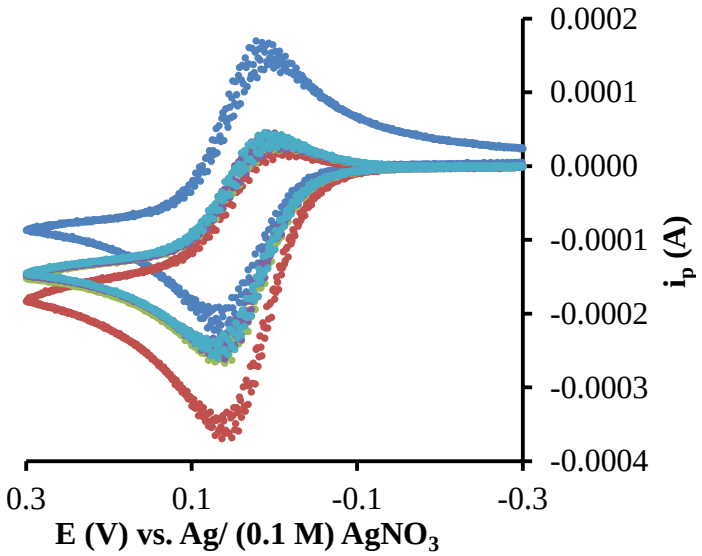

Figure 4.10: Representative multi-scan cyclic voltammograms of ferrocene in the presence of tetra-n-butylammonium acetate with a ɣ = 4 at scan rate of 0.1 V/s with 0.45 TBAP/ neat acetonitrile under anhydrous conditions vs. Ag/ (0.1 M) $AgNO_3$. Multi-scans were performed with *no pre-scan* time interval. (-) Ferrocene only (Top), (-) 1st scan with acetate (Very bottom), (-) 2nd scan with acetate, (-) 3rd scan with acetate, (-) 4th scan with acetate, and (-) 5th scan with acetate (3rd-5th scans are in the middle).

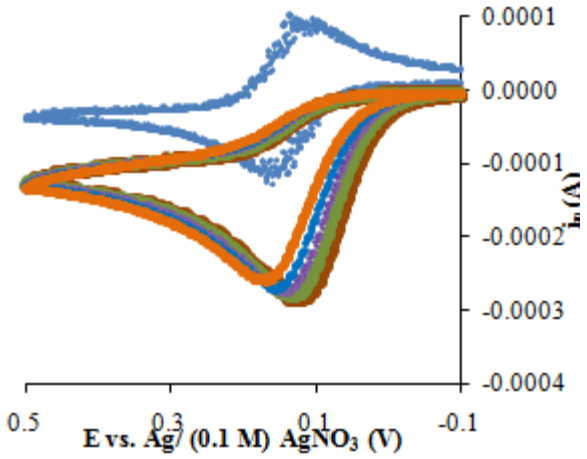

Figure 4.11. Representative multi-scan cyclic voltammograms of 4-cyanophenylferrocene in the presence of tetra-n-butylammonium acetate with a ɣ = 4 at scan rate of 0.1 V/s with 0.45 TBAP/ neat acetonitrile under anhydrous conditions vs. Ag/ (0.1 M) $AgNO_3$. Multi-scans were performed with *5 seconds pre-scan* time interval. (-) Cyanoferrocene only (Top), (-) 1st scan with acetate, (-) 2nd scan with acetate, (-) 3rd scan with acetate, (-) 4th scan with acetate, and (-) 5th scan with acetate (Slight decrease in peak current with consecutive scans).

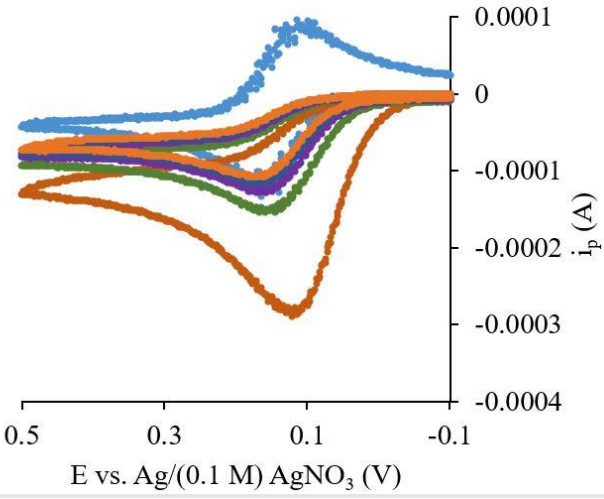

Figure 4.12. Representative multi-scan cyclic voltammograms of 4-cyanophenylferrocene in the presence of tetra-n-butylammonium acetate with a ɣ = 4 at scan rate of 0.1 V/s with 0.45 TBAP/ neat acetonitrile under anhydrous conditions vs. Ag/ (0.1 M) $AgNO_3$. Multi-scans were performed with *no pre-scan* time interval. (-) Cyanoferrocene only (Top), (-) 1st scan with acetate, (-) 2nd scan with acetate, (-) 3rd scan with acetate, (-) 4th scan with acetate, and (-) 5th scan with acetate (Significant decrease in peak current with consecutive scans).

Although recently discussed in some detail by González and coworkers,[8-10] the fouling of the electrode surface by alkyl radicals does not appear to play a significant role in varying the peak currents. Nonetheless, their findings point to contribution purely catalytic HRC process in a ferrocene/acetate system; additionally, the authors attribute discrepancies in the peak currents at various scan rates to electrode fouling by methyl radical upon decarboxylation (**Scheme 4.4**). Although it is possible that fouling could play a role in the cumulative current signal, no significant signal drop was noted upon consecutive scans without polishing the electrode for the subsequent electrolysis of acetate with ferrocene or 4-cyanophenylferrocene as mediators.

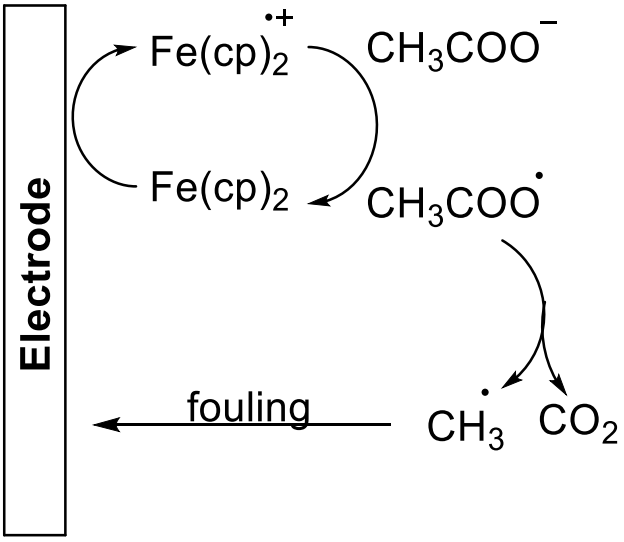

Scheme 4.4 Loss of signal due to the electrode modification by methyl radical upon homogenous redox catalysis. Adapted from Gonzalez and coworkers on the mediated redox catalysis of acetate anions by ferrocene.[9]

4.5. Conclusion.

Given the inherent experimental challenges of investigating the oxidation potential of acetate anions direct electrolysis, homogenous redox catalysis was employed as an alternative approach for investigating this compound. As described herein, ferrocene and its derivatives are well-known and well-behaved electrochemical mediators. Indeed, redox catalysis has been

reported previously for ferrocene in the presence of acetate anions. Our results, however, confirmed the following:

- The use of HRC as a process for a ferrocene/acetate system is inadequate and thus not useful for thoroughly evaluating the kinetics and thermodynamics of acetate anions. That said, our findings do indicate a quasi-catalytic HRC process for ferrocene and its derivatives when combined with acetate anions.
- Additionally, theoretical working curves for a range of purely and quasi-catalytic HRC processes —which are based on a model for the consumption of the mediator via a competing pathway—predict further deviation from catalytic behavior with more potent mediators. Subsequent experimental evidence supports this prediction and indicates a competing mechanism to HRC in the case of of *p*-cyanophenylferrocene.
- Benzoylferrocene, and ferrocene carboxyladehyde were also investigated, but results were ambiguous, which made further investigations impractical.
- Further investigations of the electrochemical response of quasi-catalytic HRC process for ferrocene and 4-cyanophenylferrocene also suggest the addition of a mediator as a competitive pathway toward HRC-based catalysis. However, the exact nature of the competing mechanism remains unknown as spectroscopic studies of mixture byproducts for ferrocene:acetate systems were inconclusive as compared to precedent literature (UV-Vis, NMR, and GC-MS). Specifically, UV-Vis studies indicated an approximate 20% decrease in the initial concentration of the mediator upon electrolysis with acetate, but further analyses showed no

evidence of ferrocenyl derivatives. Refer to **Appendix F** for detailed information on byproduct analyses.

4.6. General Procedures.

4.6.1. Electrochemical instrumentations and electrochemical apparatus.

Cyclic voltammetry and controlled current coulometry were performed on an EG&G Princeton Applied Research (EG&G/PAR) Model 283 potentiosat/galvanostat.

4.6.1.1. Cyclic voltammetry (CV).

Cyclic voltammetry was carried out in a conventional three- electrode cell, with 3.2 mm diameter glassy carbon (GC) as a working electrode with a calculated active surface area of 0.18 cm^2. A platinum coil was used as an auxiliary electrode and the reference electrode was Ag/ (0.1 M in CH_3CN, 0.337 V vs. SCE). The reference electrode was calibrated with ferrocene runs (E^o = 0.030 ± 0.005 V). Prior to use, the GC electrode was sanded and polished with alumina slurry (Buehler) in the decreasing order of 1.0 μM, 0.3 μM, and 0.05 μM on a micro-cloth and rinsed with a mixed solution of isopropyl/DI water and subsequently ultrasonicated in isopropyl alcohol/water solution prior to use. Minimal and insignificant adsorption of carboxylates by-products to the surface of the electrode were noted during consecutive scans and no polishing between consecutive scans was performed. All voltammetric measurements were performed inside a glovebox at 27 ^oC unless stated otherwise. All experiments were performed in an inert atmosphere (glovebox) with dried glassware stored in oven at 110 ^oC and all CVs were performed with 95% compensated IR and a subtracted from a corresponding background scan unless stated otherwise. Scan rates varied from 0.05 – 2.5 V/s. Background scans were performed prior to performing the initial cyclic voltammograms for ferrocenes, followed by the addition of a known concentration of tetra-n-butylammonium acetate. All concentrations were prepared *via* dilution method to produce the highest accuracy. Consecutive scans were performed with a 15 sec – 20 sec time interval for rehomogenizing the solutions.

4.6.1.2. Controlled current coulometry.

Bulk electrolysis with a controlled current coulometry was performed in a conventional 2-compartment electrolysis cell (H-like shaped) separated with a small glass frit. A platinum mesh electrode served as the working electrode with a reference electrode consisting of Ag/ (0.1 M in CH_3CN, 0.337 V vs. SCE) in one compartment, and a coiled copper wire served as an auxiliary electrode in the other compartment. All experiments were performed at ambient temperatures in an open atmosphere. A constant current of 30 mA was applied and the duration of the experiment was adjusted in accordance to the concentration of the catalyst (ferrocene and its derivatives). The reaction progress was monitored via the color change from orange to dark green. The reaction mixture was subjected to various solvent extractions and the fractions were identified via NMR, UV-VIS, and GC/GC-MS.

4.6.2. Gas chromatography (GC).

GC was performed and recorded on a Hewlett Packard HP 5890A instrument equipped with FID detector, and an HP 3393A reporting integrator, DB-5 column (30x0.32 m) or (15 x 0.32 m).

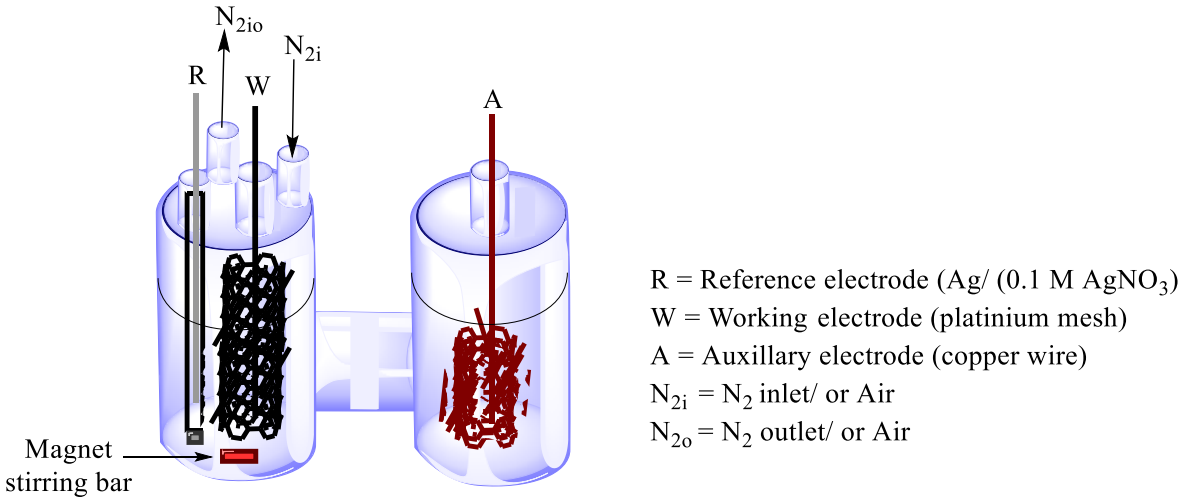

Scheme 4.5Bulk electrolysis setup for a conventional two-isolated electrochemical cell with a glass frit.

4.6.3. BASi Digisim simulation software.

A C^{++} program was utilized to simulate possible electrochemical mechanistic schemes to evaluate the qualitative cyclic voltammograms with an electron transfer occurring at the surface of the electrode. Although this study does not go into any detail about available software and fundamental theories/conditions needed to perform digital simulations to mimic mass transport in solutions for an electrochemical process, we will provide the simulation details as needed to enhance our experimental findings. For an extensive discussion of available software, as well as the theory and applicability of numerical methods of digital simulations to solve mass transport problems, the reader is referred to citations herein.[11-15] The software was operated under specific conditions to provide the most relevant quantitative analyses. Critical CV parameters included a planar geometry with semi-infinite diffusion and disabled pre-equilibrium option. For mode parameters, a value of 0.1 for expanding grid factor, a value of 0.005 D^*/k^*, a value for X_{max}/SQRT(Dt) of 2. The parameters were tested on the oxidation of ferrocene (symbol A) into ferrocenium (symbol B) as a reference model for validation with a mechanism of A + e = B (α/λ of 0.5 eV, E^o = 0V and k_s = $1x10^4$ cm/s). DigiSim software was used to obtain quantitative measurements of the rate constants for the proposed redox catalysis of ferrocene/its derivatives with tetra-n-butylammonium acetate.

4.6.4. Steady-state UV-vis spectroscopy.

Spectra were recorded on a Hewlett-Packard diode array UV-vis spectrophotometer (HP 8452A). For each solvent extraction, the solvent was tarred prior to recording measurements. Tetra-n-butylammonium acetate and tetra-n-butylammonium perchlorate salts showed no UV-signal in acetonitrile. Solvent extractions were performed with hexane, ether, and ethyl acetate in the listed order.

References

(1) Savéant, J. M.; Su, K. B. *J. Electroanal. Chem. Interfacial Electrochem.* **1984**, *171*, 341.

(2) Andrieux, C. P.; Blocman, C.; Dumas-Bouchiat, J. M.; M'Halla, F.; Savéant, J. M. *J. Electroanal. Chem. Interfacial Electrochem.* **1980**, *113*, 19.

(3) Andrieux, C. P.; Savéant, J.-M. *J. Electroanal. Chem. Interfacial Electrochem.* **1986**, *205*, 43.

(4) Andrieux, C. P.; Dumas-Bouchiat, J. M.; Saveant, J. M. *J. Electroanal. Chem. Interfacial Electrochem.* **1978**, *87*, 55.

(5) Andrieux, C. P.; Dumas-Bouchiat, J. M.; Saveant, J. M. *J. Electroanal. Chem. Interfacial Electrochem.* **1978**, *88*, 43.

(6) Andrieux, C. P.; Dumas-Bouchiat, J. M.; Savéant, J. M. *J. Electroanal. Chem. Interfacial Electrochem.* **1980**, *113*, 1.

(7) Spencer, J. N.; Virginia Tech: 2016; Vol. PhD.

(8) Hernández, D. M.; González, M. A.; Astudillo, P. D.; Hernández, L. S.; González, F. J. *Procedia Chem.* **2014**, *12*, 3.

(9) Hernández-Muñoz, L. S.; Fragoso-Soriano, R. J.; Vázquez-López, C.; Klimova, E.; Ortiz-Frade, L. A.; Astudillo, P. D.; González, F. J. *J. Electroanal. Chem.* **2010**, *650*, 62.

(10) Hernández-Muñoz, L. S.; González, F. J. *Electrochem. Commun.* **2011**, *13*, 701.

(11) Kissinger, P. T.; Heineman, W. R. *Laboratory techniques in electroanalytical chemistry*; Dekker, 1984.

(12) Britz, D. *Digital Simulations in Electrochemistry*; 2nd ed.; Springer -Verlag Berlin Heidelberg New York, 2005; Vol. 23.

(13) Rudolph, M. *J. Electroanal. Chem.* **1994**, *375*, 89.

(14) Rudolph, M. *J. Electroanal. Chem. Interfacial Electrochem.* **1991**, *314*, 13.

(15) Gottesfeld, S.; Feldberg, S. W. *J. Electroanal. Chem. Interfacial Electrochem.* **1985**, *194*, 1.

Chapter 5. Does Metal Ion Complexation Make Radical Clocks Run Fast? An Experimental Perspective

Chapter 5 is a modified version of a manuscript co-authored by Dr. J. M. Tanko, Marwa Abdel Latif, and Dr. Jared Spencer to be submitted for publication. It compromises original work toward the completion of Ph.D. degree of Marwa Abdel Latif (laser flash photolysis experiments). Dr. Jared Spencer did the theory/computation experiments. Experimental procedures and data analyses were performed by Marwa Abdel Latif, the dissertation author.

5. Introduction.

5.1. Ion complexation for the stabilization of radical clocks.

Radical clocks,[1] usually based upon unimolecular fragmentations or rearrangements with known absolute rate constants, are used to measure the rate constants for competing bimolecular products through competition kinetics. The underlying assumption in these experiments is that the unimolecular rate constant for the clock reaction is truly constant and not affected by reaction conditions.

In 2003, Horn and Clark posed the question "Does Metal Ion Complexation Make Radical Clocks Run Fast?"[2] To answer this question, these workers studied, computationally, the Δ^5-hexenyl radical rearrangement (**Scheme 5.1**), postulating that complexation of a metal ion to the double bond would decrease the activation energy. These authors found that ions (in general), were predicted to decrease the activation barrier to ring closure. For alkali metals, the predicted decrease in E_a paralleled the size of the ion. For Li^+ ion, which exhibited the most dramatic effect, the barrier decreased from 8.3 to 3.2 kcal/mol (CBS-RAD-(QCISD, B3-LYP), which equates to a predicted three order of magnitude rate acceleration in the presence of Li^+. The magnitude of this effect, of course, would likely be diminished in a polar solvent (vs. the gas phase) but the calculations

nonetheless predicted a ca. 1.7 kcal/mol reduction of the barrier in THF (obtained via explicit solvation of the reactants and transition state.)[2]

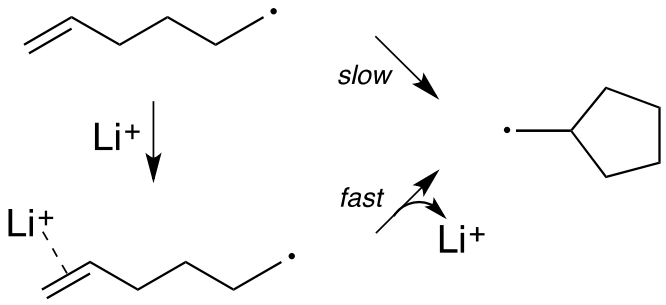

Scheme 5.1 Complexation of lithium ion to the double bond of Δ^5-hexenyl radical.

The rationale for Horn and Clark's hypothesis, i.e., that Li^+ will complex to a double bond and lower the activation barrier for *intermolecular* radical additions, has been verified both experimentally and computationally in the polymer literature, as Li^+ complexation has been demonstrated to "catalyze" the free radical polymerization of olefins, increase the propagation rate constant, etc.[3-6] However, the original question posed about radical clocks (unimolecular reactions) in their 2003 paper remains unanswered. Moreover, questions about how metal ions might affect rates of other classes of clock reactions have not yet been asked.

5.2. Objectives.

Our interest in this question comes from a slightly different perspective. Neutral free radicals can be generated by the electrochemical oxidation and reduction of anions and cations, respectively. Because electrochemical techniques such as cyclic voltammetry can be used to measure rate constants for reactions following electron transfer (illustrated for oxidation of an anion in **Scheme5.2**), and electrochemical oxidations/reductions require a supporting electrolyte,

the possibility that an ion can change the rate of a neutral radical reaction becomes an important issue.

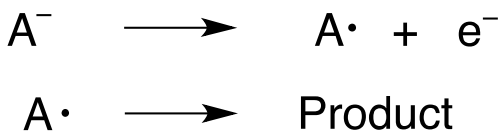

Scheme 5.2 Generated neutral alkyl radicals upon electrochemical oxidation of the corresponding anion.

To test whether the rate constant for a neutral radical clock reaction would vary in the presence of a cation, we examined the rate constant for β-scission of alkoxyl radicals. In work dating back to the early 1960s,[7] Walling and co-workers used the β-scission of t-butoxyl radical as a free radical clock to measure the rate constants for competing hydrogen abstraction reactions (**Scheme 5.3**). Walling and Wagner also suggested that k_β increased with solvent polarity (attributable to an increase in dipole moment of the transition state associated with the formation of a polar carbonyl group),[8] a hypothesis that was subsequently confirmed three decades later. [9-11]

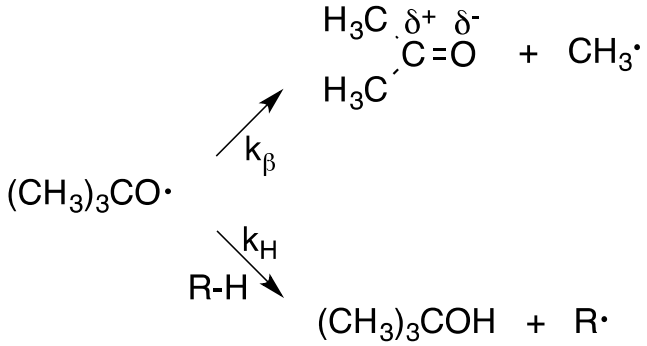

Scheme 5.3 β-scission of t-butoxyl radical favored with increase solvent polarity.

Based upon this precedent, it was quite reasonable to suspect that if the transition state for β-scission could be stabilized by a polar solvent (dipole-dipole interaction), the transition state could also be stabilized by an ion-dipole interaction as well. As a test, the rate constant for β-scission of cumyloxyl radical was measured in the presence of various electrolytes used for electrochemical studies, as well as added water. Cumyloxyl, rather than t-butoxyl, radical was used because of its characteristic absorbance at 485 nm that could be used to monitor the kinetics of the reaction.[9,12-15]

5.3. Experimental section.

A bulk solution of dicumyl peroxide was prepared in anhydrous acetonitrile in a graduated cylinder. Aliquots of 5 ml of bulk solution were transferred into 6 dr. glass vials. Appropriate masses of the desired electrolytes were added, and transferred into a cuvette sealed with a septum. The mixture was purged with N_2 for a minimum period of 10 minutes prior to photolysis. For higher concentrations of electrolytes added, solvent expansion was noted and the original concentrations were corrected.

5.4. Materials.

HPLC-acetonitrile anhydrous (Aldrich, AcroSeal ^{TM} 99.8%) was received and stored directly in a glovebox (VWR). Alumina oxide (Alfa Aesar, neutral, Brockmann Grade I) was flame-dried under vacuum prior to storage in glovebox. Acetonitrile was transferred via a glass syringe under N_2 atmosphere into a vial with a septum.

Dicumyl peroxide (98%), Lithium perchlorate ($LiClO_4$, 99.9%), Magnesium perchlorate ($Mg(ClO_4)_2$, ACS grade), Sodium perchlorate ($NaClO_4$, ACS grade) were purchased from Aldrich and used as received.

Tetra-n-butylammonium perchlorate (Bu_4NClO_4) was prepared by ion exchange reaction.[16] Tetra-n-butylammonium bromide was fully dissolved in deionized water (DI) using a magnetic stirrer and a heat gun. 70% perchloric acid was added to equimolar of tetra-n-butylammonium bromide. The Bu_4NClO_4 was washed with cold DI water (2 L) till clear aliquots were noted and tested for a neutral pH with litmus paper. The solid is dried overnight in a vacuum oven at 78 ^oC. For recrystallization, the solid was dissolved in minimal volume of ethyl acetate with continuous controlled heating and continuous stirring with a magnetic bar to yield a transparent solution. Small aliquots of hexane were added to the hot solution to yield a slowly forming but fast disappearing white precipitant. Addition of hexane and heating of the solution continued till a persistent white precipitant was formed. The solid was dissolved into solution with heating till a transparent solution was obtained. The solution is cooled down to form white needle-like crystals. The recrystallization was performed 3-5 times from ethyl acetate/hexane then dried at 80 ^oC in a vacuum oven for 24 hours. A white crystalline solid with 85% yield with a melting point of 213 ^oC was dried over P_2O_5 in a vacuum desiccator and transferred under *vacuo* into the glovebox. The literature melting point of TBAP ranges between 207-214 ^oC.

D_2O (Aldrich, 99.9atom % D) in 0.6 mL vials were purchased and used as received.

5.5. Apparatus.

5.5.1 Steady-state UV-vis spectroscopy.

Spectra were recorded on a Hewlett-Packard diode array UV-Vis spectrophotometer (HP 8452A). Laser flash photolysis (LFP) experiments were conducted using an Applied Photophysics LKS.80 spectrometer using the third harmonic of a Continuum Surelite I-10 Nd:YAG laser (4-6 ns pulse, 355 nm). Transient signals were monitored by a Hewlett-Packard Infinium digital oscilloscope and analyzed with the Applied Photophysics Spectra Kinetic Workstations software (version 4.59). Variable temperature experiments were performed with a jacketed cell holder connected to a VWR Scientific Products (PolyScience) variable temperature circulating bath (model 1150-A). The cell holder was equipped with a thermocouple to measure the temperature directly adjacent to the cuvette. Samples were thermally equilibrated prior to photolysis by placing the cuvettes in a tray in the circulating bath for at least 10 min. Afterward, the samples were placed in the spectrometer and equilibrated for an additional 10 min. (This protocol was checked by placing a thermometer directly into representative samples and verifying that the internal temperature was identical to that measured by the thermocouple over the temperature range of these studies).

5.5.1. Laser flash photolysis (LFP).

Laser flash photolysis experiments were performed with an Applied Photophysics LFP Spectrometer with a Continuum Surelite 1-10 Nd:YAG source. Steady-state UV-Vis spectra were recorded to verify that dicumyl peroxide was the only species absorbing at the excitation wavelength prior to photolysis. An absorbance range of 0.2 to 0.3 at 355 nm wavelength was recorded for a corresponded to 0.1 M of the dicumyl peroxide (di-cumyl peroxide). UV-Vis

spectrometer and all used solvents were tested for low or no absorbance at 355 nm prior to addition of dicumyl peroxide. A direct excitation of the dicumyl peroxide at 355 nm was performed and absorbance monitored using a *HP Infinium digital*oscilloscope at 485 nm. Multiple samples containing dicumyl peroxide in anhydrous acetonitrile were prepared and flashed at various laser intensities to check for any laser power dependence on the apparent rate constant. These findings show a consistent k_β within experimental error which experiments assuring no other secondary competing side reactions are occurring upon such as dimerization. Solutions containing the cumyloxyl radical precursor (di-cumyl peroxide) and desired electrolyte were prepared in acetonitrile solvent and purged for 10 minutes prior to photolysis. Replicates of the same samples were prepared for temperature dependence studies to avoid bleaching of the samples due to long exposure period to elevated temperatures. For each run, samples were allowed to equilibrate for 5-10 minutes in a temperature controlled bath with 50% solution mixture of water/ethylene glycol in addition to 5 minutes in the chamber prior to use. The chamber temperature was monitored through a built-in thermometer. Temperature dependent studies were performed from -11 ^{o}C up to 75 ^{o}C for the solvents with a ramp of 10 ^{o}C between each temperature. Rate constants were determined by the regression first order exponential fitting of the transient spectra using Applied Photophysics Spectra Kinetic Workstations software (version 4.59). Refer to **Appendix I** for detailed description of flash laser photolysis technique.

5.5.2. MO Calculations.

Calculations were performed using the Gaussian 09 computational software package.[17] Conformational analysis was performed at the B3LYP/6-31G* level of theory and basis set. All optimized reactant, transition state, and product structures as well as potential energy surface profiles were obtained at the B3LYP/6-311+(3df,2pd) level of theory and basis set (where the

unrestricted method was used for open-shell systems). All optimized structures were verified by and thermochemical corrections to the electronic energies were obtained from frequency jobs at the same theory and basis set. Single point energies for all optimized structures were obtained with the CCSD(T)/Aug-CC-pVTZ theory and basis set. Thermochemical corrections from the lower level frequency jobs were applied to the single point energies from the CCSD jobs to obtain the thermochemical data presented in **Tables 5.3 - 5.5**. For $M^+ = {}^nBu_4N^+$, the jobs were only performed at the B3LYP/6-31* level of theory and basis set as the excessive size of the anion made more expensive methods unfeasible. The visualization software MOLDEN was used to visualize the Gaussian output files.[18]

5.6. Results. Rate Constants and Activation Parameters.

Cumyloxyl radical (**Scheme 5.4**) was generated by flash photolysis of dicumyl peroxide at 355 nm in acetonitrile, and its characteristic absorption at ca. 485 nm was used to follow the kinetics.[9,12,13] Rate constants measured in the presence of various electrolytes (that were sufficiently soluble in CH_3CN) are summarized in Table **5.1**. We also determined the rate constant in the presence of H_2O or D_2O, and in the presence of electrolyte plus water. These results are summarized in **Appendix H**.

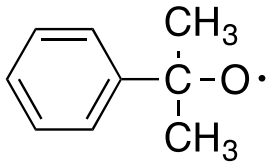

Scheme 5.3 Cumyloxyl radical generated upon photolysis.

Table 5.1
Rate constants for the β-cleavage of cumyloxyl radical in the presence of various electrolytes in CH_3CN solvent at 25 °C.

	k x 10^{-5} (s^{-1})			
Concentration (M)	$LiClO_4$	$NaClO_4$	$^nBu_4NClO_4$	$Mg(ClO_4)_2$
0		8.1 (0.2)		
0.08	9.2 (0.2)	8.4 (0.2)	8.2 (0.2)	8.3 (0.3)
0.15	10.1 (0.2)	8.6 (0.2)	8.6 (0.2)	9.5 (0.3)
0.23	10.0 (0.2)	9.0 (0.2)	8.7 (0.2)	9.7 (0.3)
0.31	11.5 (0.3)	9.4 (0.2)	9.1 (0.3)	9.2 (0.3)
0.39	12.6 (0.2)	10.2 (0.2)	9.5 (0.3)	
0.62	16.4 (0.3)	11.2 (0.2)	10.5 (0.3)	
0.77	19.2 (0.8)	11.9 (0.2)	10.7 (0.3)	
1.15			11.8 (0.4)	
1.54			12.8 (0.5)	

Arrhenius parameters for β-cleavage in CH_3CN with added electrolyte, H_2O, or D_2O were determined *via* non-linear regression analysis in accordance with the Arrhenius equation (**Eq 5.1**); reported errors are based upon 95% confidence limits. The results are summarized in **Table 5.2**.

$$k = Ae^{-E_a/RT} \qquad \textbf{Eq 5.1}$$

Table 5.2
Arrhenius parameters for the β-cleavage of cumyloxyl radical in the presence of various addends in CH_3CN solvent.

Addend	(M)	*log (A)*	E_a(kcal/mol)	k (10^{-5} s^{-1} at 30 °C)
None	0.00	11.5 (0.2)	7.68 (0.69)	11.2 (0.6)
$LiClO_4$	0.23	11.5 (0.2)	7.46 (0.27)	14.4 (0.5)
	0.39	11.6 (0.4)	7.52 (0.5)	17.6 (0.7)
	0.77	11.6 (0.9)	7.40 (0.66)	21.8 (0.7)
$NaClO_4$	0.39	11.1 (0.2)	7.00 (0.57)	13.7 (0.8)
$^nBu_4NClO_4$	0.39	11.2 (0.6)	7.15 (0.58)	12.8 (0.9)
$MgClO_4$	0.39	11.5 (0.2)	7.49 (0.74)	12.7 (0.9)
H_2O	2.1	11.3 (0.20	7.09 (0.30)	14.0 (0.6)
D_2O	2.1	11.5 (0.2)	7.43 (0.23)	13.2 (0.4)

5.7. MO Calculations.

To obtain further insight, activation energies for β-cleavage of the t-butoxyl radical (complexed to Li^+, Na^+, K^+, and $^nBu_4N^+$) were obtained through molecular orbital calculations (gas phase, **Table 5.3**). To assess the relative binding affinity of the cations (M^+) to t-butoxyl radical relative to the solvent (CH_3CN),ΔG for the following exchange reaction was determined: $CH_3CN/M^+ + {}^tBuO\bullet \rightarrow CH_3CN + {}^tBuO\bullet/M^+$; the results are summarized in **Table 5.4**.

Table 5.3
Calculated (CCSD/uB3LYP) activation free energies for β-scission of t-butoxyl radical complexed to a cation in the gas phase

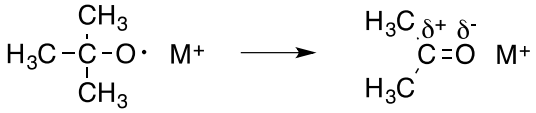

M^+	$^a\Delta G^{\ddagger}$ (kcal/mol)
none	13.8
K^+	7.6
Na^+	5.8
Li^+	2.8

Table 5.5
Calculated (CCSD/B3LYP) ΔG of binding of t-butoxyl radical cations (relative to CH_3CN) in the gas phase

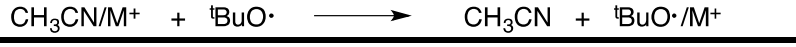

M^+	[a]ΔG (kcal/mol)
Li^+	5.3
Na^+	5.5
K^+	4.0

5.8. Discussion.

In all cases, the addition of electrolyte increased the rate constant for β-scission of the cumyloxyl radical (**Table 5.2**; **Figure 5.1**) in the order $Li^+ > Mg^{2+} \approx Na^+ > {}^nBu_4N^+$, and the magnitude of the effect increased with increasing electrolyte concentration; for clarity, the results for $Mg(ClO_4)_2$ were omitted from the figure. This study was somewhat limited by the solubility of the electrolyte in CH_3CN solvent; e.g., $KClO_4$ was not sufficiently soluble.

The activation energy for β-scission was also examined in the presence and absence of electrolyte (**Table 5.2**). Although the results seem to suggest a lowering of the barrier when M^+ is present, the effect is too small to be detected (i.e., E_a and log(A) are identical within experimental error).

To test whether the observed trend was consistent with the hypothesis that cation complexation with the developing C=O in the transition state was responsible for the observed rate enhancement, MO calculations (gas phase) were performed to model the effect of cations on the analogous β-scission of t-butoxyl radical. The results are summarized in **Table 5.3**.

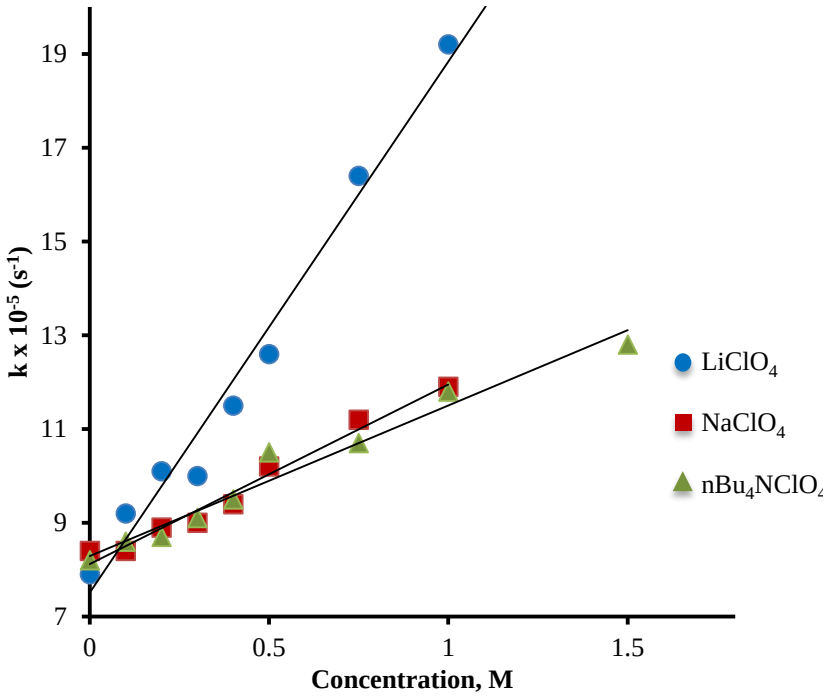

Figure 5.1. Rate constants for the β-scission of cumyloxyl radical in the presence of added electrolytes (CH_3CN solvent, ambient temperature).

Although *qualitatively* consistent with the notion that complexation of M^+ to an alkoxyl radical will lower the barrier to β-cleavage, the most striking result from the gas phase calculations is that the effect is predicted to be much, much greater than what was experimentally observed. Almost certainly, the explanation is that in solution, complexation of M^+ to an electron deficient such as an alkoxyl radical is strongly disfavored (relative to complexation to the solvent, CH_3CN). The calculations summarized in **Table 5.4** clearly support this interpretation.

We also examined whether k_β would be lowered with the addition of water, perhaps as a result of hydrogen bonding to the developing C=O in the transition state. As shown in **Figure 5.2**, in the presence and absence of electrolyte ($^nBu_4NClO_4$), the k_β increased modestly with increased water concentration.

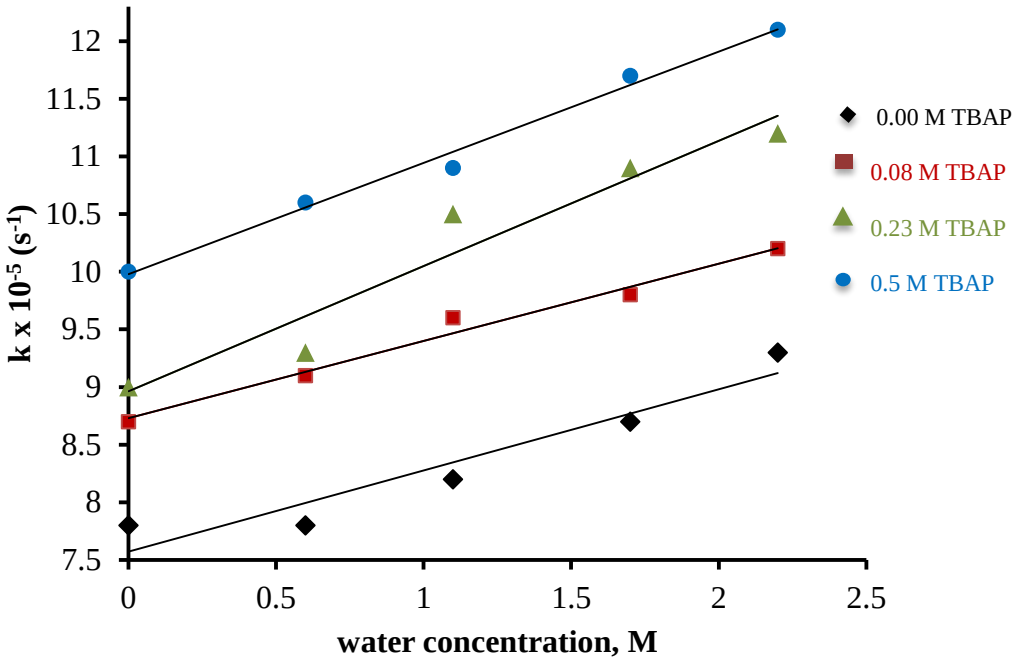

Figure 5.2. Increase in the rate constant of β-scission for cumyloxyl radical with higher water concentrations for an acetonitrile solution with a range of concentrations of tetra-n-butylammonium perchlorate.

It was also thought that if H-bonding to the transition state were important, the system might exhibit a modest secondary H/D isotope effect. Within experimental error however, there was no significant difference between H_2O and D_2O in either the observed rate constants or activation parameters (**Table 5.2**). To the extent there was an isotope effect, these measurements were not sensitive enough to detect it. Hence, these results do not reveal whether the rate increases because the transition state is stabilized by H-bonding to water, or simply because the solvent polarity increases with water addition.

5.9. Solvent polarity: Activation energy profile with variable temperatures.

The β-cleavage of cumyloxyl radical generates a polar product. Solvent-dependence of the rate constant for β-scission is known to increase with more polar solvents. The changes in the rate constant of the reaction reflects changes in the free energy of activation ($\Delta G^{\ddagger}$), with contributions from the enthalpy of activation ($\Delta H^{\ddagger}$) and/or entropy of activation ($\Delta S^{\ddagger}$) (**Eq 5.2 - 5.3**). Even though the interaction of an ion with free radical activated complex leads to significant changes in the $\Delta S^{\ddagger}$ due to impact of ions on the net charge of the complex and the rearrangement of the ions, solvent effects were attributed majorly to the changes in the dipole interactions contributing to $\Delta H^{\ddagger}$ with negligible changes to entropy of activation ($\Delta S^{\ddagger}$), in accordance with Hughes-Ingold theory.[19] In general, the quantitative contribution of ($\Delta S^{\ddagger}$) to ($\Delta G^{\ddagger}$) term is too insignificant in most reported cases (unless no change in the $\Delta H^{\ddagger}$) is noted.

$$\Delta G^{\ddagger} = \Delta H^{\ddagger} - T\Delta S^{\ddagger} \qquad \textbf{(5.2)}$$

$$k = \left(\frac{ekT}{h}\right) \exp(\Delta \mathrm{S}^{\ddagger}/\mathrm{R}) \exp(-\mathrm{E_a}/\mathrm{RT}) \qquad \textbf{(5.3)}$$

The addition of water to anhydrous acetonitrile leads to higher observed β-cleavage attributable to hydrogen bonding and/or polarity of the solvent. Steenken and coworkers investigated water effects on the β-cleavage of ring-substituted cumyloxyl radicals. Cumyloxyl radicals are suggested to carry a partial radical zwitterionic character with a partial positive charge on the ring. Water molecules are effective in stabilizing both partial charges and thus, stabilizing the excited state complex.[20]

It is important to note that hydrogen abstraction is another possibility. Hydrogen abstraction was generally deemed negligible from the water/acetonitrile solvent mix or parent peroxide.[21,22] These measurements were performed for peroxide concentrations ranging between

1.1-0.006 M. Our experimental approach was performed on solution concentrations with 0.1 M dicumyl peroxide and the possibility of hydrogen abstraction is considered insignificant. The lack of a significant solvent isotopic effect (H_2O vs. D_2O) on the β-cleavage of cumyloxyl radical further confirm the negligible contribution of hydrogen abstraction to the observed rate constant.

On the contrary, studies in DMSO solvent may be contaminated by H-atom abstraction because DMSO is a known hydrogen atom donor.[23] If hydrogen abstraction is contributing to the observed rate, it should be evident in the measured rate constants in the d_6- vs. h_6-DMSO solvents. The averaged rate constants are found to be $8.3 \pm 0.4 \times 10^5$ s^{-1} (DMSO) versus $7.6 \pm 0.2 \times 10^5$ s^{-1} (DMSO-d_6). Because these values are practically within experimental error, these results provide no clear evidence for hydrogen abstraction from DMSO (**Appendix H**). Bietti and coworkers' recent work on substrate-radical hydrogen bonding complexes with cumyloxyl radical in DMSO also reported a very low rate constant for hydrogen abstraction in DMSO but with an unexpected and unexplained high isotopic effect.[24] Thus, it is critical to choose a proper solvent system for measurements of rate constants for β-scission by which polarity is varied with low probability of hydrogen abstraction.

Lusztyk and coworkers' findings on solvent effects on the competitive β-scission and hydrogen abstraction[22] indicated only k_β varied proportionally with polarity for six solvents systems (carbon tetrachloride < benzene < chlorobenzene < tert-butanol < acetonitrile < acetic acid) due to the stabilization of the transition state of β- scission by polar solvents. The solvent polarity effects were also discussed by Steenken and others as the rate of β-cleavage of cumyloxyl radical was reported to be higher by a factor of 3 in a mixed solvent of acetonitrile/water than in anhydrous acetonitrile with k_β of 1.1×10^6 s^{-1} and 7.4×10^5 s^{-1} respectively).[21,25]

Our approach is to further examine the activation energy profile for the β- scission of cumyloxyl radical in these solvent systems for a temperature range of -293.15 K to 365 K, if it is feasible. **Figure 5.3** illustrates the variation of $\ln(k)$ as a function of $1/T$, in accordance with **Eq 5.3**. It is apparent that an overall increase in the rate of β-cleavage with solvent polarity, i.e. acetic acid, but the trend of increasing rate of cleavage does not completely follow the argued trend as published by Lusztyk and coworkers (**Table 5.5**).

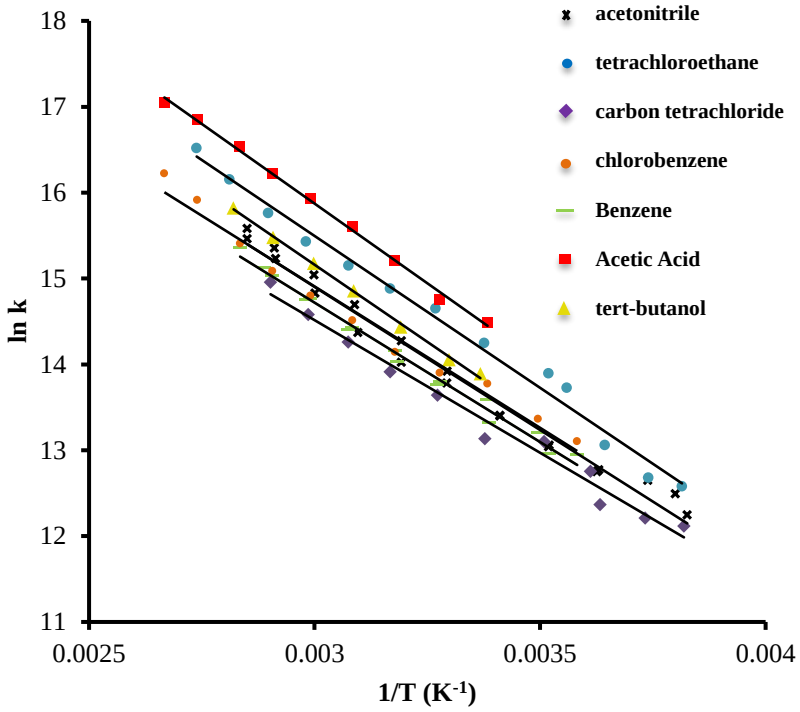

Figure 5.3. Arrhenius plot showing a solvent effect on the β-scission of cumyloxyl radical (0.75 M) with no electrolyte added.

Lusztyk argued that rate constants are dependent on solvent polarity, as shown in **Table 5.6**. Their measured values, however, do not show a significant difference within experimental error. Their findings seem to be driven by the significant difference between the most and the least polar solvents (acetic acid and carbon tetrachloride). Our measured values, although follow the general trend as predicted, further confirm the lack of significant effects of solvent polarity on β-

scission of cumyloxyl radical except for acetic acid. As carbon tetrachloride seems to not follow the predicted change, 1,1,2,2 tetrachloroethane was investigated as another highly aprotic, non-polar solvent for the β-cleavage reaction.

The rate of cleavage in tetrachloroethane is one of the highest rates reported in non-polar solvent which further confirms the "not so simple" dependence of β-cleavage on solvent polarity as the only major contributor to the demethylation rate. Our measured β-cleavage rate in acetonitrile is 7.8 ± 0.2 x 10^5 s^{-1} which falls within experimental error to the one reported by Steenken and coworkers (7.4 x 10^5 s^{-1}).[20]

Furthermore, the variations in the reported values for $\Delta H^{\ddagger}$ and $\Delta S^{\ddagger}$ do not exceed 1 kcal/mole (≈ 4.2 kJ/mol) and 6 cal/K.mol (≈ 25 J/K.mol) respectively and the slight difference are also reflected clearly in the corresponding E_a and *log A* values. Regardless of the solvent polarity, no effects of the solvent polarity on the activation energy are noted. In addition, a single construct of all of the activation energy profiles ($lnk\ vs.\ 1/T$) shows a possible convergence towards a common intersection (isokinetic point) involving most of these solvents.

Figure 5.4 illustrates further the possibility of an isokinetic relationship among these solvents at which the same activation energy is predicted at temperatures of 223.1 K and 258.2 K.[26] At very low temperatures, the rate of the reaction should be driven by enthalpy of activation (**Eq5.2**). At higher temperatures, however, entropy of activation dominates. Our experimental temperature range falls very closely to the isokinetic point and slightly under entropic control. If isokinetic point indeed exists for the β-cleavage of cumyloxyl radical, our experimental range is not sufficient to allow for the detection of subtle variations in entropy or enthalpy of activation (**Appendix H**).

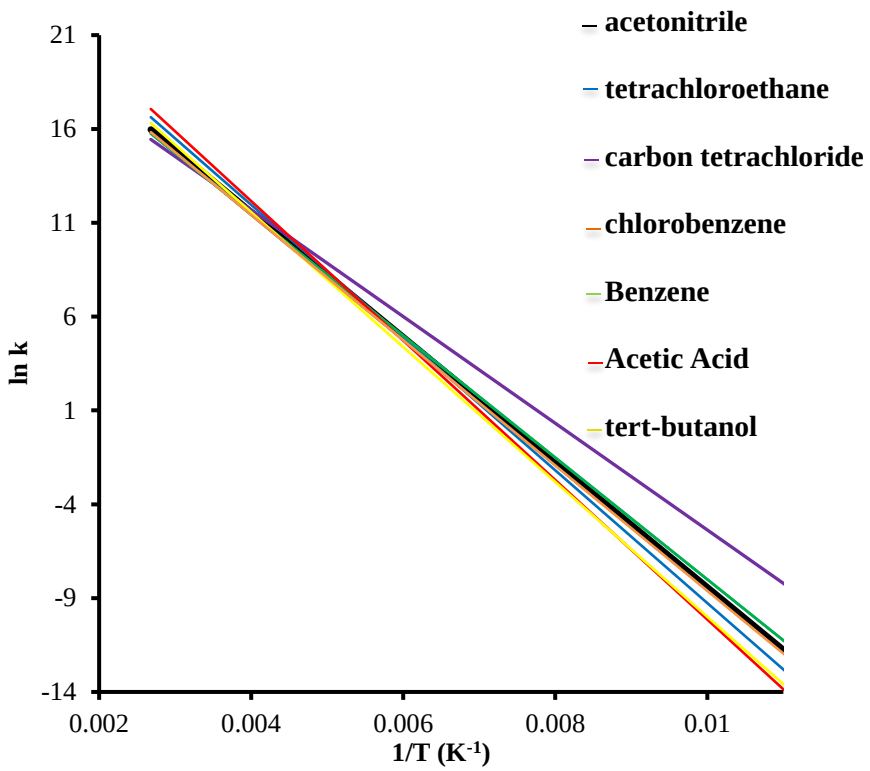

Figure 5.4. Arrhenius plot showing an isokinetic point for the β-scission of cumyloxyl radical (0.75 M) in a series of solvents with different polarity characteristics.

Table 5.6
Activation barriers calculated from Arrhenius plots with estimated enthalpy and entropy of activation for the β-scission of cumyloxyl in solvents with a range of polarities.

Solvent	E_a *(Kcal/mol)*	*log A*	$\Delta H^{\ddagger}$ $(Kcal/mol)$	$\Delta S^{\ddagger}$ $(cal/K.mol)$	[a]k *(x 10^{-5} s^{-1})*	[b]k *(x 10^{-5} s^{-1})*
Carbon tetrachloride	6.75 (0.51)	10.8 (0.4)	6.06 (0.49)	-11.62 (1.47)	7.9 (0.6)	2.6 (0.2)
1,1-2,2-tetrachloroethane	7.91 (0.78)	11.9 (-)	7.06 (0.74)	-6.89 (2.10)	18.6 (1.1)	
Acetic Acid	7.41 (0.60)	11.8 (0.6)	6.79 (0.61)	-6.85 (1.83)	25.7 (0.9)	19 (3.0)
Benzene	7.07 (0.38)	11.0 (0.3)	6.36 (0.37)	-10.44 (1.10)	8.6 (0.9)	3.7 (0.5)
chlorobenzene	8.82 (0.71)	12.2 (1.1)	7.91 (0.68)	-5.87 (0.71)	11.1 (0.9)	5.5 (2.0)
tert-butanol	7.26 (0.28)	11.4 (0.2)	6.60 (0.27)	-8.86 (0.78)	13.2 (0.6)	5.8 (1.0)
Acetonitrile	7.68 (0.69)	11.5 (-)	6.99 (0.65)	-8.11 (1.90)	11.2 (0.6)	6.3 (0.4)

[a]Calculated rate constants at 30 [o]C from Arrhenius plots; [b]Reported rate constants Steenken and coworkers.[20]

Nevertheless, one must take into consideration the shift in the slope of the line due to experimental error. The convergence is dependent on the slopes and it will certainly be affected greatly and thus, these findings are rather inconclusive without further investigation the effects of solvent polarity on similar systems showing polar free radical activated complex, i.e. decarbonylation reactions. Error bars were excluded from **Figure 5.3** and **5.4** for clarity but **Table 5.7** in **Appendix H** summarizes measured values.

5.10. Conclusions.

The results demonstrate that through complexation, the absolute rate constants for radical clock reactions such as the β-scission of alkoxyl radicals are influenced by cations (Li^{+}> Mg^{2+} ≈ Na^{+}>$^{n}Bu_4N^{+}$). This effect is attributable to stabilizing ion-dipole interactions in the transition state of the developing carbonyl group, a conclusion supported by MO calculations. In solution

however, this effect is seriously attenuated because complexation of the cation to the electrophilic alkoxyl radical (relative to the solvent, CH_3CN) is very weak. Presumably the effect would be greater in a non-polar solvent, but this would be difficult to test experimentally because of solubilities. Addressing the original question posed by Horn and Clark, yes, metal ion complexation can cause radical clocks to run fast—and for reasons that make sense based on fundamental principles. However, these results also go one step further by showing that that even if the complexation between the radical and ion is unfavorable, a significant effect can be observed if, in cases such as studied herein, there is an increase in dipole moment going from reactant → transition state.

Solvent effects on rate of β-cleavage, however, do not follow the predicted trend. A higher rate of β-cleavage is observed with increased solvent polarity as a result of a polar free radical activated complex. On the contrary, an isokinetic relationship for the β-cleavage may exist in a range of the investigated solvents. Further investigations are required to elucidate the observed phenomenon. Based on these results however, neither the trends in k_β, nor trends in the E_a (or log A) observed in different solvents provide compelling evidence that the β-scission process is subject to a significant solvent effect.

References

(1) Griller, D.; Ingold, K. U. *Acc. Chem. Res.* **1980**, *13*, 317

(2) Horn, A. H. C.; Clark, T. *J. Am. Chem. Soc.* **2003**, *125*, 2809

(3) Noble, B. B.; Smith, L. M.; Coote, M. L. *Polym. Chem.* **2014**, *5*, 4974

(4) Hirano, T.; Segata, T.; Hashimoto, J.; Miwa, Y.; Oshimura, M.; Ute, K. *Polym. Chem.* **2015**, *6*, 4927

(5) Vyakaranam, K.; Barbour, J. B.; Michl, J. *J. Am. Chem. Soc.* **2006**, *128*, 5610

(6) Clark, T. *J. Am. Chem. Soc.* **2006**, *128*, 11278

(7) Walling, C.; Jacknow, B. B. *J. Am. Chem. Soc.* **1960**, *82*, 6108

(8) Walling, C.; Wagner, P. J. *J. Am. Chem. Soc.* **1964**, *86*, 3368

(9) Avila, D. V.; Brown, C. E.; Ingold, K. U.; Lusztyk, J. *J. Am. Chem. Soc.* **1993**, *115*, 466

(10) Tsentalovich, Y. P.; Kulik, L. V.; Gritsan, N. P.; Yurkovskaya, A. V. *J. Phys. Chem. A* **1998**, *102*, 7975

(11) Baciocchi, E.; Bietti, M.; Salamone, M.; Steenken, S. *J. Org. Chem.* **2002**, *67*, 2622

(12) Avila, D. V.; Ingold, K. U.; Di Nardo, A. A.; Zerbetto, F.; Zgierski, M. Z.; Lusztyk, J. *J. Am. Chem. Soc.* **1995**, *117*, 2711

(13) Baciocchi, E.; Bietti, M.; Salamone, M.; Steenken, S. *J. Org. Chem.* **2002**, *67*, 2266

(14) Baignee, A.; Howard, J. A.; Scaiano, J. C.; Stewart, L. C. *J. Am. Chem. Soc.* **1983**, *105*, 6120.

(15) Neville, A. G.; Brown, C. E.; Rayner, D. M.; Lusztyk, J.; Ingold, K. U. *J. Am. Chem. Soc.* **1989**, *111*, 9269.

(16) House, H. O.; Feng, E.; Peet, N. P. *J. Org. Chem.* **1971**, *36*, 2371.

(17) Frisch, M. J.; Trucks, G. W.; Schlegel, H. B.; Scuseria, G. E.; Robb, M. A.; Cheeseman, J. R.; Scalmani, G.; Barone, V.; Mennucci, B.; Petersson, G. A.; Nakatsuji, H.; Caricato, M.; Li, X.; Hratchian, H. P.; Izmaylov, A. F.; Bloino, J.; Zheng, G.; Sonnenberg, J. L.; Hada, M.; Ehara, M.; Toyota, K.; Fukuda, R.; Hasegawa, J.; Ishida, M.; Nakajima, T.; Honda, Y.; Kitao, O.; Nakai, H.; Vreven, T.; Montgomery Jr., J. A.; Peralta, J. E.; Ogliaro, F.; Bearpark, M. J.; Heyd, J.; Brothers, E. N.; Kudin, K. N.; Staroverov, V. N.; Kobayashi, R.; Normand, J.; Raghavachari, K.; Rendell, A. P.; Burant, J. C.; Iyengar, S. S.; Tomasi, J.; Cossi, M.; Rega, N.; Millam, N. J.; Klene, M.; Knox, J. E.; Cross, J. B.; Bakken, V.; Adamo, C.; Jaramillo, J.; Gomperts, R.; Stratmann, R. E.; Yazyev, O.; Austin, A. J.; Cammi, R.; Pomelli, C.; Ochterski, J. W.; Martin, R. L.; Morokuma, K.; Zakrzewski, V. G.; Voth, G. A.; Salvador, P.; Dannenberg, J. J.; Dapprich, S.; Daniels, A. D.; Farkas, Ö.; Foresman, J. B.; Ortiz, J. V.; Cioslowski, J.; Fox, D. J.; Gaussian, Inc.: Wallingford, CT, USA, 2009.

(18) Schaftenaar, G.; Noordik, J. H. *J. Comput.-Aided Mol. Des.* **2000**, *14*, 123.

(19) Reichardt, C. *Solvents and solvent effects in organic chemistry*; Wiley-VCH: Weinheim, 2003; Vol. 3rd, updat and enl.

(20) Baciocchi, E.; Bietti, M.; Salamone, M.; Steenken, S. *J. Org. Chem.* **2002**, *67*, 2266.

(21) Neta, P.; Dizdaroglu, M.; Simic, M. G. *Isr. J. Chem.* **1984**, *24*, 25.

(22) Avila, D. V.; Brown, C. E.; Ingold, K. U.; Lusztyk, J. *J. Am. Chem. Soc.* **1993**, *115*, 466.

(23) Albert, J. F. In *Synthetic Organic Electrochemistry*; John Wiley & Sons.

(24) Salamone, M.; DiLabio, G. A.; Bietti, M. *J. Org. Chem.* **2012**, *77*, 10479.
(25) Banks, J. T.; Scaiano, J. C. *J. Am. Chem. Soc.* **1993**, *115*, 6409.
(26) Liu, L.; Guo, Q.-X. *Chem. Rev. (Washington, DC, U. S.)* **2001**, *101*, 673.

Chapter 6 Conclusions and Future Work

6. Broader Impact and Future work

An in-depth understanding of the kinetic and thermodynamic properties of a molecule of interest via an electrochemical single electron transfer processes allows for intellectual predictions of the behavior of the molecule as a reducing or oxidizing agent in chemical reactions. Our work has focused on investigating these properties for aliphatic and aryl carboxylate anions. We have established the first application of convolution voltammetry to oxidative dissociative electron transfer (DET) system of a series of R-substituted aliphatic carboxylates (acetate, propanoate, and pivalate). The DET mechanism for these compounds was found to be concerted and undergoes a shift towards a stepwise mechanism in the presence of water. Radical stability trend was established based on measured oxidation potentials via convolution voltammetry. The predicted trend was parallel to experimental values which is further suggestive of a concerted mechanism for these compounds. Further computational investigations of the solvation shell on the stabilization of the radical intermediate are essential to better elucidate the role of water in DET mechanism. Our approach can be adopted to establish oxidation potentials, transfer coefficients, and diffusion coefficients for a wide variety of aliphatic and aryl carboxylates if needed.

With regards to aryl carboxylates, our findings indicate a stepwise mechanism in contradictory to the aliphatic carboxylates. Further experimental and computational investigations of the oxidation of a series of substituted tetra-n-butylammonium phenylacetate will provide a valuable insight into the role of the electron density of the benzyl ring on the stabilization of the carboxyl radical intermediate. In addition, we recommend the use of silver oxide for the synthesis of tetra-n-butylammonium carboxylates to precipitate the bromide ion for the reaction of tetra-n-butylammonium bromide with the corresponding acid. This synthetic approach proved to be more

efficient alternative with higher purity than the neutralization reaction of tetra-n-butylammonium hydroxide with the corresponding acid.

Furthermore, we have established an experimental evidence via lasher flash photolysis for the effects of the counter cations on radical stability by investigating the β-scission of cumyloxyl radical. Significant increase in the rate of β-scission were noted in the presence of metal ions such as lithium. No significant difference in the activation barrier was found for higher the samples with higher ions concentrations. The high demethylation rates are reported to have minimal decrease in the activation barrier in the presence of the metal ions. Our computational approach confirms a metal to solvent complexation that can possibly be responsible for the unnoticed decrease in the activation barrier for these samples. Other metal ions are to be investigated including barium and cesium.

Additionally, no solvent polarity effects were found on the β-scission which is in disagreement with precedent literature. Only acetic acid and acetonitrile were found to follow the predicted trend. To further confirm our findings, the rate of β-scission was investigated in 1,1-2,2 –tetrachloroethane which is a non-polar aprotic solvent. The rate was found as high as that for acetic acid. The results are suggestive of a non-polar transition state for β-scission which is not stabilized with increased solvent polarity. Future work will address the solvent effects on other β-scission systems with anticipated polar and non-polar transition states.

More importantly, the high rates noted in the acetic acid solvent are intriguing as no solvent polarity was noted for other polar solvent. It has been reported previously that H-abstraction is competitive pathway with β-scission for cumyloxyl radical. In addition, a computational evidence has addressed the possibility of H-abstraction from carboxylic acid compound.[1,2] We hypothesize that higher rate of demethylation in acetic acid is due to additional H-abstraction process which

was proposed recently to occur via a stepwise mechanism.[3] In order to further confirm this prediction, the observed rate constant for the reaction H-abstraction reaction between cumyloxyl radical will be evaluated in the presence of a series of concentration of R-substituted carboxylic acids (**Scheme 6.1**).

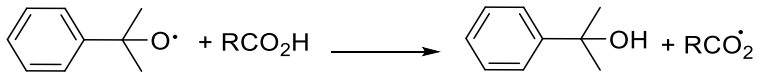

Scheme 6.1. Demethylation rates predicted to increase due to H-abstraction from the carboxylic acids

Moreover, we aim to extend our investigations of solvent and ion effects on the radical stability of benzoxyloxyl radical generated from benzoyl peroxide which undergoes decarboxylation rather than demethylation (**Scheme 6.2**).[2] The decarboxylation process will mimic closely our earlier work with aryl carboxylates as it generates a phenyl radical upon decarboxylation. The rate of decarboxylation is expected to slow down with higher solvent polarity and ion stability in accordance with our electrochemical studies.

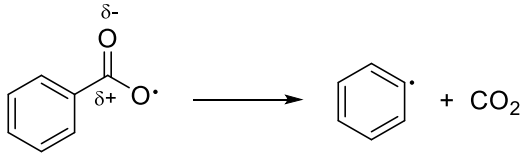

Scheme 6.2. Decarboxylation of the benzoyloxyl radical

References

(1) Avila, D. V.; Brown, C. E.; Ingold, K. U.; Lusztyk, J. *J. Am. Chem. Soc.* **1993**, *115*, 466.

(2) Salamone, M.; DiLabio, G. A.; Bietti, M. *J. Org. Chem.* **2012**, *77*, 10479.

(3) Denisov, E. T.; Shestakov, A. F. *Kinetics and Catalysis* **2013**, *54*, 22.

Appendices

Appendix A

Visual Basics convolution code (Chapter 2)

```
Sub Conv()
Const pie = (22 / 7) ^ -0.5
Dim Iconv As Double
Dim k As Integer
Dim j As Integer
Dim deltat As Double
Dim sum As Double
sum = 0
Dim n As Integer
n = UsedRange.Rows.Count
Dim lastt As Double
lastt = Cells(n, "A").Value
Dim firstt As Double
firstt = Cells(10, "A").Value
deltat = ((lastt - firstt) / (n - 10)) ^ 0.5
Dim numerator As Double
Dim denominator As Double
For k = 1 To 2800
   For j = 1 To k
   Dim firsti As Double
   Dim lasti As Double
   Dim change As Integer
   change = j + 10
   firsti = Cells(change, "C").Value
   change = j - 1 + 10
  lasti = Cells(change, "C").Value
   numerator = (lasti + firsti) / 2
   denominator = (k - j + 0.5) ^ 0.5
   sum = sum + deltat * (numerator / denominator)
   Next
   Iconv = pie * sum
   Dim c As Integer
   c = k + 10
   Cells(c, "F").Value = Iconv
   sum = 0
Next
End Sub
```

(Notes: The input data columns were defined based on the cyclic voltammograms excel file recorded by EG&G Princeton Applied Research (EG&G/PAR) Model 283 potentiosat/galvanostat. In order to utilize this code, the letter for the columns of current and time need to be adjusted in the code. For instance, this code was written based on the following

assignments of the data the cyclic voltammogram— current in column A, cell 10 (one cell below the first reported current in the column), time in column D, cell 10. The output convoluted current was assigned in column F. This code can be adjusted based on the CV profile and saved).

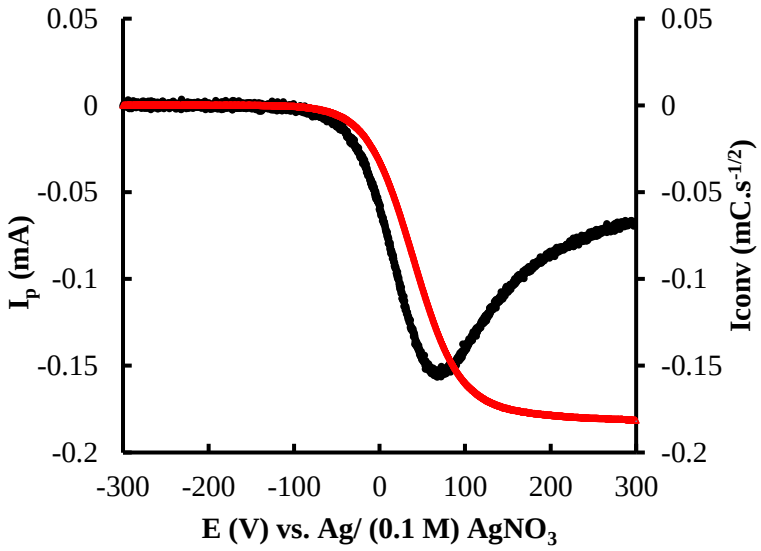

Figure 2.15. (-) Cyclic voltammogram of the forward peak current of 4 mM ferrocene in 0.45 TBAP/CH_3CN at 0.1 V/s. (-) Corresponding convoluted current.

Appendix B

Experimental error analysis associated with reported values from conventional and convolution analysis (Chapter 2 & 3)[1]

To calculate the error for the α obtained from the slope of (E_p *vs. log v*) plots

$\alpha = (\text{slope})^{-1} \times ((8.314 \times 298.15 / 96485.33))$

$\alpha = (\text{slope} \pm \text{Err})^{-1} \times (0.026)$ (similar to function formula: $f = a A^b$)

Whereas, in this particular case,

f = calculated α value, a = a constant = 0.026, b = function power of -1, and A = the slope.

The error is calculated for the function of slope^{-1} and then for the function ($a \times \text{slope}^{-1}$)

Hence, $Err_\alpha = \frac{0.026\ xErr}{(slope)^2}$

To calculate the 90%CI and 95%CI for diffusion coefficients, peak widths, and α for the conventional approach, the following equation is used: $Average \pm zx \frac{\sigma}{\sqrt{n}}$

Where,

z: the confidence level for df = n-1

n: the number of trials, and

σ: standard deviation

To calculate the diffusion coefficients using conventional analysis, the following equation was used for irreversible systems, followed by a rapid chemical step

$$i_p = nFAD_o^{\frac{1}{2}} C_0^* v^{\frac{1}{2}} \left(\frac{\alpha n_a F}{RT}\right)^{\frac{1}{2}} \pi^{\frac{1}{2}} \chi(bt)$$

Whereas,

$\pi^{1/2}\chi(bt)$ *is* a tabulated function with the value of 0.4958; hence, it is simplified into:

$$i_p = (2.99\ x10^5)\ AD_o^{\frac{1}{2}} C_0^* v^{\frac{1}{2}}$$

with i_p, $v^{1/2}$, A, C_o^*, and D represent the experimental peak current, scan rate, area of the electrode surface, initial bulk concentration, and D = diffusion coefficient, respectively.

References

(1) Bard, A. F., L. *Electrochemical Methods Fundamentals and Applications*; 2 ed.; John Wiley & Sons Inc., 2000.

Appendix C

Evaluating the code and estimation of surface area of GC electrodes by coupling cyclic voltammetry and PFG NMR (Chapter 2)

Ferrocene is a well-behaved compound that is commonly utilized as a reference. Upon oxidation, ferrocene shows a reversible one-electron transfer process. Under strictly-controlled diffusion conditions on a planar electrode, the surface area of the working GC electrode can be determined as depicted by the simplified Randles-Sevcik equation[1]:

$$i_p = 2.69\ x10^5 n^{3/2} A C D_o^{1/2} v^{1/2}$$

where I_p is the peak current (A), n is the number of electrons, A is the active surface area of the electrode (cm^2), C is the bulk concentration of ferrocene (mol/cm^3), D_o is the diffusion coefficient of ferrocene in 0.45 M TBAP/ CD_3CN (cm^2/s), and υ is the scan rate (V/s).

Although all these parameters are easily determined, the diffusion coefficient under these conditions is not provided in the literature. However, any inaccuracies in the diffusion coefficient will subsequently affect the accuracy of the resulting calculated surface area. Hence, PFG NMR was utilized to estimate an accurate D_o of (2.71 ± 0.01) x 10^{-4} cm^2/s at 27 ^oC with 0.45 TBAP/CH_3CN and fit for the area of the electrode (Figure 2.11). The active surface area was estimated to be (3.5 ± 0.1) x 10^{-2} cm^2. Convolution voltammetry shows a diffusion coefficient of (5.71 ± 0.08) x 10^{-4} cm^2/s, which was within experimental error with estimated D_o from PFG NMR measurements. The corrected surface area was used to determine the diffusion coefficients for all the substrates investigated.

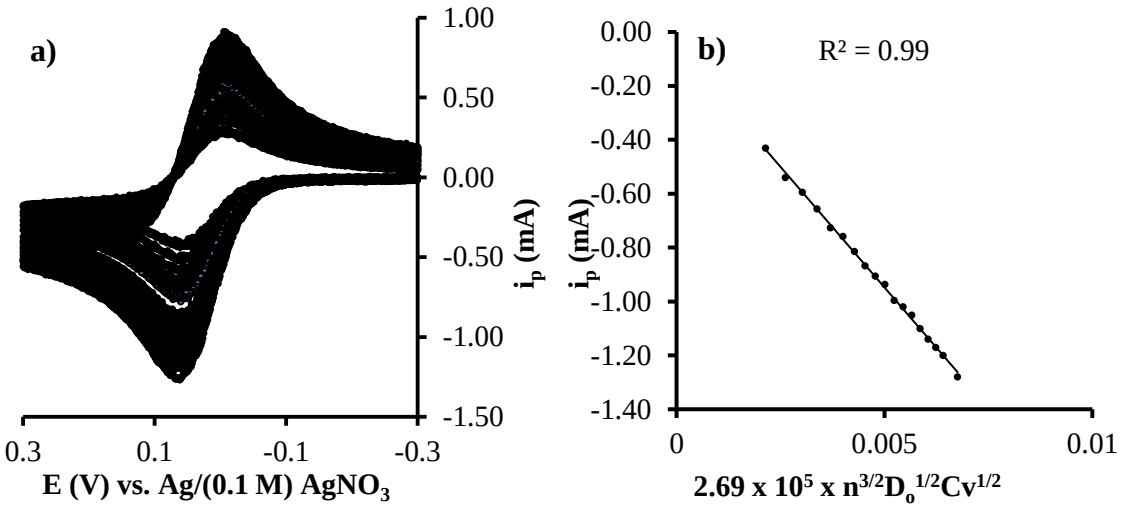

Figure 2.16. a) Anodic oxidation of 3.8 mM of ferrocene in 0.45 M TBAP/ CD_3CN vs. Ag/ (0.1 M) $AgNO_3$ with a scan range of 0.1-2.0 V/s at 27 ^{0}C, b) "Best-fit" linear plot of current as a function of scan rate to estimate area of the electrode.

References

(1) Bard, A. F., L. *Electrochemical Methods Fundamentals and Applications*; 2 ed.; John Wiley & Sons Inc., 2000.

Appendix D

Representative conventional and convolution analysis for the electrolysis of tetra-n-butylammonium acetate salt for a range of concentrations (Chapter 2)

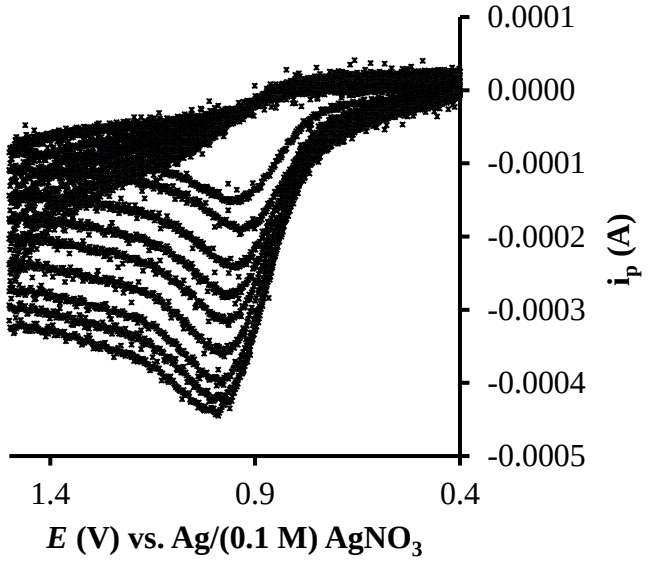

Figure 2.17. Cyclic voltammograms corresponding to the electrolysis of 2.7 mM tetra-n-butylammonium acetate in 0.45 M TBAP/ "neat" acetonitrile vs. Ag/ (0.1 M) $AgNO_3$ at scan range of 0.1 – 2.0 V/s

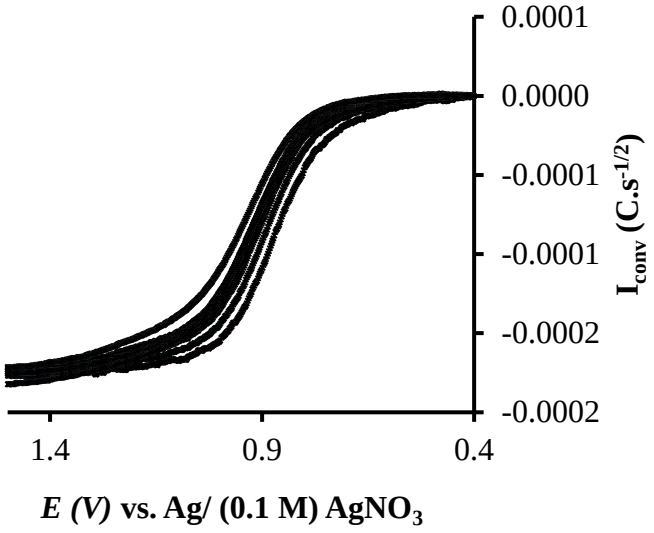

Figure 2.18. Background subtracted convolution voltammograms corresponding to the electrolysis of 2.7 mM tetra-n-butylammonium acetate in 0.45 M TBAP/ "neat" acetonitrile vs. Ag/ (0.1 M) AgNO3 at scan range of 0.1 – 2.0 V/s

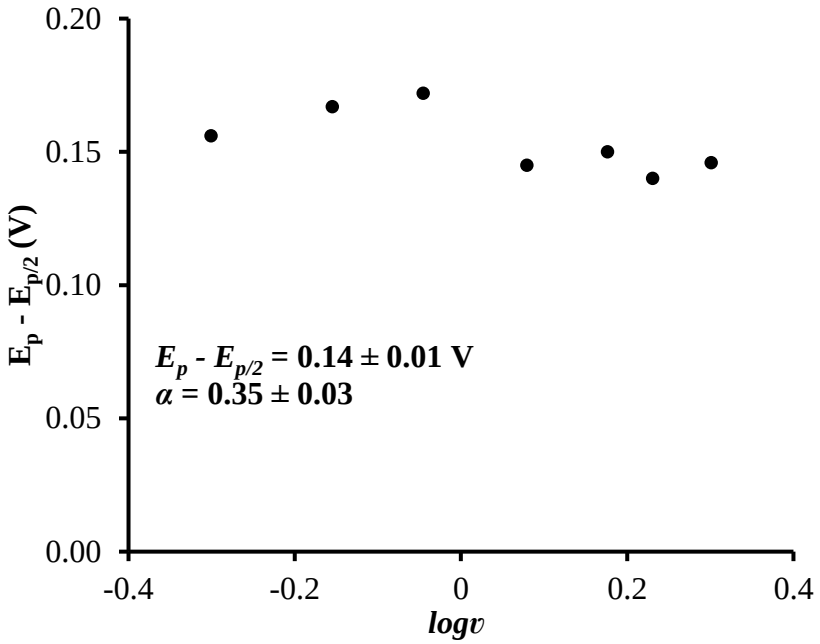

Figure 2.19. Peak width plots vs. *log v* corresponding to the electrolysis of 2.7 mM tetra-n-butylammonium acetate in 0.45 M TBAP/ "neat" acetonitrile vs. Ag/ (0.1 M) $AgNO_3$ at scan range of 0.1 – 2.0 V/s

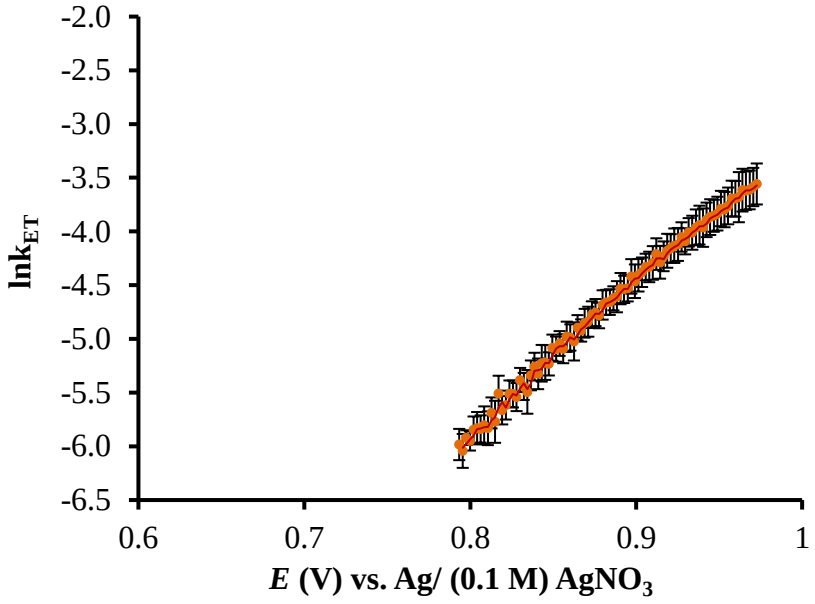

Figure 2.20. Plot of lnk_{ET} vs. E (V) corresponding to the electrolysis of 2.7 mM tetra-n-butylammonium acetate in 0.45 M TBAP/ "neat" acetonitrile vs. Ag/ (0.1 M) $AgNO_3$ at scan range of 0.1 – 2.0 V/s (95% CI error bars)

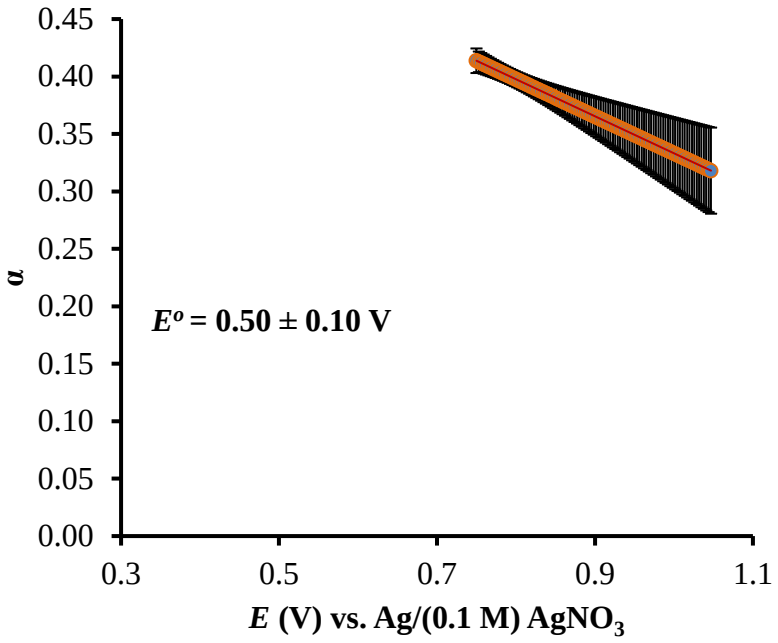

Figure 2.21. Plot of α vs. E (V) corresponding to the electrolysis of 2.7 mM tetra-n-butylammonium acetate in 0.45 M TBAP/ "neat" acetonitrile vs. Ag/ (0.1 M) $AgNO_3$ at scan range of 0.1 – 2.0 V/s (95% CI error bars)

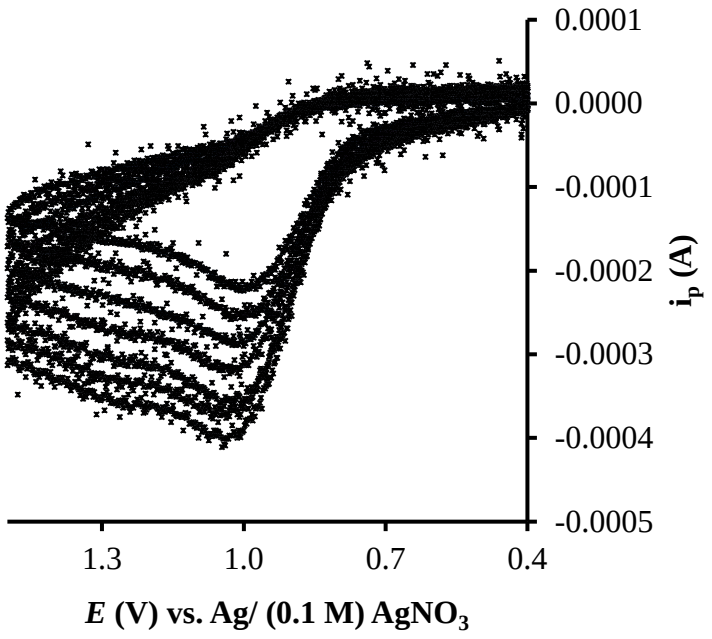

Figure 2.22. Cyclic voltammograms corresponding to the electrolysis of 3.0 mM tetra-n-butylammonium acetate in 0.45 M TBAP/ "neat" acetonitrile vs. Ag/ (0.1 M) $AgNO_3$ at scan range of 0.1 – 2.0 V/s

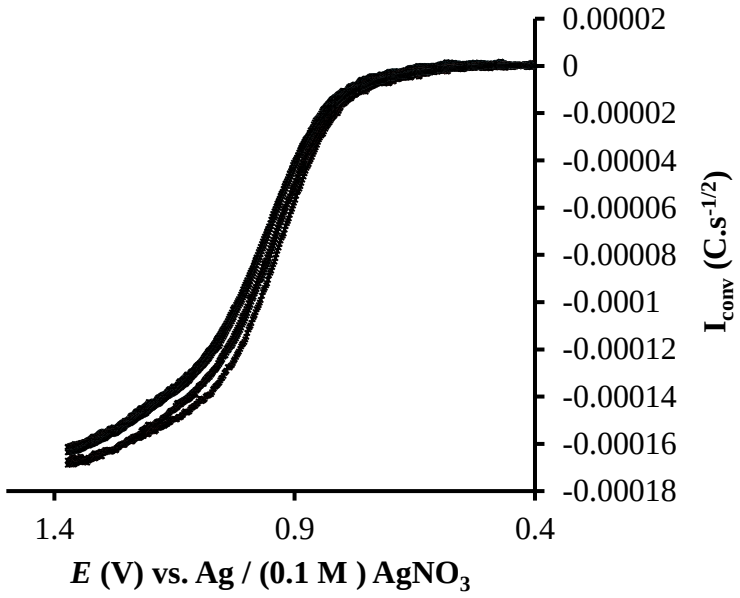

Figure 2.23. Background subtracted convolution voltammograms corresponding to the electrolysis of 2.7 mM tetra-n-butylammonium acetate in 0.45 M TBAP/ "neat" acetonitrile vs. Ag/ (0.1 M) $AgNO_3$ at scan range of 0.1 – 2.0 V/s

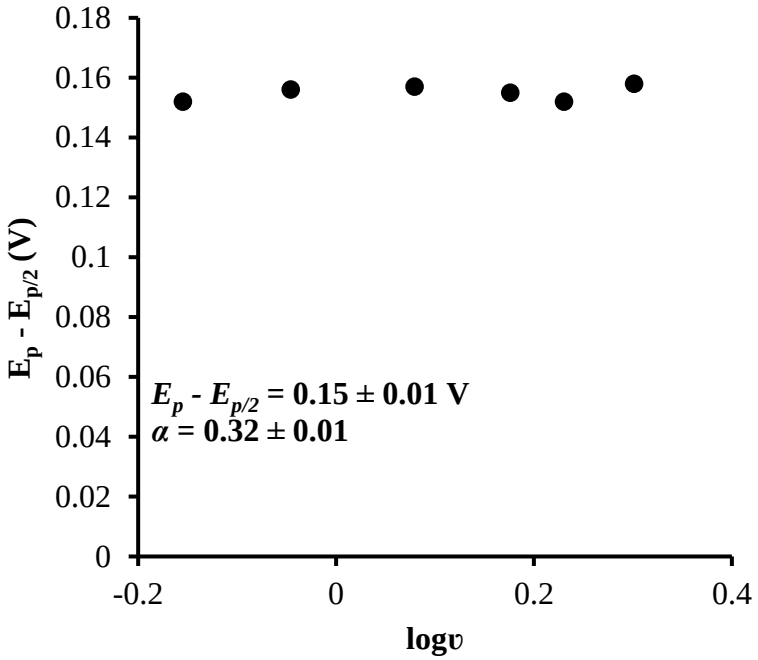

Figure 2.24. Peak width plots vs. *log v* corresponding to the electrolysis of 3.0 mM tetra-n-butylammonium acetate in 0.45 M TBAP/ "neat" acetonitrile vs. Ag/ (0.1 M) $AgNO_3$ at scan range of 0.1 – 2.0 V/s

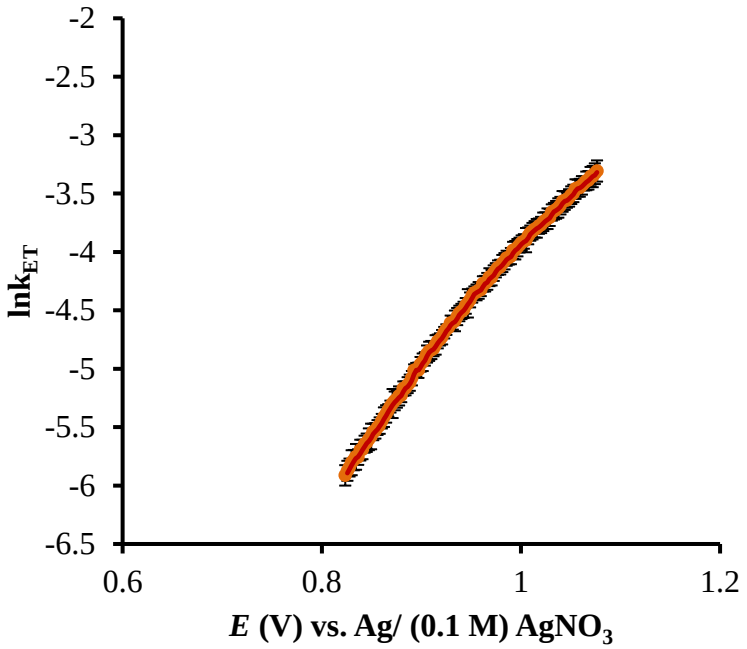

Figure 2.25. Plot of lnk_{ET} vs. *E* (V) corresponding to the electrolysis of 3.0 mM tetra-n-butylammonium acetate in 0.45 M TBAP/ "neat" acetonitrile vs. Ag/ (0.1 M) $AgNO_3$ at scan range of 0.1 – 2.0 V/s (95% CI error bars)

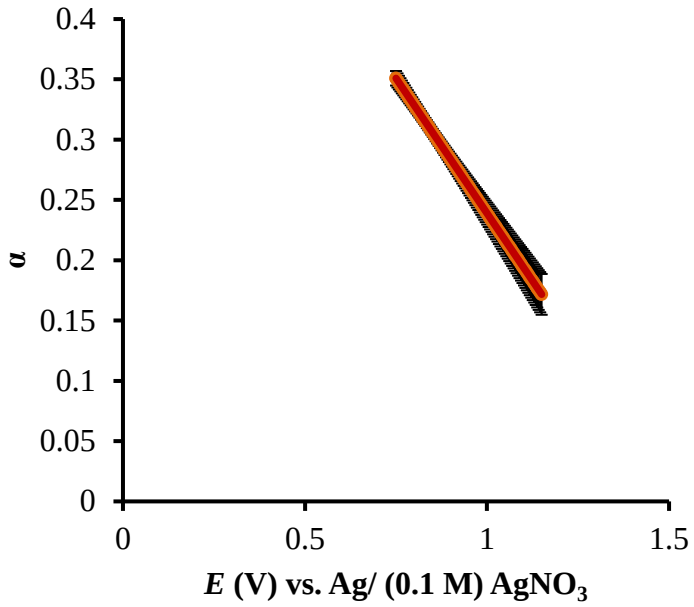

Figure 2.26. Plot of *α* vs. *E* (V) corresponding to the electrolysis of 3.0 mM tetra-n-butylammonium acetate in 0.45 M TBAP/ "neat" acetonitrile vs. Ag/ (0.1 M) $AgNO_3$ at scan range of 0.1 – 2.0 V/s (95% CI error bars)

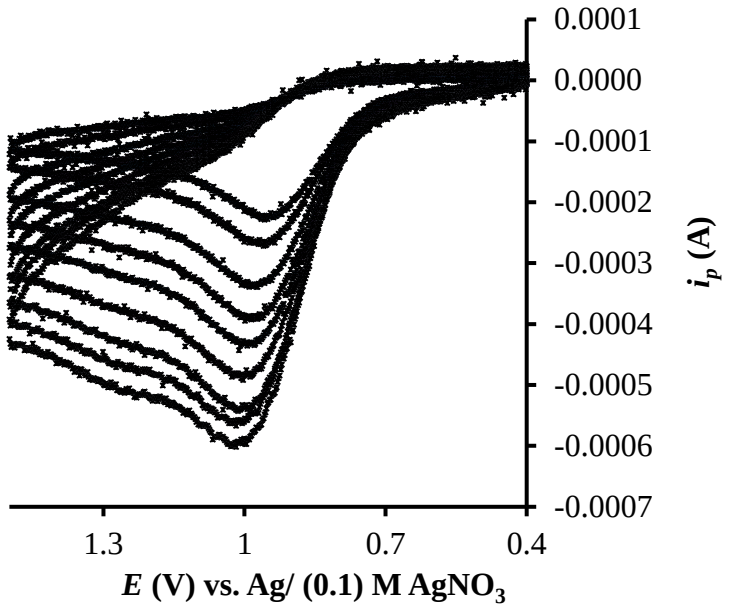

Figure 2.27. Cyclic voltammograms corresponding to the electrolysis of 4.2 mM tetra-n-butylammonium acetate in 0.45 M TBAP/ "neat" acetonitrile vs. Ag/ (0.1 M) $AgNO_3$ at scan range of 0.1 – 2.0 V/s

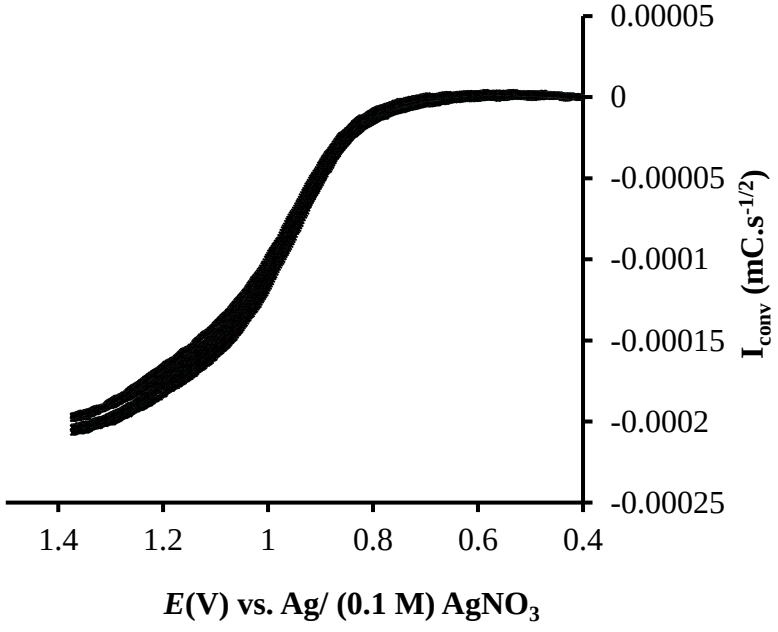

Figure 2.28. Background subtracted convolution voltammograms corresponding to the electrolysis of 4.2 mM tetra-n-butylammonium acetate in 0.45 M TBAP/ "neat" acetonitrile vs. Ag/ (0.1 M) $AgNO_3$ at scan range of 0.1 – 2.0 V/s

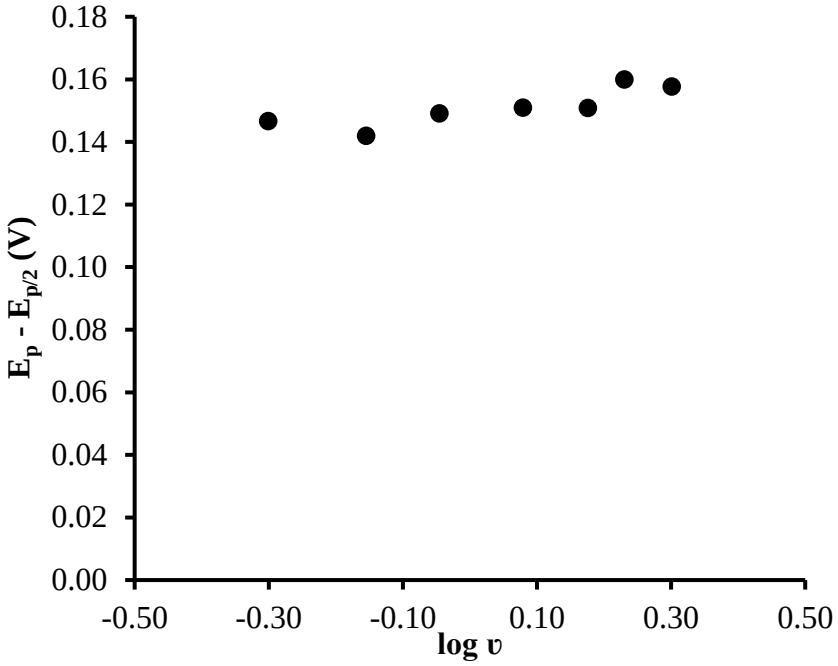

Figure 2.29. Peak width plots vs. *log v* corresponding to the electrolysis of 4.2 mM tetra-n-butylammonium acetate in 0.45 M TBAP/ "neat" acetonitrile vs. Ag/ (0.1 M) $AgNO_3$ at scan range of 0.1 – 2.0 V/s

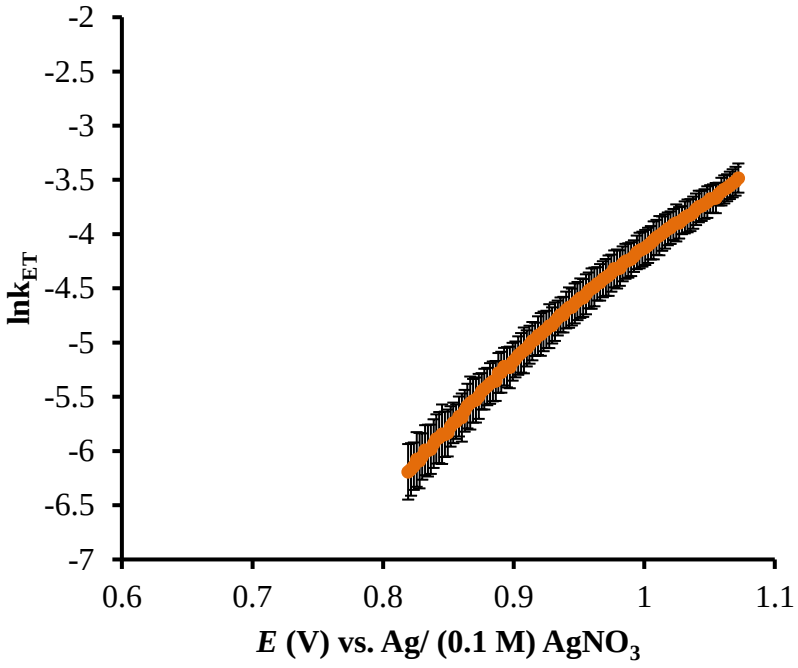

Figure 2.30. Plot of lnk_{ET} vs. E (V) corresponding to the electrolysis of 4.2 mM tetra-n-butylammonium acetate in 0.45 M TBAP/ "neat" acetonitrile vs. Ag/ (0.1 M) $AgNO_3$ at scan range of 0.1 – 2.0 V/s (95% CI error bars)

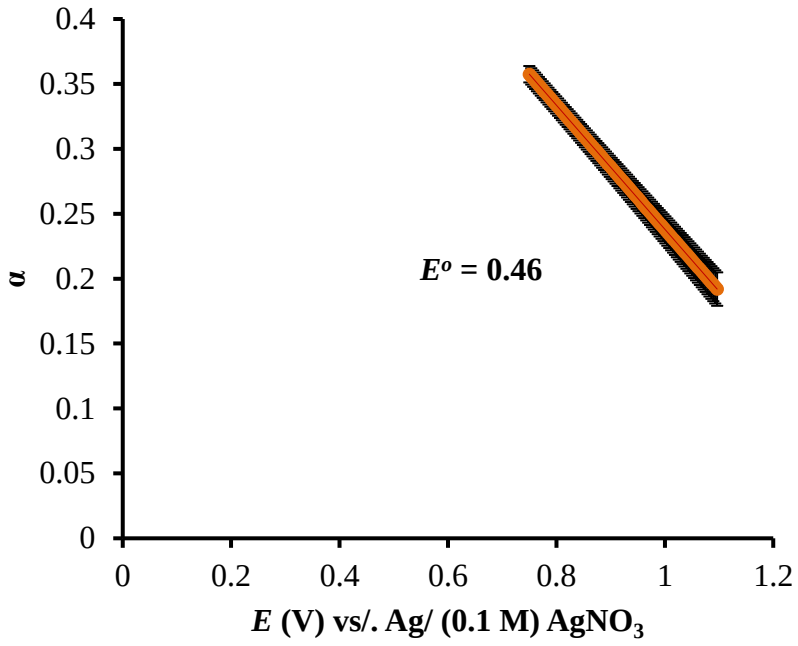

Figure 2.31. Plot of α vs. E (V) corresponding to the electrolysis of 3.0 mM tetra-n-butylammonium acetate in 0.45 M TBAP/ "neat" acetonitrile vs. Ag/ (0.1 M) $AgNO_3$ at scan range of 0.1 – 2.0 V/s (95% CI error bars)

Appendix E

Cyclic voltammograms with additions of water to ferrocene (Chapter 3)

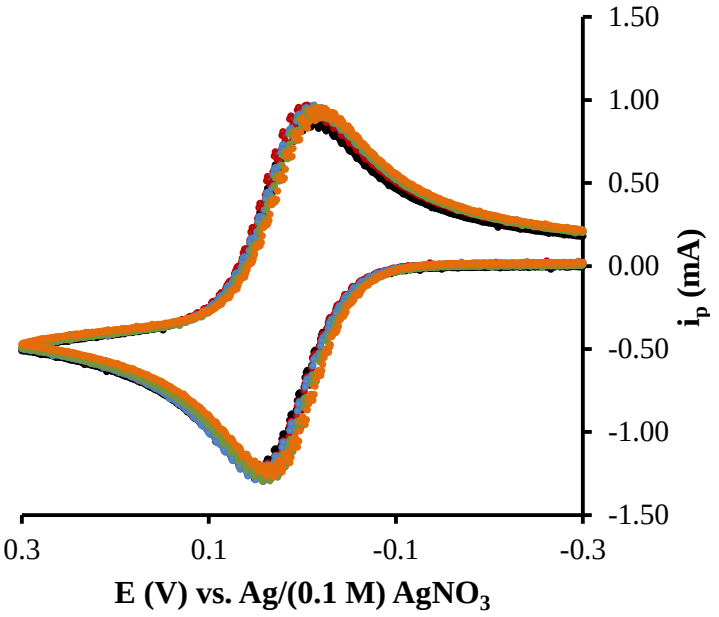

Figure 3.17. Additions of water to neat anhydrous acetonitrile ("neat" up to 1 M H_2O) with 8 mM ferrocene and 0.45 TBAP at 0.5 V/s. No shift or increased peak current was noted for the ferrocene electrolysis.

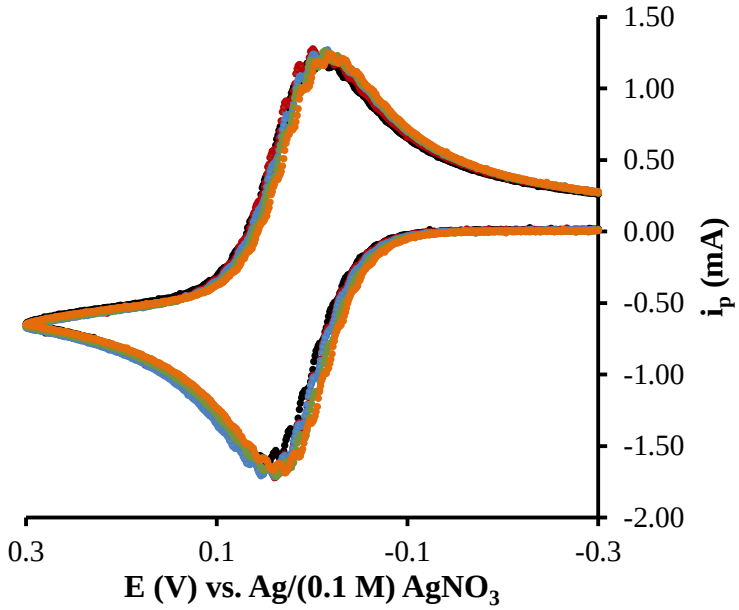

Figure 3.18, Additions of water to neat anhydrous acetonitrile ("neat" up to 1 M H_2O) with 8 mM ferrocene and 0.45 TBAP at 0.9 V/s. No shift or increased peak current was noted for the ferrocene electrolysis.

Appendix F

Identification of mixture byproducts for bulk electrolysis for the ferrocene/acetate system via UV-Vis spectroscopy, NMR, GC-MS) (Chapter 3)

Ferrocene and its derivatives are one of the most commonly investigated organometallic sandwich complexes. Ferrocene is a symmetrical molecule with no substituted functional groups, making it relatively simple to investigate. The electrolysis of ferrocene in the presence of acetate can yield a variety of ferrocenyl derivatives: acetyoxyl radical, methyl radical, and ferrocenium cation. Ferrocenyl derivatives of interest, including methylferrcoene ($Fe(C_5H_4CH_3)(C_5H_5)$),[1,2] ferrocenylmethylium cations ($Fe(C_5H_4HCH_2)(C_5H_5C_5H_5)^+$), alkanoyllferrocene ($C_5H_5FeC_5H_4COCH_3$),[3,4] ferrocenyl acetate as ferrocenyl esters and ethers ($C_5H_5FeC_5H_4OCOCH_3$),[5,6] have been extensively investigated. Spectroscopic data for these derivatives have been reported—and in particular ^{1}H NMR, ^{13}C-NMR, FT-IR, and UV-Vis absorbance. While it is possible to verify obtained results via comparative analyses to further identify byproducts, the complexity of these analyses becomes even more challenging with substituted functionality groups on ferrocene, which reinforces the importance of understanding ferrocene:acetate as a model system. All experiments were performed on control sample of ferrocene:acetate solution without electrolysis.

Identification of mixture byproducts for bulk electrolysis for the ferrocene/acetate system *via* UV-Vis spectroscopy.

Ferrocenes and their derivatives have both electrochemical and UV-Vis properties that make them ideal mediators and reliable indicators of UV-Vis patterns. The oxidation of ferrocenes results in a change in the oxidation state of the iron within the molecules, and ferrocenium ions (Fe^{3+}) are obtained with distinct UV-Vis peaks.[7] Unlike ferrocene, ferrocenium (which is a strong oxidizing agent)displays low-frequency absorption bands in the UV-Vis

spectrum. An Fe^{+2} ion shows a peak around 420 nm, whereas the corresponding peak for a Fe^{+3} ion is around 630 nm. The peaks differ slightly depending on the solvent and the structure of the molecule.[7] It is evident from electrochemical evidence that ferrocene is being regenerated upon oxidation, since the system seem to behave in a similar manner as expected for an HRC system. The advantageous UV-Vis properties of ferrocene and ferrocenium compounds provide distinct signals, which can be further quantified based on known molarities. Also, UV-Vis spectroscopy provides insights into other possible by-products produced via oxidative processes.

To investigate these properties, bulk electrolysis was employed as a preparative scale for the ferrocene-acetate system in order to investigate the mixture by-products generated upon oxidation. First, constant-current electrolysis (10^{-3} A) was applied to a known molarity of a ferrocene solution over a given period of time in an H-shaped electrochemical cell, as shown in **Scheme 4.5** (30 mM ferrocene in 25 ml solution of 0.1 M TBAP in neat acetonitrile was set for 3600 seconds for the oxidation to complete at 10^{-3} A). The solution changed color from orange to dark purplish-blue, thereby signaling the production of ferrocenium cation. The resulting solution was further examined by UV-Vis to ensure that no signal was detected for ferrocene at 420 nm, as well as to confirm the presence of a signal for the ferrocenium cation at 630 nm. Upon full oxidation of the ferrocene, tetra-n-butylammonium acetate was added to the solution with an excess factor similar to the ones performed for cyclic voltammetry, and in particular, γ = 2 and 4.

The resulting bulk solution was retrieved and a series of solvent extractions were performed prior to measuring the UV-Vis absorbance spectra. Such solvent extractions are essential for teasing out the influence of different compounds with distinct solubility properties, and providing clear UV-Vis spectra for quantification. In addition to some unknown byproducts,

the bulk solution was expected to include tetra-n-butylammonium acetate, TBAP, and ferrocene or ferrocenium as major compounds in excess; consequently, a ɣ = 2 was utilized as it served to decrease the excess amount of reactant.

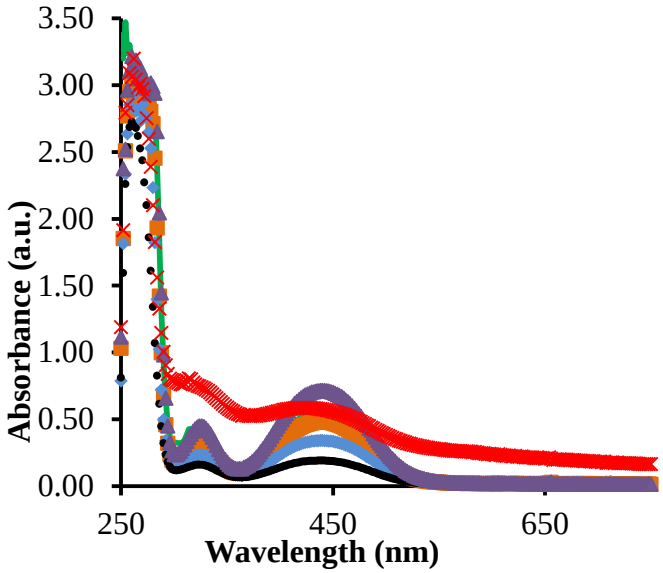

Figure 4.13. UV-Vis spectra for a series of dilutions for ferrocene in hexane to access the recovery of the ferrocene compound upon addition of acetate: 2 mM (black), 4 mM (blue), 6 mM (orange), 8 mM (purple), bulk electrolysis solution without extraction in acetonitrile (red), bulk solution with an extraction with hexane as a solvent (green). Calculated recovery was 80% based on absorbance peak at 420 nm for ferrocene.

Individual UV-Vis spectra for each compound were investigated prior to examining the bulk solution. Solvent extractions were designed based on polarity trends, and each solvent extract was repeated five times in small 2 ml additions. Prior to solvent extractions, the resulting bulk electrolysis was rotovapped to remove acetonitrile and condense the non-volatile productions. While it is possible that volatile by-products with lower molecular weight were eliminated during the process of solvent extraction, it is essential for improved spectroscopic data analyses. As shown in **Figure 4.13**, there is no distinct peak at 630 nm for ferrocenium with a significant absorbance peak at 420 nm. Due to the variety of compounds present in the solution, hexane extraction indicates the distinct peak for the ferrocene with a recovery of 80%

using ferrocene standards; in contrast, the bulk solution spectrum did not show clear results. These findings indicate a roughly 20% loss in the mediator upon the addition of the acetate to the ferrocenium bulk solution for two replicates under analogous experimental conditions. Moreover, the appearance of the peak between (250 nm – 300 nm) with reddish/orange color, which is similar to ferrocene in the ether layer, could indicate the presence of other ferrocenyl derivatives such as the methylferrocene. No other information was deduced from the other extractions using UV-Vis spectroscopy.

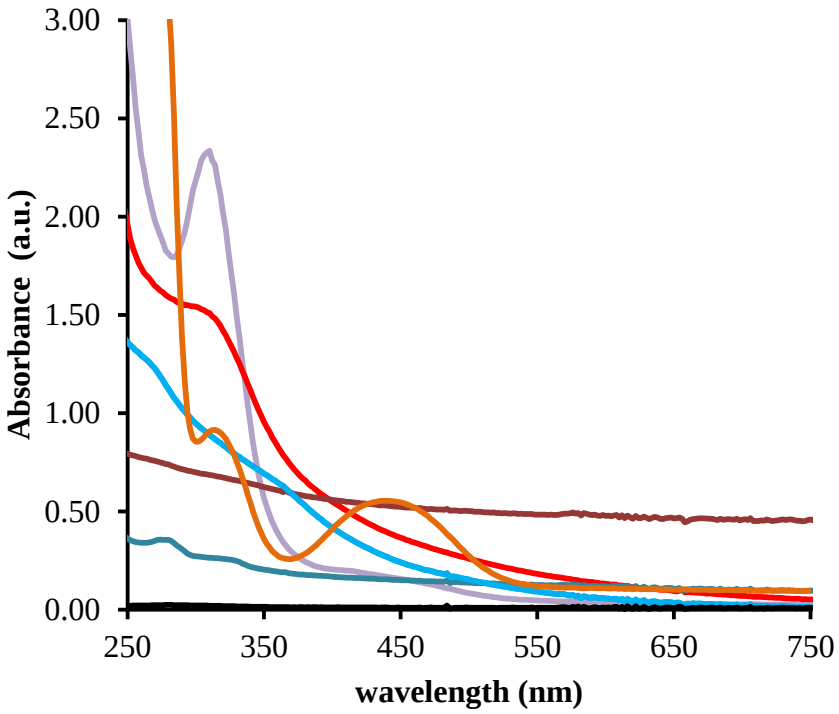

Figure 4.14. UV-Vis spectra for a series of solvent extractions with an increasing polarity for a bulk electrolysis of ɣ = 2 of ferrocene: tetra-n-butylammonium acetate: TBAP/acetonitrile (black), hexane layer (orange), ether layer (gray), ethyl acetate layer (red), chloroform (green), methanol (brown), and water layer (blue).

Another important observation pertains to the formation of a reddish-brown precipitant for all bulk electrolysis solutions regardless of the ratio of ferrocene:acetate used. Ferrocenium

solution was prepared as a control and the formation of a reddish-brown precipitant occurred over an expanded period, but less than 24 hours. The addition to the mediator is one possible explanation for the color change. It must be noted, however, that the decomposition of ferrocenium ion is another possible pathway for the color change that was facilitated by the presence of acetate anions. There is the possibility of either the ferrocenium ion and/or the ferrocene decomposing upon the addition of acetate, which generated highly unstable free radicals. In either case, an Fe^{3+}-like byproduct is expected. The decomposition of ferrocenium ions in acetonitrile has been previously reported, but in the presence of excess molecular oxygen.[8,9] Nevertheless, phenanthroline ligand was added to confirm the presence of Fe^{3+}-like byproducts in the bulk solution.[10] The rapid change in color to a deep reddish hue was noted upon the addition, which is indicative of the complexation of the ligand with iron ions in solution.

As mentioned earlier, oxygen plays a role in the decomposition of ferrocenium ion. Water also is a critical factor in the decomposition of ferrocenium, but research shows oxygen is also required for the decomposition to occur.[11] Therefore, bulk electrolysis of ferrocene was performed in a glovebox, which remained sealed under argon flow. The solution was divided into two separate vials. Tetra-n-butylammonium acetate was added to one vial prior to adding deionized water to both solutions outside the glovebox. The deionized water was then purged for three minutes with argon prior to use. After extraction with a water layer, the latter was transferred into a sealed vial containing the ligand. A light reddish-colored solution was noted for the ferrocenium only; in contrast, a deeper red color was noted for the other vial containing the acetate.

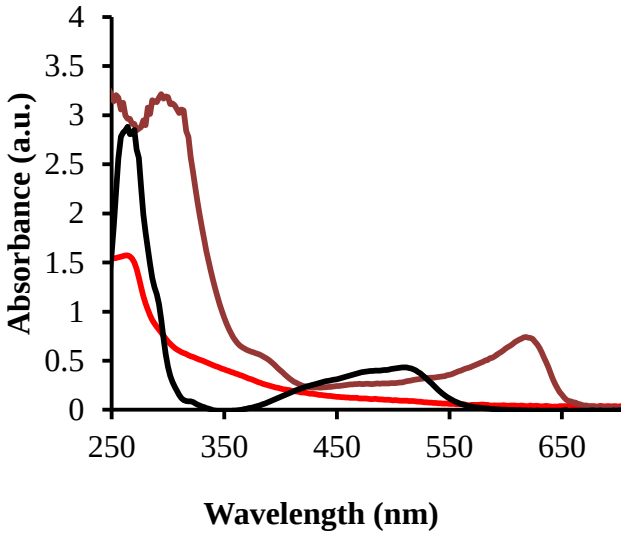

Figure 4.15. Water layer extraction for the bulk electrolysis solution in the absence of phenanthroline for ɣ = 2 of ferrocene:acetate (red), for 30 mM ferrocenium (brown), 0.13 mM ferrous sulfate (black).

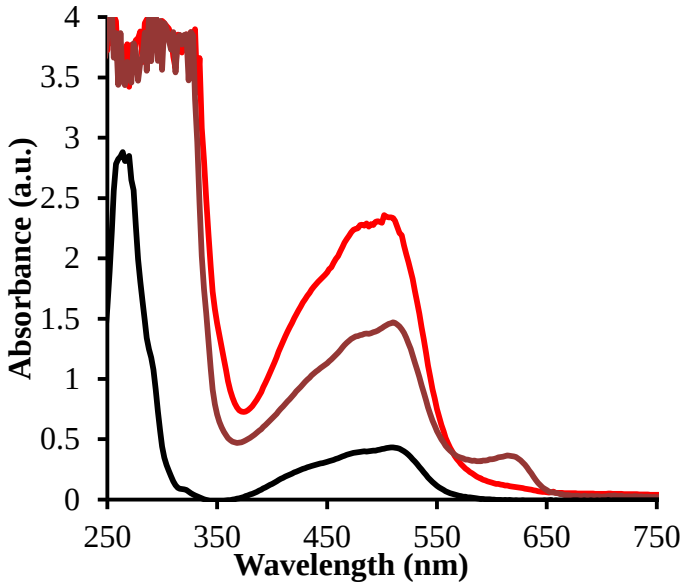

Figure 4.16. Water layer extraction for the bulk electrolysis solution in the presence of phenanthroline for ɣ = 4 of ferrocene:acetate (red), for 30 mM ferrocenium (brown), 0.13 mM ferrous sulfate (black).

As shown in **Figure 4.14**, no signal for ferrocene or ferrocenium was identified in the water layer for the bulk electrolysis reaction mixture. Only ferrocenium was noted in the

ferrocenium bulk solution with an absorbance of 0.75. Upon addition of the ligand, the absorbance of ferrocenium bulk solution decreased to 0.32 at 630 nm and a new signal was noted for the ligand-Fe^{3+} like complex roughly around 500 nm (**Figure 4.15**). Although both mixtures indicate the decomposition in the presence of water, more significant results were noted for the mixture containing acetate anions—even when no signal for ferrocenium was observed prior to the addition of the ligand. These findings show the significant role that acetate plays in decomposing the ferrocenium ion prior to the presence of oxygen or water in solution.

Bulk electrolysis mixture by-products of the ferrocene-acetate system via NMR spectroscopy.

Reaction mixtures for the bulk electrolysis of **$\gamma = 2$** of ferrocene:tetra-n-butylammonium acetate in 25 ml of 0.1 M TBAP/neat acetonitrile was prepared. TBA-acetate was added after the bulk electrolysis of the ferrocene had concluded. The reaction mixture was rotovapped and a series of solvent extractions was performed systematically in the listed order of hexane, ether, ethyl acetate, chloroform, methanol, and water. Each extraction was performed with 2-ml solvent fractions and repeated five times. After each solvent extraction was completed, the solvent was rotovapped and 1-ml of deuterated chloroform was used as a reference for NMR spectrum.

The NMR results were analyzed for major peaks and compared to precedent literature with regards to either the addition of acetate to the mediator (acetate radical or methyl radical addition to the rings will split the singlet at 4.2 ppm), or the appearance of distinct peaks relating to the decomposition of the cyclopentadiene rings (in order to identify possible by-products). However, impurities in the mixture even after solvent extractions were difficult to analyze. As shown in **Figure 4.17**, the ^{1}H NMR spectra for the bulk solution displayed a variety of

significant peaks, which were identified in comparison to analogous spectra for pure ferrocene, TBAP, and tetra-n-butylammonium acetate. The expected products in the reaction mixture, as discussed earlier, included ferrocene upon regeneration, added excess tetra-n-butylammonium acetate, TBAP, and possibly other derivatives of ferrocene or cyclopentadienes.

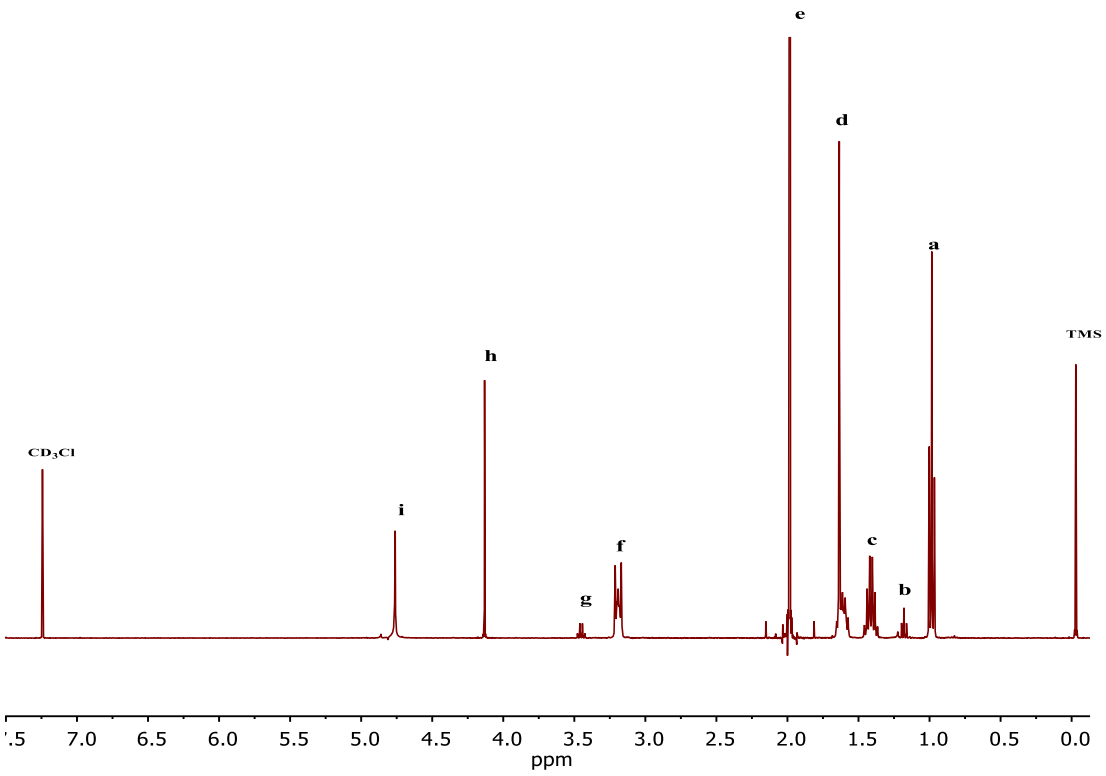

Figure 4.17. Representative NMR spectrum for a 2 ml of reaction mixture by bulk electrolysis of ɣ = 2 of ferrocene: tetra-n-butylammonium acetate in 25 ml of neat acetonitrile. Reaction mixture was rotovapped prior to adding deuterated chloroform. Peaks (a, c, d, & f) correspond to proton signals from the tetra-n-butylammonium cation, peak (h) corresponds to ferrocene, and unknown peaks (b, e, g, and i)

Since the reaction mixture was difficult to assign with complete confidence, solvent extractions were performed as mentioned earlier. Major peaks in the reaction mixture were observed in the extraction layers. The hexane layer had a distinct peak for ferrocene, which supports the findings from UV-Vis spectra. As the polarity of the solvent increases, other distinct

peaks were separated accordingly. While the UV-Vis spectrum for the ether layer did not indicate the presence of ferrocene, the NMR-spectrum indicated a ferrocene-like singlet. Since tetra-n-butylammonium acetate and tetra-n-butylammonium perchlorate salts are soluble in ethyl acetate, the corresponding peaks for these compounds can be found in the ethyl acetate layer. In chloroform, ether, and water layers new unidentified peaks appeared.

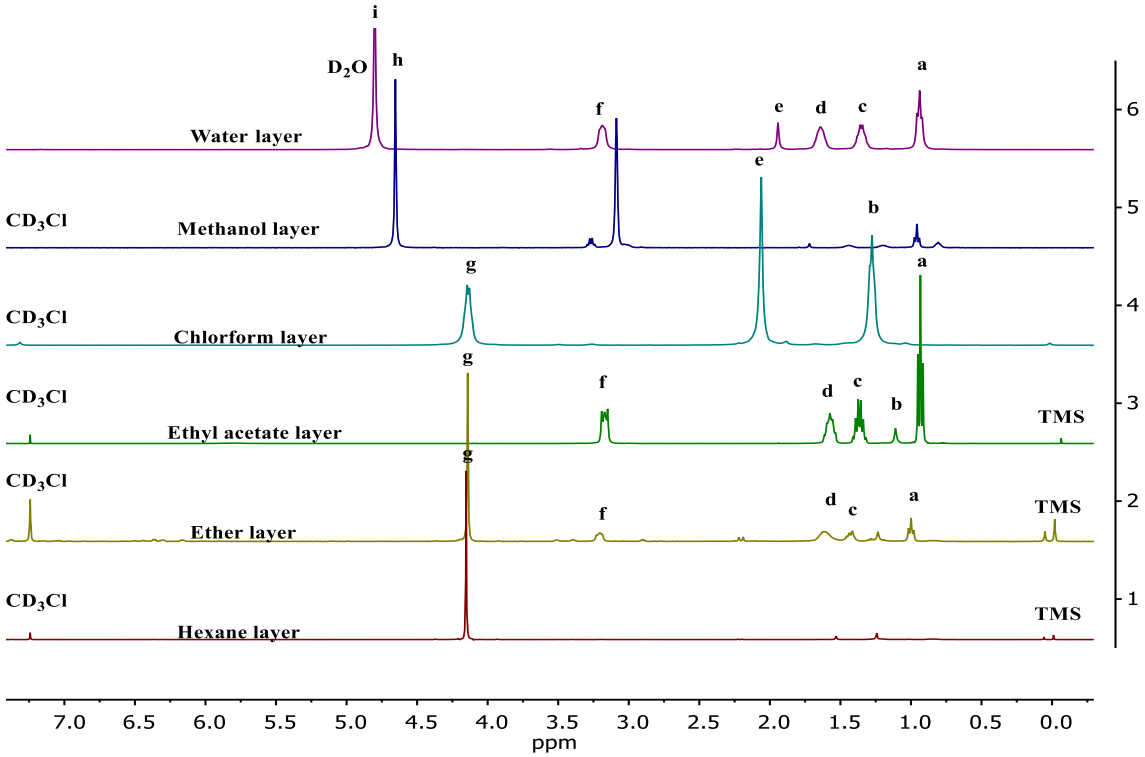

Figure 4.18. Representative NMR spectra for a series of solvent extractions for the reaction mixture of the bulk electrolysis of (1:2) of ferrocene: tetra-n-butylammonium acetate after rotovapping the reaction mixture. The solvent extraction was done systematically by adding 1 ml with 5 times extractions for each solvent. The remaining reaction mixture was rotavapped and the next solvent was added.

The reproducibility of this data was best for hexane, ether, and ethyl acetate layer extractions. As the solvent polarity increased, other distinct peaks were noted, but we were unable to formulate any conclusive results based on this behavior. In addition, one major drawback associated with solvent extraction is the need to evaporate the solvent residues

between consecutive extractions. This approach hinders the full analysis of volatile and unstable byproducts due to continuous exposure to a temperature of 40 ^{o}C under vacuum. On the other hand, if any of the byproducts can be identified, it would be possible to identify a likely mechanism for the quasi-catalytic HRC process for the ferrocene/acetate system.

Bulk electrolysis mixture by-products of the ferrocene-acetate system via GC and GC/MS.

Four major peaks were recorded from the ether layer extractions. The retention times were recorded as follows: 3.223 for acetic acid, 7.791 for n-butylamine, 8.498 for phenol, and 9.456 for ferrocene. The results did not show any other derivatives of ferrocene, but did confirm the decomposition of the tetra-n-butylammonium anion and acetate. Given the nature of these somewhat questionable results, identifying a conclusive mechanism for the ferrocene/acetate is not currently feasible.

References

(1) Kumar, D.; Singh, A. S.; Tiwari, V. K. *RSC Advances* **2015**, *5*, 31584.

(2) Hoshino, K.; Saji, T.; Ohsawa, Y.; Aoyagui, S. *Bull. Chem. Soc. Jpn.* **1984**, *57*, 1685.

(3) Donahue, C. J.; Donahue, E. R. *J. Chem. Educ.* **2013**, *90*, 1688.

(4) Rinehart, K. L.; Motz, K. L.; Moon, S. *J. Am. Chem. Soc.* **1957**, *79*, 2749.

(5) Akabori, S.; Sato, M.; Ebine, S. *Synthesis-Stuttgart* **1981**, 278.

(6) Nesmejanow, A. N.; Ssasonowa, W. A.; Drosd, V. N. *Chem. Ber.* **1960**, *93*, 2717.

(7) Manzi-Nshuti, C. W., C. Ferrocene and Ferrocenium Modified Clays and Their Styrene and EVA Composites. [Online Early Access]. DOI: 10.1016/j.polymdegradstab.2007.07.005. Published Online: 2007.

(8) Hurvois, J. P.; Moinet, C. *J. Organomet. Chem.* **2005**, *690*, 1829.

(9) Zotti, G.; Schiavon, G.; Zecchin, S.; Favretto, D. *J. Electroanal. Chem.* **1998**, *456*, 217.

(10) Lee, G. F. S., W. *Journal American Water Works Association* **1980**, *52*, 1569.

(11) Singh, A.; Chowdhury, D. R.; Paul, A. *Analyst* **2014**, *139*, 5747.

Appendix G

Simulated working curves with fitted data for the HRC model of ferrocene derivatives (Chapter 4)[1]

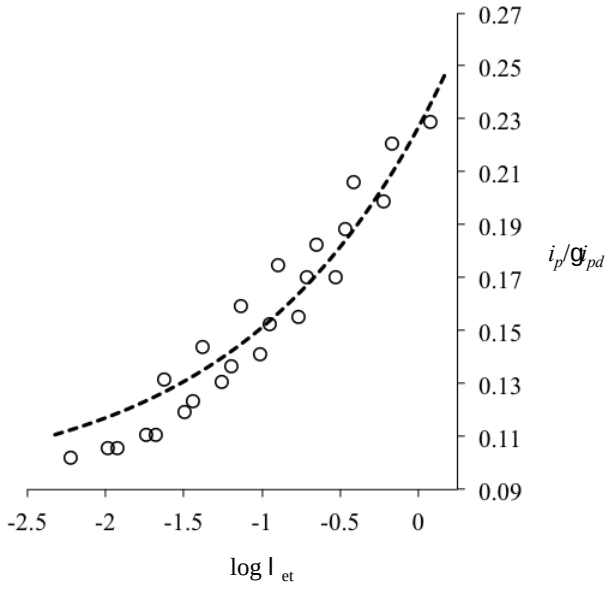

Figure 4.13. $i_p/\gamma i_{pd}$ **data fit to dimensionless working curves for tetra-*n*-butylammonium acetate in dry acetonitrile (mediator = ferrocene).** $\log\left(\frac{RT}{nF}k_{et}\right) = 1.17$, $k_{et} = (5.8 \pm 0.5)$ **x** 10^2 M^{-1} s^{-1}.

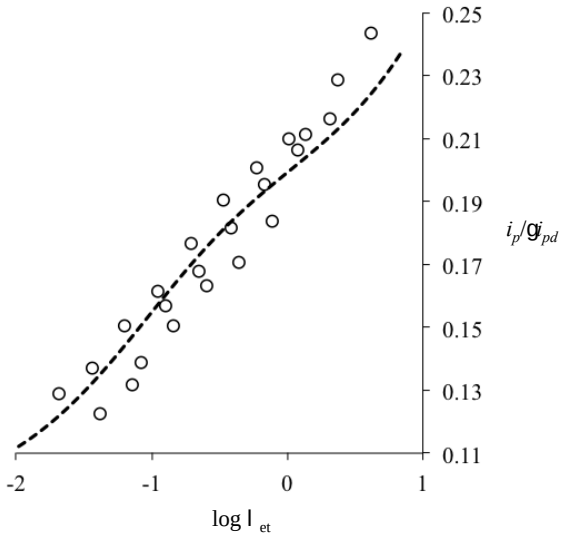

Figure 4.14. $i_p/\gamma i_{pd}$ **data fit to dimensionless working curves for tetra-*n*-butylammonium acetate in dry acetonitrile (mediator = vinylferrocene).** $\log\left(\frac{RT}{nF}k_{et}\right) = 1.84$, $k_{et} = (2.7 \pm 0.3)$ **x** 10^3 M^{-1} s^{-1}.

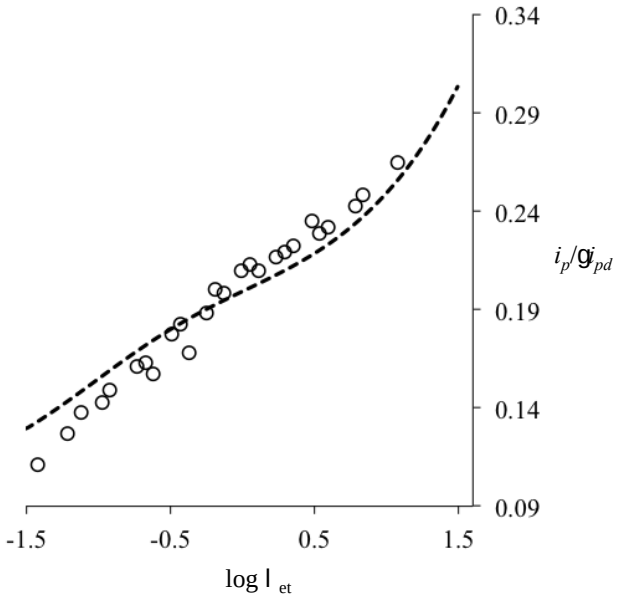

Figure 4.15. $i_p/\gamma i_{pd}$ data fit to dimensionless working curves for tetra-*n*-butylammonium acetate in dry acetonitrile (mediator = *p*-bromophenylferrocene). $\log\left(\frac{RT}{nF}k_{et}\right) = 2.494$, $k_{et} = (1.21 \pm 0.13) \times 10^4\ M^{-1}\ s^{-1}$.

References

(1) Spencer, J. N.; Virginia Tech: 2016; Vol. PhD.

Appendix H

Water and electrolyte effects on the rate of β-scission of the cumyloxyl radical *via* flash laser photolysis (Chapter 5)

Table 5.7
Measured rate constants of β-scission of cumyloxyl radical as a result of added water to an acetonitrile solution (No electrolyte is added).

Concentration	Deionized Water k (x 10^{-5} s^{-1})	Deuterated oxide k (x 10^{-5} s^{-1})
"0"	7.8 (0.2)	8.6 (0.2)
0.6	7.8 (0.2)	8.7 (0.2)
1.1	8.2 (0.2)	9.0 (0.2)
1.7	8.7 (0.2)	9.4 (0.4)
2.2	9.3 (0.5)	9.7 (0.1)

Table 5.8
Measured rate constants of β-scission of cumyloxyl radical as a result of added deionized water to an acetonitrile solution with a range of electrolyte concentrations of tetra-n-butylammonium perchlorate (TBAP).

DI water molarity (M)	No TBAP k (x 10^{-5} s^{-1})	0.08 M TBAP k (x 10^{-5} s^{-1})	0.15 M TBAP k (x 10^{-5} s^{-1})	0.23 M TBAP k (x 10^{-5} s^{-1})	0.39 M TBAP k (x 10^{-5} s^{-1})
"0"	7.8 (0.2)	8.7 (0.1)	9.0 (0.2)	9.2 (0.1)	10.0 (0.3)
0.6	7.8 (0.2)	9.1 (0.2)	9.3 (0.3)	10.0 (0.2)	10.6 (0.1)
1.1	8.2 (0.2)	9.6 (0.4)	10.5 (0.4)	9.9 (0.4)	10.9 (0.5)
1.7	8.7 (0.2)	9.8 (0.4)	--	10.5 (0.2)	11.7 (0.6)
2.2	9.3 (0.5)	10.2 (0.1)	11.2 (0.3)	11.3 (0.1)	12.1 (0.6)

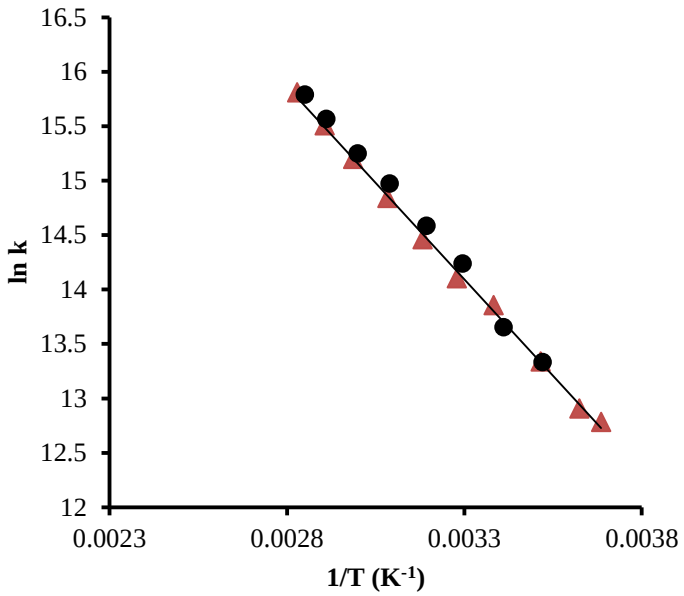

Figure 5.5. Arrhenius plot showing no apparent isotopic effect for the β-scission of cumyl radical (0.75 M) as a result of 2.1 M of added H_2O (Black circles) or D_2O (Orange triangles) into the acetonitrile solution with no electrolyte present.

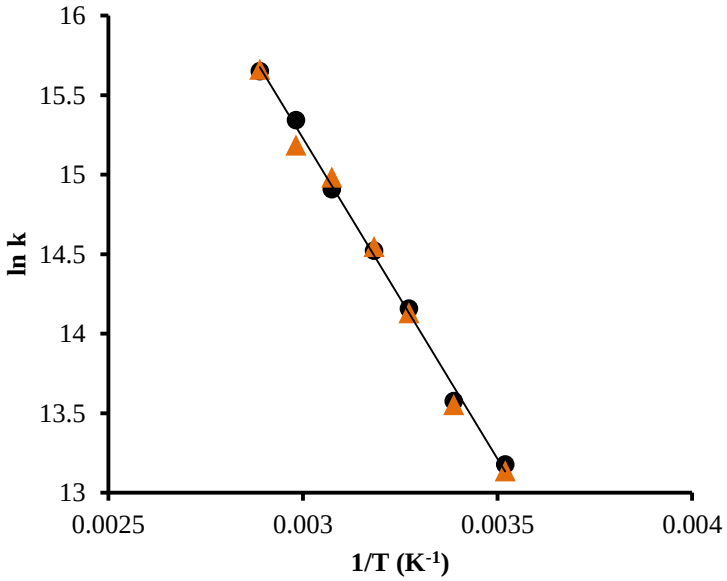

Figure 5.6. Arrhenius plot showing no apparent isotopic effect for the β-scission of cumyloxyl radical (0.75 M) as a result of 2.7 M of added H_2O (Black circles) or D_2O (Orange triangles) into the acetonitrile solution with no electrolyte present.

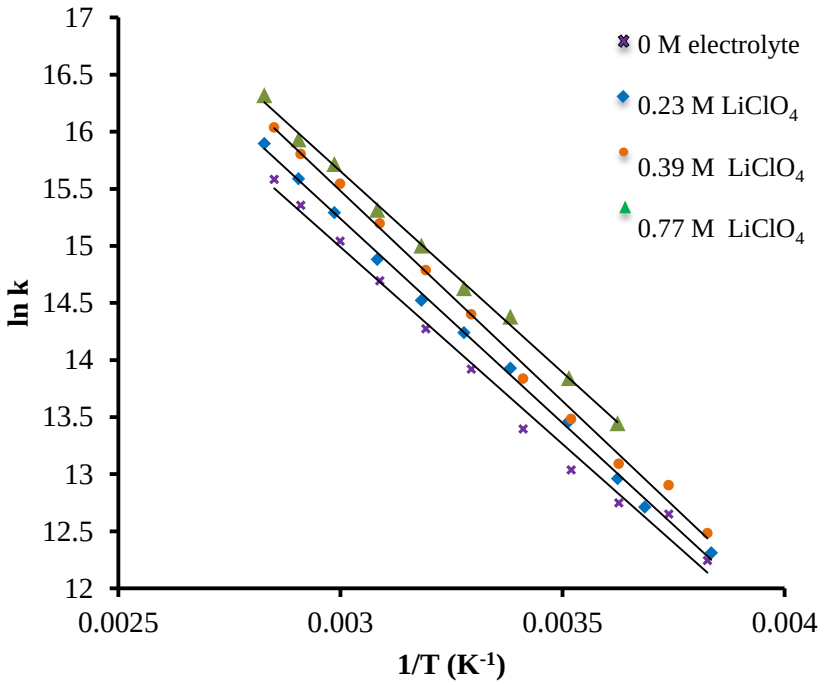

Figure 5.7. Arrhenius plot showing a solvent effect on the β-scission of cumyloxyl radical (0.75 M) with added lithium perchlorate electrolyte in anhydrous acetonitrile.

Table 5.9

Activation barriers calculated from Arrhenius plots with estimated enthalpy and entropy of activation for the β-scission of cumyloxyl in acetonitrile as a solvent with a range of molarities of added electrolytes. Subtle changes cannot be detected by the activation energy profile.

Molarity of electrolyte (M)	E_a *(Kcal/mol)*	*log A*	$\Delta H^{\ddagger}$ $(Kcal/mol)$	$\Delta S^{\ddagger}$ $(cal/K.mol)$	^{a}k *(x 10^{-5} s^{-1})*
0.23 $LiClO_4$	7.46 (0.27)	11.5 (0.2)	6.77 (0.26)	-8.18 (0.77)	14.4 (0.5)
0.39 $LiClO_4$	7.52 (0.48)	11.6 (0.4)	6.89 (0.46)	-7.43 (1.35)	17.6 (0.7)
0.77 $LiClO_4$	7.40 (0.66)	11.6 (0.9)	6.69 (0.61)	-7.60 (2.17)	21.8 (0.7)
0.39 $Mg(ClO_4)_2$	7.49 (0.74)	11.5 (-)	6.77 (0.69)	-8.54 (2.04)	12.7 (0.9)
0.39 $NaClO_4$	7.00 (0.57)	11.1 (0.2)	6.34 (0.56)	-9.82 (1.65)	13.7 (0.8)
0.39 TBAP	7.15 (0.58)	11.2 (0.6)	6.44 (0.58)	-9.60 (1.71)	12.8 (0.9)

[a]Calculated rate constants at 30 °C from Arrhenius plots

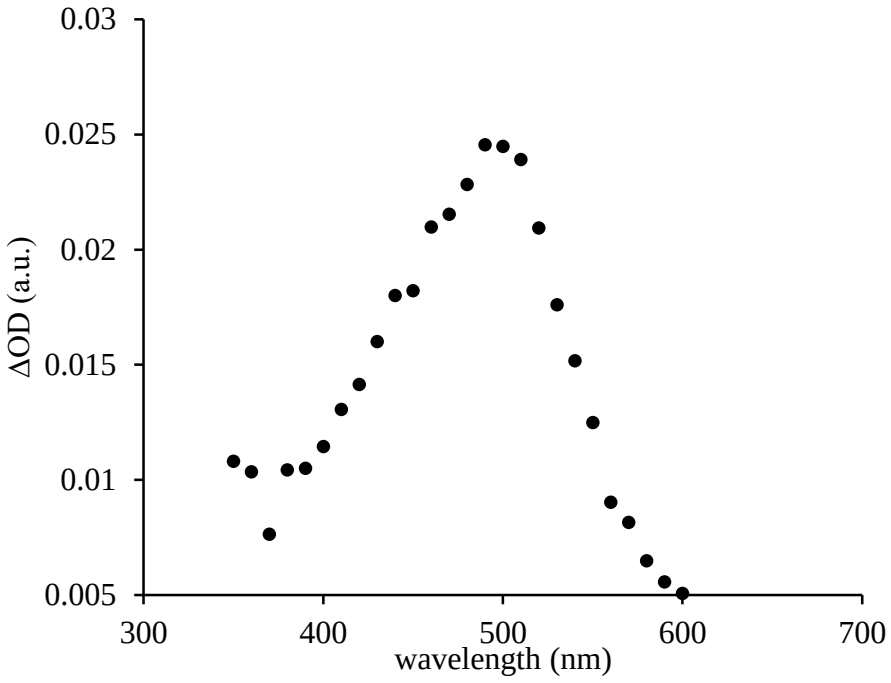

Figure 5.8. Absorbance spectrum for cumyloxyl radical with a maximum absorbance at 490 nm taken at t = 20 ns in acetonitrile at ambient room temperature.

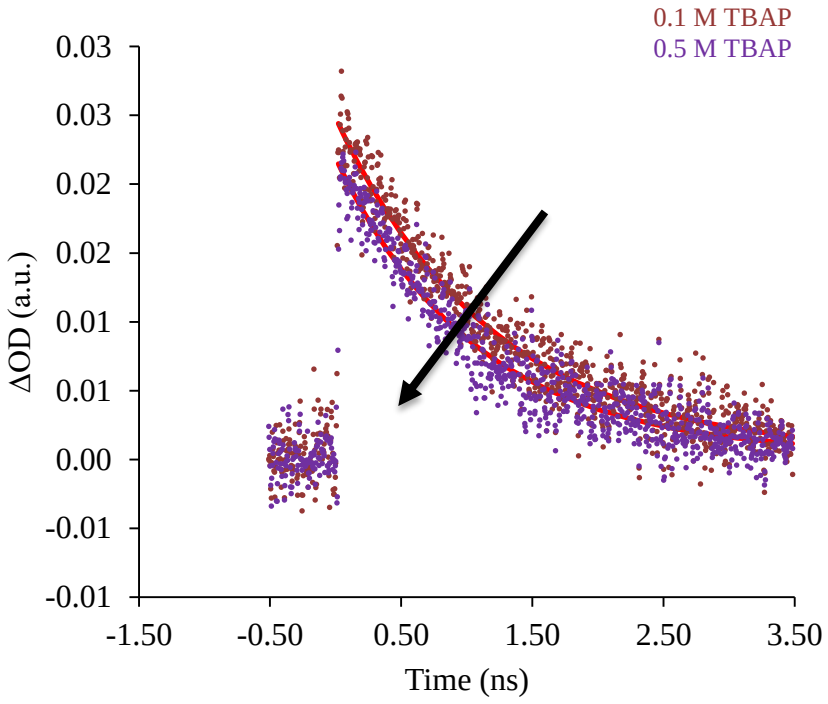

Figure 5.9. Exponential fitting corresponding to the decay of cumyloxyl radical at 490 nm at t = 20 ns as a function of increased TBAP electrolyte concentration in acetonitrile at ambient room temperature.

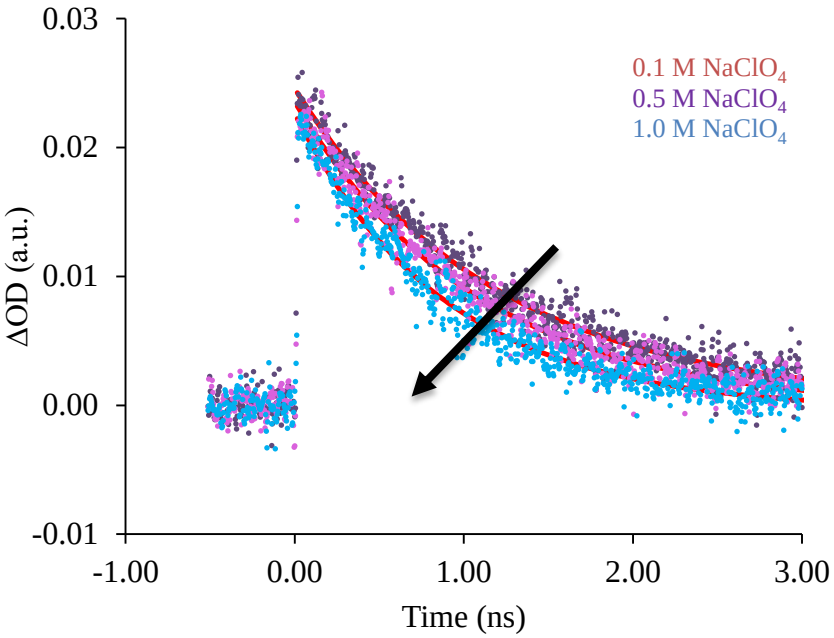

Figure 5.10. Exponential fitting corresponding to the decay of cumyloxyl radical at 490 nm at t = 20 ns as a function of increased $NaClO_4$ electrolyte concentration in acetonitrile at ambient room temperature.

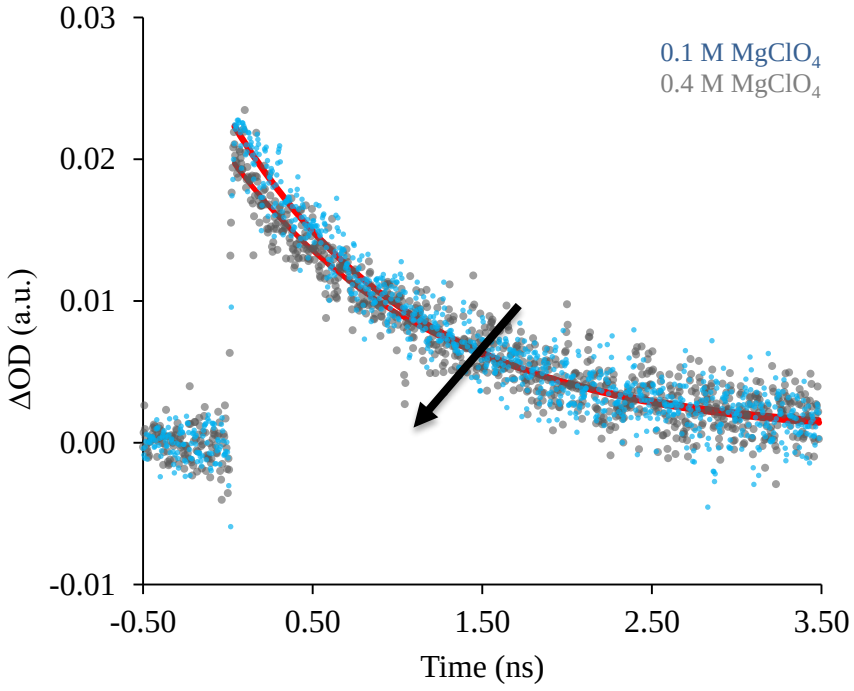

Figure 5.11. Exponential fitting corresponding to the decay of cumyloxyl radical at 490 nm at t = 20 ns as a function of increased $MgClO_4$ electrolyte concentration in acetonitrile at ambient room temperature.

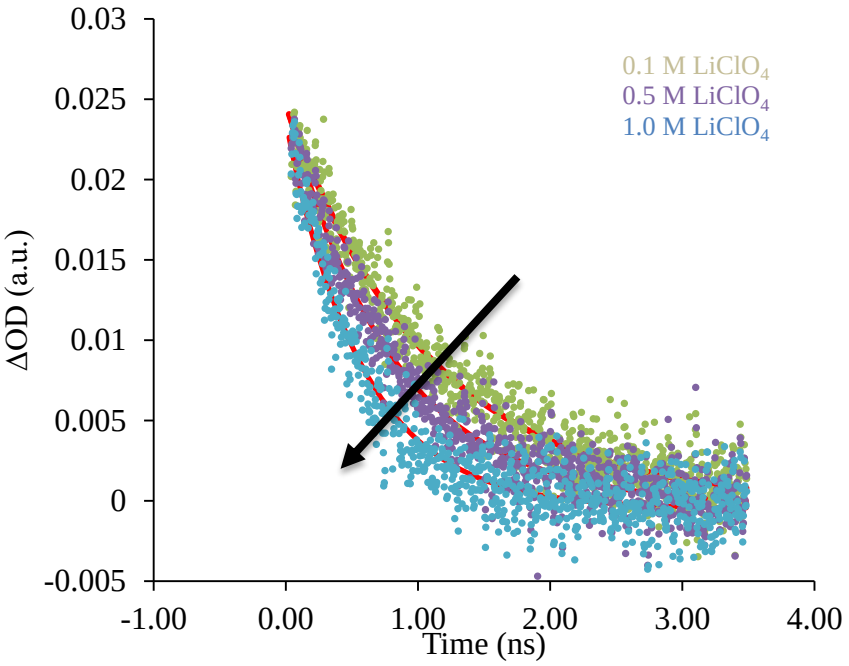

Figure 5.12. Exponential fitting corresponding to the decay of cumyloxyl radical at 490 nm at t = 20 ns as a function of increased $LiClO_4$ electrolyte concentration in acetonitrile at ambient room temperature.

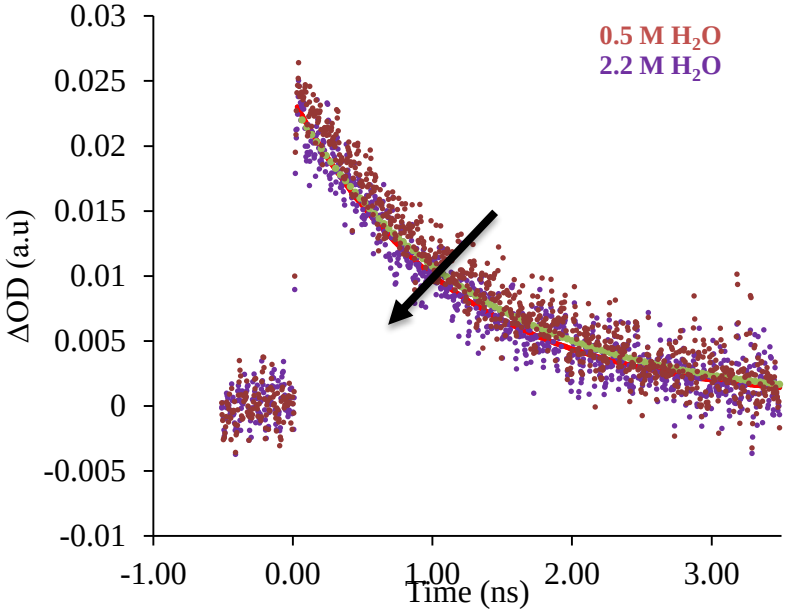

Figure 5.13. Exponential fitting corresponding to the decay of cumyloxyl radical at 490 nm at t = 20 ns as a function of increased water concentration in acetonitrile at ambient room temperature.

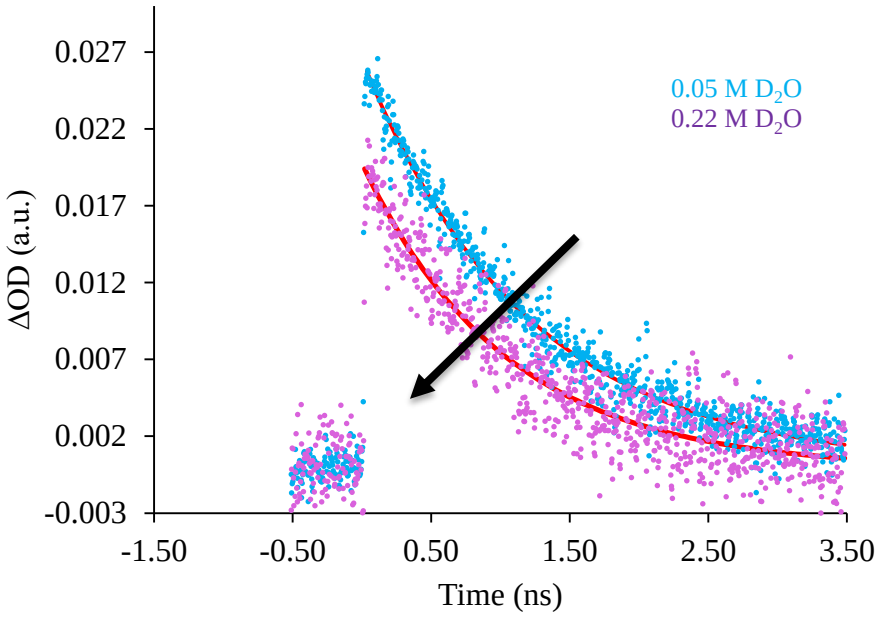

Figure 5.14. Exponential fitting corresponding to the decay of cumyloxyl radical at 490 nm at t = 20 ns as a function of increased dueterated water concentration in acetonitrile at ambient room temperature.

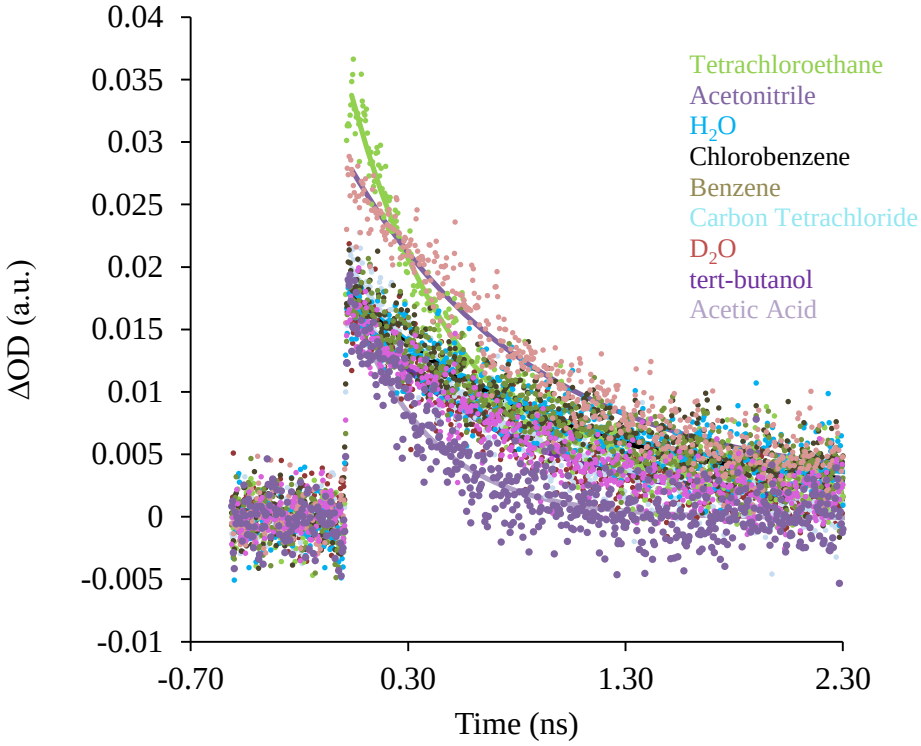

Figure 5.15. Exponential fitting corresponding to the decay of cumyloxyl radical at 490 nm at t = 20 ns as a function of solvent polarity at 30 ^{0}C.

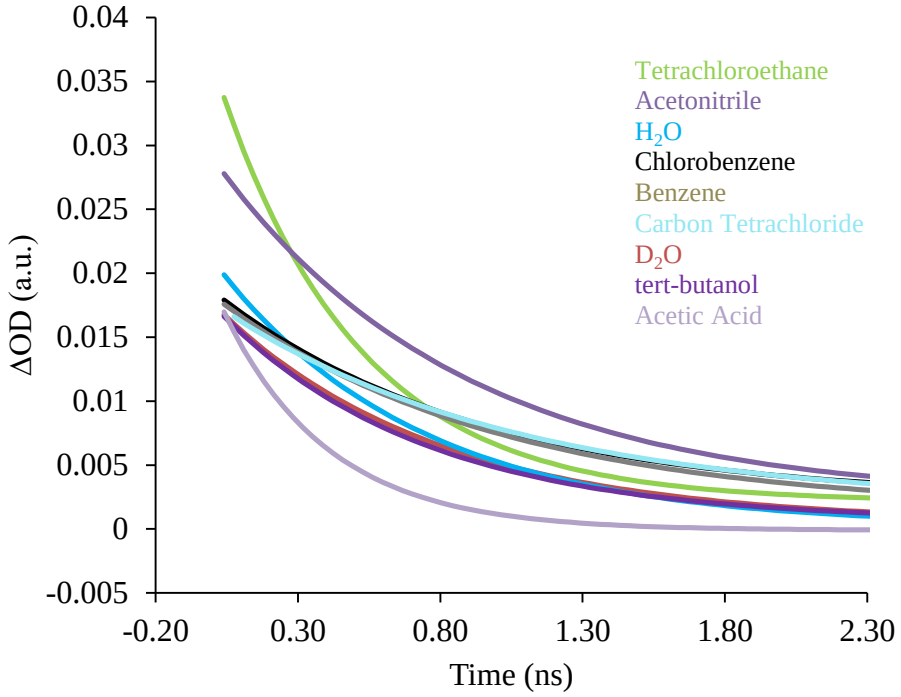

Figure 5.16. Exponential fitting corresponding to the decay of cumyloxyl radical at 490 nm at t = 20 ns as a function of solvent polarity at 30 ºC.

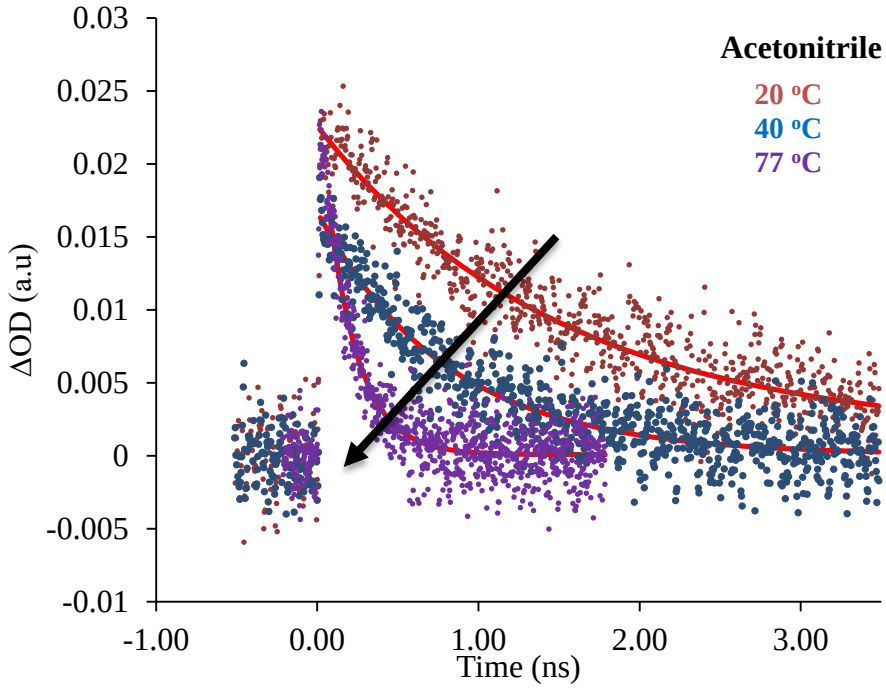

Figure 5.17. Exponential fitting corresponding to the decay of cumyloxyl radical at 490 nm at t = 20 ns as a function of increased temperature in acetonitrile.

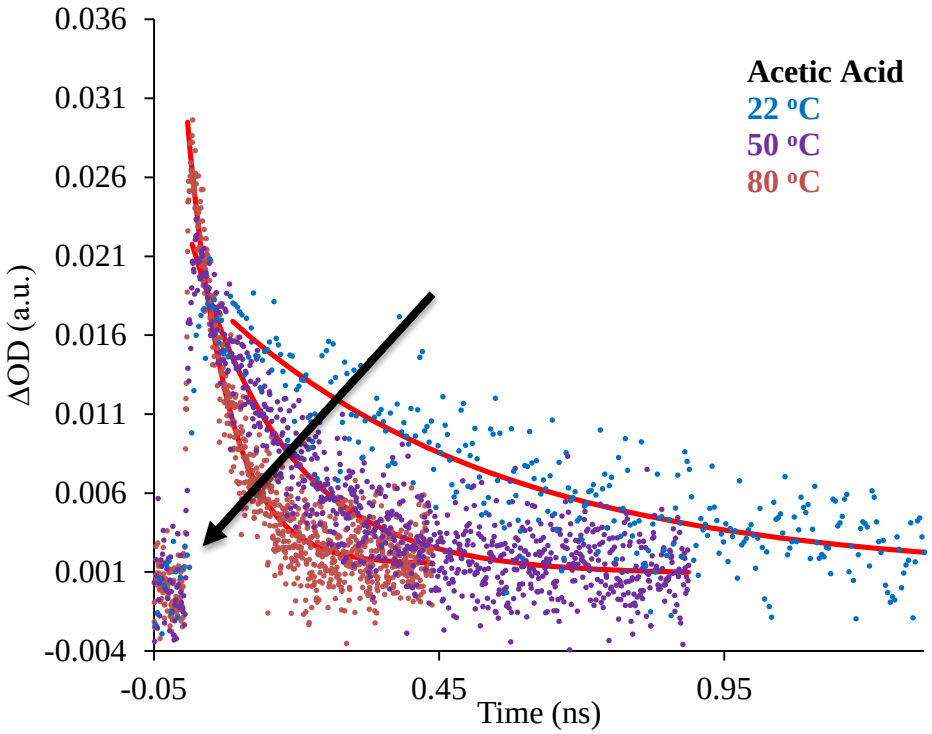

Figure 5.18. Exponential fitting corresponding to the decay of cumyloxyl radical at 490 nm at t = 20 ns as a function of increased temperature in acetic acid.

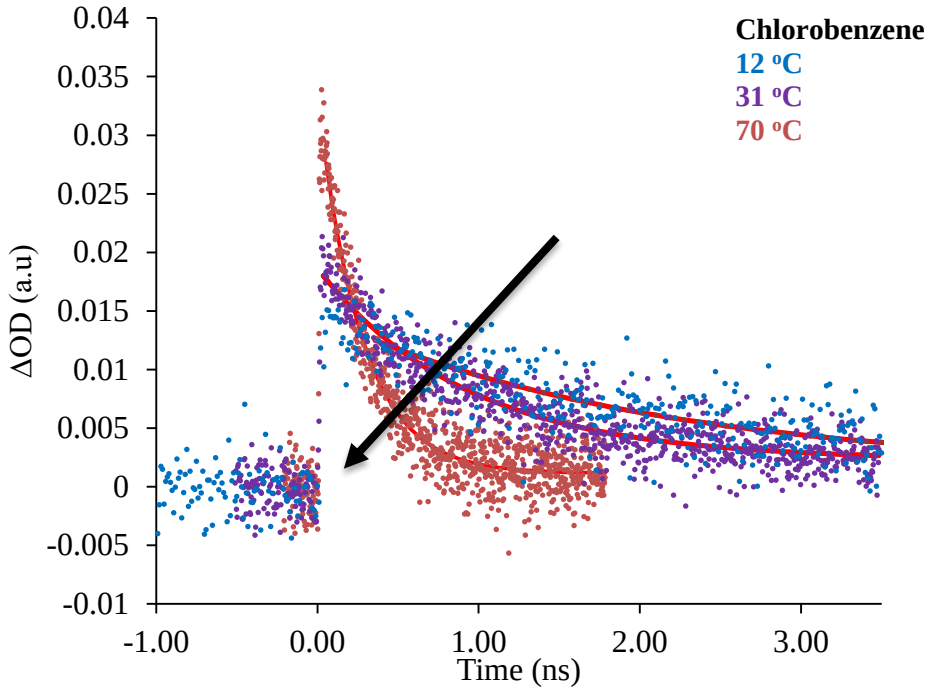

Figure 5.19. Exponential fitting corresponding to the decay of cumyloxyl radical at 490 nm at t = 20 ns as a function of increased temperature chlorobenzene.

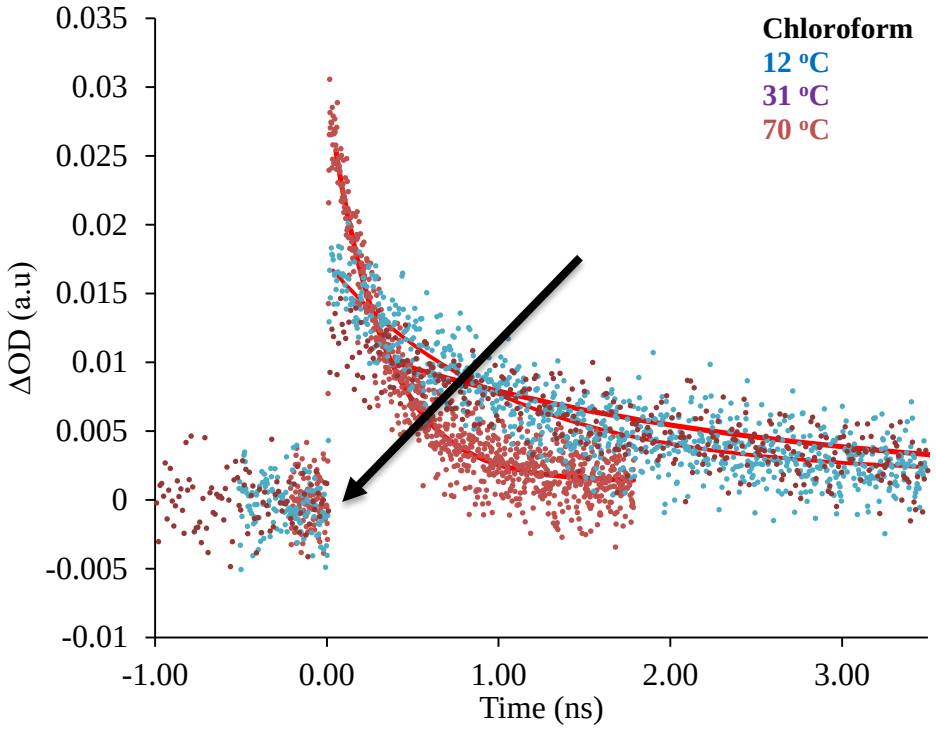

Figure 5.19. Exponential fitting corresponding to the decay of cumyloxyl radical at 490 nm at t = 20 ns as a function of increased temperature in chloroform.

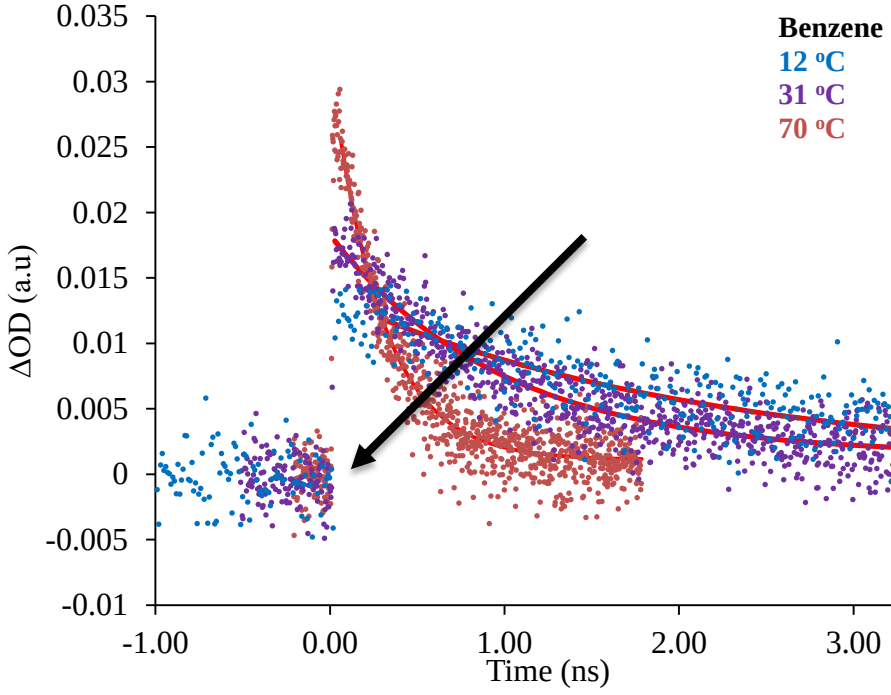

Figure 5.20. Exponential fitting corresponding to the decay of cumyloxyl radical at 490 nm at t = 20 ns as a function of increased temperature in benzene.

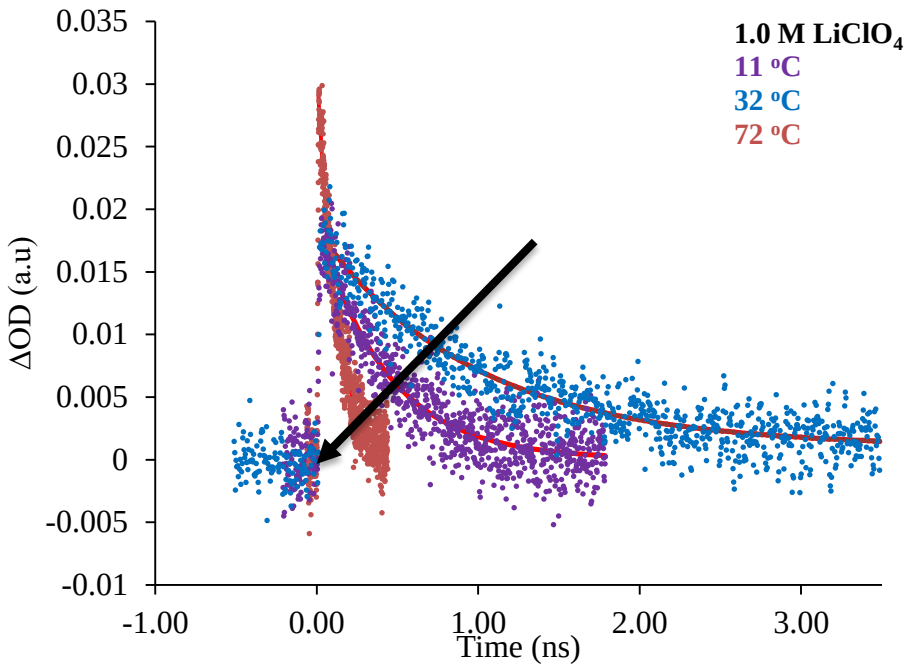

Figure 5.21. Exponential fitting corresponding to the decay of cumyloxyl radical at 490 nm at t = 20 ns as a function of increased temperature in acetonitrile in the presence of $LiClO_4$ electrolyte.

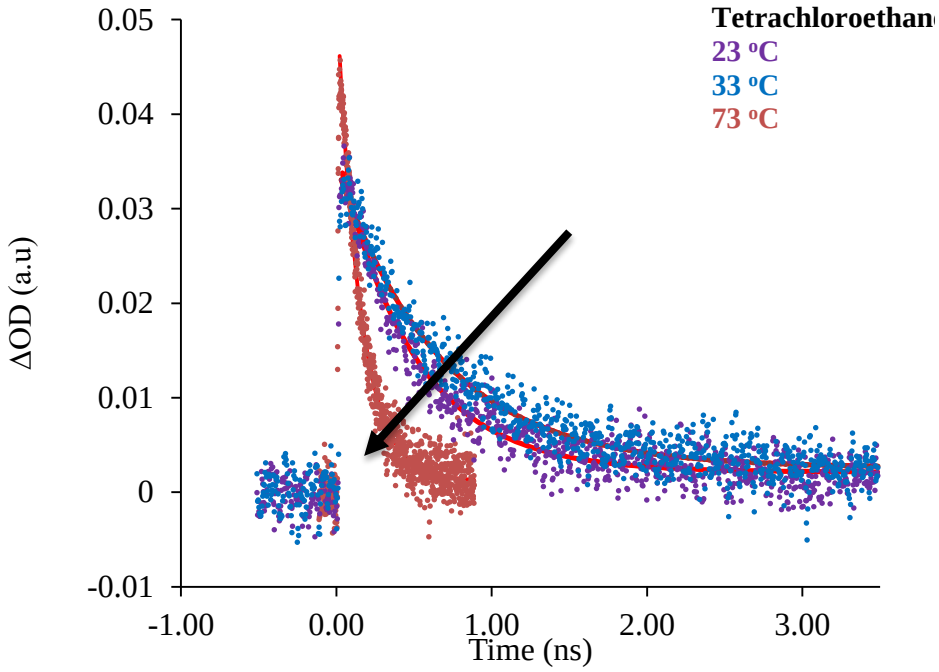

Figure 5.22. Exponential fitting corresponding to the decay of cumyloxyl radical at 490 nm at t = 20 ns as a function of increased temperature in 1,12,2-tetrachloroethane.

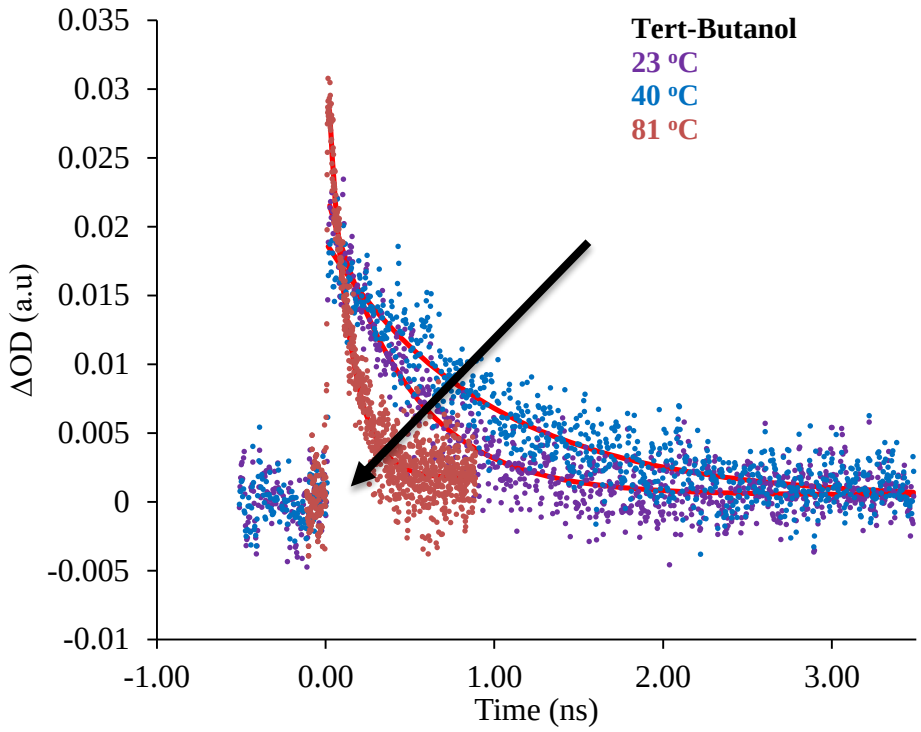

Figure 5.22. Exponential fitting corresponding to the decay of cumyloxyl radical at 490 nm at t = 20 ns as a function of increased temperature in tert-butanol.

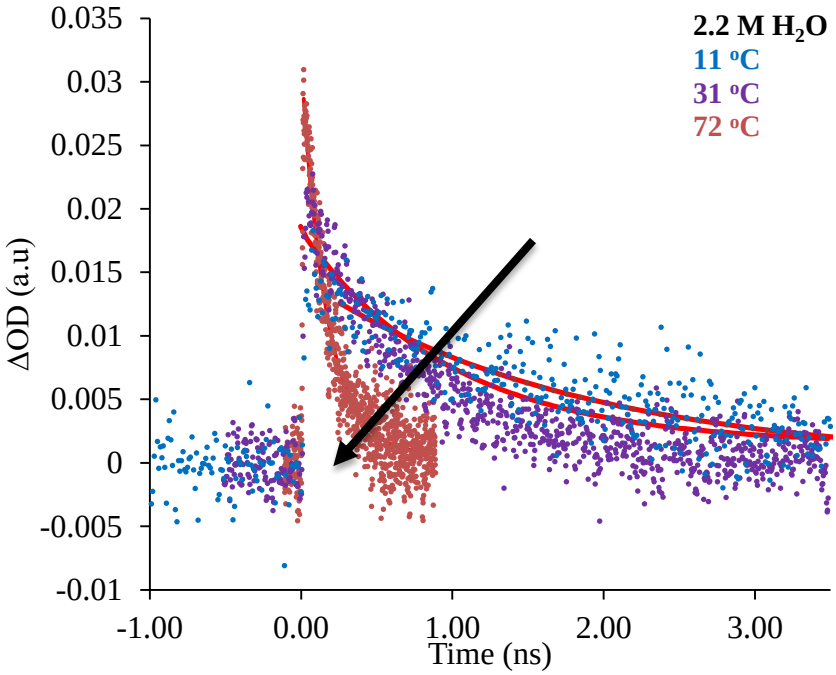

Figure 5.23. Exponential fitting corresponding to the decay of cumyloxyl radical at 490 nm at t = 20 ns as a function of increased temperature in acetonitrile with 2.2 M water concentration.

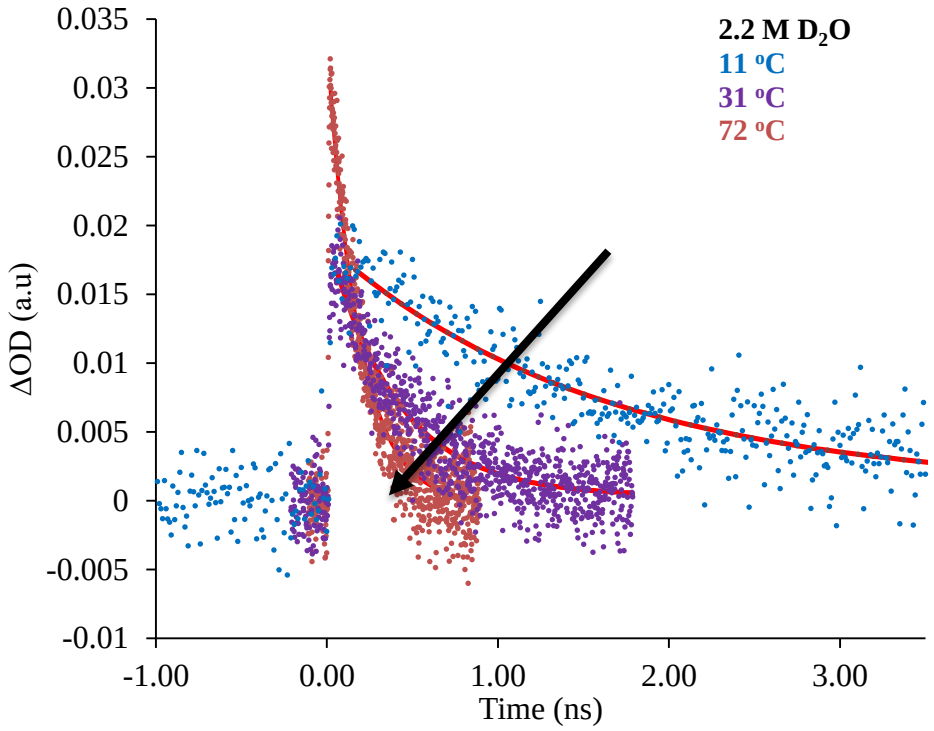

Figure 5.24. Exponential fitting corresponding to the decay of cumyloxyl radical at 490 nm at t = 20 ns as a function of increased temperature in acetonitrile with 2.2 M deuterated water concentration.

Appendix I

Flash laser photolysis (Transient absorption spectroscopy)

Flash photolysis is a fast spectrochemical technique to induce photochemical reactions such as electron transfer with rates between 10^{-5}-10^{-9} s^{-1}. The laser source in our system is a neodymium-yttrium aluminum (Nd:YAG) solid-state laser. The excitation of Nd:YAG omits an IR light frequency which is tripled into an high energy output at 355 nm. The nanosecond pulsed laser (4 – 6 nm) is directed to a sample cuvette at a right angle to a light beam from a 150 watt pulsed xenon arc source. A sample is excited at 355 nm from a ground state and the wavelength used to monitor the reaction is selected by an "Applied Photophysics" monochromator model with a 250 nm holographic diffraction grating. The monochromator is attached to a photomultiplier tube which captures the exiting light signal and amplifies the current as the light is transmitted through. The transient signal output from the photomultiplier is digitized by an oscilloscope. [1-3]

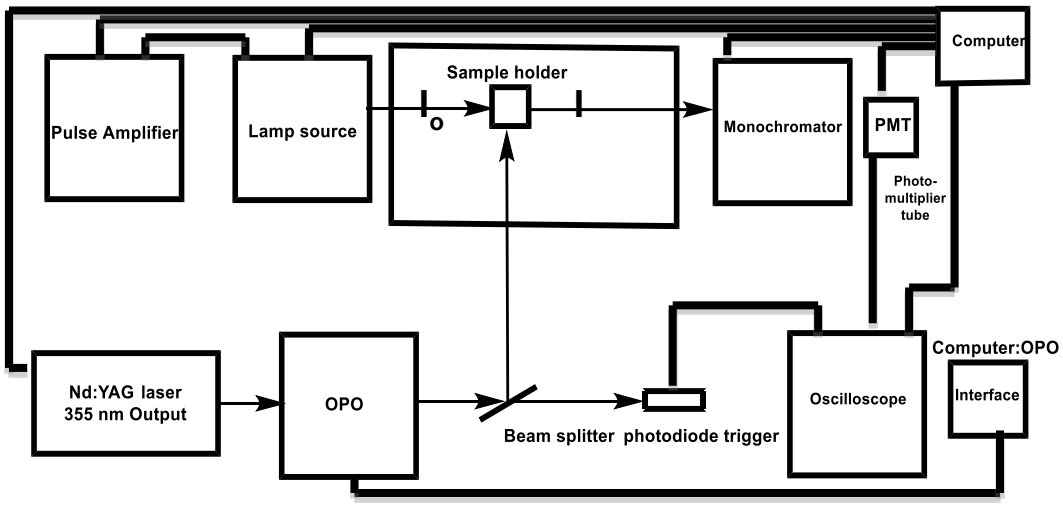

Scheme 5.5 Block diagram of Applied Photophysic LKS.80 spectrometer using the third harmonic of a Continuum Surelite I-10 Nd:YAG laser (4-6 ns pulse, 355 nm) with a Hewlett-Packard Infinium digital oscilloscope, an xenon arc lamp source, and Applied Photophysics Kinetic Workbench/LKS Spectrometer Control Panel Application (v. 3.01).

References

(1) Ellis, A. M.; Fehér, M.; Wright, T. G. *Electronic and photoelectron spectroscopy: fundamentals and case studies*; Cambridge University Press: Cambridge, UK;New York;, 2005.

(2) Hercules, D. M. *Fluorescence and phosphorescence analysis: principles and applications*; Interscience Publishers, 1966.

(3) Lakowicz, J. *Principles of Fluorescene Spectroscopy*; 3 ed. USA.